Univerzita Karlova

Přírodovědecká fakulta

Studijní program: Biochemie
Studijní obor: Biochemie

Mgr. Václav Navrátil

Vývoj analytických nástrojů pro kvantifikaci a hledání inhibitorů glutamátkarboxypeptidas II a III

Development of analytical tools for quantification and screening for inhibitors of glutamate carboxypeptidases II and III

Disertační práce

Vedoucí práce:

Doc. RNDr. Jan Konvalinka, CSc.

Praha, 2018

Charles University

Faculty of Science

Study program: Biochemistry
Branch of study: Biochemistry

Václav Navrátil

Development of analytical tools for quantification and screening for inhibitors of glutamate carboxypeptidases II and III

Vývoj analytických nástrojů pro kvantifikaci a hledání inhibitorů glutamátkarboxypeptidas II a III

Doctoral thesis

Supervisor:

Jan Konvalinka, Ph.D.

Prague, 2018

Prohlašuji, že jsem tuto disertační práci vypracoval samostatně pod vedením školitele doc. RNDr. Jana Konvalinky, CSc., a všechny použité prameny jsem řádně citoval. Tato práce ani její podstatná část nebyla předložena k získání jiného nebo stejného akademického titulu.

V Praze, dne 6. 6. 2018 .....

Acknowledgment

I would like to thank my supervisor Jan Konvalinka, who gave me the opportunity to join his great team at Institute of Organic Chemistry and Biochemistry AS CR (IOCB). I would like to express my special thanks to him due to his long-lasting support during the complete course of my time in his lab.

I would also like to thank to my closest colleagues and collaborators: Pavel Šácha, Jirka Schimer, Tom Knedlík, Honza Tykvart, Jitka Zemanová, Milan Kožíšek, Katka Rojíková, Pavel Majer and others for fruitful collaborations. I would also like to thank to other members of Jan Konvalinka's lab and to collaborators from other groups at IOCB or from other institutes.

I would like to thank also to the management of IOCB for their support of commercial applications of the presented work, especially to Zdeněk Hostomský (Director of IOCB), Martin Fusek (Head of IOCB Tech transfer company) and Jaromír Zahrádka (Head of IOCB owned investment fund I&I Prague). In this respect, also the help of Martin Dienstbier was very important.

I would also like to express my deep gratitude to my parents not only for their support during my previous study. Finally, I would like to dedicate this doctoral thesis to my wonderful wife Diana, who was supportive throughout the entire postgraduate studies and was patient with me spending a lot of my time in the lab.

Abstract

Glutamate carboxypeptidase II (GCPII) usually called prostate specific membrane antigen (PSMA) is membrane bound metallopeptidase expressed mainly in prostate carcinoma (PCa). Agents targeting GCPII suitable for both imaging and treatment of PCa are in development and they show promising results in advanced clinical trials. Some studies showed that GCPII may serve also as PCa blood serum marker, but this has not been validated due to the lack of methods suitable for accurate detection of GCPII in human blood.

Moreover, GCPII is also expressed in brain, where it cleaves inhibitory *N*-acetyl-*α*-L-aspartyl-L-glutamate (NAAG) to release excitatory L-glutamate and GCPII inhibition has been shown to be neuroprotective in animal models of several neuropathies. Tight binding inhibitors of GCPII have been identified by rational design, but all have poor bioavailability and thus cannot be used in clinics. Identifying new scaffolds by 'brute force' screening methods is thus essential; however, no such method for GCPII has been developed so far.

Glutamate carboxypeptidase III (GCPIII) is also expressed in brain and cleaves NAAG. It is thus an important protein for understanding of GCPII function as well as GCPII targeting in medicine.

Here, we focused on development of novel methods for quantification of both enzymes and screening of their inhibitors. First, we developed qRT-PCR and radioenzymatic assays to quantify GCPII and GCPIII in human and mice tissues and proved lack of GCPII in murine prostate and intestine. We also developed several orthogonal assays for detection of GCPII in blood and determined GCPII blood levels in healthy and PCa individuals. Unfortunately, we showed that GCPII is not useful as a serum marker of PCa. Finally, we developed a novel method for enzyme detection (DIANA), which is based on dual recognition of the enzyme by immobilized antibody and DNA-linked inhibitor. We showed on the example of GCPII and CAIX, which is also a putative cancer marker and potential drug target, that this method is useful not only for ultrasensitive enzyme detection but also for screening of enzyme inhibitors without the need to purify the target enzyme. This makes DIANA a superior tool for biomarker detection and drug discovery.

Abstrakt

Glutamát karboxypeptidasa II (GCPII), známá také jako prostatický specifický membránový antigen (PSMA), je membránová metalopeptidasa exprimovaná zejména na buňkách karcinomu prostaty (PCa). Látky cílící GCPII pro zobrazování a léčbu PCa jsou ve vývoji a ukazují nadějné výsledky v pokročilých fázích klinického testování. Některé studie ukázaly, že GCPII by mohla být využita také jako krevní marker PCa, což ale zatím nebylo potvrzeno kvůli absenci metod vhodných pro přesnou detekci GCPII v krvi.

GCPII je exprimována také v mozku, kde štěpí inhibiční *N*-Acetyl-*α*-L-aspartyl-L-glutamát (NAAG) na excitační L-glutamát a inhibice GCPII je neuroprotektivní ve zvířecích modelech několika neuropatií. Silné inhibitory GCPII byly nalezeny pomocí racionálního vývoje, ale všechny vykazují nedostatečnou biodostupnost aby mohly být využity v klinické praxi. Nalezení nových strukturních motivů je tedy nezbytné, nicméně zatím nebyla vyvinuta žádná metoda vhodná pro účinné testování inhibitorů GCPII.

V mozku se nalézá také málo prozkoumaná glutamát karboxypeptidasa III (GCPIII), která také štěpí NAAG. Její studium je tak nutné pro pochopení funkce GCPII a pro cílení GCPII v medicíně.

V této práci jsme se zaměřili na vývoj nových metod pro kvantifikaci obou enzymů a pro hledání jejich inhibitorů. Nejprve jsme vyvinuli qRT-PCR a radioenzymové stanovení pro kvantifikaci GCPII a III v lidských a myších tkáních a ověřili, že GCPII se v myši na rozdíl od člověka nenachází v prostatě a tenkém střevu. Dále jsme vyvinuli několik vzájemně se doplňujících stanovení pro detekci GCPII v krvi a určili jsme jimi hladiny GCPII v krvi zdravých lidí a pacientů trpících PCa. Bohužel jsme ukázali, že GCPII patrně nelze využít jako sérový marker PCa. Nakonec jsme vyvinuli zcela novou metodu detekce enzymů DIANA založenou na vazbě enzymu na protilátku a jeho detekci skrze inhibitor navázaný na DNA oligonukleotid. Na příkladu GCPII a CAIX, což je další nádorový marker a potenciální terapeutický cíl, jsme ukázali, že tato metoda je vhodná nejen pro ultracitlivou detekci enzymů, ale také pro účinné hledání jejich inhibitorů bez potřeby purifikovaného enzymu. To dělá DIANA metodu výjimečným nástrojem pro detekci biomarkerů a vývoj léčiv.

Table of contents

1. Introduction

1.1. Glutamate carboxypeptidases II and III (GCPII and GCPIII)

Glutamate carboxypeptidase II (GCPII) is homodimeric type II integral membrane glycoprotein located on the cytoplasmic membrane with active site facing to the extracellular space (uniprot entry FOLH1_HUMAN).

GCPII was first described independently as three distinct proteins: (i) as pteroyl-poly-glutamyl hydrolase sequentially cleaving off the γ-glutamates from folyl-poly-γ-glutamate (FPG) isolated from human intestine in 1986 (hence its name **folate hydrolase**, FOLH1) [1], (ii) as *N*-acetylated-alpha-linked acidic dipeptidase cleaving *N*-acetyl-*α*-L-aspartyl-L-glutamate (NAAG) to *N*-acetyl-L-aspartate (NAA) and L-glutamate isolated from rat brain in 1987 (hence its name **NAALADase**) [2] and (iii) as an antigen overexpressed in a prostate carcinoma cell line also in 1987 (hence its name **prostate specific membrane antigen, PSMA**) [3]. In the pre-genomics era, it took almost ten years for the scientific community to realize that all three represent an identical protein [4, 5]. PSMA remained the mostly used name despite recommendation of International Union for Biochemistry and Molecular Biology to call this enzyme GCPII.

GCPII is in humans predominantly expressed in prostate [6-9] and its expression is confined to the secretory epithelial cells [6]. Prostate carcinoma is derived from these cells and carcinoma cells preserve the high expression of membrane bound GCPII [10, 11] (see **Fig. 1** on page 10). It is also secreted to the seminal plasma [12]. GCPII has been observed also in neovasculature of non-prostatic solid tumors but not in normal vasculature [11, 13, 14]. GCPII is also highly expressed in kidney [10] where it localizes to luminal side of the proximal tubules [6, 11, 15], in brain [6, 16] where it has been found on neurons [15] and astrocytes [16], and in jejunal brush border [1, 6, 17]. GCPII has been found also in liver, spleen [6, 9] and in some studies also in blood [18].

GCPII represents a promising target for diagnosis and treatment of several diseases. An ^{111}In-labeled anti-GCPII antibody known under the trade name ProstaScint is used for imaging of prostate carcinoma *in vivo* [19]. New generation of tracers consisting of small

molecule inhibitor conjugated to radionuclide, which are suitable not only for imaging but also for targeted treatment, are in clinical development [20, 21]. At the same time, GCPII serum levels may also be used for diagnostics [18]. Moreover, it has been shown that GCPII inhibition may be neuroprotective in some pathological conditions of central nervous system [22-24]. Recently, its role in the development of inflammatory bowel disease has been also proposed [25, 26]. To enable clinical exploitation of GCPII, high-affinity competitive inhibitors of GCPII have been identified by rational design [27-29]. However, they bear multiple negative charges and show poor bioavailability [30, 31] and therefore identifying new inhibitor scaffolds is essential to target GCPII in human brain. The possibilities of therapeutic targeting of GCPII will be described in more detail in later sections.

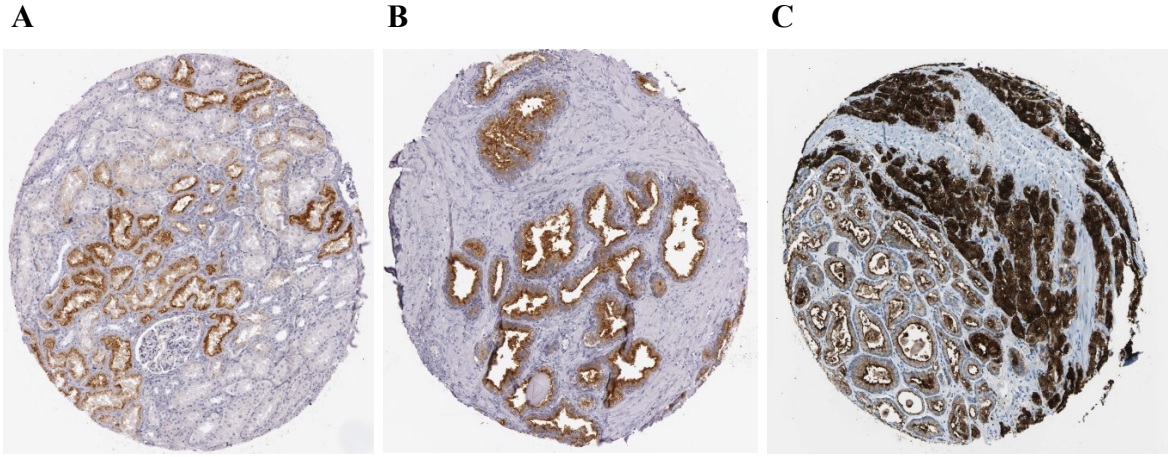

Figure 1: GCPII expression in selected healthy and cancerous tissues

Immunochemical staining of GCPII in selected tissues obtained from www.proteinatlas.org. (**A**) GCPII is expressed in proximal tubules of healthy kidney, (**B**) in secretory epithelial cell of prostate gland and (**C**) in prostate carcinoma cells (PCa), which are derived from the secretory epithelia.

Glutamate carboxypeptidase III (GCPIII) is the closest homolog of GCPII. It is also a homodimeric integral membrane glycoprotein, which is also located on the cytoplasmic membrane and shares ~70% amino acid sequence identity and the same topology with GCPII (uniprot entry NALD2_HUMAN).

GCPIII has been much less thoroughly studied than GCPII and it has been cloned and characterized only in 1999 for the first time. It has been shown that it also possesses *N*-acetylated-alpha-linked acidic dipeptidase activity (hence its name **NAALADase 2**) [32]. This activity has been later confirmed also for murine GCPIII [33]. However, both studies used unpurified GCPIII in lysates of transfected cell. Purified recombinant human GCPIII

has been vigorously characterized later by Hlouchova *et al*. This study confirmed that human GCPIII cleaves NAAG, however with about 10 fold lower efficiency than GCPII. It also showed that GCPII inhibitors inhibited GCPIII with similar potency [34]. Recently, it has been shown that mouse GCPIII can cleave also *β*-citryl-L-glutamate (BCG) to form citrate and L-glutamate [35] and that it is identical to the membrane bound BCG hydrolase initially isolated from rat testis more than thirty years ago [36, 37].

GCPIII tissue expression is not well described, as antibodies selective for GCPIII are lacking. Using RT-PCR and northern blot, highest amount of GCPIII mRNA has been found in human testes and to a lesser extent in ovary, spleen, placenta and heart [32]. Northern blot analysis showed GCPIII in mouse ovary, testes and lung [33]. The highest BCG hydrolysis was observed in mouse testis, uterus and bladder and to a lesser extent also in kidneys, lungs and other tissues [35]. In rat, highest BCG hydrolyzing activity was observed in testis, lung and heart, but it was detected also in kidney, intestine, brain and other tissues [36]. Unfortunately, different sets of tissues were analyzed in these studies and direct comparison is not possible, however, they consistently showed GCPIII presence in reproductive system (testis, ovary and uterus).

1.1.1. Substrates of GCPII and GCPIII and their physiological role

1.1.1.1. *N*-acetyl-*α*-L-aspartyl-L-glutamate (NAAG)

Both GCPII and GCPIII cleave neurotransmitter *N*-acetyl-*α*-L-aspartyl-L-glutamate (NAAG) to create N-acetyl-L-aspartate (NAA) and L-glutamate (**Fig. 2** on page 12), though GCPIII with about ten fold lower efficiency [34, 38]. NAAG is present in brain in up to milimolar concentrations, which makes it one of the most abundant peptide neurotransmitters in human brain [39, 40]. Both GCPII and GCPIII are also expressed in the brain [16, 32] and human GCPII has been shown to be present on outer membrane of astrocytes in humans [16] in mice [41] and in rats [42]. Astrocytes are cells supporting neurons and their projections surround most glutamatergic synapses [43]. GCPII on astrocytic membrane can thus participate in the modulation of synaptic transmission by cleaving NAAG and producing another neurotransmitter glutamate, which is likely the physiological role of GCPII in the brain [38, 44]. The key to understand the physiological role of NAAG cleavage are the different effects of NAAG and glutamate within the brain [45] (**Fig. 3** on page 14).

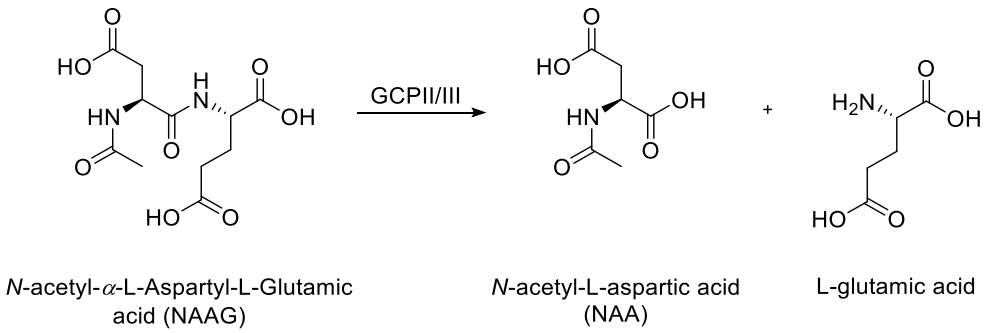

Figure 2: Cleavage of NAAG by GCPII or GCPIII in brain

Neuroprotective NAAG is cleaved by both GCPII and GCPIII and *N*-acetyl-aspartic acid and excitatory L-glutamic acid is produced.

The excitatory role of glutamate

Glutamate is an excitatory neurotransmitter, which activates both ionotropic and metabotropic glutamate receptors and excess of glutamate signaling leads to excitotoxicity. Ionotropic glutamate receptors are ligand gated ion channels and are subdivided into groups based on glutamate analogs activating them: NMDA (activated by *N*-methyl-D-aspartate), AMPA (activated by α-amino-3-hydroxy-5-methyl-4-isoxasolepropionate) and kainate receptors (reviewed in [46]). These receptors are located mostly on synaptic membrane of the downstream neuronal dendrite and are responsible for the transmission of the signal [46, 47]. Metabotropic receptors are G-coupled proteins and are also divided into three classes: group I consisting of mGluR1 and 5, group II consisting of mGluR2 and 3 and group III consisting of mGluR4, 6, 7 and 8. They act via second messengers and their response to glutamate is thus more complex; group I is activatory and promotes glutamate release when present, group II and III inhibit release of glutamate. Group I receptors are mostly located postsynaptically, whereas group II and III presynaptically; mGluR3 and 5 are also present on astrocytes (reviewed in [48]). Under normal conditions, extracellular glutamate concentration in brain is very low (<1μM) and its concentration in the synaptic cleft rises to milimolar levels only after release of the presynaptic vesicles and is again rapidly lowered by the action of excitatory amino acid transporters (EAATs) on both neurons and astrocytes [47, 49, 50]. Excessive glutamate release leads to NMDA receptor mediated increase of calcium ions in postsynaptic neurons and consequently their death followed by additional release of glutamate, which starts cascade effect of cell death [51, 52]. This process is known

as glutamate-mediated excitotoxicity and its implication has been reported in several central nervous system (CNS) disorders, including ischemic stroke [50] and neurodegenerative disorders such as Parkinson disease, Alzheimer disease and Huntington disease [53]. These effects may be, in principle, counteracted by administration of NMDA receptor antagonists such as phencyclidine or ketamine. However, these compounds elicit severe side effects in animal models and it is unclear, whether NMDA receptor can be targeted [49, 54, 55].

The neuroprotective role of NAAG

NAAG, on the other hand, has neuroprotective effects and is inactivated by GCPII. NAAG is synthetized in neurons from NAA and glutamate, is packaged to vesicles by sialin [56] and is released upon stimulus to the synaptic cleft [57]. Two reasons make the study of physiological role of NAAG very difficult: (1) contamination of NAAG preparations with glutamate, which activates with high-potency all glutamate receptors and (2) the presence of GCPII in neuronal tissues, which cleaves NAAG and produces glutamate. It is therefore necessary to use ultra-pure NAAG preparations and to employ GCPII inhibitors in physiological studies. The contamination of NAAG with glutamate may have been indeed responsible for some of the reported NAAG activities [44, 58-60]. Nevertheless, there is strong evidence that NAAG both *in vitro* and *in vivo* selectively activates mGluR3 and not other metabotropic receptors (reviewed in [24, 44, 57]). On neurons, NAAG activates presynaptic mGluR3 causing inhibition of glutamate release and thus providing a negative feedback loop [57, 61, 62]. mGluR3 is also present on the surface of astrocytes, where its activation by NAAG leads to secretion of transforming growth factor β (TGF-β) which has neuroprotective effects [63-66]. The role of NAAG in acting on NMDA receptors is less clear. Some studies showed that NAAG is not binding to NMDA receptors [60, 67], some showed it is an antagonist [68] and some showed it is even an agonist, which does not bind to other ionotropic glutamate receptors [69] and most recent study suggested that these effects may be pH dependent [70].

After release, NAAG is cleaved by GCPII and resulting NAA and glutamate are removed from extracellular space by EAATs on both neurons and astrocytes; glutamate is then transported back to the neurons in the form of glutamine [57]. NAAG is thus acting as neuroprotective agent and inhibition of its inactivation by GCPII inhibitors has been shown

to be neuroprotective [22]. Importantly, beneficial effects of GCPII inhibition are abolished in mGluR3 KO but not in mGluR2 KO mice [24] and are blocked by the administration of mGluR3 antagonists (such as LY341495) in wild type animals [61, 71, 72], which confirm that NAAG acts via this receptor.

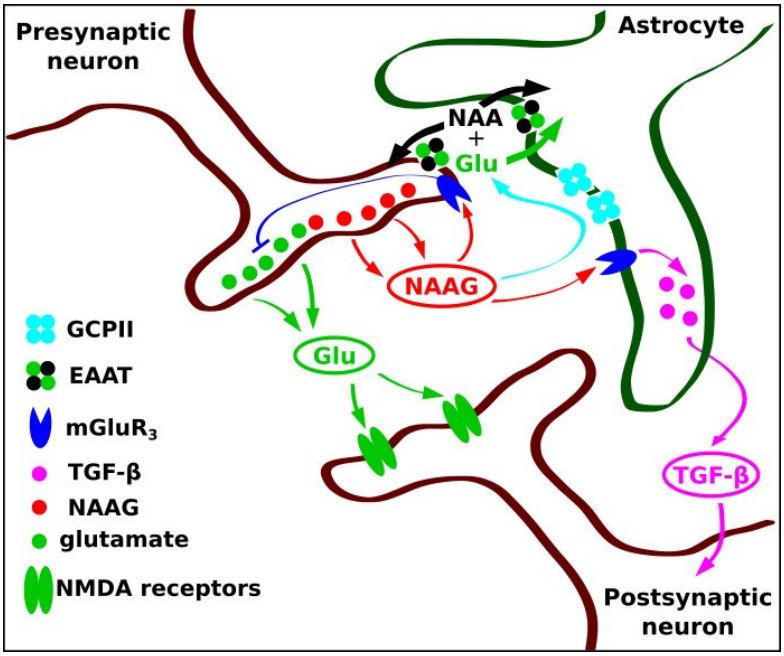

Figure 3: Proposed mechanism of action of *N*-acetyl-*α*-L-aspartyl-L-glutamate (NAAG)

During synaptic transmission, both glutamate and NAAG are released from presynaptic vesicles. Glutamate acts as excitatory neurotransmitter via its activation of ionotropic postsynaptical NMDA receptors. NAAG can activate mGluR3 both on presynaptic neuron, where it inhibits release of glutamate, and on glial cell, where it leads to secretion of neuroprotective transforming growth factor β (TGF-β). NAAG is inactivated by GCPII, which hydrolyzes NAAG to release L-glutamate and *N*-acetyl-L-aspartate (NAA), which are reabsorbed by the excitatory amino acid transporters (EAATs) on both neurons and glial cells. Adapted with changes from [73].

1.1.1.2. Folyl-poly-*γ*-glutamates (FPG)

Poly-*γ*-glutamylated forms of folate (vitamin B9) are other substrates of GCPII [4, 74] and its cleavage by GCPII is essential for absorption of dietary folates [75, 76]. Folate is an essential enzyme cofactor serving as a source of single carbon units in different oxidative states in single carbon transfer. Humans cannot synthetize folate and the only source is thus dietary folate, which is present in the poly-*γ*-glutamylated form. The *γ*-linked glutamates are sequentially cleaved off at the jejunal brush border by GCPII in humans and pigs [75, 76] but not in rats and possibly also in other organism, in which they are cleaved by *γ*-glutamyl hydrolase (GGH) which is localized in the lysosomes of enterocytes [77, 78].

Cleavage of γ-glutamyl chain yields folate, which is the only form which can be transported by the enteral folate transporter in human and mouse (proton-coupled folate transporter, PCFT1; reviewed in [79]). Folate is then directly exported to bloodstream and later absorbed by the liver, where it is either transformed to the poly-γ-glutamylated form by folyl-poly-γ-glutamate synthetase (FPGS) and stored (γ-glutamyl chain may be later removed by the action of liver GGH) or transformed to 5-methyltetrahydrofolate (5MeTHF) by the action of dihydrofolate reductase (DHFR), serine hydroxymethyl transferase (SHMT) and methylenetetrahydrofolate reductase (MTHFR) and then exported to the bloodstream. Folate is absorbed by the peripheral tissues by reduced folate carrier (RFC) where it is stored in the form of poly-γ-glutamylated folate (reviewed in [79-81]) (see **Fig. 4** on page 16 for summary). While 5MeTHF is the primary form of folate in blood plasma, the poly-γ-glutamylated folate is present at about 50-fold higher concentration in red blood cells [82]. In case poly-γ-glutamylated folate would leak out of senescent red blood cells, then glutamates needs to be cleaved off before reabsorption; the GGH present in plasma probably cannot cleave at neutral pH [82] and GCPII expressed in renal tubules may thus play a role in reabsorption of such folates.

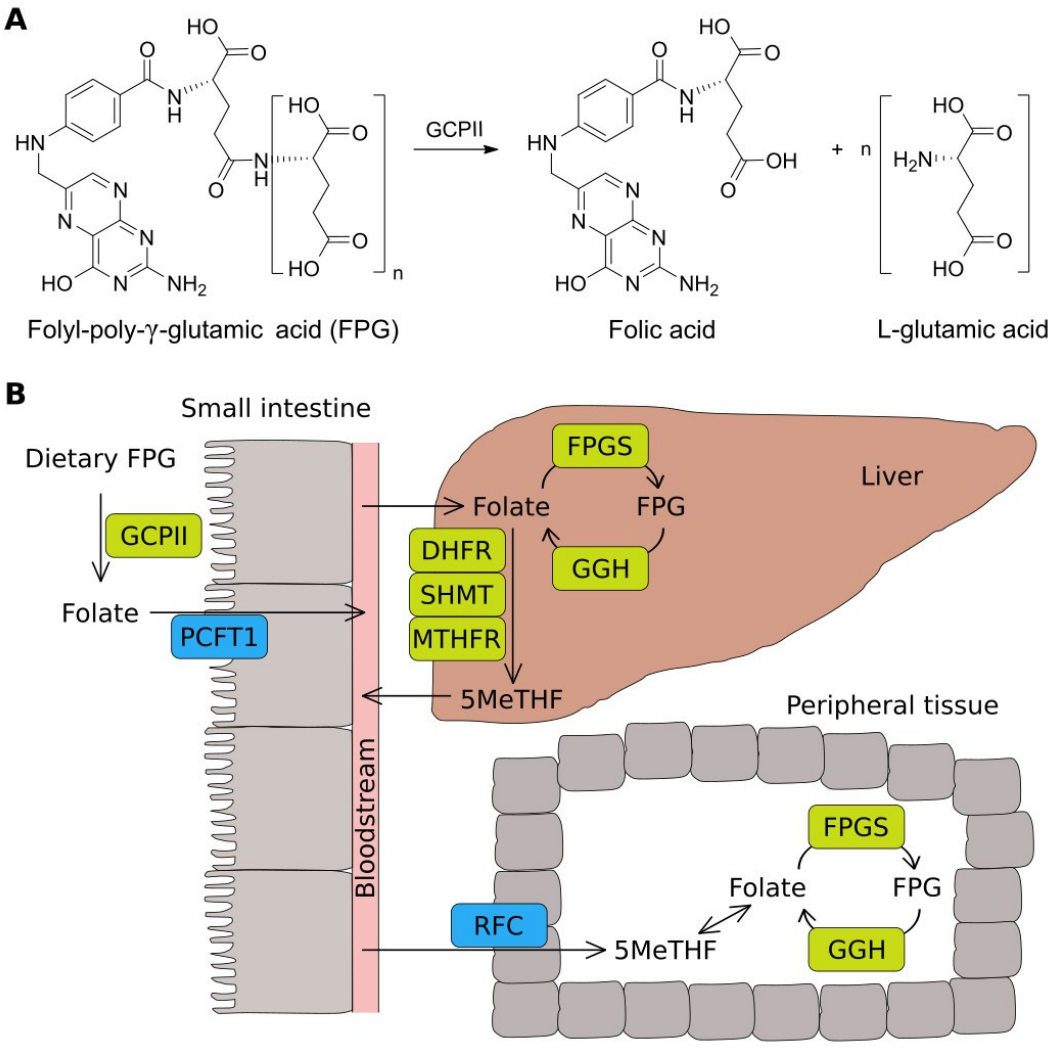

Figure 4: Metabolism of folate

(**A**, **B**) Dietary folyl-poly-γ-glutamate (FPG) is cleaved in small intestine by GCPII and folate and L-glutamate is produced. (**B**) Folate is then transported by the enteral folate transporter (proton-coupled folate transporter, PCFT1) and then directly exported to bloodstream and later absorbed by the liver, where it is either transformed to the FPG form by folyl-poly-γ-glutamate synthetase (FPGS) and stored (γ-glutamyl chain may be later removed by the action of liver GGH) or transformed to 5-methyltetrahydrofolate (5MeTHF) by the action of dihydrofolate reductase (DHFR), serine hydroxymethyl transferase (SHMT) and methylenetetrahydrofolate reductase (MTHFR) and then exported to the bloodstream. Folate is absorbed by the peripheral tissues by reduced folate carrier (RFC) where it is stored in the form of FPG. 5MeTHF is the primary form of folate in blood plasma. Inspired by [81].

1.1.1.3. *β*-citryl glutamate (BCG)

BCG has been recently identified as a novel substrate of murine GCPIII enzyme, but not murine GCPII [35] (**Fig. 5** on page 17). BCG was first identified in newborn rat brain, where its concentration reaches up to 1 milimolar while decreasing with age [83]. High levels

of BCG were detected also in other organs of newborn rats such as kidneys, heart, intestine, testis and lung and its levels decreased with age with the exception of testes, where its concentration was higher in adult rats [84]. Physiological role of BCG is not known, but there is some evidence it may play an important role during neuronal development and spermatogenesis [84, 85] and that it could serve as metal chelator [86, 87].

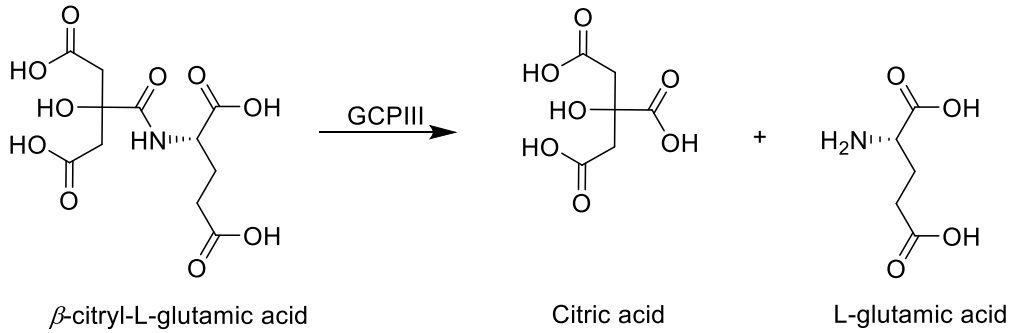

Figure 5: Cleavage of BCG by GCPIII.

β-citryl-L-glutamic acid (BCG) is cleaved to citric acid and L-glutamic acid by the action of GCPIII.

1.1.1.4. Biosynthesis of NAAG and BCG

NAAG and BCG are synthetized by Ribosomal Modification Protein RimK Like Family Members A and B (RIMKLA and RIMKLB) and *N*-acetyltransferase 8 like protein (NAT8L) in mice. RIMKLA (also called NAAGS-II) and RIMKLB (also called NAAGS-I) share 85% sequence identity and both are able to ligate NAA and glutamate to NAAG by the consumption of ATP with similar effectivity, but only RIMKLB is able to ligate citrate and glutamate to form BCG (the efficiency of RIMKLA is about 100 fold lower) [88-90]. Even though both enzymes are able to prepare NAAG, this reaction can happen only at sites expressing simultaneously also NAT8L, which is synthetizing NAA [88, 89]. Additionally, it has been shown that RIMKLA is able to catalyze also ligation of two glutamates to NAA and thus forming tripeptide *N*-acetyl-*α*-L-aspartyl-*α*-L-glutamyl-L-glutamate ($NAAG_2$), which is also present in mouse brain and is probably also substrate of murine GCPII [90]. The role of $NAAG_2$ is completely unclear and it has to be noted that it is synthetized by RIMKLA with about 1000-fold lower efficacy than NAAG and its concentration in the mouse brain regions is about 100-fold lower than of NAAG [90-92].

It is not much known about the expression profiles of these enzymes. By Northern blot, the highest expression of RIMKLA has been shown in mouse brain and spinal cord [90], while highest RIMKLB expression has been shown in mouse thymus [89]. Human RNA expression data shown at www.proteinatlas.org show high expression of NAT8L in cerebral cortex, adipose tissue, testis and kidney, highest expression of RIMKLA is observed in cerebral cortex while the expression in other tissues is low and RIMKLB is expressed quite ubiquitously, at highest levels in brain, smooth muscle, testis, endometrium and placenta. This putative RIMKLB tissue distribution coincides well with the reported GCPIII tissue profile [32].

1.1.2. Molecular structure of GCPII and GCPIII

GCPII is a homodimeric integral membrane glycoprotein located on the cytoplasmic membrane [93, 94]. Each monomer consists of 750 amino acids that form short cytoplasmic tail at N-terminus (19 amino acids), a single pass transmembrane helix (24 amino acids) and a large extracellular part (707 amino acids) bearing the active site. It is heavily N-glycosylated and molecular weight of each monomer is thus about 110KDa, deglycosylation leads to the complete loss of enzymatic activity [95-98].

This full-length protein usually called PSMA is the most prevalent form of GCPII but also truncated variant termed PSM' missing amino acids 1-59 was discovered. In contrast to membrane bound PSMA, PSM' protein is in the prostate carcinoma cell line LNCaP located in cytosol, but it is also able to cleave NAAG and is glycosylated. It is therefore product of posttranslational modification of the PSMA protein [99] rather than product of alternatively spliced mRNA variant, which is also called PSM' [100]. It is unclear, whether this soluble form is present in the blood and seminal plasma; however, GCPII was detected in these matrices by 7E11 antibody recognizing an intracellular epitope, which suggests that mostly the full-length protein is present [12, 18, 101, 102].

Crystal structure of the extracellular portion of GCPII (amino acids 44-750) has been solved and revealed active site with dinuclear zinc center coordinated by His377, Asp387, Glu425, Asp 453 and His553 and catalytic Glu424. It consists of three domains: apical (amino acids 117-351), C-terminal (591-750) and protease-like domain (57-116 and 352-590) [103, 104] (**Fig. 6** on page 19). Overall fold of all three domains is very similar to the

Transferrin receptor 1, which is not enzymatically active and shares ~25% amino acid sequence identity [105]. The fold of the protease-like domain and spatial organization of zinc coordinating residues and catalytic glutamate is common even with the distant human homolog Glutaminyl cyclase, which converts glutaminyl into pyroglutamyl peptides and shares as little as ~10% identity [106, 107]. The active site, which is formed by residues from all three domains, is deeply buried and is accessible via ~20Å long tunnel [104]. Catalytic mechanism has been modelled via QM/MM and confirmed by the crystal structure of the inactive mutant Glu424Ala in complex with NAAG. It showed carboxyl of Glu424 as proton shuttle and hydroxide anion coordinated by the zinc ions as the attacking group hydrolyzing the peptide bond. In the Michaelis complex, NAAG is bound by several positively charged residues (Arg210, Arg534, Arg536 and Lys699) [108]. Multiply positively charged active site represents a challenge for the design of non-polar inhibitors, which would be brain penetrant.

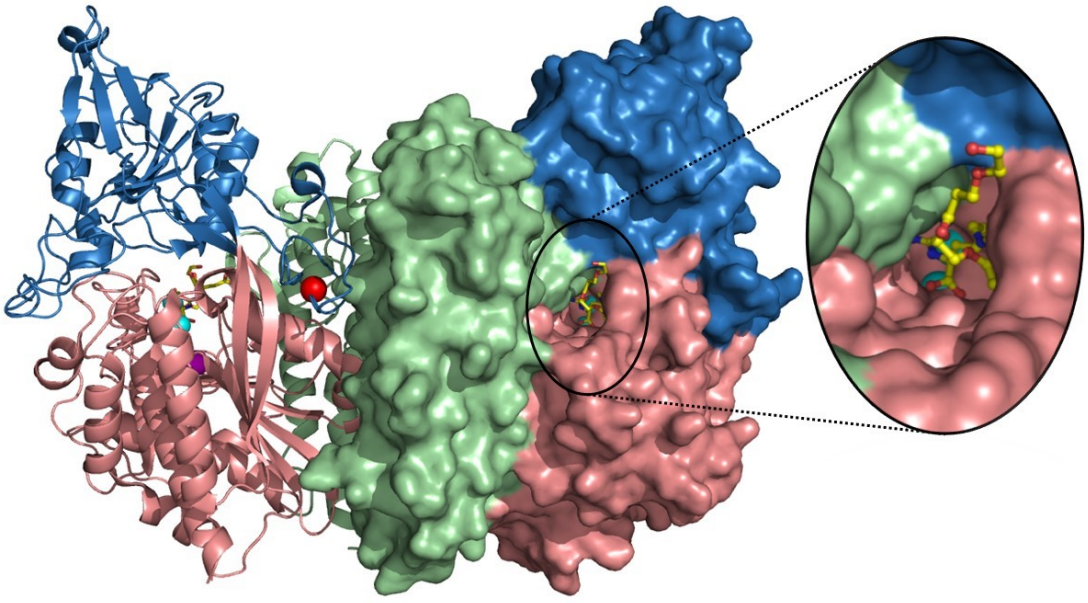

Figure 6: Crystal structure of extracellular portion of GCPII in complex with inhibitor.

Only extracellular part of GCPII homodimer is shown, one monomer is depicted in the cartoon and second in the surface representation. Each monomer consist of three domains: the C terminal (green), the apical (blue) and the protease like (pink). The deeply buried active site is created by residues from all three domains. The two zinc cations in the active site are represented as cyan spheres, calcium and chloride ions as red and magenta. Urea-based inhibitor with a polyethylene glycol linker reaching to the surface of the protein is depicted in ball and stick representation (carbon atoms in yellow, oxygen atoms in red and nitrogen atoms in blue). Structure PDB code: 4NGP [109].

GCPIII is also a homodimeric integral membrane glycoprotein. It shares also the same topology with GCPII: each monomer consists of a single transmembrane helix (24 amino acids) which connects short cytoplasmic N-termini (7 amino acids) with large extracellular part bearing the active site. Crystal structure of GCPIII has been solved and it showed very similar fold to GCPII and almost identical active site, with biggest differences being N509S substitution and lower occupancy of one of the zinc atoms [110]. This amino acid substitution between GCPII and GCPIII is common between human and mice and it is probably responsible for the ability of GCPIII to cleave BCG. Collard *et al*. showed that GCPII cannot cleave BCG and that S509N substitution in GCPIII completely abolish BCG cleaving activity but not NAAG cleaving activity [35].

1.1.3. Other putative functions of GCPII

The role of GCPII in prostate is not known and it has been speculated that it could serve as a receptor for yet undiscovered ligand [111]. This is based on the observations that (1) GCPII has similar fold as Transferrin receptor [105], (2) it undergoes both constitutive and antibody induced internalization [94, 112] and (3) it is transported after endocytosis back to the cell surface via recycling endosomal vesicles [113] (analogously to Transferrin receptor). However, no ligand has been identified so far.

GCPII was reported to participate in regulation of several cellular processes. In line with its expression in endothelial cells in neovasculature, GCPII has been shown to promote angiogenesis [114] and this regulation is linked to GCPII enzymatic activity via generation of pro-angiogenic peptides via cleavage of laminin peptides produced by the matrix metalloproteases [115, 116]. It has been also shown to promote cell proliferation [117] or to be associated with the anaphase-promoting complex [118] but these reports are still waiting to be validated by other groups.

1.1.4. Mouse is an important model organism to study GCPII function

Mouse represents an important model organism for study of physiological role of GCPII and of its possible role for treatment of different diseases. It has been most widely used for evaluating GCPII directed imaging agents of prostate cancer on xenografts (e.g. in [119-128]), for evaluating GCPII targeted therapy in prostate cancer (e.g. [20, 129-133]) and

for evaluating of beneficial effects of GCPII inhibition in several neurological disorders (reviewed in [57]). Mouse genome contains both GCPII and GCPIII orthologs, which share 85 and 88% identity to its human counterparts. It has been shown that GCPII tissue expression profile is in mouse very similar to humans, which is important for its use as a model organism. Most notably, mice express high levels of GCPII in brain, kidney and testis [35, 38, 134], but not in prostate or small intestine [15, 134].

The role of GCPII has been also studied on mice with deleted GCPII. GCPII knockouts were prepared independently by three different groups. While the Coyle group reported that GCPII deletion lead to early embryonic death [135, 136], the Neale and Zhong groups reported mice with deleted GCPII developing normally to the adulthood [38, 137]. These studies clearly showed the absence of GCPII protein in the homozygous GCPII null mice and therefore there is no clear explanation for this striking discrepancy. Both studies also did not report any significant neurological defects of the knockout mice and they even reported that knockout mice were less susceptible to traumatic and ischemic brain injury [23, 38, 137, 138]. These findings suggest that GCPII is likely a valuable target of therapeutic intervention in neurological disorders and that its targeting should not cause severe side effects.

1.1.5. Inhibitors of GCPII

Several classes of GCPII inhibitors have been discovered so far and all bind to the substrate cavity. Since the active site of GCPII is multiply positively charged and GCPII thus prefers acidic residues, the inhibitors also bear multiple negative charges [34, 104, 139]. The inhibitors also have a functional moiety, which binds to the dinuclear zinc center, while displacing the coordinated hydroxyl. Based on this group, GCPII inhibitors are divided into four major groups: phosphorus containing compounds (phosphonates, phosphinates and phosphoramidates) [27], urea derived compounds [28], thiol based compounds [29] and hydroxamates [140].

GCPII inhibitors can have low nanomolar to subnanomolar potency. This is not surprising as GCPII binds also its substrates tightly: K_M value of NAAG is ~200nM and of $FolGlu_1$ ~20nM; moreover, GCPII is also inhibited by the reaction product glutamate (K_i ~ 20μM) and its analog quisqualate (K_i ~ 200nM). 2-phosphonomethyl-pentandioic acid (2-PMPA, IC_{50} = 0.3nM) was the first synthetized subnanomolar inhibitor [27] and later also

phosphinate analogs with similar potencies were prepared [141]. More recently, also phosphoramidate inhibitors with mid nanomolar potency have been synthetized [142]. Several years after 2-PMPA, first urea based inhibitors with nanomolar potencies were synthetized [28], which turned out to be useful compounds due to straightforward synthesis and modularity [143]. Urea based compound ZJ-43 with subnanomolar potency was also synthetized [71, 72]. Later, a basic scaffold consisting of Lys-Urea-Glu was established [123]; amino group can be easily modified, which enabled easy radiolabeling of these compounds and fluorinated or iodinated compounds with mid to low picomolar potencies later called DCFPyl (see **Fig. 8** on page 27) and DCIBzL were prepared [122, 144]. The first orally available inhibitor was 2-(3-mercaptopropyl)-pentandioic acid (2-MPPA; IC_{50} = 90nM) [29]. Recently, hydroxamate inhibitor 4-Carboxy-α-[3-(hydroxyamino)-3-oxopropyl]-benzenepropanoic acid with mid nanomolar potency was prepared [140, 145]. Detailed reviews of the development of GCPII inhibitors are in [146, 147], structures of discussed inhibitors are shown in **Fig. 7**.

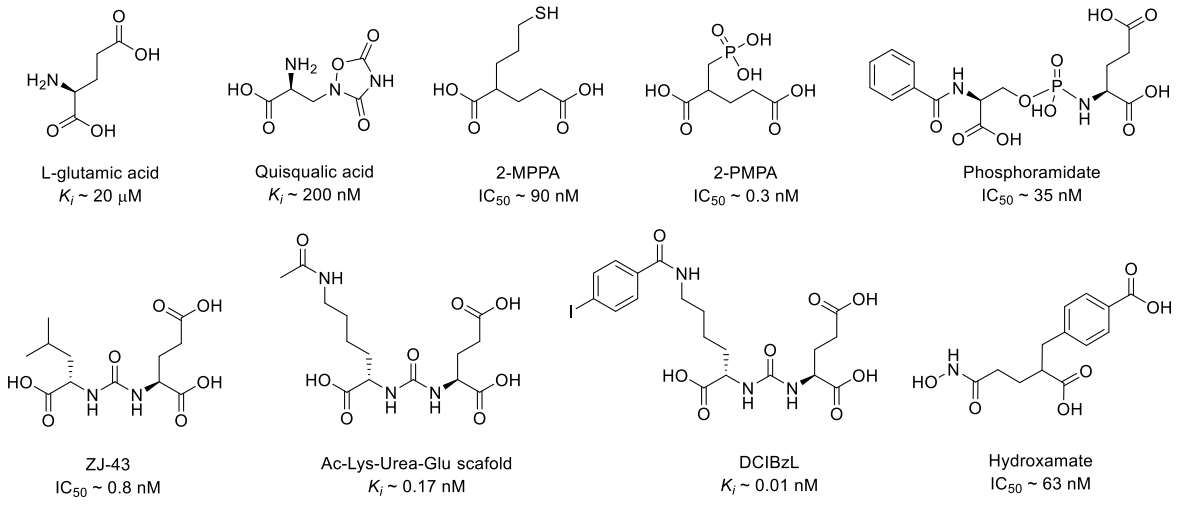

Figure 7: Structures of selected GCPII inhibitors

Structures of inhibitors discussed in text are shown, see text for more details. Inhibition potencies expressed as IC_{50} or K_i are taken from publication IV for L-glutamic acid and quisqualic acid, from ref. [148] for 2-MPPA and 2-PMPA, from ref. [142] for phosphoramidate inhibitor, from ref. [72] for ZJ-43, from publication X for Ac-Lys-Urea-Glu scaffold, from ref. [144] for DCIBzL and from ref. [145] for hydroxamate inhibitor.

1.1.6. GCPII is therapeutic target in brain

The physiological role of GCPII inactivating neuroprotective NAAG and forming excitatory glutamate and thus modulating neuronal activity makes it an attractive target for

exploration as possible drug target. First, it has been shown that GCPII inhibitors decrease concentrations of extracellular glutamate after ischemia, while increasing NAAG; at the same time, high doses of GCPII inhibitors do not cause adverse behavioral changes or deficits in learning and memory in animals [22]. Later, it has been shown that deletion of murine GCPII leads to healthy phenotype, which is more resistant to brain damage after brain injury [23, 137]. Finally, positive effects of GCPII inhibition has been demonstrated over the past two decades in a number of animal models of different neurological conditions including stroke and traumatic brain injury, pain and peripheral neuropathy, drug addiction, schizophrenia and multiple sclerosis (reviewed in [23, 44, 57, 67, 149, 150]).

However, development of human drugs targeting GCPII is challenging due to the molecular structure of known inhibitors. All potent GCPII inhibitors bear multiple negative charges, which leads to poor bioavailability. Even though fosfonate inhibitors (mainly 2-PMPA) and urea based inhibitors (mainly ZJ-43) proved very valuable in studying role of GCPII in animal models of neuropathies [22, 71, 72, 151], none of them is orally available. Even the prodrug of ZJ-43 had to be administered intraperitoneally to mice [152]. The only orally available analogs are the thiol-based compounds [29, 153] and 2-MPPA (GPI-5693, **Fig. 7**) was administered in an exploratory Phase I study to 25 healthy individuals. This study showed that it was possible to achieve plasma exposures that were effective in animal model of neuropathic pain without severe side effects on the CNS. However, gastrointestinal side effects were observed more frequently (38% of cases) and this compound was not further clinically developed [30]. There are other ongoing efforts to achieve safe and efficient GCPII inhibitor plasma and CNS concentrations. One study examined CNS levels of the most potent GCPII inhibitor 2-PMPA (**Fig. 7**) after intranasal administration and showed higher brain penetrance compared to intraperitoneal administration [31]. Another promising approach to increase oral availability and brain penetrance being investigated in animal models is the administration of prodrugs producing thiol compounds [154] or 2-PMPA [155, 156] or even hydroxamate inhibitors [157].

None of these efforts fully solved the pharmacological issues of the GCPII inhibitors and the search for novel scaffolds is thus still relevant. Recently, one effort to identify novel scaffolds via high-throughput screening using fluorescence polarization assay was reported

[158]. However, this assay was unable to identify novel inhibitory scaffolds, which may be the result of its low sensitivity as seen on the used reference compounds.

1.1.7. GCPII is theranostic target in prostate cancer

Prostate carcinoma (PCa) is the most prevalent cancer in men in western world. Fortunately, it usually forms slow growing tumors and most of the PCa affected individuals does not die due to the disease. On the other hand, it readily forms metastases in other organs including bones, it does not respond to the most chemoterapeutics and growth of the tumor is usually reduced only by androgen-deprivation therapy. In the course of the treatment, the tumor stops to respond to this therapy and metastatic castration-resistant PCa (mCRPC) develops, which eventually kills the patient. The only curative treatment is surgical removal of prostate (radical prostatectomy), but it has to be performed before the disease has spread out of the prostate, otherwise it has no beneficial effect. Therefore, an early and accurate diagnosis and the ability to discover (micro) metastases in the lymph nodes and other organs is critical [159-161].

Accurate diagnosis and imaging of both primary and metastatic PCa is challenging. Most PCa are discovered by PSA test, but the disease have to be confirmed by prostate biopsy followed by histopathological examination [162]. The primary tumor cannot be accurately imaged by usual imaging techniques due to its slow metabolic rate and its diffuse growth, which is further complicated by the low blood flow in the prostate. The slow metabolic rate complicates also the detection of metastases. Clinicians are thus seeking for techniques, which would complement the anatomic information provided by MRI or CT and would enable to discover PCa lesions. Such functional information may be provided by bone scan or positron emission tomography (PET) or single photon emission computed tomography (SPECT). Bone scan usually gives two-dimensional information and uses either ^{18}F-NaF or ^{99}Tc-MDP (methylenediphosphonate), can detect only bone lesions and suffers from low selectivity. On the other hand, PET provides three-dimensional information and is suitable for the whole body scan. However, ^{18}F-FDG (fluoro-deoxyglucose), which is used for PET of other malignancies, does not perform well in PCa. Today, ^{11}C and ^{18}F choline derivatives are used as PCa tracers, but they suffer from several drawbacks and there is a clear need for the development of new tracers (reviewed in [160, 163]).

Development of a PCa targeted imaging agent would not only improve PCa diagnostics and disease staging; but it may also be used for targeted treatment when loaded with appropriate radionuclide. While the soluble PSA protein secreted by the prostate carcinoma cells has turned out to be a useful serum marker and an excellent tool to monitor residual disease after radical prostatectomy [161], membrane bound GCPII (PSMA) may be the ideal anchor to target imaging and/or therapeutic agents to the prostate carcinoma (reviewed in [160, 163-167]). Many agents suitable for both diagnostics and therapy of PCa (hence theranostic agents) are now in clinical development and are briefly discussed below.

1.1.7.1. Imaging of prostate cancer

Primary challenges of PCa imaging are: (1) to detect primary tumor in the prostate to facilitate an early diagnosis; (2) to detect (micro)metastases in lymph nodes and other organs to enable correct selection of patients suitable for radical prostatectomy and (3) to detect metastases in the patients after radical prostatectomy to enable early start of their therapy.

Antibodies for PCa imaging

First GCPII targeted imaging agents were radiolabeled antibodies. An ^{111}In-labeled antibody 7E11 suitable for SPECT sold under the trade name ProstaScint is used for imaging of prostate carcinoma *in vivo* [19]. However, this antibody recognizes an intracellular epitope, which is hidden on live cells [102]. It is thus used only marginally in clinical praxis [168]. To overcome these limitations, antibody J591 recognizing an extracellular epitope was prepared [14]. Its conjugates with ^{111}In and ^{89}Zr suitable for imaging were prepared and tested in clinical trials [169, 170]. Even though the ^{89}Zr labeled antibody showed promising sensitivity, interests of the clinicians moved to the development of small molecule imaging agents. They have at least one big advantage compared to antibodies: thanks to their fast pharmacokinetics, it is possible to image PCa shortly after injection of the tracer (few hours) [171], while it is necessary to wait several days after injection of antibody conjugates [170, 172] and radioisotopes with much shorter half-life can be used, which minimizes the radiation dose (hours *vs.* days).

Small molecules for PCa imaging

The use of radiolabeled GCPII inhibitors to target prostate cancer is being intensively studied during the recent few years. **Fig. 8** on page 27 shows structures of selected synthetized and tested compounds, which are discussed in this text. They consist of the "targeting moiety" which is mostly the scaffold Lys-Urea-Glu and which is linked through a various linker to the halogenated or metal chelating moiety. The structure of the linker is important for the potency and biodistribution [127] and the metal chelator is usually either HBED-CC [128] or DOTA [126]. Mostly used radioligands are suitable either for SPECT (^{99}Tc, or ^{111}In or ^{123}I) or for PET (^{18}F, ^{68}Ga, ^{124}I). Several fluorinated agents have been synthetized: DCFBC [124], which is an example of targeting moiety distinct from the Lys-Urea-Glu moiety used in all other compounds listed in **Fig. 8**, DCFPyl [144] and newer PSMA-1007 [173]. Several ^{99m}Tc containing compounds were also prepared: ^{99m}Tc-L1 [123], series of compounds around MIP-1404 (Molecular insight pharmaceuticals code) [174, 175] and newest ^{99m}Tc-PSMA-I&S [176]. Iodinated compound DCIBzl (**Fig. 7**) and almost identical MIP-1095 were prepared with several different isotopes [122, 144, 177]. Finally, agents chelating ^{68}Ga were also prepared: ^{68}Ga-PSMA-HBED-CC also called as ^{68}Ga-PSMA-11 or ^{68}Ga-DKFZ-PSMA-11 [128] and newer compounds with optimized linker moiety ^{68}Ga-PSMA-617 [126, 127] or ^{68}Ga-PSMA I&T [20], both with DOTA chelator enabling also binding of ^{177}Lu or ^{225}Ac for therapy (see **Fig. 8**).

All these compounds were tested not only in animals, but also in human trials and many of them showed promising results. The state of the art is summarized for example in [160, 163-165, 167] and only selected compounds and clinical trials will be discussed here.

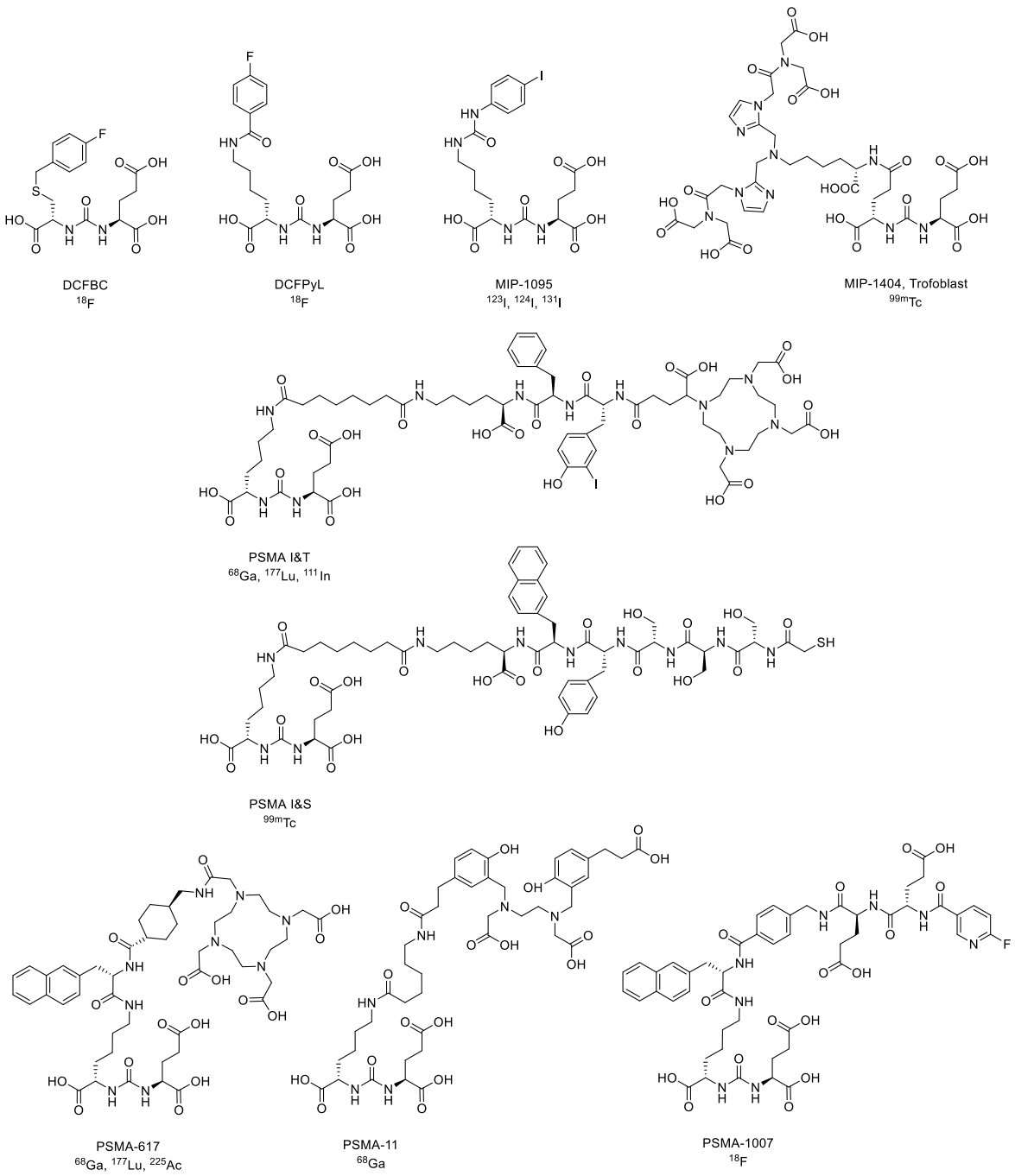

Figure 8: Structures of small molecules for PCa imaging and treatment

Structures of compounds discussed in text are shown, see text for more details. Tested radionuclides for each compound are also listed.

Clinical evaluation of ^{68}Ga-PSMA-11

Definitely, the most tested agent is the ^{68}Ga-PSMA-11 (**Fig. 8**) which is approaching phase III clinical trial. Many retrospective and prospective trials with imaging of tumor

metastases in patients with biochemically recurrent cancer (BCR, defined as the rise of PSA serum level above 0.2 ng/ml in patients after radical prostatectomy and meaning that further treatment is necessary) were done, each with tens to hundreds patients [178-183] in total with more than thousand patients [184]. These studies consistently showed detection of at least one lesion in ~90% of patients with PSA level above 2.0 ng/ml, in ~75% with PSA above 1 ng/ml and in ~50% with PSA under 1.0 ng/ml or even 0.5 ng/ml. At the same time, no false positives were observed and specificity was virtually 100% [163]. A case study report comparing imaging by ^{68}Ga-PSMA-11 and generic ^{18}F-FDG is shown in **Fig. 9** on page 31.

Several studies also compared ^{68}Ga-PSMA-11 performance side by side with the state of the art imaging with ^{11}C or ^{18}F choline derivatives [179, 181, 182, 185, 186]. ^{68}Ga-PSMA-11 was much more sensitive especially at low PSA levels: it was able to find up to 4-fold more lesions in patients with low PSA levels [181] and in most studies all choline positive lesions were positive also with ^{68}Ga-PSMA-11 (with the exception of few lesions in [182]), while ^{68}Ga-PSMA-11 was able to find lesions in up to 44% of choline negative patients [179]. However, the tracer shows also some background: intense staining is observed in kidney and salivary glands, moderate in lacrimal glands, liver, spleen, small and large intestine.

These promising results lead to the evaluation, whether ^{68}Ga-PSMA-11 may be useful even for the discovery of primary tumors, i.e. primary diagnosis. In these studies comprising almost 100 individuals, patients were imaged before radical prostatectomy and PET/MRI was correlated to the histopathological results and MRI. PET imaging had higher sensitivity of about 70-90% and specificity 90% [187-190].

Finally, its ability to discover lymph-node metastases was also tested on a cohort of 130 patients undergoing prostatectomy with pelvic lymphadenoctemy [191]. ^{68}Ga-PSMA-11 PET was superior to morphological imaging with CT or MRI and it was able to find ~68% of the histologically positive lymph nodes with 99% specificity. These data show consistently superior performance of this tracer and many clinical studies are currently under way, including Phase II/III study (clinicaltrials.gov ID NCT02678351).

Clinical evaluation of other ^{68}Ga ligands

Another ^{68}Ga tracer is the recently prepared ^{68}Ga-PSMA-I&T (**Fig. 8**). It showed similar performance to ^{68}Ga-PSMA-11 in first study with 83 patients [192]. It has been also

loaded with slower decaying isotope ^{111}In for radioguided surgery. Such surgery could remove also small lymph node metastases during or after prostatectomy and lead to longer disease free survival. The proof-of-principle was shown on five patients (one with primary PCa, four with BCR) in [191]. Follow-up study with 31 patients with BCR (PSA level 0.5-2.5) showed decrease of PSA level after surgery by at least 50% in 77% of patients, PSA dropped below 0.2 ng/ml in 60% of cases [193].

In addition, ^{68}Ga-PSMA-617 tracer has been prepared (**Fig. 8**). It has been primarily designed for loading with ^{177}Lu for treatment, but also ^{68}Ga loaded variant was prepared. The linker region was thoroughly optimized, which lead to better biodistribution and, in contrast to PSMA-11, it does not accumulate in kidney or spleen (up to 50-fold decrease) and tumor get the highest dose [126, 127]. This is extremely important for its intended use for therapy.

Clinical evaluation of ^{18}F ligands

Several ^{18}F compounds have been prepared and tested. The first ^{18}F-DCFBC (**Fig. 8**) was tested in small studies with less than 20 patients and it showed poor performance compared to the gallium tracers. Its high background is probably caused by its slow clearance from blood [194-196]. Nevertheless, there is at least one larger active study on clinicaltrials.gov (90 individuals, NCT03173924).

Much better is the compound ^{18}F-DCFPyL (**Fig. 8**) which showed better performance than ^{68}Ga-PSMA-11 in sensitivity and tumor to background ratio. Its low background is probably thanks to its rapid renal clearance [197-199]. However, it has been tested only on limited number of patients (<50) but several clinical trials with hundreds of subjects are active (NCT03471650, NCT03160794, NCT03181867, NCT03173924 and NCT03232164).

An even improved ^{18}F tracer have been synthetized in 2017: ^{18}F-PSMA-1007 (**Fig. 8**) is cleared from blood rapidly, but not via kidney and it does not accumulate in urinary bladder, which may be especially useful for finding primary tumors in prostate. It is cleared with similar rate as ^{68}Ga-PSMA-11 (ideal signal to background is therefore 2-3 hours after tracer injection). Imaging of only ~10 patients has been reported so far [171] but also a case study has been reported showing the detection of micro metastasis in patient with PSA < 0.08ng/ml [200]. Studies with larger number of patients will probably follow to evaluate the potential of ^{18}F-PSMA-1007.

Clinical evaluation of other ligands

The first imaging agents tested in human were the ^{123}I loaded MIP-1072 and MIP-1095 [201] (**Fig. 8**). The latter also showed very low renal clearance and retention of up to 48 hours, which may be important for its possible therapeutic use with ^{131}I [201]. Later, also ^{124}I loaded MIP-1095 was tested with 28 patients and it showed high uptake only in salivary and lacrimal glands, whereas only moderate in kidney, liver and intestine [202].

Technetium loaded tracers were also prepared for SPECT imaging. ^{99m}Tc-MIP-1404 showed good performance in patients [203] and now finishes Phase III study (NCT02615067) under the trade name Trofolostat (**Fig. 8**).

There is also one another PCa tracer under clinical evaluation, which is not GCPII targeted: ^{18}F-fluorocyclobutane-1-carboxylic acid (fluciclovine), which is a synthetic analog of L-leucine and is preferentially taken up by the PCa cells and gliomas via the amino acid transporter ASCT2. Such tracer may be useful in imaging of dedifferentiated PCa which have lost GCPII expression (reviewed in [163]) and there is indeed at least one active clinical trial evaluating simultaneous administration of ^{68}Ga-PSMA-11 and ^{18}F-fluciclovine (clinicaltrials.gov identifier NCT03515577).

Finally, also fluorescent conjugates targeting GCPII made from both small molecules and antibodies have been developed and tested in animals [120, 125, 204]. They may find use in fluorescence guided surgery (see e.g. da Vinci system from Intuitive surgical, Inc.) which would be superior to the radio-guided surgery thanks to the real-time imaging [205]. In addition, certain nanoparticle based systems have been developed for both antibodies and small molecules targeting GCPII [206-208]. Some of these systems are designed to be useful also for therapy, nice example is the conjugate of GCPII inhibitor and maytansinoid 1 (DM-1) loaded with ^{68}Ga [133]. Any of these conjugates have yet been tested in human trials.

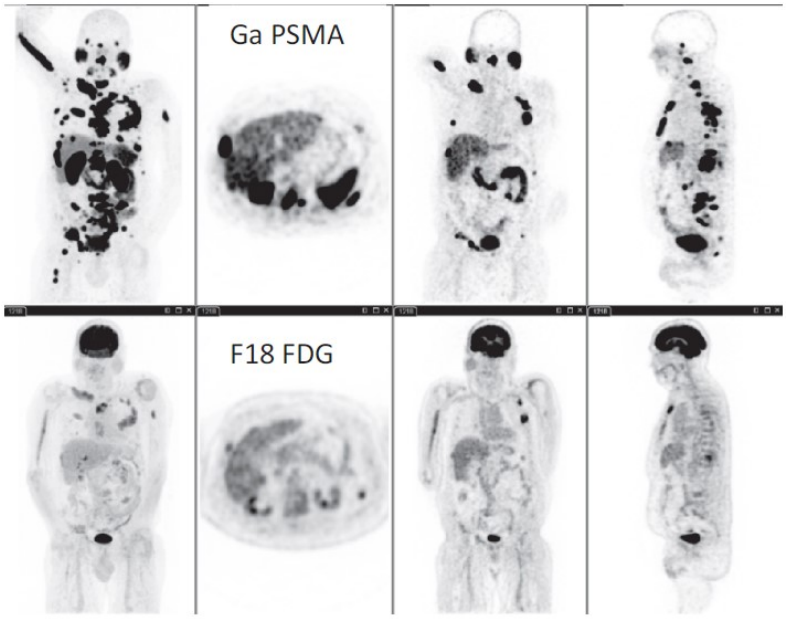

Figure 9: Case study of ^{18}F-FDG vs. ^{68}Ga-PSMA PET in metastatic prostate cancer

Upper part shows intense staining of metastatic PCa with ^{68}Ga-PSMA ligand while the bottom part shows very weak staining of metastatic PCa with ^{18}F-FDG (fluoro-deoxyglucose). Note the intense staining of brain with ^{18}F-FDG vs. virtually no staining with ^{68}Ga-PSMA. Adopted from ref. [166].

1.1.7.2. Detection in blood serum

While the targeting of GCPII for imaging of PCa is extremely promising, its possible role as a serum marker is unclear. Since we focused on this topic in the studies presented in this thesis, the current state of knowledge is thoroughly discussed later in the introduction to publication III as well as in discussion and is therefore skipped here.

1.1.7.3. Treatment of prostate cancer

There is only small step from targeted imaging agents to targeted therapy: to replace a positron emitting radionuclide suitable for PET having half-life of ~1-2 hours (^{18}F, ^{68}Ga) with toxic α (^{225}Ac) or β^- emitter (^{131}I or ^{177}Lu) having half life of ~5-10 days. The half-life of the isotope has to be shorter than the stability of the antibody in plasma to lower the toxicity. Another possibility is to ligate the antibody or targeting moiety to a toxic compound to form antibody drug conjugates (ADCs) or small molecule drug conjugates (SMDCs). Small molecules have some advantages: (1) they are not immunogenic (antibodies have to be humanized), (2) have shorter clearance time and non-selective toxicity due to the cleavage

of the conjugates is low and (3) have larger availability and tissue penetrance, which may be especially important in the prostate tissue which has low blood supply.

Antibodies for PCa treatment

First agents tested for targeted PCa therapy were antibodies. The antibody 7E11 labeled with ^{90}Y was tested in phase I and phase II [209, 210] but it failed to elucidade any PSA decline while showing significant toxicity and its development has thus been stopped.

The antibody J591 conjugated with ^{177}Lu was tested in Phase II trial with 47 patients suffering from mCRPC. It elucidated both PSA decline and significantly higher overall survival (22 *vs.* 12 months in the group with lower dosis, p=0.03) in 32 patients treated with Phase I maximum tolerated dose (MTD) of 70mCi/m^2, but many patients suffered from dose limiting toxicities (DLT): as much as ~50% suffered from grade 4 thrombocytopenia necessitating blood transfusions. At the same time, even slightly lower dose (65mCi/m^2) showed much lower efficacy and the adverse side effect are thus limiting the use of this conjugate [211, 212]. Even though there are still several active trials evaluating J591 antibody (unconjugated, ^{177}Lu or ^{225}Ac labeled) at clinicaltrials.gov, there was no Phase III trial and no approval.

Also ADCs with various toxins were prepared and tested in human trials: e.g. (1) conjugate with DM-1 showed little efficacy and dose-limiting neurotoxicity in human trial, probably due to the cleavage of disulfide bond between antibody and toxin [129, 213]; (2) conjugate of monomethyl auristatin E (MMAE) [131, 132], which was recently tested on very limited number of patients (n=6) and four of them showed decline of PSA of at least 30% but detailed results have not yet been disclosed (clinicaltrials.gov identifier NCT02020135).

Small molecules for PCa treatment

Most recent advances are in the field of small molecule conjugates and most thoroughly tested is the ^{177}Lu-PSMA-617 conjugate (**Fig. 8**). It has been tested on several hundreds patients in different hospitals [214-224]. These studies on mCRPC showed up to 80% response rate, at least 50% decline in PSA level in 30-60% patients, up to 12 months progression free survival and some complete responders, while low serum levels of alkaline

phosphatase were predictive of better response and longer survival (see also [166]). The toxicity was acceptable, with grade 4 toxicities in less than 10%. Highest dose was reached in tumor, while the dose in kidney and parotid was about 3-fold lower [217]. Several trials with hundreds of patients are active (e.g. NCT03042468, NCT03042312 and NCT03454750). This conjugate was also prepared and tested with α-emitting ^{225}Ac. First results look very promising showing similar response rate as with ^{177}Lu and ~10% of complete responses lasting over two years [225-227].

A newer ^{177}Lu-PSMA-I&T (**Fig. 8**) has been tested in 100 mCRPC patients. It showed acceptable toxicity with grade 4 in less than 10% with the most prevalent side effect being dry mouth. At least 50% decline in PSA level has been observed in 32% and median progression free survival was 4 months [21, 228]. These data suggest lower efficacy than with ^{177}Lu-PSMA-617. Finally, ^{131}I MIP-1095 (**Fig. 8**) was tested in two studies and it showed reduction in PSA of at least 50% in 60-70% patients and tolerable toxicity [202, 229].

These data confirm that GCPII is a valuable target for targeted therapy and hopefully it is just a matter of time until anti-GCPII agents will help PCa patients. The possibility of both imaging and targeting the same protein is appealing, since it may be easy to select the most responsive patients in advance [230].

1.2. Methods for selective protein detection

Many diseases are screened by detecting blood levels of selected target proteins, e.g. liver or heart damage or prostate cancer, and selective and sensitive detection of protein in complex biological matrices is thus major challenge in clinical analytics.

1.2.1. Immunoassays

Nowadays golden standard for selective protein detection in biological matrices are immunoassays with sandwich ELISA being the most prominent example [231]. They have been developed in 1960s and 1970s [232, 233]. Their huge impact is evidenced by the fact, that Rosalyn Yallow has been awarded with Nobel prize in 1977 for her pioneering work in the field of immunoassays, which enabled the first detection of insulin in human plasma [233]. Web of Science search for ELISA returns about 150,000 results (10,000 per year in recent years), which shows its extensive and persisting use in research.

In sandwich ELISA, an analyte is captured by an immobilized antibody, then probed with a second enzyme-linked antibody and quantified via a reaction catalyzed by the linked enzyme [231]. The linked enzyme is most commonly horseradish peroxidase and is detected mostly with chromogenic substrates such as OPD (o-phenylenediamine dihydrochloride) or TMB (3,3',5,5'-tetramethylbenzidine) [234] or with chemiluminescent substrate luminol (5-amino-2,3-dihydro-1,4-phthalazinedione) [235]. Such detection usually yields detection limits as low as 10 pg/ml of target protein (see e.g. Quantikine ELISA for human CAIX from RnD Systems). In automated assays used in the clinics, the enzyme is usually substituted by acridinium esters which produce chemiluminescent signal upon addition of alkaline hydrogen peroxide [236]. Such automated immunoassays are capable of detecting several pg/ml of prostate specific membrane antigen (PSA) in blood serum (see e.g. Abbott Architect total PSA kit, IVD Ref. 7K70).

To increase the sensitivity, enzyme-linked antibodies have been replaced by DNA-linked antibodies allowing detection by quantitative polymerase chain reaction (qPCR) in the so called immuno-PCR methods [237] (**Fig. 10** on page 35). Ruzicka *et al*. showed the use of non-covalent DNA-antibody conjugate [238] while Hendrickson *et al.* showed the use of covalent DNA-antibody conjugate [239]. A number of different immuno-PCR protocols

for a number of distinct targets have been developed [240, 241] and they have been shown to detect serum levels of PSA lower than 1 pg/ml [242].

In some cases ELISA tests do not provide the result with sufficient sensitivity and/or selectivity. In such cases, Western blot (WB) is commonly used. Typical example is the use of WB to confirm diagnosis of Lyme disease in which borrelia specific antibodies in patients serum are detected directly on antigens from lysed borrelia cultures [243-245]. WB was also the first diagnostic test for HIV detection and has long been used as confirmatory test for HIV infection [246, 247]. It has been also used in the early attempts to detect GCPII in human blood [101].

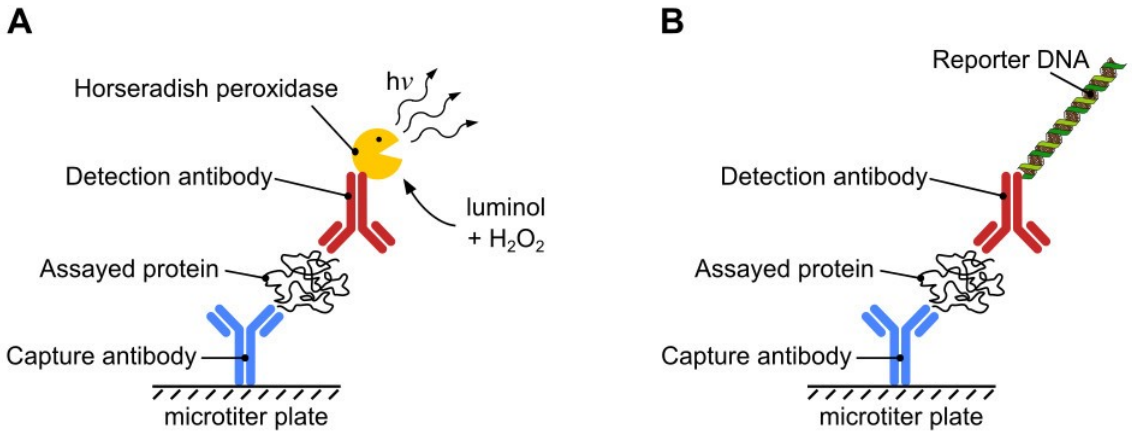

Figure 10: Sandwich ELISA and direct immuno-PCR

Comparison of sandwich ELISA, where the amount of the assayed protein is determined via enzymatic reaction of horseradish peroxidase, which is covalently attached to the detection antibody. Peroxidase catalyzes either chemiluminescent or chromogenic reaction. In immuno-PCR, the enzyme has been replaced by a DNA oligonucleotide, which is determined in quantitative PCR (qPCR).

1.2.2. Enzymatic assays

In many cases, the target protein is an enzyme, which enables its direct quantification via its enzymatic activity. Notoriously known example is the detection of Alanine amino transferase (ALT) and Aspartate amino transferase (AST) to asses liver damage [248, 249]. These tests are usually simple spectrophotometric assays, while the detected chemical is usually formed from the target enzyme product via coupled (enzymatic) reactions [250]. Higher sensitivity and selectivity is achieved by the use of radiolabeled substrate enabling

direct quantification of the product [251]. The downside is the more complex protocol due to the necessity of separation of the product and the use of harmful radioisotopes.

1.2.3. Detection of mRNA via qRT-PCR

Alternatively, cellular or tissue expression of a target protein can be determined via the quantification of its messenger RNA (mRNA) via quantitative reverse transcription polymerase chain reaction (qRT-PCR). The advantages are sensitivity, selectivity and dynamic range and there is no need for target recognizing antibodies, while the downsides are complexity of the protocol as well as the fact that in some cases mRNA levels do not correlate to the protein level due to posttranslational regulation. The protocol consists of multiple steps: (1) tissue extraction, (2) tissue homogenization, (3) RNA isolation, (4) analysis of RNA degradation, (5) reverse transcription of mRNA into complementary DNA (cDNA) and (6) quantitative PCR (qPCR). In qPCR, the target cDNA is selectively amplified by a pair of primers and detected mostly either via SYBR Green (which fluorescence lights up after intercalation into double stranded DNA) or via double hydrolysis probe complementary to the amplified sequence (also called TaqMan probe, which fluorescence lights up after cleavage by the polymerase). Fluorescence is read during each PCR cycle and a threshold cycle (C_t) is determined as the cycle in which the fluorescence raised above arbitrary threshold, which is indirectly proportional to the logarithm of initial target DNA concentration [252, 253]. Newer and more reproducible way is determining of C_q via second derivative maximum introduced by Roche. The amount of target cDNA is then determined by comparing determined C_q to the serially diluted standard of known concentration.

Unfortunately, many steps are prone to confounding errors and have to be performed in a standardized fashion. Tissues have to be processed or deep frozen immediately after dissection, otherwise changes in gene expression occur. The isolated RNA has to be pure and intact. Reverse transcription is inhibited by some tissue contaminants such as heparin and internal controls have to be introduced (most useful is the incorporation of reference genes). Finally, primers have to be designed and tested to selectively amplify the target sequence and not homologous sequences as well as genomic DNA [254].

1.3. Methods for screening of enzyme inhibitors and receptor ligands

Enzymes and receptors are important targets in medicine due to their involvement in many human diseases [255]. There are numerous examples of diseases treated by enzyme inhibitors: high blood pressure, certain cancer types, several infectious diseases such as influenza, HIV or hepatitis *etc*. About half of the marketed drugs target five main protein families: proteases, kinases, ion channels, G-protein coupled receptors (GPCRs) and nuclear receptors (NRs) [256]. One of the major scopes of drug discovery is thus the search for enzyme inhibitors and receptor ligands, which is usually done by screening large libraries of low molecular weight compounds [257].

1.3.1. In vitro assays

Inhibition potency of compounds toward an isolated enzyme is determined directly by measuring the change of its catalytic activity in the presence of the compound. Typically, pro-fluorescent peptides are used as probes for proteases [258, 259]. Signal producing product may be produced also by coupled enzymatic reactions, which is a strategy frequently used by kinases [260] and which is also commercially available (Kinase-Glo assays from Promega). The disadvantage of using coupled enzymatic detection is the appearance of false positives inhibiting these coupled enzymes and the necessity to run counterscreens on those enzymes [261]. An alternative way to detect ADP produced by kinases has been developed by Bellbrook labs [262]. In this approach, anti-ADP antibody binds fluorescently labeled ADP, which is outcompeted by the ADP produced by tested kinase, which result in the change of fluorescence polarization (FP).

Binding potency of compounds toward enzymes and receptors can be determined also via detection of its ability to displace active site probe. Typically, such probe is fluorescently labeled and its displacement is measured by the changes in FP and unbound probe does not need to be separated from the protein [158, 263, 264]. Their simple protocol is compensating higher false positive rate of FP assays. Other ways of labelling the active site probe are also possible, but they usually necessitates immobilization of the target protein and separating

bound and unbound labeled probes. Such approaches are used due to their applicability to screen whole enzyme families such as kinases [265] or serine proteases [266].

Finally, the interaction between a purified protein and compound can be determined also based on the thermal stabilization of the protein after the binding of the compound in a thermal shift assay [267].

1.3.2. Cellular assays

Unfortunately, assays listed in previous section require purified proteins, which can be a great obstacle, because (1) certain proteins cannot be prepared in purified form and (2) cellular context and binding partners are crucial for many targets.

Therefore, cellular assays are becoming increasingly popular. Assays using fluorescent sensors measuring intracellular Ca^{2+} levels for measuring ion channel activation have been developed [268, 269]. Moreover, assays based on enzyme fragment complementation [270] or bioluminescence (fluorescence) resonance energy transfer; BRET (FRET) [271] have been developed for screening of ligands of GPCRs. In addition, phenotypic screens observing multiple parameters at once (i.e. high-content screening) are being commonly used [272, 273].

Even though these assays proved to be a valuable addition to the screening toolbox, they sometimes suffer from low reproducibility due to the fact, that cells are living organisms influenced by environmental factors.

2. Results

2.1. Aims of the thesis

1. Development of qRT-PCR methods enabling selective detection of GCPII and its closest homolog GCPIII in human and mice and their quantification in a set of human and mice tissues. Comparison of GCPII tissue expression between human and mice.

2. Development of several orthogonal assays enabling selective quantification of GCPII protein in human blood (sandwich ELISA, DIANA and radioenzymatic assay). Validation of the possibility to use GCPII as a blood serum marker of prostate cancer.

3. Development of novel method for ultrasensitive detection of enzymes and screening for their inhibitors based on the use DNA-linked low molecular weight active site binders of target enzymes. Assessment of its performance on two model targets GCPII and CAIX, which are potential drug targets and potential cancer markers.

2.2. Publications

2.2.1. Publications included in the thesis

I. Navratil, M., Tykvart, J., Schimer, J., Pachl, P., Navratil, V., Rokob, T.A., Hlouchova, K., Rulisek, L., and Konvalinka, J.: **Comparison of human glutamate carboxypeptidases II and III reveals their divergent substrate specificities**. *FEBS J. 2016*, 283(13):2528-2545.

II. Knedlik T., Vorlova B., Navratil V., Tykvart J., Sedlak F., Vaculin S., Franek M., Sacha P., and Konvalinka J.: **Mouse glutamate carboxypeptidase II (GCPII) has a similar enzyme activity and inhibition profile but a different tissue distribution to human GCPII**. *FEBS Open Bio 2017*, 7(9):1362-1378.

III. Knedlik T., Navratil V., Vik V., Pacik D., Sacha P., and Konvalinka J.: **Detection and quantitation of glutamate carboxypeptidase II in human blood**. *Prostate 2014*, 74(7):768-780.

IV. Navratil V., Schimer J., Tykvart J., Knedlik T., Vik V., Majer P., Konvalinka J., and Sacha P.: **DNA-linked Inhibitor Antibody Assay (DIANA) for sensitive and selective enzyme detection and inhibitor screening**. *Nucleic Acids Res. 2017*, 45(2):e10.

2.2.2. Publications not included in the thesis

V. Hlouchova, K., Navratil, V., Tykvart, J., Sacha, P., and Konvalinka, J.: **GCPII variants, paralogs and orthologs**. *Curr. Med. Chem. 2012*, 19(9):1316-1322.

VI. Marusincova, H., Husarova, L., Ruzicka, J., Ingr, M., Navratil, V., Bunkova, L., and Koutny, M.: **Polyvinyl alcohol biodegradation under denitrifying conditions**. *International Biodeterioration & Biodegradation 2013*, 84:21-28.

VII. Navratil, V., Klusak, V., and Rulisek, L.: **Theoretical aspects of hydrolysis of peptide bonds by zinc metalloenzymes**. *Chemistry 2013*, 19(49):16634-16645.

VIII. Tykvart, J., Navratil, V., Sedlak, F., Corey, E., Colombatti, M., Fracasso, G., Koukolik, F., Barinka, C., Sacha P., and Konvalinka J.: **Comparative analysis of monoclonal antibodies against prostate-specific membrane antigen (PSMA)**. *Prostate 2014*, 74(16):1674-1690.

IX. Tykvart, J., Barinka, C., Svoboda, M., Navratil, V., Soucek, R., Hubalek, M., Hradilek, M., Sacha, P., Lubkowski, J., and Konvalinka, J.: **Structural and biochemical characterization of a novel aminopeptidase from human intestine**. *J. Biol. Chem. 2015*, 290(18):11321-11336.

X. Tykvart, J., Schimer, J., Jancarik, A., Barinkova, J., Navratil, V., Starkova, J., Sramkova, K., Konvalinka, J., Majer, P., and Sacha, P.: **Design of highly potent urea-based, exosite-binding inhibitors selective for glutamate carboxypeptidase II**. *J. Med. Chem. 2015*, 58(10):4357-4363.

XI. Sacha P., Knedlik T., Schimer J., Tykvart J., Parolek J., Navratil V., Dvorakova P., Sedlak F., Ulbrich K., Strohalm J., Majer P., Subr V., and Konvalinka J.: iBodies: **Modular Synthetic Antibody Mimetics Based on Hydrophilic Polymers Decorated with Functional Moieties**. *Angew. Chem. Int. Ed. Engl. 2016*, 55(7):2356-2360.

2.2.3. Publication 1: Comparison of human glutamate carboxypeptidases II and III reveals their divergent substrate specificities

Motivation of the study

GCPIII has been for a long time considered a twin-protein of GCPII. It has been shown that it has preference for similar N-acetylated dipeptides as GCPII and that it is also able to cleave NAAG, but with lower efficiency than GCPII [34, 274]. It has been also shown that it is responsible for a significant portion of NAAG cleaving activity *in vivo* [38]. Only recently, it has been shown that GCPIII cleaves BCG, which is not cleaved by the GCPII [35]. This novel observation may represent the physiological role of GCPIII and may also enable selective quantification of this enzyme in human tissues, which was not possible until now due to lack of selective antibodies. Since Collard *et al*. studied only the mouse proteins, we decided to examine whether his findings apply also to recombinant human purified GCPII and GCPIII.

Summary

Here, we determined kinetic parameters for human GCPII and GCPIII for all three known substrates of the two enzymes NAAG, BCG and γ-glutamylated folates (designated as $FolGlu_x$). We also examined, whether the GCPII and GCPIII activities show the same dependence on concentrations of selected bivalent cations as reported for their mouse counterparts [35]. We also made use of the determined substrate selectivities of GCPII and GCPIII to quantify both enzymes in homogenates of human tissues. Finally, we also determined amount of GCPII and GCPIII mRNA levels in human tissues via qRT-PCR.

First, we have shown that both enzymes are able to cleave all three substrates, but with various efficiencies. Moreover, GCPIII displayed a strong dependence of activity on bivalent cations, which was dependent not only on the type of cation used but also on the substrate. BCG cleavage was activated ~100-fold by calcium or manganese cations but not by zinc cations, whereas NAAG cleavage was activated ~10-fold by manganese or zinc cations but not by calcium cations. The maximum catalytic efficiency for BCG was ~10-fold higher than the maximum efficiency for NAAG. On the other hand, GCPII activity was completely independent on the concentration of any of the bivalent cations tested. The magnitude of

GCPII NAAG cleaving activity equaled to the maximum BCG activity of GCPIII, while its BCG activity was about five orders of magnitude lower. GCPII was also more effective in cleavage of γ-glutamylated folates.

To understand the mode of binding of BCG to both enzymes, we have also solved crystal structure of GCPII inactive form with bound BCG and built a QM/MM model of GCPIII in complex with BCG. In both cases, the glutamate moiety was bound to the S1' pocket as it is usual with other substrates. The crystal structure showed only few interactions of citrate moiety with GCPII, which may explain its low potency as a GCPII substrate. The QM/MM model showed more interactions of BCG with GCPIII than in with GCPII. We also tried to address the possibility of exchange of one of the active site zinc ions by calcium ion. This was suggested previously by Collard *et al*. and may explain the calcium dependent activation of BCG cleavage; however, our QM/MM model did not clearly answer this question.

Finally, we have exploited the fact, that GCPIII catalyzed BCG cleavage is in the presence of calcium ions much faster than the NAAG cleavage and *vice versa* for GCPII catalyzed cleavage, to quantify the amount of both proteins in human tissue homogenates. We have found the highest GCPII amount in brain, kidney and prostate, while the highest concentration of GCPIII was in testis (**Fig. 11** on page 44). To corroborate these results, we have developed selective qRT-PCR assays for both enzymes and quantified their amount in a panel of human tissue cDNA libraries obtained from Clontech (Human MTC Panel I and II). We have chosen this commercially available set, because this panel has been normalized to expression of several housekeeping genes and each tissue library was pooled from several individuals and should thus represent a population mean. Obtained expression profile corresponded well to the activity-based profile; highest GCPII expression was observed in prostate, liver, kidney and brain, while GCPIII was observed in testis, ovary and placenta.

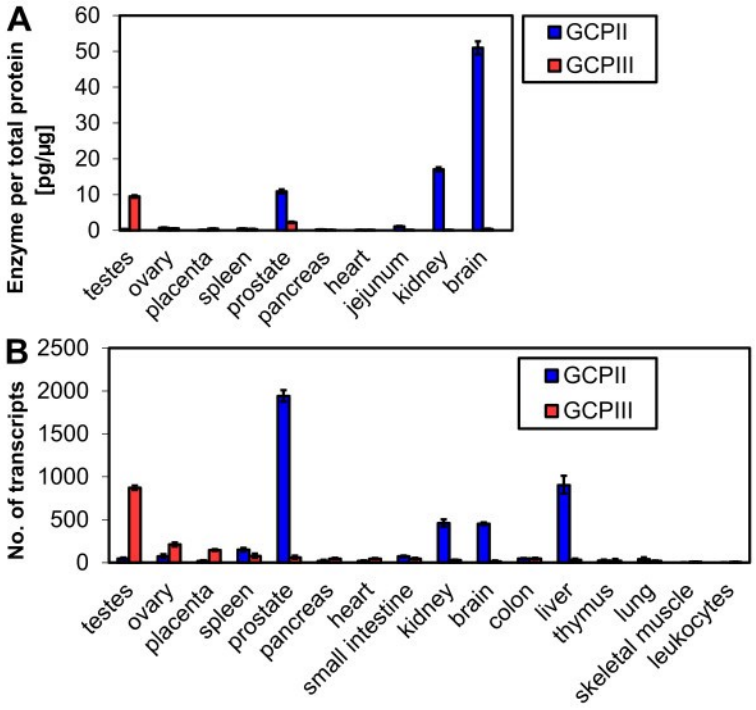

Figure 11: GCPII/III protein and mRNA levels of in human tissues.

(**a**) GCPII and GCPII levels in selected human tissues determined via NAAG and BCG hydrolyzing activity compared to total protein level in tissue homogenates. (**b**) Levels of GCPII and GCPIII mRNAs determined via qPCR. The "No. of transcripts" represents the amount of transcripts determined in 1.0 µL of 10-fold diluted tissue cDNA library obtained from Clontech (Human MTC Panel I and II), with values representing the mean from triplicate measurements. Error bars represent standard deviation.

My contribution

I developed the qRT-PCR assays for human GCPII and GCPIII, tested their selectivity and determined the amount of GCPII and GCPIII via qPCR in cDNA libraries. I also analyzed all amplification reactions on agarose gel electrophoresis. I contributed to the data analysis and writing of the manuscript.

2.2.4. Publication 2: Mouse glutamate carboxypeptidase II (GCPII) has a similar enzyme activity and inhibition profile but a different tissue distribution to human GCPII

Motivation of the study

GCPII is a promising target for multiple conditions and mouse is an important model organism. Mice have been used to study targeting of human prostate carcinoma xenografts *in vivo* as well as to study its role in brain. Murine GCPII knockouts have been developed to address the role of GCPII and the influence of GCPII inhibition in a variety of mouse models for neuropathologies have been examined (see section 1.1.4. for more details).

It is therefore necessary to understand the biology of murine GCPII. Is it expressed in the same organs as in humans? Does it have the same substrate specificity? Do the inhibitors inhibit murine GCPII with the same potency as human GCPII? These are some of the questions, which have to be answered before the results of a mice study can be generalized to human biology. Such characterization was done for rat and pig orthologs [6] but only little information is available for mouse ortholog [35, 38, 134]. Most importantly, no direct comparison for mouse *vs.* human GCPII is available and we therefore decided to prepare purified recombinant murine GCPII and compare it to its human counterpart.

Summary

Here, we present an enzymological characterization of purified recombinant murine GCPII and a study of GCPII expression profile in mice tissues.

First, we cloned, expressed and purified murine GCPII and determined its kinetic parameters, substrate specificity and inhibition profile. Both human and murine GCPII cleave NAAG and $FolGlu_1$ substrates with the same k_{cat}, while human GCPII has ~5-10 times lower K_M values for both substrates and thus higher catalytic efficiencies. Both enzymes were more >10-fold effective in cleaving $FolGlu_1$ compared to NAAG. They also cleaved randomized library of N-acetylated dipeptides with similar selectivity, however, the preference of glutamate in C-terminal position seemed more pronounced for the mouse ortholog. Moreover, our test set of inhibitors showed the same potency against both proteins. Both proteins thus showed a very similar enzyme characteristics and inhibition profiles.

We then focused on analysis of tissue expression via multiple orthogonal assays. We employed radioenzymatic assay, western blot, qRT-PCR and for selected tissues also immunohistochemistry. Multiple methods have been used, because the antibody-based methods cannot distinguish between GCPII and GCPIII due to the slight crossreactivity of the GCP-04 antibody with GCPIII (see publication VIII). Fortunately, radioenzymatic assay detecting NAAG cleavage is about 100-fold more sensitive for GCPII than GCPIII (see publication I for more details) and it has been shown that GCPII accounts for most of the NAAG activity in mouse [38]. Finally, data from these methods were correlated with qRT-PCR determination, which was able to selectively detect both GCPII and GCPIII mRNAs. The expression profiles from all methods correlated well in most tissues.

We have found highest GCPII expression in brain and kidney, which is consistent with previous reports [35, 38, 134] and corresponds to GCPII expression in human [6]. Interestingly, the expression in kidney is localized to proximal tubules, which suggest that GCPII may indeed play a role in reabsorbing folate from urine. We have also found significant amount in salivary glands, which corresponds well to the human, where high GCPII expression in the salivary glands was demonstrated by the high uptake of GCPII targeted radiotracers [165]. Generally, the GCPII expression correlated well to humans with two important exceptions: we observed no expression of GCPII in prostate, which is in line with previous reports [15, 134], and only little or no expression in small intestine, which may suggest that GCPII does not play important role in dietary folate absorption in mice. These discrepancies represent an important warning when considering mice as models for prostate cancer or when deciphering GCPII biological role from mouse models (**Fig. 12** on page 47).

Taken together, murine GCPII does not differ significantly in its enzymatic properties from human GCPII and its expression profile is similar to human in most tissues with the exception of prostate and small intestine.

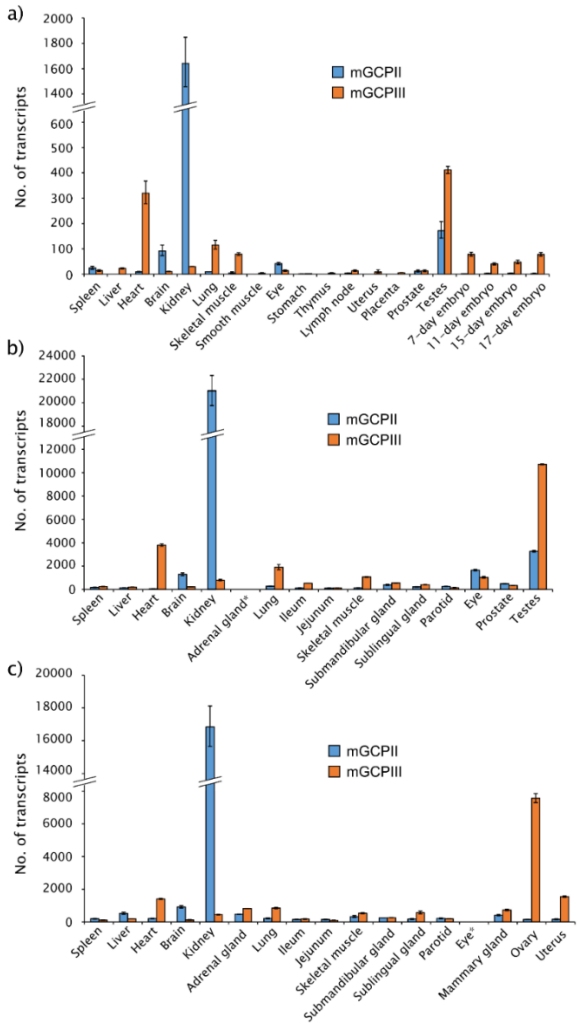

Figure 12: Quantification of murine GCPII and GCPIII transcripts using qPCR.

(**a**) Quantification of murine GCPII and GCPIII trascripts (designated as mGCPII and mGCPIII) using qPCR in commercial mouse tissue cDNA libraries from Clontech. The 'No. of transcripts' corresponds to the amount of transcripts in 1.0 µl of 10-fold diluted cDNA libraries. (**b**) and (**c**) Quantification of mGCPII and mGCPIII transcripts using qRT-PCR in cDNA libraries prepared from mouse tissues dissected from one female (**b**) and one male mouse (**c**). The 'No. of transcripts' corresponds to the amount of transcripts per 10 ng of total RNA as a starting material for cDNA synthesis. (**a-c**) Error bars show standard deviations from triplicate measurements. * Not determined.

My contribution

I was responsible for the qRT-PCR part of the study. I developed the qRT-PCR assays for murine GCPII and GCPIII, tested their selectivity and then determined GCPII and GCPIII amounts via qPCR in cDNA libraries and analyzed all amplification reactions on agarose gel electrophoresis. I also isolated RNA, tested its integrity and reverse transcribed it to cDNA. I contributed to the data analysis, discussion of the results and writing of the manuscript.

2.2.5. Publication 3: Detection and quantitation of glutamate carboxypeptidase II in human blood

Motivation of the study

Prostate cancer (PCa) is the most prevalent cancer among men and it is most commonly diagnosed via quantification of PSA in blood serum [275]. However, it suffers from false-positives leading to unnecessary prostate biopsies [162]. It also cannot precisely distinguish patients who would benefit from radical prostatectomy treatment [276] and the reduction of the rate of death in patients who undergo treatment because of positive PSA test remains elusive [277-279]. PSA test in men without symptoms has thus been questioned by some authorities such as U.S. Preventive services task force [161].

Therefore, there is a strong need to discover new PCa markers with higher predictive value and GCPII might represent such marker. Initial studies determining GCPII levels in blood serum by western blot led to inconsistent results and some studies even claimed that there is no GCPII in human blood [17, 101, 280], however a newer study showed significantly elevated GCPII serum levels in PCa patients compared to healthy individuals [18]. However, this study analyzed only limited number of patients and relied on SELDI method, which is not suitable for diagnostics. Reliable methods has to be developed in order to validate those findings and potentially enable the use of GCPII for improving diagnostics of prostate carcinoma.

We thus decided to develop several orthogonal assays suitable to detect GCPII in human blood samples, which we reported in this publication and publication IV.

Summary

In this report, we showed that the ability to cleave NAAG in human blood is unique to GCPII. We utilized this fact to develop radioenzymatic assay to quantify GCPII in human blood plasma samples. In this manner, we validated that GCPII is indeed present in human blood, but its levels are lower than reported in study by Xiao *et. al* [18].

First, we validated that GCPII is present in human blood and that we can detect NAAG hydrolyzing activity. The presence of GCPII was probed by immunoprecipitating the GCPII from blood plasma via our biotinylated 2G7 antibody and bound protein was then analyzed

on western blot and mass spectrometry. GCPII was detected in both methods: II-04 antibody showed intense band on western blot of expected molecular weight for full length GCPII (>100KDa) and mass spectrometry identified peptides covering 34% of the GCPII sequence including peptide covering intracellular part of GCPII. These results suggest, that GCPII is present in blood as a full length form. Next, we tested dilution series of three plasma samples and were able to detect NAAG hydrolyzing activity in all of them with linear dose response in the range of 10- to 100-fold diluted plasma. Moreover, we selected one sample and tried whether its activity can be inhibited by a series of known GCPII inhibitors. We found that the activity was almost completely inhibited by each compound, which provided us basic evidence that the activity comes from GCPII.

We then determined the GCPII levels in plasma samples of 19 healthy individuals (4 women and 15 men) by measuring their NAAG activities and comparing them with a dilution series of our recombinant purified GCPII standard. The median concentration was 1.7 ng/ml in women (range 1.3 to 4.3 ng/ml) and 3.2 ng/ml in men (range 1.3 to 17.2 ng/ml), see **Tab. 1** on page 50 for more details. Interestingly, there is only weak difference between men and women and also these concentrations are 10 to 100 fold lower than determined by Xiao [18].

Finally, we wanted to confirm whether all of the NAAG activity comes from GCPII, or whether there is a contribution from another enzyme. The only other enzymes reported to have NAAG cleaving activity are GCPIII [34], and plasma glutamate carboxypeptidase (PGCP) [281]. We did several additional experiments to exclude those two enzymes. First, we tested the influence of 500 nM 2-PMPA, which is a potent known GCPII inhibitor (K_i = 0.3 nM), and found out that the activity is completely abolished in all 19 individuals. Unfortunately, GCPIII is potently inhibited by 2-PMPA and other GCPII inhibitors as well [34]. To exclude GCPIII, we determined BCG hydrolyzing activity of all samples diluted in buffer containing 5 mM $CaCl_2$. Under such conditions, GCPIII cleaves BCG with about 100 fold higher efficiency than it cleaves NAAG (efficiency of NAAG cleavage is the same with or without calcium ions, see Table 2 in Publication I for more details). The observed BCG cleaving activity was in all samples much lower than the NAAG cleaving activity and GCPIII thus cannot be the enzyme responsible for NAAG cleavage. To exclude PGCP, we cloned, purified and characterized this enzyme. The PGCP protein showed a strong SerMet cleavage

activity as described previously [281, 282], but this activity could not be blocked by 500 nM 2-PMPA. Moreover, we were not able to detect any NAAG cleaving activity, even by using 5 µg of the purified PGCP (10^6 fold more than the amount of GCPII needed to produce significant activity).

Taken together, we have shown evidence that the enzyme responsible for NAAG cleavage in human serum is indeed GCPII and that we are able to determine its levels by examining rate of NAAG hydrolysis with our radioenzymatic assay.

Table 1: Radioenzymatic detection of GCPII levels in the blood plasma of healthy volunteers.

	Age (years)	GCPII in plasma (ng/ml)
female 1	22	1.4 ± 0.3
female 2	31	1.3 ± 0.3
female 3	43	1.9 ± 0.3
female 4	46	4.3 ± 0.3
male 1	20	3.7 ± 0.6
male 2	22	4.0 ± 0.6
male 3	24	2.3 ± 0.4
male 4	25	5.7 ± 0.8
male 5	26	1.8 ± 0.3
male 6	26	1.4 ± 0.3
male 7	27	1.3 ± 0.3
male 8	27	3.4 ± 0.7
male 9	28	4.6 ± 0.7
male 10	28	1.5 ± 0.3
male 11	33	3.2 ± 0.5
male 12	34	17.2 ± 5.0
male 13	45	2.4 ± 0.6
male 14	50	3.0 ± 0.4
male 15	52	9.9 ± 1.0

Quantification of NAAG cleaving activity was used to determine GCPII concentration in the heparin blood plasma samples of healthy volunteers. The samples were measured in duplicates in three separate experiments and the results are mean ± standard deviation. Recombinant extracellular GCPII was used as a standard of NAAG-hydrolyzing activity. No significant correlation between GCPII levels and the age or sex was observed.

My contribution

I conceived the study. I made first proof-of-principle experiments evaluating the possibility to detect low amounts of GCPII via enzymatic activity. I tested binding affinity of several novel anti-GCPII antibody clones, selected the 2G7 clone and optimized its purification protocol; this clone showed much better performance than our previous II-05 clone. I also contributed to the data analysis and writing of the manuscript.

2.2.6. Publication 4: DNA-linked Inhibitor Antibody Assay (DIANA) for sensitive and selective enzyme detection and inhibitor screening

Motivation of the study

Enzymes are important targets in diagnostics and treatment due to their involvement in etiology of most human diseases. Currently, many diseases are diagnosed by quantification of disease-related enzymes in biological samples, with sandwich ELISA being the golden standard. Moreover, many diseases are treated by drugs inhibiting disease-related enzymes and therefore the search of such inhibitory molecules is one of the major scopes of drug discovery. To find these inhibitors, small-molecule libraries are commonly screened by methods based on enzyme kinetics or on displacement of fluorescent active site probe. However, such screens usually consume large amounts of purified enzyme, which is in some cases not possible to prepare. Therefore, we combined approaches used in both fields and attempted to develop "first assay of its kind" which would be suitable for both ultrasensitive enzyme quantification and screening of enzyme inhibitors and which would overcome the current state of the art technologies in sensitivity and its applicability to screen inhibitors with unpurified enzyme.

Moreover, such method would be especially useful for our protein of interest, GCPII. Nowadays, there is no reliable and sensitive assay useful for detection of GCPII in blood in clinical setting and the development of such assay would facilitate validation of GCPII as prostate carcinoma serum marker. At the same time, novel GCPII inhibitors with improved pharmacokinetics are urgently needed for the development of brain penetrant neuroprotective agents, but no assay is available, which would enable sensitive screening of GCPII inhibitors (see section 1.1.6. for more details).

Summary

Here, we describe the development of a novel multi-well plate based method for ultrasensitive enzyme quantification and quantitative inhibitor screening and evaluation of this method on two putative cancer markers and potential drug targets: GCPII and CAIX. In the DNA-linked Inhibitor ANtibody Assay (DIANA), the target enzyme is captured by an immobilized antibody, probed with the detection probe consisting of a small-molecule

inhibitor attached to a reporter DNA, and subsequently detected by qPCR (**Fig. 13A**). The dual recognition by antibody and inhibitor provides selectivity, while qPCR provides sensitivity and broad linear range. Moreover, the detection probe binds to the active site of the enzyme, which can be used to evaluate the inhibition potency of other compounds.

First, we prepared the detection probes recognizing GCPII and CAIX. We were able to covalently link known inhibitors of these enzymes to a DNA oligonucleotoide without the loss of their activity. However, the affinity of original CAIX inhibitor was much lower than that of GCPII inhibitor. We thus prepared an oligonucleotide with two inhibitor moieties, which lead to an increase in potency of about 50 fold. Therefore, we used this bivalent probe for all CAIX experiments. The structures of the probes are shown in **Fig. 13B**.

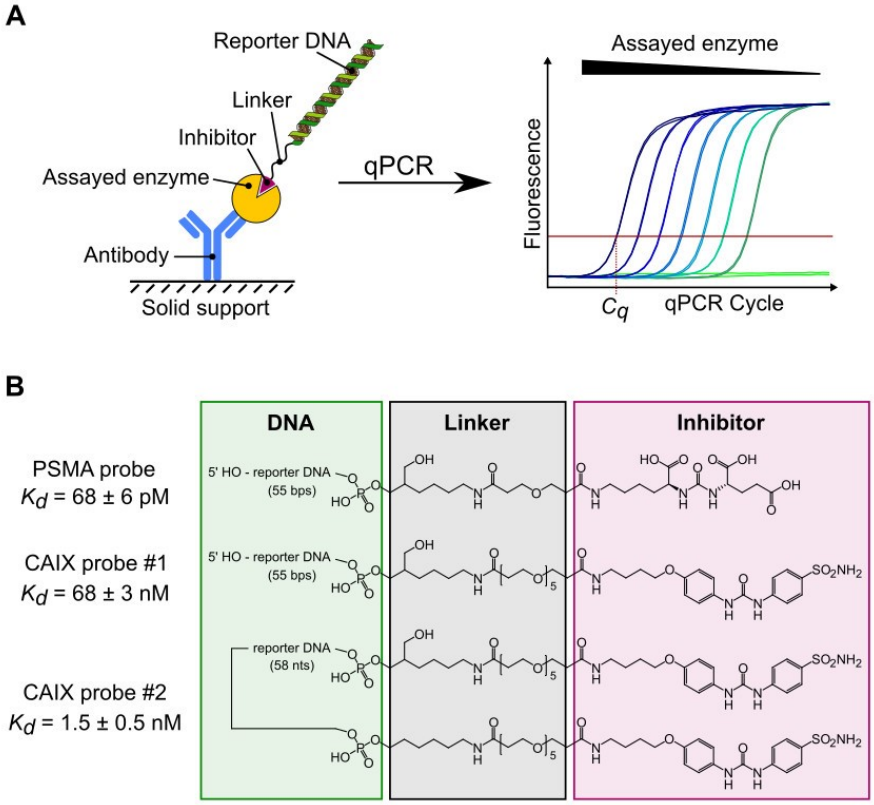

Figure 13: Schematic representation of enzyme detection by DIANA.

(**a**) A covalent conjugate of an oligonucleotide (marked as reporter DNA) and low molecular weight competitive inhibitor of the target enzyme is used as a detection probe. This probe binds to the active site of the target enzyme, which has been captured on the solid support by an immobilized antibody. The amount of detection probe bound to the enzyme is detected by qPCR in terms of the threshold cycles (C_q), which are indirectly proportional to the logarithm of its concentration. (**b**) Structures of the detection probes used for quantification of GCPII (marked here as PSMA) and CAIX. Each probe consists of reporter DNA (green box) covalently attached via a linker region (black box) to a competitive inhibitor of GCPII or CAIX (magenta box).

Next, we tested the ability of the proposed sandwich of immobilized antibody and detection probe to quantify both target enzymes. We detected as little as 1.1 zeptomole of GCPII standard (100 ag) and as little as 46 zeptomoles (2.5 fg) of CAIX standard. The linear range was more than six orders of magnitude for GCPII detection and more than five orders of magnitude for CAIX detection (see **Fig. 14A-B** on page 54).

Next, we analyzed the amount of GCPII and CAIX in serum samples from 12 healthy men, 12 men with prostate carcinoma (PCa), and 10 men and 2 women with clear cell renal cell carcinoma (ccRCC). GCPII concentrations in serum ranged from 0.10 to 6.0 ng/ml, with a median value of 0.45 ng/ml. Interestingly, mean concentration did not differ significantly among the three groups, suggesting that serum GCPII is not elevated in either ccRCC or PCa. CAIX concentrations ranged from 0.034 to 0.61 ng/ml, with a median value of 0.12 ng/ml. Mean CAIX concentration was significantly elevated not only in patients with ccRCC, which is in line with previous reports [283, 284], but also in PCa patients which is novel observation (see **Fig. 14C-D** on page 54).

We also evaluated the sensitivity of DIANA assay in serum samples by outcompeting the selective binding of the probe by free inhibitor. In this manner, we estimated the average limit of detection of GCPII in a 1-µl sample to be 0.8 pg/ml (range 0.4 to 2.4 pg/ml) and of CAIX in a 10-µl sample to be 1.1 pg/ml (range 0.7 to 2.8 pg/ml). These detection limits were two to three orders of magnitude below the actual GCPII and CAIX enzyme concentrations for most of the analyzed clinical samples. To put this in context, the detection of GCPII via sandwich ELISA was about 100-fold less sensitive even though 10-fold higher volume was used, while CAIX sandwich ELISA was about 10-fold less sensitive by using 10-fold higher volume. The linear range of both ELISA assays was approximately two orders of magnitude.

We have shown that DIANA assay can detect extremely low amounts of enzymes and with broad linear range in complex biological matrices. At the same time, it recognizes only the active form, because the probe binds to the intact active site. We therefore decided to explore also the possibilities to determine inhibition potencies of other compounds by incubating the target enzyme with the probe in the presence of such test compounds. Based on the superior performance characteristics, we proposed that we could be able to determine inhibition potency of the test compound by testing just a single well (**Fig. 15A** on page 55).

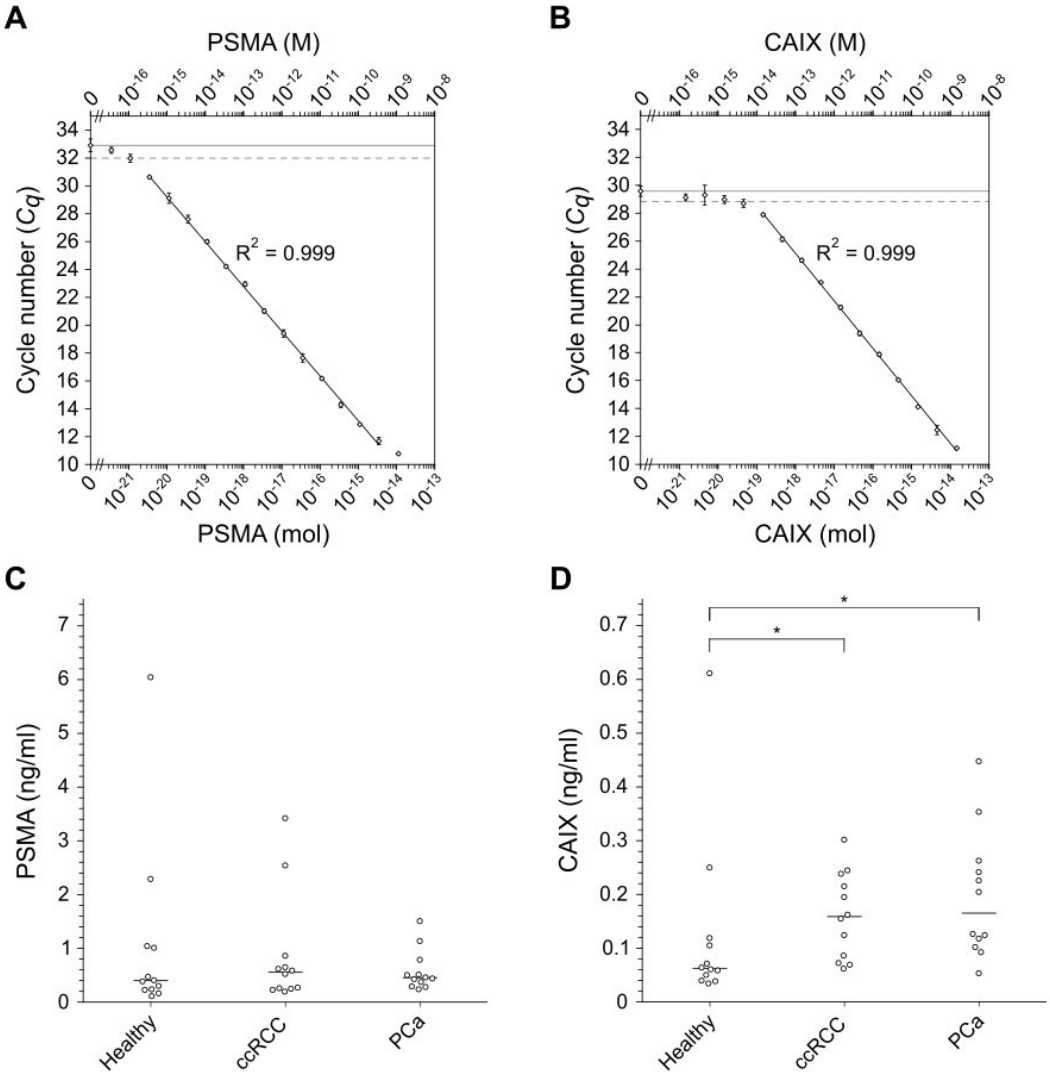

Figure 14: Ultrasensitive detection of GCPII (marked as PSMA) and CAIX by DIANA and comparison of their serum levels between healthy and diseased individuals.

(**a**,**b**) Plots of average C_q values vs. amount of human recombinant purified GCPII standard diluted in buffered solution (**a**), or average C_q values vs. amount of human CAIX present in HT-29 cell lysate diluted in buffered solution (**b**). Upper x-axes indicate molar concentration, while lower x-axes indicate the corresponding molar amount per well. Horizontal lines show the average background signal; dashed horizontal lines show the average background signal plus 2 s.d. Error bars show s.d. of quadruplicate measurements. (**c**,**d**) Plots of GCPII (**c**) and CAIX (**d**) serum levels determined by DIANA in samples from 12 healthy males, 12 males with histologically proven PCa and 10 males and 2 females with histologically proven ccRCC. Horizontal lines indicate median concentrations; * indicates statistically significant differences between the groups with $p < 0.05$ as determined by the two tailed Mann-Whitney test.

First, we examined a dilution series of selected known inhibitors and calculated their potency from each tested concentration. The determined K_i values of GCPII inhibitors were constant over six orders of magnitude of the compounds' concentration. We have seen similar

behavior also for CAIX inhibitors, only the range of the useful inhibitor concentration was narrower due to the use of cell lysate containing only a little of endogenous CAIX and also due to the bivalency of the probe. These results confirmed the possibility of determining inhibitor potency just from single well, which we later evaluated on larger set of inhibitors.

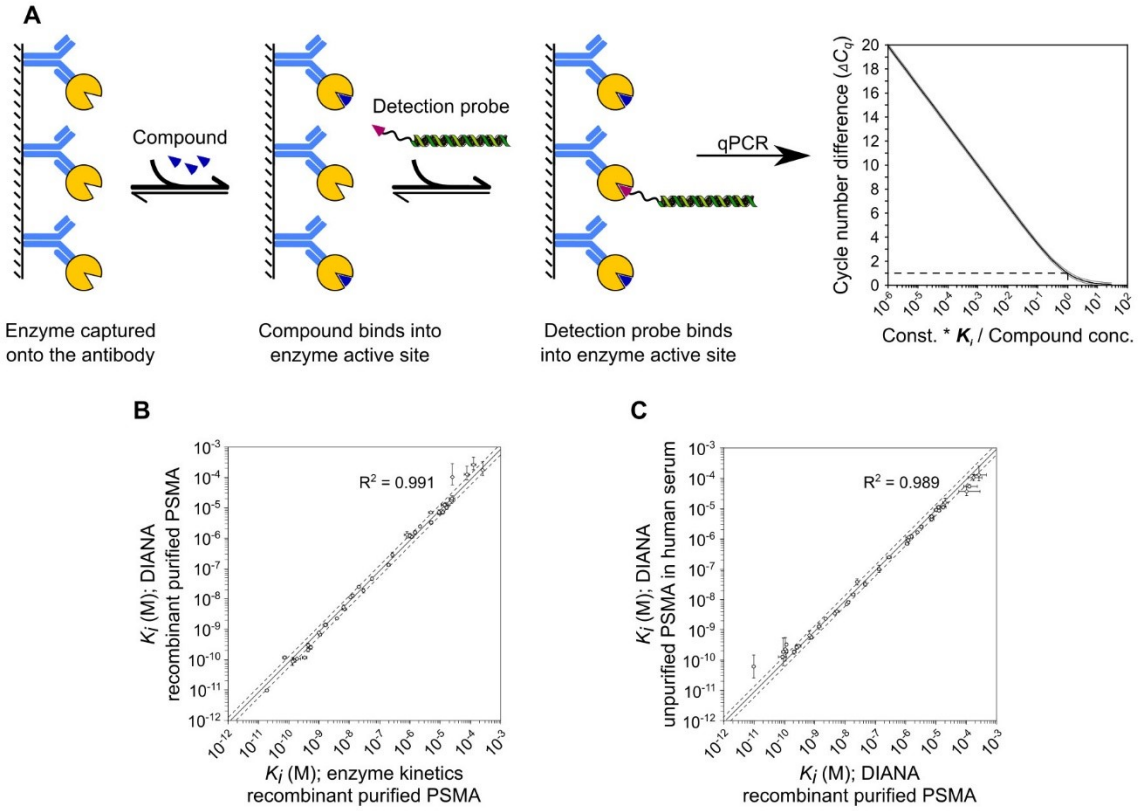

Figure 15: Determination of inhibitor potencies from single well by DIANA.

(**a**) Detection probe was incubated with target enzyme in the presence of evaluated compound. In case the test compound binds to the enzyme, the amount of bound probe is lowered. This change in the amount of bound probe (determined as ΔC_q between well with the compound and control well without any compound) and concentration of the compound were then used in calculation of its inhibition constant (K_i; formula valid for monovalent probe is shown): $K_i = (2^{-\Delta Cq} / (1 - 2^{-\Delta Cq})) * I_{tot} / (1 + (P_{tot} / K_d))$. I_{tot} is the total concentration of the tested inhibitor, P_{tot} is the total concentration of probe and K_d is the dissociation constant of the probe. Constant is equal to the term $1 + (P_{tot} / K_d)$, which can be approximated by one if probe concentration P_{tot} is held below its K_d. (**b**) Plot of K_i values of 41 GCPII (marked as PSMA) inhibitors determined by titrating recombinant purified GCPII with inhibitor and measuring kinetics (x-axis) *vs.* K_i values determined by DIANA from a single well containing 100 µM inhibitor and recombinant purified GCPII (y-axis). (**c**) Plot of K_i values of 41 GCPII inhibitors determined by DIANA from a single well containing 100 µM inhibitor with recombinant purified GCPII (x-axis) *vs.* K_i values determined by DIANA from two measurements with unpurified endogenous GCPII in 1 µl of human serum in the presence of either 100 µM or 100 nM inhibitor (y-axis). (**b-c**) Lines show linear regression of log-transformed values; dashed lines indicate values that are 1.5-fold higher or lower than the linear fit. Error bars show s.d. of duplicate measurements in the case of DIANA, or s.e. of the titration in the case of enzyme kinetics.

Finally, we selected 41 known competitive inhibitors of GCPII and determined their K_i values by single-well measurements at a constant concentration of inhibitor (100 μM). We compared these values with values determined by regular substrate cleavage assay with serial dilution of inhibitor and HPLC readout (**Fig. 15B**). The two methods showed excellent agreement ($R^2 = 0.991$) over the entire range of K_i values covering seven orders of magnitude from mid-picomolar to mid-micromolar. The high selectivity and sensitivity of DIANA even allowed us to determine K_i values for this set of GCPII inhibitors in the same manner using human serum rather than purified GCPII. The values measured in this way agreed well with those determined using recombinant GCPII (**Fig. 15C**) over the entire range of K_i values ($R^2 = 0.989$). We performed similar comparison of K_i values determined by single-well DIANA measurements and enzyme kinetics assay also for a set of known CAIX inhibitors and we observed good correlation as well. This showed us that DIANA accurately measures K_i values from a single inhibitor concentration and that purified enzyme is not needed.

We have shown that DIANA is suitable for both ultrasensitive enzyme quantification and quantitative evaluation of inhibitors with unpurified enzyme, which overcomes the limits of current state of the art methodologies in sensitivity and linear range. It is multi-well plate based, automatable and it has the unique ability to determine the compound's potency from a single well, which makes it an ideal candidate for screening of enzyme inhibitors in compound libraries. These performance characteristics make it a superior tool for disease detection and drug discovery.

My contribution

I designed the study. I developed the DIANA protocol and conducted all DIANA experiments. I derived the theoretical background for inhibitor screening and validated it experimentally. I also developed the sandwich ELISA for GCPII. I analyzed the data and wrote the manuscript.

3. Discussion and conclusions

Selective quantification of GCPII and GCPIII in human and mice tissues

In publication I, we have done thorough enzymatic characterization of human GCPII and GCPIII and exploited their divergent substrate specificities to determine their amounts in human tissues. We also determined their tissue expression by qRT-PCR assay. This study thus represents a first comprehensive quantification of both enzymes in human tissues at both mRNA and protein level.

Results from both enzymatic assay and qRT-PCR assay were in a good agreement. GCPII levels were consistent with our previous data obtained by western blot [6] and with data available from other groups [10-12]. The expression of GCPIII mRNA in testis, ovary and placenta is in good agreement with previous report [32]. There are no previous data on quantification of human GCPIII in tissues at protein level, but the predominant expression in testis agrees well with GCPIII expression in mouse and even collocalizes with the BCG which has been also found predominantly in testes of rat adults [84]. Since GCPIII reaches its maximum BCG cleaving activity at near physiological two-milimolar concentration of calcium cations and collocalizes with BCG, the cleavage of BCG is likely the physiological function of GCPIII.

In publication II, we presented an enzymological characterization of purified murine GCPII and a study of GCPII expression profile in mouse. We have shown that murine GCPII does not differ significantly in its enzymatic properties from human GCPII and its expression profile is similar to human in most tissues with the exception of prostate and small intestine as determined by several orthogonal methods.

Using qRT-PCR and other methods, we have seen GCPII expression also in mouse testis, while we have not detected any GCPII in human testis (publication I). We speculate, that this may be connected to the lack of GCPII in mouse prostate and that it may represent a difference in mouse anatomy rather than in GCPII physiology. While human GCPII enters the seminal plasma via secretion in the prostate gland [6, 12], murine GCPII may enter seminal fluid at a different occasion in mouse, i.e. in seminiferous tubules, efferent ducts or epididymis and still play the same physiological role.

Using qRT-PCR, we have also quantified the amount of GCPIII in mouse tissues. We have found significant expression of GCPIII in testes, ovary, uterus, heart and embryo. This is in line with previous reports [33, 35] and corresponds to the expression of GCPIII in human tissues as we have seen in publication I and as was previously reported [32]. It also corresponds to the prevalence of BCG in mouse tissues [84].

Methods for GCPII quantification in blood and its role as PCa serum marker

In publication III, we have developed a radioenzymatic assay to quantify GCPII in human serum. First, we have shown that NAAG cleaving activity in human serum is unique to GCPII as we excluded the only known possible enzymes having the same activity: GCPIII and PGCP. We then quantified the rate of NAAG hydrolysis in blood plasma samples drawn from 19 healthy individuals and calculated the amount of GCPII present in these samples, while using recombinant purified GCPII as standard. The median serum concentration was 1.7 ng/ml in females (range 1.3 to 4.3 ng/ml) and 3.2 ng/ml in men (range 1.3 to 17.2 ng/ml).

At the time we started working on methods for GCPII quantification, it was not only unclear, whether its concentration is elevated in prostate cancer patients, but even the fact that GCPII is present in human blood was not quite consistently demonstrated and the absolute GCPII level remained unclear. First reports using western blot yielded inconsistent results and they were not able to quantify the GCPII amount [17, 101, 280, 285, 286]. The only sandwich ELISA was reported by Sokoloff *et al.* [12]. Unfortunately, this report only stated that this ELISA is able to detect GCPII in blood, but did not showed any GCPII concentrations. Another report using SELDI assay was published by Xiao *et al.* and stated that GCPII is present in blood at 100 to 1,000 ng/ml and is significantly elevated in PCa patients compared to BPH group [18]. After we started working on this project, a plethora of new reports was published [287-293]. However, they did not shed light on the GCPII concentrations in blood, only few reached sufficient sensitivity and actually determined GCPII in blood, but they analyzed very limited number of samples (~10) [288, 289]. They confirmed the serum levels of about 100-1,000 ng/ml reported previously by Xiao *et al*.

During the last years, we have developed several methods for GCPII quantification in human blood samples: radioenzymatic assay (exploiting NAAG cleavage and described in publication III), sandwich immunoassay recognizing native GCPII (ELISA described in

publication IV and XI) and DIANA assay recognizing active GCPII, which could be seen as a combination of previous methods (publication IV). We first compared the results from these methods to each other. The radioenzymatic assay gave on average about four fold higher blood concentrations than our sandwich ELISA, but otherwise these two methods correlated very well (these results are not part of this thesis, see page 65 for comparison of the two methods on blood samples from 110 human individuals in ref. [294]). At the same time, DIANA gave about 0.85 fold lower values than sandwich ELISA with perfect correlation between the two methods as tested on 36 human serum samples (publication IV). All three methods thus showed similar results and we therefore believe, that the concentrations of GCPII in human serum is in the range of approx. 0.10 to 10 ng/ml, with a median value below 1.0 ng/ml.

These values are, however, about 100-fold lower than previously reported. There might be at least three reasons for such discrepancies: (1) use of different standards; we have used our own and well characterized recombinant purified GCPII or (2) all our methods recognize native protein, whereas previously reported methods may detect also denature protein or protein fragments, which may have lead to higher detected GCPII levels or (3) different handling of the blood samples. To investigate the second possibility, we developed a method for denaturing GCPII in blood serum and a sandwich ELISA consisting of our II-02 and II-04 antibodies, which recognize epitopes on denature GCPII in near proximity in the extracellular domain (see publication VIII for epitope mapping). This sandwich is thus able to detect total GCPII amount including denature and/or fragmented species. We have then compared the results from native and denature sandwiches on 110 blood samples (both healthy and PCa affected individuals) and we have seen a perfect correlation between the two methods and the denatured sandwich gave about 70% of the levels of native sandwich (development and use of this ELISA recognizing denature GCPII is not part of this thesis, see results on page 66 in ref. [294]). To exclude the third possibility, we have tested the blood levels in all our subjects in heparin (radioenzymatic assay) and citrate (sandwich ELISA) plasma and in serum (DIANA assay) and have not seen any significant difference. Consequently, we have not identified the reason for the observed discrepancies of GCPII serum levels.

However, even such levels are quite high if we expect that blood GCPII comes from prostate. They are comparable to concentrations of PSA, which is actually used to diagnose PCa. Both PSA [295] and GCPII [6, 11] are expressed by the epithelial cells lining the secretory glands and are found in high concentration in the prostatic fluid, which becomes part of the seminal plasma. However, PSA is a soluble protein present in seminal plasma in concentration of about 1 mg/ml [296] whereas GCPII is a membrane bound protein and is present in seminal plasma at only 0.01 mg/ml [12]. As we have detected similar levels of GCPII in blood of men and women, which is in line with report from Sokoloff *et al*. [12] (unfortunately this study did not reported the absolute values), we speculate that the source of GCPII may be an extraprostatic tissue.

To finally tackle the question, whether GCPII concentration is elevated in blood of PCa patients, we determined the GCPII blood levels in both patient samples and samples from healthy individuals. Using ELISA and DIANA, we determined GCPII levels in small groups of healthy individuals and PCa patients (12 individuals in each group) and we have not seen any difference between the groups (publication IV). To shed more light on this question, we collected and analyzed with our three methods (radioenzymatic assay, sandwich ELISA for both native and denature GCPII) 110 samples from generalized PCa cases (n=8), localized PCa cases (n=33), cases with benign prostate hyperplasia (BPH; n=23), healthy males (n=15), PCa cases after radical prostatectomy with undetectable PSA levels (n=11) and females (n=20); these results are not part of this thesis, see ref. [294] for more details. We have found out that median GCPII levels were around 0.8 ng/ml in first four groups and around 0.4 ng/ml in the last two groups, but these differences were not statistically significant. GCPII did thus not significantly decreased after surgical removal of the prostate even though the PSA levels dropped to undetectable values. To confirm these results, we collected paired samples from six patients drawn before and after prostatectomy, and we have not seen any decrease in GCPII levels even more than a year after surgery. We also made ROC analysis for the ability of PSA or GCPII to distinguish between PCa and BPH and while PSA worked quite well for our samples (cutoff 4.0 ng/ml with 90% sensitivity and 35% false positives; area under curve 0.775), GCPII levels were not useful at all (area under curve 0.455). Taken together, these data strongly suggest that GCPII in blood originate from extraprostatic tissue and that its detection cannot be used for prostate cancer diagnosis.

DIANA assay for ultrasensitive detection of enzymes and screening for their inhibitors

In publication IV, we reported the development of DIANA assay suitable for enzyme detection and screening of enzyme inhibitors. This assay is analogous to the immuno-PCR assay described in [239], in which the target protein is captured by an immobilized antibody and then probed by another DNA-linked antibody, which is detected in qPCR. In DIANA assay, the DNA-linked antibody has been replaced by detection probe consisting of a DNA oligonucleotide covalently linked to a small molecule that binds to the active site of a target enzyme. We showed that DIANA represents a powerful method with some important implications, which are discussed in following paragraphs.

We showed that DIANA can detect very low amount of target enzyme in complex biological matrices and has very broad linear range. We detected (sub)femtogram amount of GCPII and CAIX which was by several orders of magnitude less than was detected with corresponding sandwich ELISA. Such sensitivity is comparable or even better to the most sensitive sandwich immunoassays, including immuno-PCR [239], immuno-PCR on gold nanoparticles (Bio-Barcode assay [242]), proximity ligation assay [297], and proximity extension assay [298]. The linear range of DIANA for GCPII and CAIX detection ranged between five and six orders of magnitude; this means that it is not necessary to test different dilutions of the samples, as it is sometimes necessary with sandwich ELISA. DIANA also selectively detects only the active form of the enzyme, which is likely to be the more clinically relevant form.

The binding of the detection probe to the enzyme active site, the high sensitivity, selectivity and wide linear range of DIANA make it well-suited for screening of competitive inhibitors of target enzymes which ability to outcompete the detection probe is measured. We have shown that it is possible to accurately evaluate inhibitor potencies even when using untreated biological matrices such as human serum, which contains very low amounts of endogenous target enzyme. We have also shown that it is possible to accurately determine inhibitor potency from single well, which is unique to this method. We have also shown that both weak (up to submilimolar) and tight inhibitors (up to subnanomolar) are accurately ranked by DIANA. The solid-phase assay format also allows testing of notorious trouble

makers, such as fluorescent or colored compounds, since they are washed out before analysis and therefore cannot interfere with the qPCR readout.

As with other ultrasensitive solid-phase assays, the sensitivity of DIANA is limited by non-selective adsorption of the detection probe, which leads to the necessity of using a high potency probes. In our hands, the non-selective adsorption of the probe was much lower than the non-selective adsorption of a DNA-linked antibody (unpublished data), which is likely the cause for higher sensitivity of DIANA compared to immuno-PCR. Nevertheless, this background binding still limited the sensitivity and subnanomolar probe affinity was needed to detect zeptomole amounts of GCPII. However, such potent ligands have been prepared only for a limited number of targets. As we showed here for CAIX, in some cases, tight-binding probes can be prepared from weaker ligands by including several copies of the ligand moiety in order to induce multiple binding of the probe. Otherwise, the sensitivity will decrease in proportion to the decreasing affinity of the ligand, which may limit the use of weaker ligands for DIANA-based diagnostics. However, we propose that this will not limit the use of DIANA for screening of inhibitors and that up to micromolar ligands can be used to prepare the detection probe, as it is possible to use higher enzyme concentration.

DIANA can be rapidly developed for a number of targets. Many potent class-specific inhibitors are known, e.g. pepstatin [299], staurosporin [265], or acetazolamide [300] and they can be used to prepare detection probes for screening of inhibitors. In such cases, recombinant target enzyme can be captured not only via selective antibody, but also via an expression tag, as we have shown on the example of GCPII and GCPIII, which enables straightforward development of DIANA for new targets. Detection probes prepared from promiscuous inhibitors are still useful for detection of enzymes in complex biological matrices, in such cases a selective antibody is used for capturing the enzyme, which complements the assay selectivity. We have shown that this works for highly homologous proteins and we were able to selectively detect GCPII and not GCPIII, though we used probe binding to both proteins. Similarly, we used a selective antibody for CAIX, which can distinguish this isoform from all other isoforms. Finally, we propose that DIANA can be used not only for enzymes, but also for any functional protein, including receptors or transporters, for which a sufficiently potent small-molecule ligand is available (details are in supplementary information of publication IV).

Besides assays for GCPII, GCPIII and CAIX shown in publication IV, we developed DIANA assay also for several other targets (unpublished data). We also partially automated DIANA and used it to screen for inhibitors of GCPII and CAIX at our IOCB facility and we indeed identified several novel scaffolds for both enzymes, which are now being further developed (unpublished data). During these screens, we confirmed that DIANA is very robust and is very sensitive in hit discovery and test compounds can be screened at lower concentrations than in other assays. At the same time, it has very low false positive rate.

We therefore believe in a big potential of DIANA not only in diagnostics, but also in screening for enzyme inhibitors, where it can be applied to difficult targets, which are hard to tackle with other methods. Thanks to its multi-well plate based straightforward protocol, it can be run both manually and in automated setting. It can thus become a widely used method both in academic environment and in industrial applications.

4. Abbreviations

2-MPPA	2-(3-mercaptopropyl)-pentandioic acid
2-PMPA	2-phosphonomethyl-pentandioic acid
5MeTHF	5-methyltetrahydrofolate
ADC	Antibody drug conjugate
AMPA	α-amino-3-hydroxy-5-methyl-4-isoxasolepropionate
BCG	β-citryl-L-glutamate
BCR	Biochemically recurrent (prostate) cancer
BPH	Benign prostate hyperplasia
CAIX	Carbonic anhydrase IX
ccRCC	Clear cell renal cell carcinoma
CNS	Central nervous system
CT	Computed tomography
DIANA	DNA-linked Inhibitor ANtibody Assay
DHFR	Dihydrofolate reductase
DM-1	Maytansinoid 1
EAATs	Excitatory amino acid transporters
ELISA	Enzyme-Linked ImmunoSorbent Assay
FDG	Fluoro-deoxyglucose
FOLH1	Folate hydrolase (GCPII)
FDG	Fluoro-deoxyglucose
FP	Fluorescence polarization
FPG	Folyl-poly-γ-glutamate
FPGS	Folyl-poly-γ-glutamate synthetase
GGH	γ-glutamyl hydrolase
GCPII (PSMA)	Glutamate carboxypeptidase II (Prostate specific membrane antigen)
GCPIII	Glutamate carboxypeptidase III
GPCRs	G-protein coupled receptors
mCRPC	Metastatic castration-resistant PCa
mGluR3	Metabotropic glutamate receptor 3
MTHFR	Methylenetetrahydrofolate reductase
MRI	Magnetic resonance imaging

NAA	*N*-acetyl-L-aspartate
NAAG	*N*-acetyl-α-L-aspartyl-L-glutamate
NAALADase	*N*-acetylated-alpha-linked acidic dipeptidase (GCPII)
NAALADase 2	*N*-acetylated-alpha-linked acidic dipeptidase 2 (GCPIII)
NAT8L	*N*-acetyltransferase 8 like protein
NMDA	*N*-methyl-D-aspartate
PCa	Prostate carcinoma
PCFT1	Proton-coupled folate transporter
PET	Positron emission tomography
PSA	Prostate specific antigen
PSMA (GCPII)	Prostate specific membrane antigen (Glutamate carboxypeptidase II)
PSM'	Truncated form of PSMA (GCPII)
qPCR	Quantitative polymerase chain reaction
qRT-PCR	Quantitative reverse transcriptase and polymerase chain reaction
RIMKLA	Ribosomal Modification Protein RimK Like Family Member A
RIMKLB	Ribosomal Modification Protein RimK Like Family Member B
RFC	Reduced folate carrier
ROC	Receiver operating characteristics
RT-PCR	Reverse transcriptase and polymerase chain reaction
SHMT	Serine hydroxymethyl transferase
SELDI	Surface-enhanced laser desorption/ionization
SMDC	Small molecule drug conjugates
SPECT	Single photon emission computed tomography
TGF-β	Transforming growth factor β

5. List of Figures and Tables

6. References

1. Chandler, C.J., Wang, T.T. and Halsted, C.H., J. Biol. Chem., 1986. **261**(2):928-933.
2. Robinson, M.B., Blakely, R.D., Couto, R. and Coyle, J.T., J. Biol. Chem., 1987. **262**(30):14498-14506.
3. Horoszewicz, J.S., Kawinski, E. and Murphy, G.P., Anticancer Res., 1987. **7**(5):927-936.
4. Pinto, J.T., Suffoletto, B.P., Berzin, T.M., Qiao, C.H., Lin, S., Tong, W.P.*, et al.*, Clin. Cancer Res., 1996. **2**(9):1445-1451.
5. Carter, R.E., Feldman, A.R. and Coyle, J.T., Proc. Natl. Acad. Sci. U.S.A., 1996. **93**(2):749-753.
6. Rovenska, M., Hlouchova, K., Sacha, P., Mlcochova, P., Horak, V., Zamecnik, J.*, et al.*, Prostate, 2008. **68**(2):171-182.
7. Cunha, A.C., Weigle, B., Kiessling, A., Bachmann, M. and Rieber, E.P., Cancer Lett., 2006. **236**(2):229-238.
8. Israeli, R.S., Powell, C.T., Corr, J.G., Fair, W.R. and Heston, W.D., Cancer Res., 1994. **54**(7):1807-1811.
9. O'Keefe, D.S., Bacich, D.J. and Heston, W.D., Prostate, 2004. **58**(2):200-210.
10. Kinoshita, Y., Kuratsukuri, K., Landas, S., Imaida, K., Rovito, P.M., Wang, C.Y. and Haas, G.P., World. J. Surg., 2006. **30**(4):628-636.
11. Silver, D.A., Pellicer, I., Fair, W.R., Heston, W.D.W. and CordonCardo, C., Clin. Cancer Res., 1997. **3**(1):81-85.
12. Sokoloff, R.L., Norton, K.C., Gasior, C.L., Marker, K.M. and Grauer, L.S., Prostate, 2000. **43**(2):150-157.
13. Chang, S.S., Reuter, V.E., Heston, W.D.W., Bander, N.H., Grauer, L.S. and Gaudin, P.B., Cancer Res., 1999. **59**(13):3192-3198.
14. Liu, H., Moy, P., Kim, S., Xia, Y., Rajasekaran, A., Navarro, V.*, et al.*, Cancer Res., 1997. **57**(17):3629-3634.
15. Huang, X., Bennett, M. and Thorpe, P.E., Prostate, 2004. **61**(1):1-11.
16. Sacha, P., Zamecnik, J., Barinka, C., Hlouchova, K., Vicha, A., Mlcochova, P.*, et al.*, Neuroscience, 2007. **144**(4):1361-1372.
17. Troyer, J.K., Beckett, M.L. and Wright, G.L., Int. J. Cancer, 1995. **62**(5):552-558.
18. Xiao, Z., Adam, B.L., Cazares, L.H., Clements, M.A., Davis, J.W., Schellhammer, P.F.*, et al.*, Cancer Res., 2001. **61**(16):6029-6033.
19. Taneja, S.S., Rev. Urol., 2004. **6 Suppl 10**:S19-28.
20. Weineisen, M., Schottelius, M., Simecek, J., Baum, R.P., Yildiz, A., Beykan, S.*, et al.*, J. Nucl. Med., 2015. **56**(8):1169-1176.
21. Heck, M.M., Retz, M., D'Alessandria, C., Rauscher, I., Scheidhauer, K., Maurer, T.*, et al.*, J. Urology, 2016. **196**(2):382-390.
22. Slusher, B.S., Vornov, J.J., Thomas, A.G., Hurn, P.D., Harukuni, I., Bhardwaj, A.*, et al.*, Nat. Med., 1999. **5**(12):1396-1402.
23. Bacich, D.J., Wozniak, K.M., Lu, X.C.M., O'Keefe, D.S., Callizot, N., Heston, W.D.W. and Slusher, B.S., J. Neurochem, 2005. **95**(2):314-323.
24. Olszewski, R.T., Bzdega, T. and Neale, J.H., Schizophr. Res., 2012. **136**(1-3):160-161.
25. Rais, R., Jiang, W., Zhai, H., Wozniak, K.M., Stathis, M., Hollinger, K.R.*, et al.*, JCI Insight, 2016. **1**(12).
26. Date, A.A., Rais, R., Babu, T., Ortiz, J., Kanvinde, P., Thomas, A.G.*, et al.*, J. Control. Release, 2017. **263**:132-138.
27. Jackson, P.F., Cole, D.C., Slusher, B.S., Stetz, S.L., Ross, L.E., Donzanti, B.A. and Trainor, D.A., J. Med. Chem., 1996. **39**(2):619-622.

28. Kozikowski, A.P., Nan, F., Conti, P., Zhang, J.H., Ramadan, E., Bzdega, T.*, et al.*, J. Med. Chem., 2001. **44**(3):298-301.
29. Majer, P., Jackson, P.F., Delahanty, G., Grella, B.S., Ko, Y.S., Li, W.*, et al.*, J. Med. Chem., 2003. **46**(10):1989-1996.
30. van der Post, J.P., de Visser, S.J., de Kam, M.L., Woelfler, M., Hilt, D.C., Vornov, J.*, et al.*, Brit. J. Clin. Pharmaco., 2005. **60**(2):128-136.
31. Rais, R., Wozniak, K., Wu, Y., Niwa, M., Stathis, M., Alt, J.*, et al.*, Plos One, 2015. **10**(7).
32. Pangalos, M.N., Neefs, J.M., Somers, M., Verhasselt, P., Bekkers, M., van der Helm, L.*, et al.*, J. Biol. Chem., 1999. **274**(13):8470-8483.
33. Bzdega, T., Crowe, S.L., Ramadan, E.R., Sciarretta, K.H., Olszewski, R.T., Ojeifo, O.A.*, et al.*, J. Neurochem., 2004. **89**(3):627-635.
34. Hlouchova, K., Barinka, C., Klusak, V., Sacha, P., Mlcochova, P., Majer, P.*, et al.*, J. Neurochem., 2007. **101**(3):682-696.
35. Collard, F., Vertommen, D., Constantinescu, S., Buts, L. and Van Schaftingen, E., J. Biol. Chem., 2011. **286**(44):38220-38230.
36. Miyake, M., Innami, T. and Kakimoto, Y., Biochim. Biophys. Acta, 1983. **760**(2):206-214.
37. Asakura, M., Nagahashi, Y., Hamada, M., Kawai, M., Kadobayashi, K., Narahara, M.*, et al.*, Biochim. Biophys. Acta, 1995. **1250**(1):35-42.
38. Bacich, D.J., Ramadan, E., O'Keefe, D.S., Bukhari, N., Wegorzewska, I., Ojeifo, O.*, et al.*, J. Neurochem., 2002. **83**(1):20-29.
39. Neale, J.H., Bzdega, T. and Wroblewska, B., J. Neurochem., 2000. **75**(2):443-452.
40. Pouwels, P.J. and Frahm, J., NMR Biomed., 1997. **10**(2):73-78.
41. Cassidy, M. and Neale, J.H., Neuropeptides, 1993. **24**(5):271-278.
42. Berger, U.V., Luthi-Carter, R., Passani, L.A., Elkabes, S., Black, I., Konradi, C. and Coyle, J.T., J. Comp. Neurol., 1999. **415**(1):52-64.
43. Ventura, R. and Harris, K.M., J. Neurosci., 1999. **19**(16):6897-6906.
44. Neale, J.H., J. Neurochem., 2011. **119**(5):891-895.
45. Carpenter, K.J. and Dickenson, A.H., Curr. Opin. Pharmacol., 2001. **1**(1):57-61.
46. Traynelis, S.F., Wollmuth, L.P., McBain, C.J., Menniti, F.S., Vance, K.M., Ogden, K.K.*, et al.*, Pharmacol. Rev., 2010. **62**(3):405-496.
47. Nedergaard, M., Takano, T. and Hansen, A.J., Nat. Rev. Neurosci., 2002. **3**(9):748-755.
48. Niswender, C.M. and Conn, P.J., Annu. Rev. Pharmacol. Toxicol., 2010. **50**:295-322.
49. Murrough, J.W., Abdallah, C.G. and Mathew, S.J., Nat. Rev. Drug. Discov., 2017. **16**(7):472-486.
50. Camacho, A. and Massieu, L., Arch. Med. Res., 2006. **37**(1):11-18.
51. Arundine, M. and Tymianski, M., Cell. Mol. Life Sci., 2004. **61**(6):657-668.
52. Rahn, K.A., Slusher, B.S. and Kaplin, A.I., Curr. Med. Chem., 2012. **19**(9):1335-1345.
53. Fan, M.M. and Raymond, L.A., Prog. Neurobiol., 2007. **81**(5-6):272-293.
54. Olney, J.W., Labruyere, J. and Price, M.T., Science, 1989. **244**(4910):1360-1362.
55. Olney, J.W., Labruyere, J., Wang, G., Wozniak, D.F., Price, M.T. and Sesma, M.A., Science, 1991. **254**(5037):1515-1518.
56. Lodder-Gadaczek, J., Gieselmann, V. and Eckhardt, M., Biochem. J., 2013. **454**(1):31-38.
57. Vornov, J.J., Hollinger, K.R., Jackson, P.F., Wozniak, K.M., Farah, M.H., Majer, P.*, et al.*, Adv. Pharmacol., 2016. **76**:215-255.
58. Fricker, A.C., Mok, M.H., de la Flor, R., Shah, A.J., Woolley, M., Dawson, L.A. and Kew, J.N., Neuropharmacology, 2009. **56**(6-7):1060-1067.
59. Chopra, M., Yao, Y., Blake, T.J., Hampson, D.R. and Johnson, E.C., J. Pharmacol. Exp. Ther., 2009. **330**(1):212-219.
60. Losi, G., Vicini, S. and Neale, J., Neuropharmacology, 2004. **46**(4):490-496.
61. Sanabria, E.R., Wozniak, K.M., Slusher, B.S. and Keller, A., J. Neurophysiol., 2004. **91**(1):182-193.

62. Kamiya, H., Shinozaki, H. and Yamamoto, C., J. Physiol., 1996. **493 (Pt 2)**:447-455.
63. Bruno, V., Battaglia, G., Casabona, G., Copani, A., Caciagli, F. and Nicoletti, F., J. Neurosci., 1998. **18**(23):9594-9600.
64. Thomas, A.G., Liu, W., Olkowski, J.L., Tang, Z., Lin, Q., Lu, X.C. and Slusher, B.S., Eur. J. Pharmacol., 2001. **430**(1):33-40.
65. Thomas, A.G., Olkowski, J.L. and Slusher, B.S., Eur. J. Pharmacol., 2001. **426**(1-2):35-38.
66. Bruno, V., Wroblewska, B., Wroblewski, J.T., Fiore, L. and Nicoletti, F., Neuroscience, 1998. **85**(3):751-757.
67. Neale, J.H., Olszewski, R.T., Zuo, D., Janczura, K.J., Profaci, C.P., Lavin, K.M.*, et al.*, J. Neurochem., 2011. **118**(4):490-498.
68. Bergeron, R., Coyle, J.T., Tsai, G. and Greene, R.W., Neuropsychopharmacology, 2005. **30**(1):7-16.
69. Valivullah, H.M., Lancaster, J., Sweetnam, P.M. and Neale, J.H., J. Neurochem., 1994. **63**(5):1714-1719.
70. Khacho, P., Wang, B., Ahlskog, N., Hristova, E. and Bergeron, R., Neurobiol. Dis., 2015. **82**:580-592.
71. Olszewski, R.T., Bukhari, N., Zhou, J., Kozikowski, A.P., Wroblewski, J.T., Shamimi-Noori, S.*, et al.*, J. Neurochem., 2004. **89**(4):876-885.
72. Yamamoto, T., Hirasawa, S., Wroblewska, B., Grajkowska, E., Zhou, J., Kozikowski, A.*, et al.*, Eur. J. Neurosci., 2004. **20**(2):483-494.
73. Tykvart, J., Ph.D. Thesis, 2015. Charles University in Prague.
74. Navratil, M., Ptacek, J., Sacha, P., Starkova, J., Lubkowski, J., Barinka, C. and Konvalinka, J., FEBS J., 2014. **281**(14):3228-3242.
75. Halsted, C.H., Ling, E.H., Luthi-Carter, R., Villanueva, J.A., Gardner, J.M. and Coyle, J.T., J. Biol. Chem., 1998. **273**(32):20417-20424.
76. Wang, T.T., Chandler, C.J. and Halsted, C.H., J. Biol. Chem., 1986. **261**(29):13551-13555.
77. Yao, R., Schneider, E., Ryan, T.J. and Galivan, J., Proc. Natl. Acad. Sci. U.S.A., 1996. **93**(19):10134-10138.
78. Shafizadeh, T.B. and Halsted, C.H., J. Nutr., 2007. **137**(5):1149-1153.
79. Visentin, M., Diop-Bove, N., Zhao, R. and Goldman, I.D., Annu. Rev. Physiol., 2014. **76**:251-274.
80. Donnelly, J.G., Crit. Rev. Clin. Lab. Sci., 2001. **38**(3):183-223.
81. Gueant, J.L., Namour, F., Gueant-Rodriguez, R.M. and Daval, J.L., Trends Endocrinol. Metab., 2013. **24**(6):279-289.
82. Pfeiffer, C.M. and Gregory, J.F., 3rd, Clin. Chem, 1996. **42**(11):1847-1854.
83. Miyake, M., Kakimoto, Y. and Sorimachi, M., Biochim. Biophys. Acta, 1978. **544**(3):656-666.
84. Miyake, M., Kume, S. and Kakimoto, Y., Biochim. Biophys. Acta, 1982. **719**(3):495-500.
85. Narahara, M., Tachibana, K., Adachi, S., Iwasa, A., Yukii, A., Hamada-Kanazawa, M.*, et al.*, Biol. Pharm. Bull., 2000. **23**(11):1287-1292.
86. Hamada-Kanazawa, M., Narahara, M., Takano, M., Min, K.S., Tanaka, K. and Miyake, M., Biol. Pharm. Bull., 2011. **34**(9):1455-1464.
87. Narahara, M., Hamada-Kanazawa, M., Kouda, M., Odani, A. and Miyake, M., Biol. Pharm. Bull., 2010. **33**(12):1938-1943.
88. Collard, F., Stroobant, V., Lamosa, P., Kapanda, C.N., Lambert, D.M., Muccioli, G.G.*, et al.*, J. Biol. Chem., 2010. **285**(39):29826-29833.
89. Becker, I., Lodder, J., Gieselmann, V. and Eckhardt, M., J. Biol. Chem., 2010. **285**(38):29156-29164.
90. Lodder-Gadaczek, J., Becker, I., Gieselmann, V., Wang-Eckhardt, L. and Eckhardt, M., J. Biol. Chem., 2011. **286**(19):16693-16706.

91. Lodder-Gadaczek, J., Ph.D. Thesis, 2013. Rheinische Friedrich-Wilhelms-Universität Bonn.
92. Navratil, M., Ph.D. Thesis, 2016. Charles University in Prague.
93. Israeli, R.S., Powell, C.T., Fair, W.R. and Heston, W.D., Cancer Res., 1993. **53**(2):227-230.
94. Liu, H., Rajasekaran, A.K., Moy, P., Xia, Y., Kim, S., Navarro, V.*, et al.*, Cancer Res., 1998. **58**(18):4055-4060.
95. Barinka, C., Mlcochova, P., Sacha, P., Hilgert, I., Majer, P., Slusher, B.S.*, et al.*, Eur. J. Biochem, 2004. **271**(13):2782-2790.
96. Barinka, C., Sacha, P., Sklenar, J., Man, P., Bezouska, K., Slusher, B.S. and Konvalinka, J., Protein Sci., 2004. **13**(6):1627-1635.
97. Holmes, E.H., Greene, T.G., Tino, W.T., Boynton, A.L., Aldape, H.C., Misrock, S.L. and Murphy, G.P., Prostate Suppl., 1996. **7**:25-29.
98. Ghosh, A. and Heston, W.D., Prostate, 2003. **57**(2):140-151.
99. Mlcochova, P., Barinka, C., Tykvart, J., Sacha, P. and Konvalinka, J., Prostate, 2009. **69**(5):471-479.
100. Su, S.L., Huang, I.P., Fair, W.R., Powell, C.T. and Heston, W.D., Cancer Res., 1995. **55**(7):1441-1443.
101. Beckett, M.L., Cazares, L.H., Vlahou, A., Schellhammer, P.F. and Wright, G.L., Clin. Cancer Res., 1999. **5**(12):4034-4040.
102. Troyer, J.K., Feng, Q., Beckett, M.L. and Wright, G.L., Jr., Urol. Oncol., 1995. **1**(1):29-37.
103. Davis, M.I., Bennett, M.J., Thomas, L.M. and Bjorkman, P.J., Proc. Natl. Acad. Sci. U.S.A., 2005. **102**(17):5981-5986.
104. Mesters, J.R., Barinka, C., Li, W., Tsukamoto, T., Majer, P., Slusher, B.S.*, et al.*, EMBO J., 2006. **25**(6):1375-1384.
105. Lawrence, C.M., Ray, S., Babyonyshev, M., Galluser, R., Borhani, D.W. and Harrison, S.C., Science, 1999. **286**(5440):779-782.
106. Fischer, W.H. and Spiess, J., Proc. Natl. Acad. Sci. U.S.A., 1987. **84**(11):3628-3632.
107. Huang, K.F., Liu, Y.L., Cheng, W.J., Ko, T.P. and Wang, A.H., Proc. Natl. Acad. Sci. U.S.A., 2005. **102**(37):13117-13122.
108. Klusak, V., Barinka, C., Plechanovova, A., Mlcochova, P., Konvalinka, J., Rulisek, L. and Lubkowski, J., Biochemistry, 2009. **48**(19):4126-4138.
109. Tykvart, J., Schimer, J., Barinkova, J., Pachl, P., Postova-Slavetinska, L., Majer, P.*, et al.*, Bioorg. Med. Chem., 2014. **22**(15):4099-4108.
110. Hlouchova, K., Barinka, C., Konvalinka, J. and Lubkowski, J., FEBS J, 2009. **276**(16):4448-4462.
111. Rajasekaran, A.K., Anilkumar, G. and Christiansen, J.J., Am. J. Physiol. Cell. Physiol., 2005. **288**(5):C975-981.
112. Rajasekaran, S.A., Anilkumar, G., Oshima, E., Bowie, J.U., Liu, H., Heston, W.*, et al.*, Mol. Biol. Cell, 2003. **14**(12):4835-4845.
113. Anilkumar, G., Rajasekaran, S.A., Wang, S., Hankinson, O., Bander, N.H. and Rajasekaran, A.K., Cancer Res., 2003. **63**(10):2645-2648.
114. Conway, R.E., Petrovic, N., Li, Z., Heston, W., Wu, D. and Shapiro, L.H., Mol. Cell. Biol., 2006. **26**(14):5310-5324.
115. Conway, R.E., Joiner, K., Patterson, A., Bourgeois, D., Rampp, R., Hannah, B.C.*, et al.*, Angiogenesis, 2013. **16**(4):847-860.
116. Conway, R.E., Rojas, C., Alt, J., Novakova, Z., Richardson, S.M., Rodrick, T.C.*, et al.*, Angiogenesis, 2016. **19**(4):487-500.
117. Colombatti, M., Grasso, S., Porzia, A., Fracasso, G., Scupoli, M.T., Cingarlini, S.*, et al.*, Plos One, 2009. **4**(2):e4608.
118. Rajasekaran, S.A., Christiansen, J.J., Schmid, I., Oshima, E., Ryazantsev, S., Sakamoto, K.*, et al.*, Mol. Cancer Ther., 2008. **7**(7):2142-2151.

119. Chen, Y., Dhara, S., Banerjee, S.R., Byun, Y., Pullambhatla, M., Mease, R.C. and Pomper, M.G., Biochem. Biophys. Res. Commun., 2009. **390**(3):624-629.
120. Novakova, Z., Foss, C.A., Copeland, B.T., Morath, V., Baranova, P., Havlinova, B.*, et al.*, Prostate, 2017. **77**(7):749-764.
121. Foss, C.A., Mease, R.C., Fan, H., Wang, Y., Ravert, H.T., Dannals, R.F.*, et al.*, Clin. Cancer Res., 2005. **11**(11):4022-4028.
122. Maresca, K.P., Hillier, S.M., Femia, F.J., Keith, D., Barone, C., Joyal, J.L.*, et al.*, J. Med. Chem., 2009. **52**(2):347-357.
123. Banerjee, S.R., Foss, C.A., Castanares, M., Mease, R.C., Byun, Y., Fox, J.J.*, et al.*, J. Med. Chem., 2008. **51**(15):4504-4517.
124. Mease, R.C., Dusich, C.L., Foss, C.A., Ravert, H.T., Dannals, R.F., Seidel, J.*, et al.*, Clin. Cancer Res., 2008. **14**(10):3036-3043.
125. Chen, Y., Pullambhatla, M., Banerjee, S.R., Byun, Y., Stathis, M., Rojas, C.*, et al.*, Bioconjug. Chem., 2012. **23**(12):2377-2385.
126. Benesova, M., Bauder-Wust, U., Schafer, M., Klika, K.D., Mier, W., Haberkorn, U.*, et al.*, J. Med. Chem., 2016. **59**(5):1761-1775.
127. Benesova, M., Schafer, M., Bauder-Wust, U., Afshar-Oromieh, A., Kratochwil, C., Mier, W.*, et al.*, J. Nucl. Med., 2015. **56**(6):914-920.
128. Eder, M., Schafer, M., Bauder-Wust, U., Hull, W.E., Wangler, C., Mier, W.*, et al.*, Bioconjug. Chem., 2012. **23**(4):688-697.
129. Henry, M.D., Wen, S., Silva, M.D., Chandra, S., Milton, M. and Worland, P.J., Cancer Res., 2004. **64**(21):7995-8001.
130. Wolf, P., Alt, K., Wetterauer, D., Buhler, P., Gierschner, D., Katzenwadel, A.*, et al.*, J. Immunother., 2010. **33**(3):262-271.
131. Ma, D., Hopf, C.E., Malewicz, A.D., Donovan, G.P., Senter, P.D., Goeckeler, W.F.*, et al.*, Clin. Cancer Res., 2006. **12**(8):2591-2596.
132. DiPippo, V.A., Olson, W.C., Nguyen, H.M., Brown, L.G., Vessella, R.L. and Corey, E., Prostate, 2015. **75**(3):303-313.
133. Kumar, A., Mastren, T., Wang, B., Hsieh, J.T., Hao, G. and Sun, X., Bioconjug. Chem., 2016. **27**(7):1681-1689.
134. Bacich, D.J., Pinto, J.T., Tong, W.P. and Heston, W.D., Mamm. Genome, 2001. **12**(2):117-123.
135. Tsai, G., Dunham, K.S., Drager, U., Grier, A., Anderson, C., Collura, J. and Coyle, J.T., Synapse, 2003. **50**(4):285-292.
136. Han, L., Picker, J.D., Schaevitz, L.R., Tsai, G., Feng, J., Jiang, Z.*, et al.*, Synapse, 2009. **63**(8):625-635.
137. Gao, Y., Xu, S., Cui, Z., Zhang, M., Lin, Y., Cai, L.*, et al.*, J. Neurochem., 2015. **134**(2):340-353.
138. Cao, Y., Gao, Y., Xu, S., Bao, J., Lin, Y., Luo, X.*, et al.*, BMC Neurosci., 2016. **17**:15.
139. Barinka, C., Rinnova, M., Sacha, P., Rojas, C., Majer, P., Slusher, B.S. and Konvalinka, J., J. Neurochem., 2002. **80**(3):477-487.
140. Stoermer, D., Liu, Q., Hall, M.R., Flanary, J.M., Thomas, A.G., Rojas, C.*, et al.*, Bioorg. Med. Chem. Lett., 2003. **13**(13):2097-2100.
141. Jackson, P.F., Tays, K.L., Maclin, K.M., Ko, Y.S., Li, W., Vitharana, D.*, et al.*, J. Med. Chem., 2001. **44**(24):4170-4175.
142. Liu, T., Toriyabe, Y., Kazak, M. and Berkman, C.E., Biochemistry, 2008. **47**(48):12658-12660.
143. Kozikowski, A.P., Zhang, J., Nan, F., Petukhov, P.A., Grajkowska, E., Wroblewski, J.T.*, et al.*, J. Med. Chem., 2004. **47**(7):1729-1738.
144. Chen, Y., Foss, C.A., Byun, Y., Nimmagadda, S., Pullambhatla, M., Fox, J.J.*, et al.*, J. Med. Chem., 2008. **51**(24):7933-7943.

145. Novakova, Z., Wozniak, K., Jancarik, A., Rais, R., Wu, Y., Pavlicek, J., *et al.*, J. Med. Chem., 2016. **59**(10):4539-4550.
146. Ferraris, D.V., Shukla, K. and Tsukamoto, T., Curr. Med. Chem., 2012. **19**(9):1282-1294.
147. Zhou, J., Neale, J.H., Pomper, M.G. and Kozikowski, A.P., Nat. Rev. Drug. Discov., 2005. **4**(12):1015-1026.
148. Tsukamoto, T., Majer, P., Vitharana, D., Ni, C.Y., Hin, B., Lu, X.C.M., *et al.*, J. Med. Chem., 2005. **48**(7):2319-2324.
149. Neale, J.H., Olszewski, R.T., Gehl, L.M., Wroblewska, B. and Bzdega, T., Trends Pharmacol. Sci., 2005. **26**(9):477-484.
150. Zhong, C., Luo, Q. and Jiang, J., Int. J. Neurosci., 2014. **124**(12):867-873.
151. Yamamoto, T., Saito, O., Aoe, T., Bartolozzi, A., Sarva, J., Zhou, J., *et al.*, Eur. J. Neurosci., 2007. **25**(1):147-158.
152. Feng, J.F., Van, K.C., Gurkoff, G.G., Kopriva, C., Olszewski, R.T., Song, M., *et al.*, Brain Res., 2011. **1395**:62-73.
153. Wozniak, K.M., Wu, Y., Vornov, J.J., Lapidus, R., Rais, R., Rojas, C., *et al.*, J. Pharmacol. Exp. Ther., 2012. **343**(3):746-754.
154. Ferraris, D.V., Majer, P., Ni, C., Slusher, C.E., Rais, R., Wu, Y., *et al.*, J. Med. Chem., 2014. **57**(1):243-247.
155. Nedelcovych, M., Dash, R.P., Tenora, L., Zimmermann, S.C., Gadiano, A.J., Garrett, C., *et al.*, Mol. Pharm., 2017. **14**(10):3248-3257.
156. Majer, P., Jancarik, A., Krecmerova, M., Tichy, T., Tenora, L., Wozniak, K., *et al.*, J. Med. Chem., 2016. **59**(6):2810-2819.
157. Rais, R., Vavra, J., Tichy, T., Dash, R.P., Gadiano, A.J., Tenora, L., *et al.*, J. Med. Chem., 2017. **60**(18):7799-7809.
158. Alquicer, G., Sedlak, D., Byun, Y., Pavlicek, J., Stathis, M., Rojas, C., *et al.*, J. Biomol. Screen., 2012. **17**(8):1030-1040.
159. Attard, G., Parker, C., Eeles, R.A., Schroder, F., Tomlins, S.A., Tannock, I., *et al.*, Lancet, 2016. **387**(10013):70-82.
160. Cuccurullo, V., Di Stasio, G.D. and Mansi, L., World J. Nucl. Med., 2018. **17**(2):70-78.
161. Moyer, V.A. and Force, U.S.P.S.T., Ann. Intern. Med., 2012. **157**(2):120-134.
162. Schroder, F.H., Hugosson, J., Roobol, M.J., Tammela, T.L., Ciatto, S., Nelen, V., *et al.*, N. Engl. J. Med., 2009. **360**(13):1320-1328.
163. Evans, J.D., Jethwa, K.R., Ost, P., Williams, S., Kwon, E.D., Lowe, V.J. and Davis, B.J., Pract. Radiat. Oncol., 2018. **8**(1):28-39.
164. Kopka, K., Benesova, M., Barinka, C., Haberkorn, U. and Babich, J., J. Nucl. Med., 2017. **58**(Suppl 2):17S-26S.
165. Lutje, S., Heskamp, S., Cornelissen, A.S., Poeppel, T.D., van den Broek, S.A., Rosenbaum-Krumme, S., *et al.*, Theranostics, 2015. **5**(12):1388-1401.
166. Emmett, L., Willowson, K., Violet, J., Shin, J., Blanksby, A. and Lee, J., J. Med. Radiat. Sci., 2017. **64**(1):52-60.
167. Eiber, M., Fendler, W.P., Rowe, S.P., Calais, J., Hofman, M.S., Maurer, T., *et al.*, J. Nucl. Med., 2017. **58**(Suppl 2):67S-76S.
168. Bander, N.H., Nat. Clin. Pract. Urol., 2006. **3**(4):216-225.
169. Bander, N.H., Trabulsi, E.J., Kostakoglu, L., Yao, D., Vallabhajosula, S., Smith-Jones, P., *et al.*, J. Urol., 2003. **170**(5):1717-1721.
170. Osborne, J.R., Green, D.A., Spratt, D.E., Lyashchenko, S., Fareedy, S.B., Robinson, B.D., *et al.*, J. Urol., 2014. **191**(5):1439-1445.
171. Giesel, F.L., Hadaschik, B., Cardinale, J., Radtke, J., Vinsensia, M., Lehnert, W., *et al.*, Eur. J. Nucl. Med. Mol. Imaging, 2017. **44**(4):678-688.
172. Foss, C.A., Mease, R.C., Cho, S.Y., Kim, H.J. and Pomper, M.G., Curr. Med. Chem., 2012. **19**(9):1346-1359.

173. Cardinale, J., Schafer, M., Benesova, M., Bauder-Wust, U., Leotta, K., Eder, M.*, et al.*, J. Nucl. Med., 2017. **58**(3):425-431.
174. Hillier, S.M., Maresca, K.P., Lu, G., Merkin, R.D., Marquis, J.C., Zimmerman, C.N.*, et al.*, J. Nucl. Med., 2013. **54**(8):1369-1376.
175. Osborne, J., Akhtar, N.H., Vallabhajosula, S., Nikolopoulou, A., Maresca, K.P., Hillier, S.M.*, et al.*, J. Clin. Oncol., 2012. **30**(5).
176. Robu, S., Schottelius, M., Eiber, M., Maurer, T., Gschwend, J., Schwaiger, M. and Wester, H.J., J. Nucl. Med., 2017. **58**(2):235-242.
177. Hillier, S.M., Maresca, K.P., Femia, F.J., Marquis, J.C., Foss, C.A., Nguyen, N.*, et al.*, Cancer Res., 2009. **69**(17):6932-6940.
178. Afshar-Oromieh, A., Avtzi, E., Giesel, F.L., Holland-Letz, T., Linhart, H.G., Eder, M.*, et al.*, Eur. J. Nucl. Med. Mol. Imaging, 2015. **42**(2):197-209.
179. Bluemel, C., Krebs, M., Polat, B., Linke, F., Eiber, M., Samnick, S.*, et al.*, Clin. Nucl. Med., 2016. **41**(7):515-521.
180. Eiber, M., Maurer, T., Souvatzoglou, M., Beer, A.J., Ruffani, A., Haller, B.*, et al.*, J. Nucl. Med., 2015. **56**(5):668-674.
181. Morigi, J.J., Stricker, P.D., van Leeuwen, P.J., Tang, R., Ho, B., Nguyen, Q.*, et al.*, J. Nucl. Med., 2015. **56**(8):1185-1190.
182. Schwenck, J., Rempp, H., Reischl, G., Kruck, S., Stenzl, A., Nikolaou, K.*, et al.*, Eur. J. Nucl. Med. Mol Imaging, 2017. **44**(1):92-101.
183. Verburg, F.A., Pfister, D., Heidenreich, A., Vogg, A., Drude, N.I., Voo, S.*, et al.*, Eur. J. Nucl. Med. Mol Imaging, 2016. **43**(3):397-403.
184. Perera, M., Papa, N., Christidis, D., Wetherell, D., Hofman, M.S., Murphy, D.G.*, et al.*, Eur. Urol., 2016. **70**(6):926-937.
185. Afshar-Oromieh, A., Haberkorn, U., Eder, M., Eisenhut, M. and Zechmann, C.M., Eur. J. Nucl. Med. Mol. Imaging, 2012. **39**(6):1085-1086.
186. Afshar-Oromieh, A., Zechmann, C.M., Malcher, A., Eder, M., Eisenhut, M., Linhart, H.G.*, et al.*, Eur. J. Nucl. Med. Mol. Imaging, 2014. **41**(1):11-20.
187. Eiber, M., Weirich, G., Holzapfel, K., Souvatzoglou, M., Haller, B., Rauscher, I.*, et al.*, Eur. Urol, 2016. **70**(5):829-836.
188. Fendler, W.P., Schmidt, D.F., Wenter, V., Thierfelder, K.M., Zach, C., Stief, C.*, et al.*, J. Nucl. Med., 2016. **57**(11):1720-1725.
189. Rahbar, K., Weckesser, M., Huss, S., Semjonow, A., Breyholz, H.J., Schrader, A.J.*, et al.*, J. Nucl. Med., 2016. **57**(4):563-567.
190. Zamboglou, C., Drendel, V., Jilg, C.A., Rischke, H.C., Beck, T.I., Schultze-Seemann, W.*, et al.*, Theranostics, 2017. **7**(1):228-237.
191. Maurer, T., Gschwend, J.E., Rauscher, I., Souvatzoglou, M., Haller, B., Weirich, G.*, et al.*, J. Urol., 2016. **195**(5):1436-1443.
192. Berliner, C., Tienken, M., Frenzel, T., Kobayashi, Y., Helberg, A., Kirchner, U.*, et al.*, Eur. J. Nucl. Med. Mol. Imaging, 2017. **44**(4):670-677.
193. Rauscher, I., Duwel, C., Wirtz, M., Schottelius, M., Wester, H.J., Schwamborn, K.*, et al.*, Bju Int., 2017. **120**(1):40-47.
194. Cho, S.Y., Gage, K.L., Mease, R.C., Senthamizhchelvan, S., Holt, D.P., Jeffrey-Kwanisai, A.*, et al.*, J. Nucl. Med., 2012. **53**(12):1883-1891.
195. Rowe, S.P., Gage, K.L., Faraj, S.F., Macura, K.J., Cornish, T.C., Gonzalez-Roibon, N.*, et al.*, J. Nucl. Med., 2015. **56**(7):1003-1010.
196. Rowe, S.P., Macura, K.J., Ciarallo, A., Mena, E., Blackford, A., Nadal, R.*, et al.*, J. Nucl. Med., 2016. **57**(1):46-53.
197. Dietlein, M., Kobe, C., Kuhnert, G., Stockter, S., Fischer, T., Schomacker, K.*, et al.*, Mol. Imaging Biol., 2015. **17**(4):575-584.

198. Rowe, S.P., Macura, K.J., Mena, E., Blackford, A.L., Nadal, R., Antonarakis, E.S., *et al.*, Mol. Imaging Biol., 2016. **18**(3):411-419.
199. Szabo, Z., Mena, E., Rowe, S.P., Plyku, D., Nidal, R., Eisenberger, M.A., *et al.*, Mol. Imaging Biol., 2015. **17**(4):565-574.
200. Giesel, F.L., Kesch, C., Yun, M., Cardinale, J., Haberkorn, U., Kopka, K., *et al.*, Clin. Genitourin. Cancer, 2017. **15**(3):e497-e499.
201. Barrett, J.A., Coleman, R.E., Goldsmith, S.J., Vallabhajosula, S., Petry, N.A., Cho, S., *et al.*, J. Nucl. Med., 2013. **54**(3):380-387.
202. Zechmann, C.M., Afshar-Oromieh, A., Armor, T., Stubbs, J.B., Mier, W., Hadaschik, B., *et al.*, Eur. J. Nucl. Med. Mol. Imaging, 2014. **41**(7):1280-1292.
203. Vallabhajosula, S., Nikolopoulou, A., Babich, J.W., Osborne, J.R., Tagawa, S.T., Lipai, I., *et al.*, J. Nucl. Med., 2014. **55**(11):1791-1798.
204. Chen, Y., Chatterjee, S., Lisok, A., Minn, I., Pullambhatla, M., Wharram, B., *et al.*, J. Photochem. Photobiol. B, 2017. **167**:111-116.
205. Neuman, B.P., Eifler, J.B., Castanares, M., Chowdhury, W.H., Chen, Y., Mease, R.C., *et al.*, Clin. Cancer Res., 2015. **21**(4):771-780.
206. Banerjee, S.R., Foss, C.A., Horhota, A., Pullambhatla, M., McDonnell, K., Zale, S. and Pomper, M.G., Biomacromolecules, 2017. **18**(1):201-209.
207. Chen, Z., Penet, M.F., Krishnamachary, B., Banerjee, S.R., Pomper, M.G. and Bhujwalla, Z.M., Biomaterials, 2016. **80**:57-67.
208. Chen, Z., Penet, M.F., Nimmagadda, S., Li, C., Banerjee, S.R., Winnard, P.T., Jr., *et al.*, ACS Nano, 2012. **6**(9):7752-7762.
209. Deb, N., Goris, M., Trisler, K., Fowler, S., Saal, J., Ning, S., *et al.*, Clin. Cancer Res., 1996. **2**(8):1289-1297.
210. Kahn, D., Austin, J.C., Maguire, R.T., Miller, S.J., Gerstbrein, J. and Williams, R.D., Cancer Biother. Radiopharm., 1999. **14**(2):99-111.
211. Bander, N.H., Milowsky, M.I., Nanus, D.M., Kostakoglu, L., Vallabhajosula, S. and Goldsmith, S.J., J. Clin. Oncol., 2005. **23**(21):4591-4601.
212. Tagawa, S.T., Milowsky, M.I., Morris, M., Vallabhajosula, S., Christos, P., Akhtar, N.H., *et al.*, Clin. Cancer Res., 2013. **19**(18):5182-5191.
213. Milowsky, M.I., Galsky, M.D., Morris, M.J., Crona, D.J., George, D.J., Dreicer, R., *et al.*, Urol. Oncol., 2016. **34**(12):530 e515-530 e521.
214. Ahmadzadehfar, H., Eppard, E., Kurpig, S., Fimmers, R., Yordanova, A., Schlenkhoff, C.D., *et al.*, Oncotarget, 2016. **7**(11):12477-12488.
215. Ahmadzadehfar, H., Rahbar, K., Kurpig, S., Bogemann, M., Claesener, M., Eppard, E., *et al.*, EJNMMI Res., 2015. **5**(1):114.
216. Ahmadzadehfar, H., Wegen, S., Yordanova, A., Fimmers, R., Kurpig, S., Eppard, E., *et al.*, Eur. J. Nucl. Med. Mol. Imaging, 2017. **44**(9):1448-1454.
217. Baum, R.P., Kulkarni, H.R., Schuchardt, C., Singh, A., Wirtz, M., Wiessalla, S., *et al.*, J. Nucl. Med., 2016. **57**(7):1006-1013.
218. Brauer, A., Grubert, L.S., Roll, W., Schrader, A.J., Schafers, M., Bogemann, M. and Rahbar, K., Eur. J. Nucl. Med. Mol. Imaging, 2017. **44**(10):1663-1670.
219. Kratochwil, C., Giesel, F.L., Stefanova, M., Benesova, M., Bronzel, M., Afshar-Oromieh, A., *et al.*, J. Nucl. Med., 2016. **57**(8):1170-1176.
220. Rahbar, K., Ahmadzadehfar, H., Kratochwil, C., Haberkorn, U., Schafers, M., Essler, M., *et al.*, J. Nucl. Med., 2017. **58**(1):85-90.
221. Rahbar, K., Bode, A., Weckesser, M., Avramovic, N., Claesener, M., Stegger, L. and Bogemann, M., Clin. Nucl. Med., 2016. **41**(7):522-528.
222. Rahbar, K., Boegemann, M., Yordanova, A., Eveslage, M., Schafers, M., Essler, M. and Ahmadzadehfar, H., Eur. J. Nucl. Med. Mol. I, 2018. **45**(1):12-19.

223. Rahbar, K., Bogeman, M., Yordanova, A., Eveslage, M., Schafers, M., Essler, M. and Ahmadzadehfar, H., Eur. J. Nucl. Med. Mol. Imaging, 2018. **45**(2):243-246.
224. Rahbar, K., Schmidt, M., Heinzel, A., Eppard, E., Bode, A., Yordanova, A.*, et al.*, J. Nucl. Med., 2016. **57**(9):1334-1338.
225. Kratochwil, C., Bruchertseifer, F., Giesel, F.L., Weis, M., Verburg, F.A., Mottaghy, F.*, et al.*, J. Nucl. Med., 2016. **57**(12):1941-1944.
226. Kratochwil, C., Bruchertseifer, F., Rathke, H., Bronzel, M., Apostolidis, C., Weichert, W.*, et al.*, J. Nucl. Med., 2017. **58**(10):1624-1631.
227. Kratochwil, C., Bruchertseifer, F., Rathke, H., Hohenfellner, M., Giesel, F.L., Haberkorn, U. and Morgenstern, A., J. Nucl. Med., 2018. **59**(5):795-802.
228. Heck, M., Schwaiger, S., Knorr, K., Retz, M., Maurer, T., Janssen, F.*, et al.*, J. Urology, 2018. **199**(4):E304-E304.
229. Afshar-Oromieh, A., Haberkorn, U., Zechmann, C., Armor, T., Mier, W., Spohn, F.*, et al.*, Eur. J. Nucl. Med. Mol. Imaging, 2017. **44**(6):950-959.
230. Yadav, M.P., Ballal, S., Tripathi, M., Damle, N.A., Sahoo, R.K., Seth, A. and Bal, C., Eur. J. Nucl. Med. Mol. Imaging, 2017. **44**(1):81-91.
231. Lequin, R.M., Clinical Chemistry, 2005. **51**(12):2415-2418.
232. Engvall, E. and Perlmann, P., Immunochemistry, 1971. **8**(9):871-&.
233. Yalow, R.S. and Berson, S.A., J Clin. Invest., 1960. **39**(7):1157-1175.
234. Goka, A.K.J. and Farthing, M.J.G., J. Immunoassay, 1987. **8**(1):29-41.
235. Khan, P., Idrees, D., Moxley, M.A., Corbett, J.A., Ahmad, F., von Figura, G.*, et al.*, Appl. Biochem. Biotech., 2014. **173**(2):333-355.
236. Natrajan, A., Sharpe, D., Costello, J. and Jiang, Q., Anal. Biochem., 2010. **406**(2):204-213.
237. Sano, T., Smith, C.L. and Cantor, C.R., Science, 1992. **258**(5079):120-122.
238. Ruzicka, V., Marz, W., Russ, A. and Gross, W., Science, 1993. **260**(5108):698-699.
239. Hendrickson, E.R., Truby, T.M., Joerger, R.D., Majarian, W.R. and Ebersole, R.C., Nucleic Acids Res., 1995. **23**(3):522-529.
240. Niemeyer, C.M., Adler, M. and Wacker, R., Nat. Protoc., 2007. **2**(8):1918-1930.
241. Niemeyer, C.M., Adler, M. and Wacker, R., Trends Biotechnol., 2005. **23**(4):208-216.
242. Thaxton, C.S., Elghanian, R., Thomas, A.D., Stoeva, S.I., Lee, J.S., Smith, N.D.*, et al.*, P. Natl. Acad. Sci. U.S.A., 2009. **106**(44):18437-18442.
243. Dressler, F., Whalen, J.A., Reinhardt, B.N. and Steere, A.C., J. Infect. Dis., 1993. **167**(2):392-400.
244. Hauser, U., Lehnert, G., Lobentanzer, R. and Wilske, B., J. Clin. Microbiol., 1997. **35**(6):1433-1444.
245. Mavin, S., Evans, R., Cornulier, T. and Bowman, A.S., J. Microbiol. Meth., 2018. **146**:71-76.
246. Papadopuloseleopulos, E., Turner, V.F. and Papadimitriou, J.M., Biotechnol., 1993. **11**(6):696-707.
247. Branson, B.M., J. Acq. Imm. Def., 2010. **55**:S102-S105.
248. Gowda, S., Desai, P.B., Hull, V.V., Math, A.A., Vernekar, S.N. and Kulkarni, S.S., Pan Afr. Med. J., 2009. **3**:17.
249. Kim, W.R., Flamm, S.L., Di Bisceglie, A.M., Bodenheimer, H.C. and A, P.P.C.A., Hepatology, 2008. **47**(4):1363-1370.
250. Huang, X.J., Choi, Y.K., Im, H.S., Yarimaga, O., Yoon, E. and Kim, H.S., Sensors-Basel, 2006. **6**(7):756-782.
251. de Bono, J.P., Warrick, N., Bendall, J.K., Channon, K.M. and Alp, N.J., Nitric Oxide, 2007. **16**(1):1-9.
252. Livak, K.J. and Schmittgen, T.D., Methods, 2001. **25**(4):402-408.
253. Schmittgen, T.D., Zakrajsek, B.A., Mills, A.G., Gorn, V., Singer, M.J. and Reed, M.W., Anal. Biochem., 2000. **285**(2):194-204.

254. Bustin, S.A., Benes, V., Garson, J.A., Hellemans, J., Huggett, J., Kubista, M.*, et al.*, Clin. Chem., 2009. **55**(4):611-622.
255. Zheng, C.J., Han, L.Y., Yap, C.W., Ji, Z.L., Cao, Z.W. and Chen, Y.Z., Pharmacol. Rev., 2006. **58**(2):259-279.
256. Hopkins, A.L. and Groom, C.R., Nat. Rev. Drug. Discov., 2002. **1**(9):727-730.
257. Hughes, J.P., Rees, S., Kalindjian, S.B. and Philpott, K.L., Brit. J. Pharmacol., 2011. **162**(6):1239-1249.
258. Grant, S.K., Sklar, J.G. and Cummings, R.T., J. Biomol. Screen., 2002. **7**(6):531-540.
259. Pierrat, O.A., Strisovsky, K., Christova, Y., Large, J., Ansell, K., Bouloc, N.*, et al.*, ACS Chem. Biol., 2011. **6**(4):325-335.
260. Charter, N.W., Kauffman, L., Singh, R. and Eglen, R.M., J. Biomol. Screen., 2006. **11**(4):390-399.
261. Inglese, J., Johnson, R.L., Simeonov, A., Xia, M., Zheng, W., Austin, C.P. and Auld, D.S., Nat. Chem. Biol., 2007. **3**(8):466-479.
262. Lowery, R.G. and Kleman-Leyer, K., Expert Opin. Ther. Tar., 2006. **10**(1):179-190.
263. Banks, P., Gosselin, M. and Prystay, L., J. Biomol. Screen., 2000. **5**(3):159-168.
264. Parker, G.J., Law, T.L., Lenoch, F.J. and Bolger, R.E., J. Biomol. Screen., 2000. **5**(2):77-88.
265. Karaman, M.W., Herrgard, S., Treiber, D.K., Gallant, P., Atteridge, C.E., Campbell, B.T.*, et al.*, Nat. Biotechnol., 2008. **26**(1):127-132.
266. Bachovchin, D.A., Koblan, L.W., Wu, W., Liu, Y., Li, Y., Zhao, P.*, et al.*, Nat. Chem. Biol., 2014. **10**(8):656-663.
267. Pantoliano, M.W., Petrella, E.C., Kwasnoski, J.D., Lobanov, V.S., Myslik, J., Graf, E.*, et al.*, J. Biomol. Screen., 2001. **6**(6):429-440.
268. Gee, K.R., Brown, K.A., Chen, W.N.U., Bishop-Stewart, J., Gray, D. and Johnson, I., Cell. Calcium, 2000. **27**(2):97-106.
269. Zheng, W., Spencer, R.H. and Kiss, L., Assay Drug Dev. Techn., 2004. **2**(5):543-552.
270. Eglen, R.M. and Singh, R., Comb. Chem. High Throughput Screen., 2003. **6**(4):381-387.
271. Boute, N., Jockers, R. and Issad, T., Trends Pharmacol. Sci., 2002. **23**(8):351-354.
272. Gasparri, F., Expert Opin. Drug. Dis., 2009. **4**(6):643-657.
273. Zanella, F., Lorens, J.B. and Link, W., Trends in Biotechnology, 2010. **28**(5):237-245.
274. Barinka, C., Rinnova, M., Sacha, P., Rojas, C., Majer, P., Slusher, B.S. and Konvalinka, J., J. Neurochem., 2002. **80**(3):477-487.
275. Catalona, W.J., Richie, J.P., Ahmann, F.R., Hudson, M.A., Scardino, P.T., Flanigan, R.C.*, et al.*, J. Urology, 1994. **151**(5):1283-1290.
276. Eifler, J.B., Feng, Z., Lin, B.M., Partin, M.T., Humphreys, E.B., Han, M.*, et al.*, Bju Int., 2013. **111**(1):22-29.
277. Wilt, T.J., J. Natl. Cancer Inst. Monogr., 2012. **2012**(45):184-190.
278. Bill-Axelson, A., Holmberg, L., Garmo, H., Rider, J.R., Taari, K., Busch, C.*, et al.*, N. Engl. J. Med., 2014. **370**(10):932-942.
279. Hamdy, F.C., Donovan, J.L., Lane, J.A., Mason, M., Metcalfe, C., Holding, P.*, et al.*, N. Engl. J. Med., 2016. **375**(15):1415-1424.
280. Murphy, G.P., Kenny, G.M., Ragde, H., Wolfert, R.L., Boynton, A.L., Holmes, E.H.*, et al.*, Urology, 1998. **51**(5A):89-97.
281. Gingras, R., Richard, C., El-Alfy, M., Morales, C.R., Potier, M. and Pshezhetsky, A.V., J. Biol. Chem., 1999. **274**(17):11742-11750.
282. Zajc, T., Suban, D., Rajkovic, J. and Dolenc, I., Protein Expr. Purif., 2011. **75**(2):119-126.
283. Zavada, J., Zavadova, Z., Zat'ovicova, M., Hyrsl, L. and Kawaciuk, I., Brit. J. Cancer, 2003. **89**(6):1067-1071.
284. Sim, S.H., Messenger, M.P., Gregory, W.M., Wind, T.C., Vasudev, N.S., Cartledge, J.*, et al.*, Brit. J. Cancer, 2012. **107**(7):1131-1137.

285. Murphy, G.P., Maguire, R.T., Rogers, B., Partin, A.W., Nelp, W.B., Troychak, M.J., *et al.*, Prostate, 1997. **33**(4):281-285.
286. Rochon, Y.P., Horoszewicz, J.S., Boynton, A.L., Holmes, E.H., Barren, R.J., Erickson, S.J., *et al.*, Prostate, 1994. **25**(4):219-223.
287. Esmaeili, E., Ghiass, M.A., Vossoughi, M. and Soleimani, M., Sci. Rep., 2017. **7**(1):194.
288. Kadimisetty, K., Malla, S., Sardesai, N.P., Joshi, A.A., Faria, R.C., Lee, N.H. and Rusling, J.F., Analytical Chemistry, 2015. **87**(8):4472-4478.
289. Kadimisetty, K., Mosa, I.M., Malla, S., Satterwhite-Warden, J.E., Kuhns, T.M., Faria, R.C., *et al.*, Biosens. Bioelectron., 2016. **77**:188-193.
290. Liu, J., Lu, C.Y., Zhou, H., Xu, J.J. and Chen, H.Y., ACS Appl. Mater. Interfaces, 2014. **6**(22):20137-20143.
291. Liu, N., Liang, W., Ma, X., Li, X., Ning, B., Cheng, C., *et al.*, Biosens. Bioelectron., 2013. **47**:92-98.
292. Mohan, K., Donavan, K.C., Arter, J.A., Penner, R.M. and Weiss, G.A., Journal of the American Chemical Society, 2013. **135**(20):7761-7767.
293. Tardivo, M., Toffoli, V., Fracasso, G., Borin, D., Dal Zilio, S., Colusso, A., *et al.*, Biosens. Bioelectron., 2015. **72**:393-399.
294. Vik, V., Ph.D. Thesis, 2014. Masaryk University in Brno.
295. Balk, S.P., Ko, Y.J. and Bubley, G.J., J. Clin. Oncol., 2003. **21**(2):383-391.
296. Diamandis, E.P. and Yu, H., Urol. Clin. North. Am., 1997. **24**(2):275-282.
297. Fredriksson, S., Dixon, W., Ji, H., Koong, A.C., Mindrinos, M. and Davis, R.W., Nat. Methods, 2007. **4**(4):327-329.
298. Lundberg, M., Eriksson, A., Tran, B., Assarsson, E. and Fredriksson, S., Nucleic Acids Res., 2011. **39**(15).
299. Rich, D.H., Bernatowicz, M.S., Agarwal, N.S., Kawai, M., Salituro, F.G. and Schmidt, P.G., Biochemistry, 1985. **24**(13):3165-3173.
300. Supuran, C.T., Nat. Rev. Drug. Discov., 2008. **7**(2):168-181.

7. Appendix: Reprints of the publications described in the thesis

7.1. Publication I

Navratil, M., Tykvart, J., Schimer, J., Pachl, P., Navratil, V., Rokob, T.A., Hlouchova, K., Rulisek, L., and Konvalinka, J.:

Comparison of human glutamate carboxypeptidases II and III reveals their divergent substrate specificities.

FEBS J 2016, 283(13):2528-2545.

Supplementary information Data S1 containing pdb structures is available online.

The FEBS Journal

FEBS PRESS science publishing by scientists

Comparison of human glutamate carboxypeptidases II and III reveals their divergent substrate specificities

Michal Navrátil[1,2], Jan Tykvart[1,2], Jiří Schimer[1,2], Petr Pachl[1], Václav Navrátil[1,2], Tibor András Rokob[3], Klára Hlouchová[1,2], Lubomír Rulíšek[1] and Jan Konvalinka[1,2]

1 Institute of Organic Chemistry and Biochemistry, Gilead Sciences and IOCB Research Centre, Academy of Sciences of the Czech Republic, Prague, Czech Republic
2 Department of Biochemistry, Faculty of Natural Sciences, Charles University in Prague, Czech Republic
3 Institute of Organic Chemistry, Research Centre for Natural Sciences, Hungarian Academy of Sciences, Budapest, Hungary

Keywords
arene-binding site; GCPIII; prostate-specific membrane antigen; QM/MM calculations; β-citryl-L-glutamate

Correspondence
J. Konvalinka, Institute of Organic Chemistry and Biochemistry, Gilead Sciences and IOCB Research Centre, Academy of Sciences of the Czech Republic, Flemingovo n. 2, 166 10 Prague, Czech Republic
Fax: +420 220 183 578
Tel: +420 220 183 218
E-mail: konval@uochb.cas.cz

(Received 10 March 2016, revised 25 April 2016, accepted 18 May 2016)

doi:10.1111/febs.13761

Glutamate carboxypeptidase III (GCPIII) is best known as a homologue of glutamate carboxypeptidase II [GCPII; also known as prostate-specific membrane antigen (PSMA)], a protease involved in neurological disorders and overexpressed in a number of solid cancers. However, mouse GCPIII was recently shown to cleave β-citrylglutamate (BCG), suggesting that these two closely related enzymes have distinct functions. To develop a tool to dissect, evaluate and quantify the activities of human GCPII and GCPIII, we analysed the catalytic efficiencies of these enzymes towards three physiological substrates. We observed a high efficiency of BCG cleavage by GCPIII but not GCPII. We also identified a strong modulation of GCPIII enzymatic activity by divalent cations, while we did not observe this effect for GCPII. Additionally, we used X-ray crystallography and computational modelling (quantum and molecular mechanical calculations) to describe the mechanism of BCG binding to the active sites of GCPII and GCPIII, respectively. Finally, we took advantage of the substantial differences in the enzymatic efficiencies of GCPII and GCPIII towards their substrates, using enzymatic assays for specific detection of these proteins in human tissues. Our findings suggest that GCPIII may not act merely as a complementary enzyme to GCPII, and it more likely possesses a specific physiological function related to BCG metabolism in the human body.

Database
The X-ray structure of GCPII Glu424Ala in complex with BCG has been deposited in the RCSB Protein Data Bank under accession code 5F09.

Abbreviations
3D, three-dimensional; AAS, atomic absorption spectroscopy; ABS, arene-binding site; ACN, acetonitrile; BCG, β-citryl-L-glutamic acid (β-citrylglutamate, beta-citrylglutamate, beta-citryl-L-glutamic acid, beta-citryl-L-glutamate); BSA, bovine serum albumin; C12E8, octaethylene glycol monododecyl ether; DBU, 1,8-Diazabicycloundec-7-ene; DIEA, N,N-Diisopropylethylamine; EtOAc, ethylacetate; FolGlu$_n$, folyl-*n*-γ-L-glutamic acid; G3PDH, glyceraldehyde 3-phosphate dehydrogenase; GCPII, glutamate carboxypeptidase II; GCPIII, glutamate carboxypeptidase III; HPLC, high-performance liquid chromatography; HRMS, high-resolution mass spectrometry; MeOH, methanol; MD/MM, molecular dynamical/molecular mechanical calculations; NAAG, *N*-acetyl-L-aspartyl-L-glutamic acid; NMR, nuclear magnetic resonance; OPA, orthophtalaldehyde; ORF, open reading frame; Pd(C), palladium on activated charcoal; PSMA, prostate-specific membrane antigen; QM/MM, quantum mechanical and molecular mechanical calculations; QM/MM/MD, quantum mechanical, molecular mechanical and molecular dynamical calculations; qPCR, quantitative polymerase chain reaction; rhGCPII, recombinant human glutamate carboxypeptidase II; SDS/PAGE, sodium dodecylsulfate polyacrylamide gel electrophoresis; TFA, trifluoroacetic acid; TLC, thin-layer chromatography.

Introduction

Glutamate carboxypeptidase III (GCPIII) is a binuclear zinc metallopeptidase that belongs to the MEROPS M28B peptidase subfamily (ID M28.012) [1]. GCPIII shares 67% sequence identity and 81% sequence similarity with glutamate carboxypeptidase II (GCPII, EC 3.4.17.21), one of the most well-characterized members of the M28B subfamily [2]. Additionally, GCPIII adopts an almost identical 3D structure and possesses very similar enzymatic activity to GCPII [3]. It is also predicted to be a type II transmembrane protein with amino acids 9–31 forming the transmembrane part of the structure [4] and its protease domain facing the extracellular milieu.

The physiological functions of GCPII include degradation of *N*-acetyl-L-aspartyl-L-glutamate (NAAG, Fig. 1), the most abundant peptide neurotransmitter in the brain [3,5], and processing of polyglutamylated folates ($FolGlu_n$, Fig. 1), vitamin B9 precursors, enabling the absorption of free folate in the small intestine [6,7]. Furthermore, GCPII, also known as prostate-specific membrane antigen (PSMA), has been investigated as a promising prostate cancer marker [8,9] and an interesting molecular address for specific anticancer drug delivery [10,11]. Because both GCPII and GCPIII have similar enzymatic activities and there is no specific monoclonal antibody against GCPIII [12], unravelling the distinct physiological functions of GCPII and GCPIII has been challenging.

Until recently, GCPIII was recognized mainly as a potentially complementary enzyme to GCPII. However, in 2011, Collard *et al.* [13] identified a novel physiological substrate for mouse GCPIII, β-citryl-L-glutamic acid (BCG, Fig. 1), which is cleaved to citrate and L-glutamate by GCPIII but not GCPII. Interestingly, the study also showed that the efficiency of NAAG vs. BCG cleavage by GCPIII is metal-dependent. The presence of zinc or manganese ions facilitates NAAG cleavage, and the presence of calcium or manganese ions facilitates cleavage of BCG. The researchers hypothesized that the ability of GCPIII to cleave BCG in the presence of specific metal ions may be caused by replacement of one of its two active site zinc ions by these metals [13].

BCG was first identified as a physiologically relevant molecule in the 1970s, when it was isolated from newborn rat brains [14]. Additionally, BCG-hydrolysing activity, as well as BCG itself, has been detected in rat testes [15,16]. Although BCG has been known for several decades, its precise physiological function remains unclear. One hypothesis suggested that BCG may serve as an endogenous low-molecular-weight chelator of iron or other biogenic metals [17]. However, the recent unambiguous assignment of BCG-hydrolysing activity to GCPIII increased the potential for elucidation of BCG's physiological role. Furthermore, the identification of GCPIII as a BCG hydrolase suggests that GCPIII may not function merely as a compensatory enzyme for GCPII, but may play a different, physiologically relevant role in humans.

We have shown previously that the GCPII tissue expression profile differs in human and animal models, which might have implications for its specific roles [18]. The findings concerning GCPIII/BCG metabolism have been obtained using animal models, mostly mice or rats. GCPIII tissue distribution in the human body is unknown, and it is crucial to validate and properly characterize this novel metal-dependent enzymatic activity for human GCPIII. Therefore, we set out to perform a careful comparative analysis of human GCPII and GCPIII activities towards their physiological substrates NAAG, BCG and polyglutamylated folates. Additionally, we describe the binding of BCG into the active sites of GCPII and GCPIII using X-ray crystallography and high-level (QM/MM) molecular modelling, respectively. Finally, employing the enzymological data, we were able to specifically detect GCPII and GCPIII protein levels in human tissues, a feat that had been impossible to achieve so far.

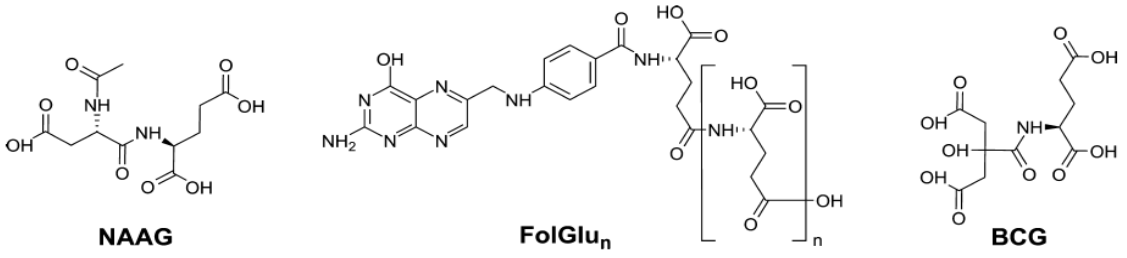

Fig. 1. Chemical structures of investigated substrates. From left to right: *N*-acetyl-L-aspartyl-L-glutamic acid (NAAG), *n*-γ-L-glutamylated folic acid ($FolGlu_n$) and β-citryl-L-glutamic acid (BCG).

Specific molecular recognition of these two close enzyme homologues will enable the use of GCPII as a selective molecular address for the anticancer drug delivery and to validate its potential for the diagnosis and prognosis of prostate cancer.

Results

BCG hydrolysis by GCPIII depends on divalent metal cations

Using recombinant human GCPII and GCPIII [19], we analysed hydrolysis of three physiological substrates in the presence or absence of calcium, manganese(II) and zinc cations. The chemical structures of the tested compounds, NAAG, $FolGlu_n$ and BCG are shown in Fig. 1.

The enzymological data, summarized in Fig. 2, indicate that BCG is selectively hydrolysed by human GCPIII. Although it is also cleaved by GCPII, the catalytic efficiency for the GCPIII-catalysed reaction is up to five orders of magnitude greater [Fig. 2A, k_{cat}/K_M (GCPII) = 1.7×10^2 $s^{-1}\cdot M^{-1}$ vs. k_{cat}/K_M (GCPIII, Ca^{2+}) = 1.33×10^7 $s^{-1}\cdot M^{-1}$]. Additionally, we found that the catalytic efficiency of human GCPIII is highly metal-dependent. The presence of calcium ions increased the BCG cleavage efficiency by two orders of magnitude [k_{cat}/K_M (GCPIII) = 1.8×10^5 $s^{-1}\cdot M^{-1}$ vs. k_{cat}/K_M (GCPIII, Ca^{2+}) = 1.33×10^7 $s^{-1}\cdot M^{-1}$], while zinc ions facilitated NAAG and $FolGlu_1$ cleavage [k_{cat}/K_M (GCPIII, NAAG) = 2.16×10^5 $s^{-1}\cdot M^{-1}$ vs. k_{cat}/K_M (GCPIII, NAAG, Zn^{2+}) = 2.27×10^6 $s^{-1}\cdot M^{-1}$]. Manganese ions seemed to increase GCPIII activity towards all tested substrates. The activation effect of these divalent cations is mainly driven by an increase in k_{cat} values, while the K_M values are less affected (Fig. 2B,C). Importantly, we also tested the ability of these cations to activate GCPII, and we did not observe any notable metal-dependent activity (data not shown).

These data suggest that in the presence of calcium cations, GCPII and GCPIII can be specifically detected based on their different enzymatic activities.

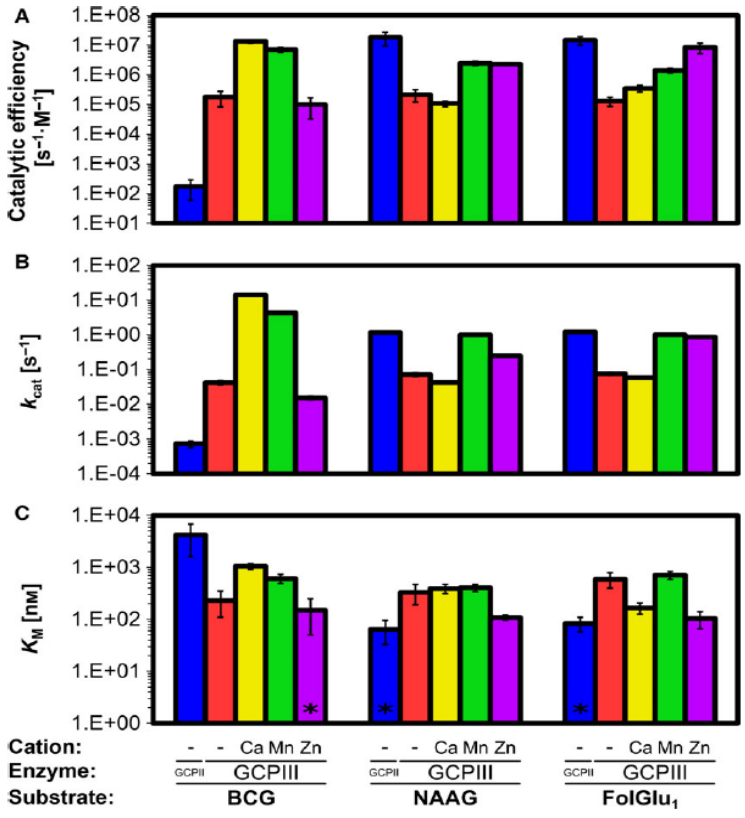

Fig. 2. Characterization of BCG-, NAAG- and $FolGlu_1$-hydrolysing activity of GCPIII in the absence or presence of divalent cations (Ca^{2+}, Mn^{2+} or Zn^{2+}) and comparison to GCPII. The reaction buffer was 25 mM bistrispropane, pH 7.5, supplemented with the cations where specified (Ca^{2+} 2.5 mM, Mn^{2+} 0.25 mM and Zn^{2+} 0.10 mM). Error bars represent SD. K_M and k_{cat} values were obtained by nonweighted hyperbolic fit into a single saturation curve consisting of 6–11 data points (n = 1). The panels show comparisons of (A) catalytic efficiencies, (B) k_{cat} values and (C) K_M values of GCPIII and GCPII towards the panel of substrates BCG, NAAG and $FolGlu_1$ in the presence or absence of calcium, manganese and zinc ions. Asterisks indicate that the K_M value was lower than the lowest substrate concentration (see Materials and methods for more information).

GCPII processes NAAG or $FolGlu_1$ with a two order of magnitude higher catalytic efficiency than GCPIII, while GCPIII processes BCG with a five order of magnitude higher catalytic efficiency than GCPII.

The GCPII arene-binding site facilitates processing of polyglutamylated folates

The GCPII structure includes an exosite called the arene-binding site (ABS), which comprises Arg463, Arg511 and Trp541 and is involved in the binding of the pteroate moiety during the cleavage of glutamylated folates [7,20]. A similar feature has not been described in the structure of GCPIII. We investigated the catalytic efficiency of GCPIII towards polyglutamylated folates ($FolGlu_{1–6}$), which bind to the ABS of GCPII, and compared it with previous data on GCPII cleavage efficiency of $FolGlu_{1–6}$ [7]. As shown in Fig. 3, GCPIII processes $FolGlu_{2–6}$ with much lower catalytic efficiency than GCPII, while processing of monoglutamylated folate ($FolGlu_1$) is comparable between the two enzymes (Fig. 3A). The difference resides mainly in the higher K_M values for GCPIII (Fig. 3B,C). These results are in good agreement with previously reported structural data showing that GCPII is unable to fully utilize the ABS for binding of the pteroate moiety of $FolGlu_1$, while the $FolGlu_{2–3}$ substrates are able to bind into this exosite [7].

Occupancy of active site zinc ions is lower for GCPIII than GCPII

The previously reported X-ray structures of GCPIII suggested that the active site Zn1 and Zn2 atoms have only partial occupancies in the 0.80–0.95 and 0.45–0.80 ranges, respectively [21]. To further corroborate these findings, we applied an atomic absorption spectroscopy technique to GCPII and GCPIII to determine the precise amount of zinc atoms per molecule (for experimental details, see Materials and methods). We determined that GCPII contains 1.40 zinc atoms per molecule and GCPIII contains 1.13. These results further support the partial occupancy of Zn2 within the GCPIII structure.

BCG binding mode in the GCPII active site: X-ray structure

To elucidate the differences in BCG cleavage by GCPII and GCPIII, we prepared a diffraction-quality crystal of inactive GCPII Glu424Ala in complex with BCG. We solved the structure by molecular replacement and refined the final model to 1.85 Å resolution

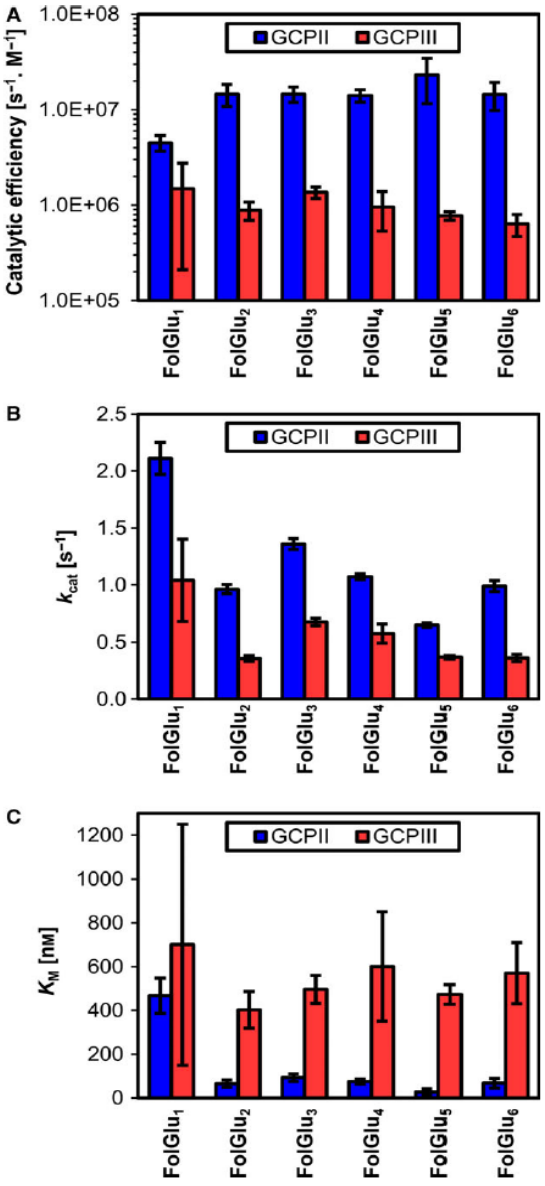

Fig. 3. Comparison of the $FolGlu_{1–6}$-hydrolysing activity of GCPIII and GCPII: (A) catalytic efficiencies, (B) k_{cat} values and (C) K_M values. The reaction buffer was 25 mM Tris/HCl, pH 7.5, without any added cations. Data for cleavage of $FolGlu_{1–6}$ by GCPII were measured previously [7]. Error bars represent SD. K_M and k_{cat} values were obtained by nonweighted hyperbolic fit into a single saturation curve consisting of 6–10 data points (n = 1).

Table 1. Data collection and refinement statistics.

Compound	BCG
PDB ID	5F09
Data collection statistics	
Space group	*I222*
Cell parameters	
a (Å)	100.899
b (Å)	130.916
c (Å)	159.118
α, β, γ (°)	90,90,90
No. of molecules in AU	1
Wavelength (Å)	0.918
Resolution (Å)	1.85
Highest resolution shell (Å)	1.96–1.85
No. of unique refl.	89 051 (13 967)
Multiplicity	4.51 (4.43)
Completeness (%)	98.8 (97.1)
R_{meas} (%)[a]	8.1 (94.1)
Average I/σ (I)	13.29 (1.96)
Wilson B (Å^2)[b]	39.43
Refinement statistics	
Resolution range (Å)	30.00–1.85
Highest resolution shell (Å)	1.90–1.85
No. of refl. in working set	84 147 (4444)
No. of refl. in test set	6105 (322)
R value (%)[c]	0.155 (0.311)
R_{free} value (%)[d]	0.181 (0.336)
RMSD bond length (Å)	0.014
RMSD angle (°)	1.690
No. of atoms in AU	6402
No. of protein atoms in AU	5804
No. of ligand atoms in AU	22
No. of ion atoms in AU	4
No. of water molecules in AU	562
Mean B value (Å^2)	21.91
Ramachandran plot statistics[e]	
Res. in favoured regions (%)	97.2
Res. in allowed regions (%)	2.7
Outliers	Val382

The data in parentheses denote the highest resolution shell. [a]R_{meas} is the redundancy-independent merging R factor [25]. [b]Estimated by SFcheck [26,27]. [c]R value = $||F_o| - |F_c||/|F_o|$, where F_o and F_c are the observed and calculated structure factors, respectively. [d]R_{free} is equivalent to R value but is calculated for 5% of the reflections chosen at random and omitted from the refinement process. [e]As calculated by MolProbity [28,29]. The AviTEV-tag and first 11 amino acids from the extracellular part of GCPII are not visible in the structure.

(PDB ID 5F09; data collection and refinement statistics are shown in Table 1). The binding mode of BCG within GCPII is depicted in Fig. 4A. The glutamate moiety of BCG binds into the S1′ pocket of GCPII in an identical manner as described for FolGlu$_n$ or NAAG substrates [7,22]. It forms hydrogen bonds with the side chains of Arg210, Asn257 and Tyr552, and also with Lys699 and Tyr700 forming the so-called 'glutarate sensor' [23]. However, in this structure, the glutamate moiety shows weaker electron density (see Fig. 4B) than in crystal structures of complexes with better substrates (e.g. FolGlu$_n$ or NAAG [7,22]). Interestingly, the glutarate sensor adopts two equally populated conformations, the 'closed' and 'open' form (see Fig. 4C). Unlike the glutamate moiety, the citrate moiety of BCG forms only one identifiable interaction with the enzyme: a salt bridge between one of the citrate carboxyl groups and the guanidine group of Arg534. This lack of interaction in the S1 pocket may be responsible for the substantially lower affinity of BCG towards GCPII, compared to that of other substrates such as NAAG. Accordingly, the citrate moiety of BCG had much less well-defined electron density than the glutamate moiety (see Fig. 4B), suggesting that this portion of BCG is not present in one particular conformation within the GCPII active site and likely possesses some degree of rotational freedom. These findings suggest that the binding of BCG, and in particular its citrate moiety, into the GCPII active site might partially prevent the closing of the glutarate sensor. Finally, it should be noted that we refined BCG to 70% occupancy, which is yet another indication that the binding affinity of BCG for GCPII is poor.

BCG binding mode in the GCPIII active site: QM/MM calculations

The technical difficulties of obtaining diffraction-quality crystals for GCPIII in complex with BCG led us to approximate the structure of GCPIII in complex with BCG by quantum mechanics/molecular mechanics (QM/MM). We computed a QM/MM homology model of GCPIII in complex with BCG (see Fig. 5A). The comparison of the obtained GCPII and GCPIII structures in complex with BCG suggests that the overall binding mode of this substrate is very similar in both enzymes (see Fig. 5B). However, in contrast to the flexibility of the BCG citrate moiety in the structure of the GCPII-BCG complex, both citrate carboxylates are coordinated – specifically by Ser444, Arg524 and Arg526 in the QM/MM model of GCPIII. Additionally, the orientation of the BCG hydroxyl group in GCPIII enables its coordination by Gly508. In the GCPII-BCG structure, the orientation of this hydroxyl group is different, and prevents such an interaction.

Thermodymamics of Zn^{2+}/Ca^{2+} binding in the active site: QM/MM calculations

After obtaining plausible QM/MM models of GCPIII in complex with NAAG and BCG, it is

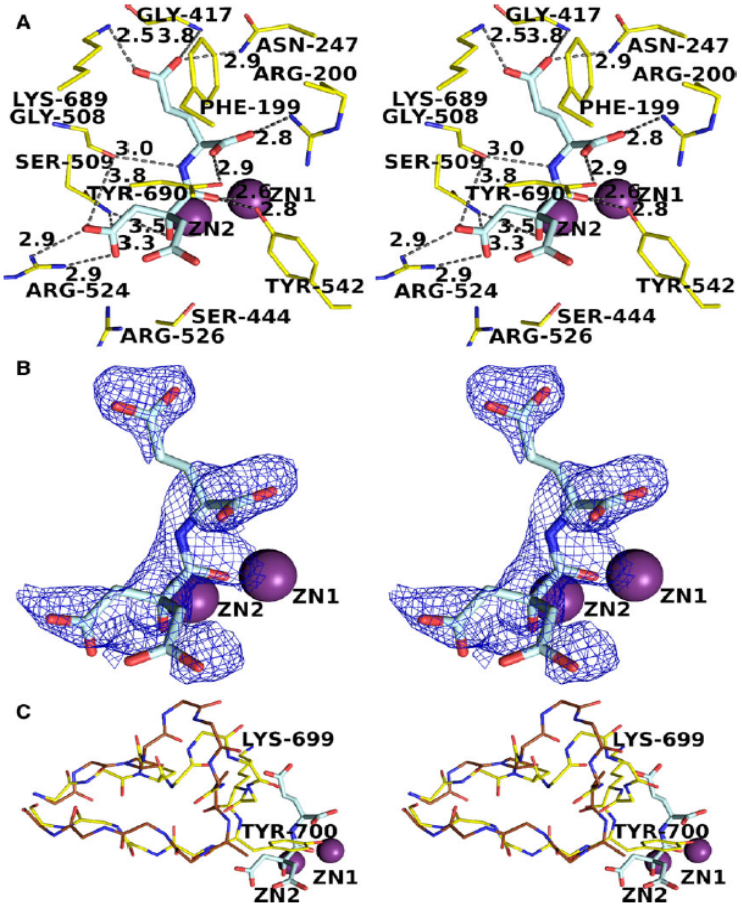

Fig. 4. X-ray structure of GCPII Glu424Ala in complex with β-citryl-L-glutamic acid (BCG, PDB ID 5F09). Images are rendered in cross-eye stereo representation. Active site zinc ions are shown in violet, GCPII protein in yellow and BCG in pale cyan. In panel (A), Tyr700 is truncated to provide an unobscured view. Distances are shown in Å. Images were created using PYMOL [24]. (A) Detail of the active site of GCPII with bound BCG. (B) The electron density map $2F_o - F_c$ for BCG in the GCPII-BCG complex (PDB ID 5F09), contoured at 1.0σ. (C) The structure of GCPII in complex with BCG features the glutarate sensor in two conformations, closed (yellow) and open (brown). Glutarate sensor is depicted as main chain only except for Lys699 and Tyr700 (only stubs are shown for the open conformation).

computationally straightforward to address the possibility of replacing one Zn^{2+} in the active site with a Ca^{2+} ion. This hypothesis has been put forward previously [13], and here, we tested it using advanced QM/MM modelling, which is arguably more rigorous and accurate than MD/MM simulations (or even less elaborate models [13]). We surmised that the QM/MM equilibrium structures and associated energetics may provide structural definition of potential calcium binding in the GCPII/III active site as well as a clue to explaining the observed differences in catalytic efficiency of GCPII and GCPIII in the absence or presence of Ca^{2+}. We carried out 12 QM/MM simulations varying the enzyme (GCPII and GCPIII), substrate (NAAG and BCG) and active site metals (Zn1–Zn2, Ca1–Zn2, Zn1–Ca2). Eight of the QM/MM equilibrium geometries (optimized structures, Zn1–Zn2, Zn1–Ca2) for the QM part (~ 280 atoms comprising the active site) are deposited in Data S1. In brief, substitution of Ca^{2+} for Zn^{2+} in the Zn2 position (which is in all cases favoured by approximately 10–15 kcal·mol^{-1} compared to Ca1-Zn2 structures) induces several structural perturbations to the active site (see Fig. 6). In comparison with the X-ray structure of GCPII in complex with BCG (PDB ID 5F09), the heterometallic cluster Zn1-Ca2 is rotated relative to the homometallic Zn1-Zn2 cluster so that Ca2 can be bound in a typical pentagonal bipyramidal manner, whereby His367 and a partially ionized hydroxyl of the citrate moiety are the axial ligands. An active site water forms part of the pentagonal coordination base, and residues Asp443 and Asp377 are correspondingly shifted to accommodate the Ca2 atom. Finally, we compared the energetics of calcium binding in the

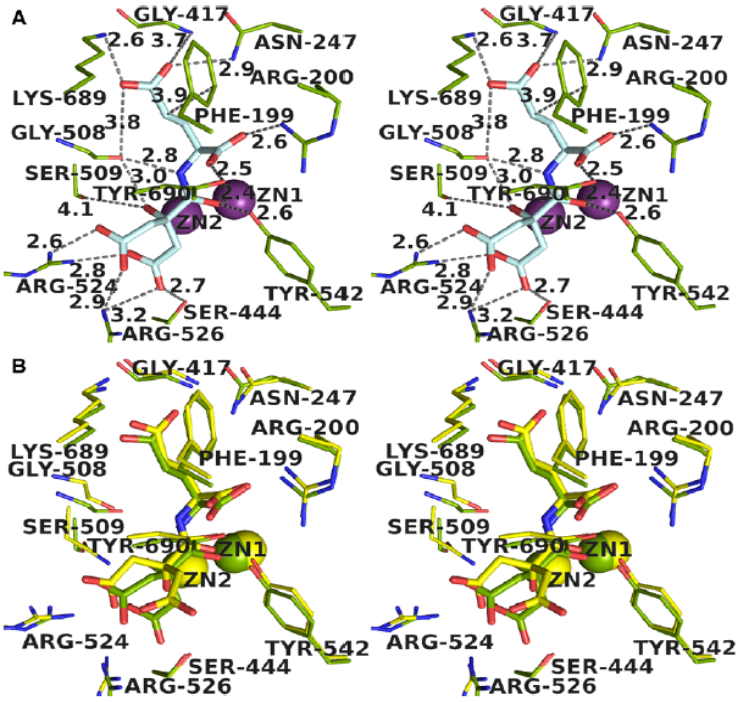

Fig. 5. QM/MM model of GCPIII in complex with BCG and its comparison to the X-ray structure of GCPII Glu424Ala in complex with β-citryl-L-glutamic acid (BCG, PDB ID 5F09). Images are rendered in cross-eye stereo representation. Numbering of amino acid residues in GCPIII is lower by 10 in comparison to GCPII. Tyr700/Tyr690 is truncated to provide an unobscured view. Distances are shown in Å. Zinc atoms are shown as spheres. Images were created using PYMOL [24]. (A) The QM/MM model of GCPIII in complex with BCG shows that GCPIII binds BCG in a way that allows more interactions. Protein is coloured green, BCG pale cyan, zinc atoms violet. (B) Overlay of GCPII-BCG complex with the QM/MM model of GCPIII-BCG complex. It shows that BCG is bound in a very similar manner to both GCPII and GCPIII. The only two differences are the presence of Ser509 in GCPIII instead of Asn519 in GCPII and how the citrate moiety is bound. GCPII-BCG complex is coloured yellow, and GCPIII-BCG in green.

GCPII and GCPIII sites in the presence of substrate (BCG vs. NAAG). Employing the QM (DFT+D3/TPSSh/def2-TZVP)/MM values, the calculations predict rather contradictory effects. For NAAG as a substrate, calculated affinity of calcium for the active site was marginally greater for GCPIII (~ 0.5 kcal·mol^{-1}). We found the opposite pattern for BCG; the calcium substitution was ~ 10 kcal·mol^{-1} 'easier' for the GCPII-BCG complex than the GCPIII-BCG complex. Therefore, the calculations suggest that the observed differences in the catalytic efficiencies may not depend on the stability constants of calcium ions that potentially fill the partially occupied Zn2 sites. Further investigation into the observed metal ion dependence is beyond the scope of the current study.

GCPII and GCPIII expression levels can be specifically determined by enzymatic assays and correspond to mRNA levels

Based on the results obtained from the enzymological characterization of human GCPII and GCPIII, we employed the NAAG cleavage assay for specific detection of GCPII and the BCG cleavage assay for specific detection of GCPIII in a representative sample of human tissues, analogously to an earlier report [13] (Fig. 7A). Both assays were performed in the presence of calcium ions because it affords the highest difference in GCPII and GCPIII catalytic efficiencies for the substrates employed (for quantitative information, see Materials and methods). Simultaneously, we quantified the amount of mRNA coding for GCPII and GCPIII in a set of human tissues to confirm the functionality of the proposed enzymatic detection assays.

The amounts of GCPII and GCPIII transcripts were analysed in commercially available panels of human tissue cDNA libraries (Human MTC Panel I and II) by quantitative PCR (qPCR). Each transcript was amplified by a specific assay set consisting of a primer pair for amplification and a fluorescent probe for visualization. The cDNA amplification products were resolved by agarose gel electrophoresis. Besides the occasional weak formation of primer dimers in the GCPII assay set and the occasional weak formation of higher molecular weight products in the GCPIII assay, only the product of expected size was observed in all reactions. No products were formed in the negative controls without template DNA, indicating that there

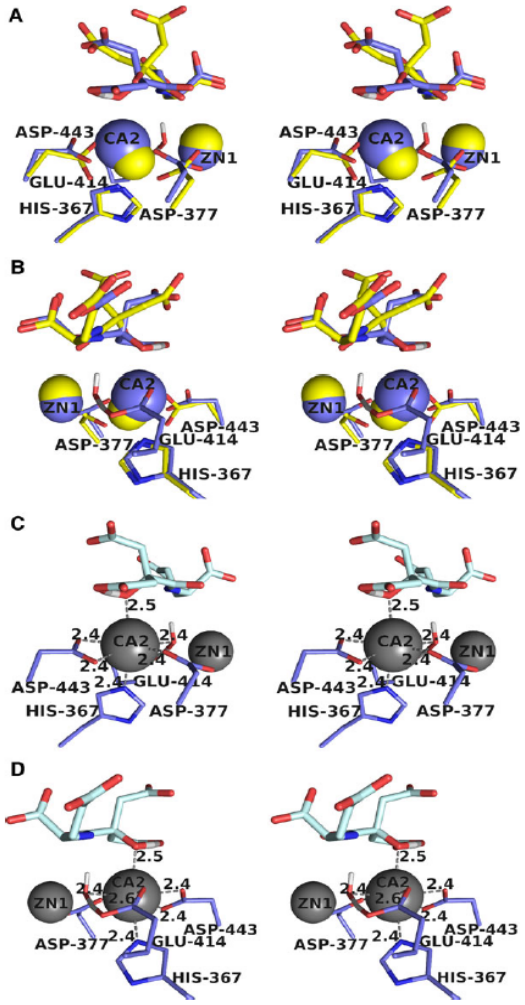

Fig. 6. QM/MM model of GCPIII in complex with BCG and with Zn2 atom replaced by calcium (II) (GCPIII-BCG-Ca2) compared to the X-ray structure of GCPII in complex with BCG (GCPII-BCG, PDB ID 5F09). Images are rendered in cross-eye stereo representation. BCG is depicted in stick representation. Please note that there is also a hydrogen atom of BCG hydroxyl group shown in light grey, which is attracted by the ionized carboxyl group of the citrate moiety, so that the hydroxyl becomes partially ionized to coordinate the Ca2 atom. Metal atoms are shown as spheres. (A) A comparison of GCPIII-BCG-Ca2 QM/MM model (blue) with GCPII-BCG (yellow). (B) The same as in (A), but rotated along *y* axis by 180°. (C) Detailed view of the coordination matrix of Ca2 in the GCPIII-BCG-Ca2 QM/MM model. BCG is coloured pale cyan, protein blue, and Zn1-Ca2 cluster grey. Coordination distances are shown in Å. (D) The same as in (C), but rotated along *y* axis by 180°.

were no false positives or negatives due to amplification of other nontargeted sequences (data not shown).

We also tested the selectivity of each assay set by amplification of plasmids with subcloned sequences of full-length GCPII or GCPIII and of isolated genomic DNA. Both assay sets amplified only the target of interest, and not the homologous transcript, and they did not tend to detect the genomic sequence. We tested selectivity against the genomic sequence because cDNA libraries are often contaminated with the genome. To this point, we also quantified the amount of the genome in the cDNA libraries by another assay set, which showed us that the contamination was very low to undetectable.

Amplification of a dilution series of plasmids with subcloned sequences of either GCPII or GCPIII showed linear dependency of determined C_q values on the logarithm of template concentration over the complete range of concentrations used. It also revealed a PCR efficiency of over 80% for both assay sets.

The absolute amounts of both transcripts detected in tissue cDNA libraries are shown in Fig. 7B. Because the cDNA libraries were normalized to several different housekeeping genes (G3PDH, alpha-tubulin, phospholipase A2, beta-actin) and are mostly pooled from multiple individuals, the results between tissues should be comparable and should represent tissue distribution of both transcripts.

As shown in Fig. 7, the protein levels of GCPII and GCPIII (Fig. 7A) determined by enzymatic assays correlate with the mRNA levels determined by qPCR (Fig. 7B). These data indicate that the enzymatic assays can be used for specific discrimination of GCPII and GCPIII expression levels in various human tissues. We detected a greater than one order of magnitude higher amount of GCPIII compared to GCPII in the testes. On the other hand, GCPIII expression in the brain, kidney and small intestine is one to two orders of magnitude lower than that of GCPII.

Discussion

In this study, we demonstrated that human GCPIII shares a similar metal-dependent enzymological profile as previously described for its mouse orthologue [13]. We observed facilitation of BCG-hydrolysing activity by Ca^{2+} ions and NAAG-hydrolysing activity by Zn^{2+} ions. Additionally, we discovered that GCPIII also processes polyglutamylated folates ($FolGlu_n$) and that this activity is facilitated by Zn^{2+} ions in a similar manner as NAAG hydrolysis.

The concentration of calcium cations used for the enzymological studies, 2.5 mM, was chosen to

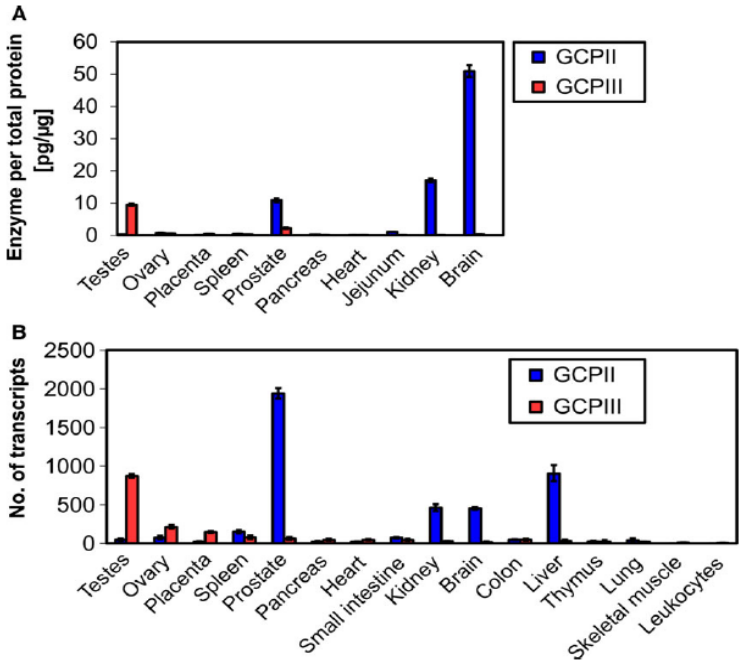

Fig. 7. GCPII/III protein and mRNA levels in human tissues. Error bars represent SD [$n = 2$ for (A), $n = 3$ for (B)]. For an easy comparison of protein and mRNA levels, tissues in (A) and (B) are juxtaposed. (A) Concentration of GCPII/III proteins in selected human tissues. The reaction buffer was 20 mM Tris, 0.15 M NaCl, 2.5 mM $CaCl_2$, 0.1% (v/v) Tween 20, pH 7.4. (B) Quantitative PCR (qPCR) determination of mRNA coding for GCPII and GCPIII. The 'No. of transcripts' shows the amount of transcripts determined in 1.0 µL of 10-fold diluted tissue cDNA library (for more experimental details see Materials and methods).

approximate the common concentrations of these cations in human plasma (despite its free, so-called ionic, concentration is usually two times lower [30]). Although free zinc concentration is very low in blood plasma [31], 0.10 mM concentration was used in our study, mainly because we wanted to characterize the saturation kinetics and because GCPIII is half-saturated by zinc at a relatively low concentration (approximately 6 µM, unpublished observation). Furthermore, zinc in the CNS serves as an orthograde, transcellular messenger [32], and it is also secreted by pancreas at the amount 1–2 $mg \cdot day^{-1}$ [33] (see also below). Because both metals substantially facilitated the corresponding enzymatic activities of GCPIII, GCPIII has the potential to act as either a BCG- or NAAG/$FolGlu_n$-hydrolysing enzyme. Its activity could likely be fine-tuned by the Ca^{2+} and Zn^{2+} concentrations in a particular tissue. Therefore, we suggest that GCPIII may have different enzymatic functions within the human body based on its tissue localization, the accessibility of its substrates and the concentration of divalent cations in that particular tissue. For a proper estimation of the function of GCPIII, its expression profile will need to be correlated with the distribution of its endogenous substrates, in particular BCG.

We attempted to address the structural basis for the differences in substrate specificities between these two homologues. Inspection of the GCPII and GCPIII 3D structures revealed that, although their active sites are structurally almost identical, there are two notable differences: substitution of Asn519 in GCPII with Ser509 in GCPIII and substitution of Trp541 in GCPII with Lys531 in GCPIII. The Asn to Ser substitution enables two conformations of the Zn2-coordinating amino acid Asp443 and is thus likely responsible for the lower occupancy of the Zn2 ion within the GCPIII active site [21], while the Trp to Lys substitution likely disrupts the ABS [7,20]. Disruption of the ABS in GCPIII can be exploited for development of inhibitors that are highly specific towards GCPII [34]. We corroborated these results by showing that endogenous substrates such as $FolGlu_n$, which utilize the ABS in GCPII [7], have substantially lower affinity (higher K_M value) towards GCPIII compared to GCPII. These findings suggest that even though GCPIII is also expressed at low levels in small intestine, the processing of polyglutamylated folates will likely be performed primarily by GCPII. GCPII inhibitors are currently heavily investigated as potential theranostic agents against prostate cancer [10] and various neurological disorders. Therefore, it is advisable to design compounds that would not hinder

the BCG-hydrolysing activity of its homologue GCPIII, although its physiological relevance is not quite clear yet.

Furthermore, we attempted to elucidate the mechanism of calcium-dependent BCG cleavage by determining structures of GCPII and GCPIII in complex with BCG. Unfortunately, due to experimental difficulties, we were able to prepare only protein crystals of GCPII in complex with BGC. Therefore, we built a QM/MM model of the GCPIII-BCG complex. As a control for our QM/MM approach, we also built a QM/MM structural model of GCPII in complex with NAAG and BCG (which are available as X-ray structures, PDB IDs 3BXM [22] and 5F09, respectively). The QM/MM models of GCPII in complex with NAAG or BCG and X-ray structures of inactive GCPII (Glu424Ala) in complex with these compounds are almost identical, with root-mean-square deviation values of 0.069 and 0.189 Å, respectively (except for the citrate moiety, which adopts a different conformation – the same conformation as in the GCPIII-BCG model, data not shown).

Our structural data show an overall similar binding of BCG into the GCPII and GCPIII active sites, which was expected because the major difference in the catalytic efficiencies of these two enzymes comes from substrate turnover number (k_{cat}) rather than substrate binding (K_M) (see Fig. 2B,C). Considering our observation that GCPII is not activated by divalent cations, we investigated the hypothesis that the mechanism behind the activation of GCPIII-BCG-hydrolysing activity might presumably involve replacement of the loosely coordinated Zn2 ion from GCPIII's active site with a different ion, such as Ca^{2+}. However, the QM/MM calculations did not provide a clear indication that the replacement of the Zn2 ion with Ca^{2+} would be thermodynamically more favourable for BCG as a substrate rather than NAAG and rather exclude this hypothesis. However, it should be kept in mind that QM/MM calculations do not provide any information about whether Ca^{2+} is present or absent in the partially occupied GCPIII active site. In addition, our computed values do not provide any indication whether BCG – presumably a better chelator than NAAG – assists in the Ca^{2+} uptake into the active site. This issue might be, in principle, assessed experimentally (X-ray crystallography or X-ray absorption techniques) and complemented by QM/MM/MD calculations of the activation energies of individual complexes (to analyse the kinetic origin of the observed metal ion dependency) which is well beyond the scope of the presented work.

Finally, we utilized enzymological data for specific detection of GCPII and GCPIII protein levels in several human tissues. Because there are no commercially available specific antibodies against human GCPIII, this approach represents a method for detection and discrimination between these two enzymes in human tissues. The fact that we detected lower levels of GCPIII than GCPII in brain and small intestine, the tissues where cleavage of NAAG and polyglutamylated folates, respectively, takes place, supports the assumption that BCG is the main physiological substrate of GCPIII in humans. The high level of GCPIII expression in human testes, and the high BCG-hydrolysing activity also detected in rat testes [16], further strengthens this hypothesis. We believe that a reliable determination of the GCPIII expression profile on a protein level, combined with data on BCG levels in human tissues, will help to dissect and elucidate the primary physiological function of GCPIII in the human body.

Regarding mRNA of GCPII in human tissues, there is one discrepancy to be addressed. Cunha *et al.* [35] also determined the amount of GCPII (PSMA in the medical literature) in Clontech tissue cDNA libraries. Their primers, like ours, were designed to detect only the PSMA splice variant and not the intracellular variant of PSMA. The relative PSMA expression levels in various tissues that they determined [35] are in good agreement with our results, except for PSMA expression in prostate. We determined the ratio of expression of PSMA in the prostate and liver (the tissue with second highest PSMA expression) to be approximately 2, compared to 12 in the previous report. Although the tissue libraries were normalized to four different reference genes by the vendor, Cunha *et al.* renormalized their results to only one of these genes, beta-actin. Unfortunately, they do not describe the details of the beta-actin assay or the amounts of beta-actin determined. Therefore, it is not clear whether the higher specificity of PSMA expression in their study was caused by lower levels of beta-actin in prostate, or whether the different results can be attributed to different tissue library lots.

In summary, we present a thorough enzymatic and structural characterization of the behaviour of human GCPII and GCPIII towards their physiological substrates. We also identified metal-dependent enzymatic activity of human GCPIII, which we did not observe for human GCPII. Finally, we confirmed BCG to be a specific substrate of human GCPIII. Utilizing these findings, we mapped the expression patterns of GCPII and GCPIII in a panel of human tissues. Compared to GCPII expression, we detected higher levels of

GCPIII in testes and lower levels in brain, kidney and prostate. Additionally, this study is also the first to show mRNA levels of GCPIII in the human tissues.

Materials and methods

Crystallization and data collection

Inactive GCPII with the engineered mutation Glu424Ala [22] and AviTag™ affinity tag (Avidity, Aurora, CO, USA) [19] was crystallized using the hanging drop vapour diffusion method as described earlier [36] with the following modifications: (a) 1.0 μL precipitant was added to a 1.0 μL drop of protein (concentrated to 3.6 $mg \cdot mL^{-1}$) in 20 mM bistrispropane, 20 mM NaCl, pH 7.4, and sealed over a 0.50 mL reservoir of the same precipitant; (b) 0.1 μL of 2.1 mM BCG in MilliQ water (Merck Millipore, Billerica, MA, USA) was added to the crystallization drop after 11 weeks and again after 13 weeks (resulting in a calculated ratio of protein : substrate equal to 19 μM : 0.21 mM); (c) the crystal was frozen in liquid nitrogen after 15 weeks; and (d) precipitant was made up of 33% (v/v) pentaerythritol propoxylate PO/OH 5/4 (Hampton Research, Aliso Viejo, CA, USA), 1.5% (w/v) PEG 3350 (Merck KGaA, Darmstadt, Germany) and 0.10 M Tris/HCl (Merck KGaA), pH 8.0, in distilled water. In the drop, one single crystal appeared after several weeks. Crystallization approach of adding BCG right at the setup was unsuccessful. Diffraction data were collected at 100 K at the beamline BL1412 operated by the Joint Berlin MX-Laboratory at the BESSY II electron storage ring (Berlin-Adlershof, Germany) [37], using a Pilatus 6M detector (Dectris, Baden, Switzerland). Scaling and merging was done with the programs XDS [38] and its graphical user interface XDSAPP [39].

Structure determination was performed by molecular replacement using the program MOLREP from the CCP4 software package [27,40,41]. The previously solved structure of recombinant human GCPII (PDB ID 4NGP [11]) without inhibitor and water molecules was used as the starting model. Refinement calculations were performed with the program REFMAC 5.7 [42,43], and the refinement protocol was interspersed with manual corrections to the model using WINCOOT 0.7 [44]. The final models, together with experimental amplitudes, were deposited into the RCSB Protein Data Bank under the accession number 5F09. A summary of structural parameters is displayed in Table 1. Images were created with the programs PYMOL [24] and FFT and MAPMASK [45].

QM/MM calculations

All QM/MM calculations were carried out with the COMQUM program [46], which combines the quantum mechanical approach, applied to the region most relevant for the studied process, and the classical mechanical approach for the rest of the protein. In the current version, the program employs TURBOMOLE 6.6 suite [47] for the QM part and AMBER 8.0 with the *ff14SB* force field for the MM part [48]. ComQum utilizes the standard hydrogen-link approach, and the technical details of the QM/MM computational protocol have been described elsewhere [22].

All quantum chemical calculations were performed at the density functional theory (DFT) level. Geometry optimizations were carried out at the Perdew–Burke–Ernzerhof (PBE) level [49]. The DFT/PBE calculations were expedited by expanding the Coulomb integrals in an auxiliary basis set: the resolution-of-identity (RI-J) approximation. The def-SV(P) basis set was employed for all atoms. The single-point energies were then calculated using the TPSSH method [50] as implemented in TURBOMOLE 6.6. For these calculations, the def2-TZVPD basis set was employed for all atoms.

The protein (GCPII) setup

Structural models used in QM/MM calculations were based on the 1.71 Å X-ray crystallographic structure of the inactive Glu424Ala mutant of GCPII in complex with NAAG (PDB ID 3BXM [22]) and the 1.37 Å structure of the GCPIII with L-glutamate (3FF3 [21]). BCG was positioned in the active site using the GCPII (Glu424Ala)/NAAG and GCPIII/L-Glu structures as templates. The protein was equilibrated using the standard approach [22]: (a) minimizing the positions of all hydrogen atoms in the initial structure, (b) adding a solvation sphere with a radius of 50 Å (~ 12 700 and 11 500 water molecules in total for GCPII and III, respectively) and (c) running a 1 ns simulated annealing molecular dynamics followed by the final minimization of the whole system (with all nonhydrogens atoms kept at their crystallographic positions throughout). Both GCPII and GCPIII structures were neutralized by addition of ions (two Na^+ for GCPII and four Cl^- for GCPIII). We assumed the standard protonation states at pH 7 for all amino acids. For the histidine residues, the protonation status was assigned based on a detailed study of the hydrogen bond network around the residue and the solvent accessibility. In the GCPII structure, histidines 82, 347, 377, 553 and 573 were assumed to be protonated on the N^{δ} atom; histidines 56, 112, 124, 295, 396, 475, 689 and 697 on the N^{ε} atom; and histidines 345 and 618 on both nitrogens. In the GCPIII structure, histidines 124, 367, 543, 637 and 721 were assumed to be protonated on the N^{δ} atom; histidines 102, 285, 335, 608, 615, 679 and 687 on the N^{ε} atom; and histidine 72 on both nitrogens.

The quantum system consisted of ~ 280 active site atoms and is deposited in Data S1. The so-called system 2 (part of the system that is relaxed in the QM/MM calculations by MM method) comprised 48 amino acids in the vicinity

of the quantum system, and it has been selected on a per-residue based cut-off distance of 2.5 Å from the quantum system. The rest of the protein (system 3) was kept frozen in all QM/MM simulations.

Synthesis of β-citryl-L-glutamic acid (BCG)

General information

All chemicals were purchased from Sigma-Aldrich, unless stated otherwise. β-citrylglutamate (BCG) was purified using preparative scale HPLC Waters Delta 600 (Waters Corporation, Milford, MA, USA) (flow rate 7 mL·min^{-1}), with column Waters SunFire C18 OBD Prep Column, 5 µm, 19 × 150 mm (Waters Corporation). The purity of BCG was tested on the analytical Jasco PU-1580 HPLC instrument (Jasco, Easton, MD, USA) (flow rate 1 mL·min^{-1}, R_t is shown below) employing the Waters C18 Analytical Column, 5 µm, 250 × 5 mm (Waters Corporation). The final product was of at least 99% purity. Structure was further confirmed by high-resolution mass spectrometry (HRMS) at LTQ Orbitrap XL (Thermo Scientific, Waltham, MA, USA) and by NMR at Bruker Avance I™ 400 MHz (Bruker, Billerica, MA, USA).

Synthesis of β-citrylglutamate

Overall scheme for the six-step synthesis of BCG is shown below (Scheme 1). Detailed description of each step and its resulting intermediate or final compound (designated **1** to **5** or **6**, respectively) is given in the following text in the order of the synthesis (Scheme 1).

1. 2-tert-butyl 1,3-dimethyl 2-hydroxypropane-1,2,3-tricarboxylate

About 5.3 g of dimethyl citrate (24 mmol, prepared as described in [51]) was suspended in 15 mL of isobutylene and 0.5 mL of sulfuric acid was added while cooled to −78 °C. The reaction mixture cleared over time. After 18 h of stirring at room temperature, the reaction mixture was cooled down to −78 °C and poured to ice bath saturated with bicarbonate. The water phase was then washed three times by ethylacetate (EtOAc) (50 mL) and the organic

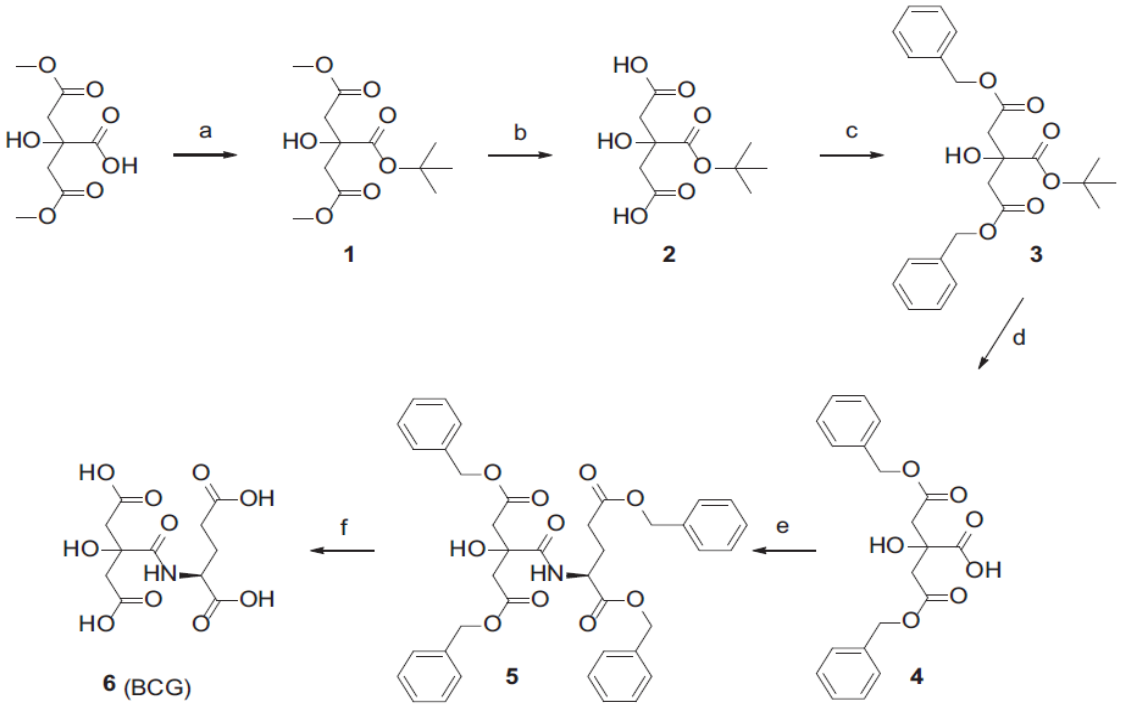

Scheme 1. The scheme for synthesis of β-citryl-L-glutamic acid (BCG). The synthesis proceeded via five intermediate compounds, designated **1**–**5**, whereby BCG is compound **6**. (a) Isobutylene, H_2SO_4; (b) NaOH, MeOH/H_2O; (c) DBU, benzyl bromide, ACN; (d) TFA; (e) NH_2Glu(OBzl)OBzl, *O*-(Benzotriazol-1-yl)-*N*,*N*,*N*′,*N*′-tetramethyluronium tetrafluoroborate, DIEA, dimethylformamide; (f) H_2, Pd(C), MeOH.

phases were combined, dried and evaporated yielding 5.3 g of pure product (yield = 80%).

2. 3-(tert-butoxycarbonyl)-3-hydroxypentanedioic acid

About 5.2 g of compound **1** (18.7 mmol) was dissolved in 20 mL of methanol and was cooled down to 0 °C. About 20 mL of 2 M NaOH was then added in portions during 5 min. The reaction was left to proceed for 6 h. The reaction mixture was then diluted by 200 mL of EtOAc and was extracted two times by 10% $KHSO_4$ (2 × 100 mL). The organic phase was then dried and evaporated to yield 3.5 g of product (yield = 75%).

3. 1,3-dibenzyl 2-tert-butyl 2-hydroxypropane-1,2,3-tricarboxylate

About 1 g of compound **2** (4.03 mmol, 1.0 eq) was suspended in 20 mL of acetonitrile (ACN) along with 1.2 mL of 1,8-Diazabicycloundec-7-ene (DBU) (8.86 mmol, 2.0 eq). About 1.05 mL of benzyl bromide was added in one portion and the reaction mixture was refluxed for 2 h. The TLC analysis (EtOAc) showed no starting material and the whole mixture was evaporated. The crude product was dissolved in 100 mL of EtOAc and was washed two times with 10% $KHSO_4$, two times with saturated $NaHCO_3$ and once with brine, and the organic phase was dried and evaporated to obtain the titled compound as white solid (1.2 g, yield = 70%). The product was used in next step without further purification (purity approximately 90%).

4. 1,3-dibenzyl 2-hydroxypropane-1,2,3-tricarboxylate

About 1.1 g of compound **3** (2.57 mmol) was dissolved in 3 mL of trifluoroacetic acid (TFA). The reaction mixture was stirred and sonicated alternately for 25 min and then the TFA was removed by flow of nitrogen. The residue was then dissolved in EtOAc and was washed three times with water to get rid of the residual TFA. The organic phase was then dried and evaporated. About 940 mg of compound **4** was obtained (yield = 95%) and it was used in the synthesis without further purification.

5. 2-{(1S)-[1,3-bis(benzylcarboxy)prop-1-yl]-carbamoyl}-1,3-bis(benzylcarboxy)-2-carboxy-2-hydroxy-propan-2-amide

About 500 mg of compound **4** (1.35 mmol, 1.1 eq) was dissolved in 5 mL of dimethylformamide along with 564 mg of 2-(1H-benzotriazol-1-yl)-1,1,3,3-tetramethyluronium hexauorophosphate (1.49 mmol, 1.1 eq) and 840 µL of *N*,*N*-Diisopropylethylamine (DIEA) (4.65 mmol, 3.5 eq). The mixture was left stirring for 15 min and then 486 mg of H_2N-Glu(OBn)-COOBn*Tos (1.49 mmol, 1.0 eq) was added in one portion. After 2.5 h, all volatiles were evaporated and the residue was dissolved in 50 mL of EtOAc. The organic phase was washed two times with 10% $KHSO_4$, two times with saturated $NaHCO_3$ and once with brine. About 600 mg of compound **5** (yield = 60%) was obtained as an oily product after evaporation and column chromatography on silica (EtOAc, TLC R_f = 0.25).

6. 3-{[(1S)-1,3-dicarboxypropyl]carbamoyl}-3-hydroxy-pentanedioic acid (ß-citrylglutamate, BCG)

About 50 mg of compound **5** was dissolved in 2 mL of methanol (MeOH) and catalytical amount of palladium on activated charcoal [Pd(C)] was added. The reaction mixture was first purged with flow of nitrogen, then with flow of hydrogen. The benzyl groups were then removed during 3 h using slightly elevated pressure of hydrogen (1.05 Atm). TLC analysis showed that all the reactants disappeared and the reaction mixture was filtered and evaporated. The product was purified using preparative scale HPLC (isocratic 2.5% ACN, R_t = 6 min). About 10 mg was isolated upon dry freezing (isolated yield = 42%). ^{1}H NMR (401 MHz, DMSO) δ 12.31 (bs, 4H), 7.74 (d, J = 8.0 Hz, 1H), 5.73 (bs, 1H), 4.25 (td, J = 8.3, 4.8 Hz, 1H), 2.77 (d, J = 15.6 Hz, 1H), 2.68 (d, J = 15.7 Hz, 1H), 2.66 (d, J = 15.2 Hz, 1H), 2.58 (d, J = 15.2 Hz, 1H), 2.37–2.21 (m, 2H), 2.07–1.98 (m, 1H), 1.89–1.78 (m, 1H). ^{13}C NMR (101 MHz, DMSO) δ 174.01, 173.40, 172.94, 171.41, 171.26, 73.47, 51.12, 42.90, 42.45, 29.66, 26.78. Analytical HPLC R_t = 4.0 min. HRMS (ESI-) m/z for $C_{19}H_{22}O_7N_2$ $[M-H]^-$ calculated 389.13433, found 389.13424.

Expression and purification of recombinant human GCPII, GCPIII and GCPII inactive variant

The expression and purification protocols for all used human recombinant proteins in this study, Avi-tagged extracellular portion of GCPII [19], GCPIII [12], the inactive variant of GCPII [7] and tag-free extracellular portion of GCPII [52], have been described earlier.

GCPII and GCPIII activity assay

Because GCPIII activity is metal-dependent, MilliQ (Merck Millipore) was used to prepare all solutions. Reactions with BCG, NAAG (Merck KGaA) and folyl-*n*-γ-L-glutamic acids ($FolGlu_{1-6}$) (Schircks Laboratories, Jona, Switzerland) were performed in 25 mM Tris/HCl, pH 7.5, (Merck KGaA) or 25 mM bistrispropane HCl, pH 7.5, (Merck KGaA) in a total volume of 215 µL in a 96-well plate immersed in a water bath (Grant Instruments, Shepreth, UK) at 37.0 °C [or in a lower throughput setting in 1.5 mL eppendorf tubes using a thermo-block Bioer MB120 (MB-102; Bioer, Hangzhou, China)]. Concentrations of substrate stock solutions were determined by amino acid analysis [53]. All components were pipetted on ice, and reactions

were started by adding substrate following a 5- to 13-min preincubation at 37.0 °C. After 20 min, the reactions were terminated by inhibiting the enzyme and by changing the pH to 5.8 by addition of 10.0 μL stopping solution composed of 0.37 M phosphoric acid (Penta, Prague, Czech Republic) and 22 μM 2-(phosphonomethyl)-pentanedioic acid in MilliQ water (Merck Millipore) (when 25 mM bis-trispropane buffer, pH 7.5, was used) or 3.48 μL of 0.41 M phosphoric acid (Penta), 72 μM 2-(phosphonomethyl)-pentanedioic acid and 7.2 μM 2-mercaptoethanol (Merck KGaA) in MilliQ water (Merck Millipore) (when 25 mM Tris/HCl buffer, pH 7.5, was used). Reaction conditions were designed to yield 10–30% substrate turnover. The method for quantifying $FolGlu_{1-6}$ substrates and $FolGlu_{0-5}$ products was the same as described elsewhere [7], while hydrolysis of NAAG and BCG was assessed with a novel assay (see below for details). Using GraFit, we fitted a saturation curve to 6–11 data points for every substrate (whereby each point represented a single or average of a duplicate experiment). Because of low K_M values, the assay was sometimes restricted by the limit of quantification of the employed analytic method (indicated by an asterisk in Fig. 2 and below), meaning that the K_M value was smaller than the lowest experimental substrate concentration. In Fig. 2, the lowest substrate concentrations were, from left to right, 1.5, 0.20, 0.20, 0.20, 0.32*, 0.088*, 0.20, 0.20, 0.20, 0.10, 0.14*, 0.045, 0.031, 0.030, 0.034 μM.

Quantification of glutamate in the enzymatic assay

To quantify glutamate as a product of NAAG and BCG cleavage, a novel method was developed. It is based on a highly concentrated solution of orthophthalaldehyde (OPA), a commonly used reagent for amino acid derivatization [53]. The new derivatization formulation was a 0.10 M OPA, 0.30 M 3-mercaptopropionic acid, 4% acetonitrile (v/v) and 0.94 M bistrispropane, pH 9.6 solution. A 11.0 μL portion of the solution was added to 99 μL of a reaction containing the cleavage product glutamate. This improvement made it possible to surpass the need to concentrate the sample by lyophilization and redissolving it [7]. Sample derivatization and analysis was performed on an Agilent 1200 or 1260 instrument (Agilent Technologies, Santa Clara, CA, USA) similarly as described previously [7], except that the analysis method was slightly modified. The new method consisted of 13.80 min at 0.7% B, 0.05 min transition to 80.0% B, 1.00 min at 80.0% B, 0.05 min transition back to 0.70% B, 0.60 min at 0.7% B, injection of 20.0 μL of 16-fold diluted 85% phosphoric acid (w/w; Penta), pH 2.5, (NaOH; Penta) to dissolve precipitate of metal hydroxides, and 10.50 min at 0.7% B. The automatic derivatization procedure and injection performed by the instrument just prior to analysis took approximately 7 min.

Atomic absorption spectroscopy to determine Zn occupancy in the GCPIII active site

Following purification, approximately 10 μM GCPII and GCPIII was dialysed against 10 mM MOPS (Duchefa, Biochemie, Haarlem, the Netherlands; pH adjusted by KOH), pH 7.4, using Slide-A-Lyzer™ MINI Dialysis Devices (Thermo Scientific). The buffer was prepared from MilliQ water (Merck Millipore) and subjected to Chelex 100 (Bio-Rad, Hercules, CA, USA) before use. Dialysis devices and glass vials used for protein preparation were washed twice with EDTA solution and thoroughly with MilliQ (Merck Millipore) water. Samples were analysed on an Analyst 800 spectrometer (Perkin-Elmer, Waltham, MA, USA) with electrothermal atomization using an EDL Zn lamp. Temperatures of pyrolysis and atomization were 700 °C and 1500 °C, respectively. Palladium was employed as a modifier. The limit of detection for zinc was 0.1 $ng \cdot mL^{-1}$. For the analysis itself, samples were diluted 200-fold. The analysed volume was 10 mL. Measurements were performed at least in triplicate. The protein concentration was quantified by amino acid analysis [53].

Quantification of GCPII/III at the protein and mRNA levels

Enzymatic assay

The total protein concentrations of tissue lysates were estimated by a modified Bradford method (Protein Assay; Bio-Rad), using BSA (Thermo Scientific) as a standard and 97 mM HEPES (Merck KGaA) and 0.15 M NaCl (Penta) pH 7.5 (NaOH; Penta) as a buffer. For the activity assay, tissue lysates were diluted 5.3- to 7300-fold overall. Buffer used for the specific detection of both GCPII and GCPIII was prepared from MilliQ water (Merck Millipore), composed of 20 mM Tris (Merck KGaA), 0.15 M NaCl (Penta), 2.5 mM $CaCl_2$ (Merck KGaA) and 0.1% (v/v) Tween 20 (USB, Cleveland, OH, USA), pH 7.4 (HCl, Penta) and filtered through a 0.22 μm filter (Merck Millipore). As a substrate, [^{3}H]NAAG and [^{3}H]BCG were used at 5 nM final concentration (mixed with cold substrates in a 19 : 1 molar ratio to yield a total substrate concentration of 100 nM) in a previously described radiometric assay [5], in which the column volume was 1.0 or 0.5 mL and elution was performed with 2.4 or 1.2 mL of 1 M HCOOH (Penta), respectively. The usual time of incubation was 17 h at 37.0 °C.

This particular buffer confers the needed differences in specificities of GCPII towards NAAG and GCPIII towards BCG: When GCPII is quantified according to NAAG hydrolysis, GCPIII must be approximately 60-fold more concentrated to yield a comparable turnover. On the other hand, when GCPIII is quantified according to BCG hydrolysis, GCPII does not cleave BCG at all even if its concentration is 180-fold higher (data not shown).

Quantitative PCR

Amounts of GCPII transcript (encoded by the gene FOLH1) were quantified by an assay set of forward and reverse primers (sequences 5′-CGG CTT CCT CTT CGG GTG-3′ and 5′-GAT GTT CTC AGC TTT CAA TTC ATC C-3′) and a fluorescent hydrolysis probe (sequence 5′-ATC CTC CAA TGA AGC TAC TAA CAT TAC TCC AA-3′). This set was designed to amplify nucleotides 366–471 in the GCPII transcript (NM_004476) to yield an amplified product of 106 bps, which covers regions of exons 1 and 2 and corresponds to amino acids 35–70 in the longest open reading frame (ORF). The forward primer is complementary to the exon 1–exon 2 junction, and it was designed to enable selective amplification of the wild-type GCPII protein-coding splice variant (usually termed PSMA). This assay set was also designed to amplify neither genomic sequences nor the prostate specific membrane antigen like protein transcript, which is encoded by the pseudogene FOLH1B.

Amounts of GCPIII transcript were quantified by an assay set of forward and reverse primers (sequences 5′-TTT GGA CTT CTG GGT TCC AC-3′ and 5′-TGC TTC TCT CCT GGA GTA TTT TG-3′) and a fluorescent hydrolysis probe, Universal probe #30 (Roche, 04687639001, Basel, Switzerland). This set was designed to amplify nucleotides 1291–1354 in the GCPIII transcript (NM_005467) which covers regions in exons 11 and 12 and corresponds to amino acids 416–437 in the longest ORF. The expected size of the amplified product was 64 bases; the size of a possibly amplified genomic DNA sequence was 5308 bases.

As a standard for absolute quantification, serial 10-fold dilutions covering concentrations from 10^7 to 10^2 copies per reaction of pcDNA4 plasmid with subcloned protein-coding sequence of either GCPII (longest ORF from NM_004476 coding amino acids 1–750, i.e. full-length GCPII) or GCPIII (longest ORF from NM_005467 coding amino acids 1–740, i.e. full-length GCPIII) were amplified with both assay sets. The initial concentration of plasmid DNA (purified by QIAprep Spin Miniprep Kit; Qiagen, Venlo, Netherlands) prior to dilution was determined spectrophotometrically by absorption at 260 nm (Nanodrop ND-1000; Thermo Scientific). To enable precise comparison between the determined amounts of both transcripts, obtained calibration curves were further normalized against each other by quantification of common regions in both plasmids. The ampicillin resistance gene region was quantified with a set of primers of sequences 5′-GCA GAA GTG GTC CTG CAA CT-3′ and 5′-AGC TTC CCG GCA ACA ATT A-3′ and Universal probe #58 (Roche). In this way, two calibration curves were obtained for each plasmid, one for the amplification of target transcript and one for the common sequence. Finally, the slope and intercept values of both curves were transformed for each plasmid so that the transformed slope and intercept values of the curves for the common sequence were equal and corresponded to the average value between the two plasmids.

To assess the selectivity of qPCR amplification, both pcDNA4 plasmids with subcloned protein-coding sequences of either GCPII or GCPIII (10^6 copies per reaction) were amplified in the same qPCR setup by both assay sets, and possible products were inspected by agarose gel electrophoresis. For the same reason, amplification of isolated human genomic DNA was tested in the same way. The amount of genomic DNA was quantified by a set of primers of sequences 5′-GAG AAC CGT TTG AAT GAA ACT GAG-3′ and 5′-TTG GAT GAA CAG GAA TAC TTG GAA GA-3′ and a fluorescent hydrolysis probe of sequence 5′-ACA GCC TCT GCA ATT CCA CGC CTA T-3′, which detects the intron–exon junction of the FOLH1 gene (gene coding for GCPII).

The amount of both GCPII and GCPIII transcripts was then measured in 1.0 μL of 10-fold diluted tissue cDNA libraries obtained from Clontech (Human MTC Panel I and II; Takara Bio, Kyoto, Japan).

All qPCR reactions were carried out in triplicate in FrameStar 480/96 multiwell plates (4titude, Dorking, UK) sealed with adhesive foil (Roche) using a LightCycler 480 II instrument (Roche) in a total volume of 10 μL. Each reaction consisted of a LightCycler 480 Probe Master (Roche) diluted according to the manufacturer's instructions, forward and reverse primer (1 μM final concentration each), fluorescent probe (final concentration of Roche universal probes was 50 nM; final concentration of custom probes was 100 nM) and 1 μL of sample or template DNA (positive and nontemplate controls as well as interplate calibrators were included on each plate). Initial denaturation for 3 min at 95 °C was followed by 45 cycles of 10 s at 95 °C, 30 s at 66 °C and 30 s at 72 °C. The threshold cycle numbers (C_q) were then determined from fluorescence intensities acquired during the qPCR runs by second derivative maximum method using LIGHTCYCLER 480 software (Roche). The presence and the size of PCR products was analysed in all qPCR reactions by agarose gel electrophoresis.

Acknowledgements

We thank Prof Barbara Slusher (School of Medicine, John Hopkins University, MD, USA) for her kind gift of the 2-PMPA inhibitor; Radko Souček for amino acid analysis; Dr Sebastian Zoll for data collection, scaling and molecular replacement; Jana Starková for cultivation of S2 cells; Dr Vlasta Korunová for AAS; and Dr Pavel Šácha for recloning the inactive GCPII Glu424Ala into the vector pMT/Bip/AviTEV/rhGCPII. The financial support of the Czech Science Foundation (GA CR, projects P208-12-G016 and 14-31419S) and InterBioMed I project LO 1302 and

LO 1304 (to PP) from the Ministry of Education of the Czech Republic is gratefully acknowledged.

Author contributions

MN performed protein purification, crystallization and kinetic studies; JT and PP performed X-ray structure refinement and validation; JS synthesized BCG; KH prepared protein samples for AAS; LR and TAR worked out the QM/MM models; VN quantified GCPII/III in human tissues; JK initiated and led the project; MN, JT, LR, KH, VN and JK analysed the data and wrote the manuscript.

References

1 Hlouchova K, Navratil V, Tykvart J, Sacha P & Konvalinka J (2012) GCPII variants, paralogs and orthologs. *Curr Med Chem* **19**, 1316–1322.
2 Pangalos MN, Neefs JM, Somers M, Verhasselt P, Bekkers M, van der Helm L, Fraiponts E, Ashton D & Gordon RD (1999) Isolation and expression of novel human glutamate carboxypeptidases with N-acetylated alpha-linked acidic dipeptidase and dipeptidyl peptidase IV activity. *J Biol Chem* **274**, 8470–8483.
3 Hlouchova K, Barinka C, Klusak V, Sacha P, Mlcochova P, Majer P, Rulisek L & Konvalinka J (2007) Biochemical characterization of human glutamate carboxypeptidase III. *J Neurochem* **101**, 682–696.
4 Bzdega T, Crowe SL, Ramadan ER, Sciarretta KH, Olszewski RT, Ojeifo OA, Rafalski VA, Wroblewska B & Neale JH (2004) The cloning and characterization of a second brain enzyme with NAAG peptidase activity. *J Neurochem* **89**, 627–635.
5 Robinson MB, Blakely RD, Couto R & Coyle JT (1987) Hydrolysis of the brain dipeptide N-acetyl-L-aspartyl-L-glutamate. Identification and characterization of a novel N-acetylated alpha-linked acidic dipeptidase activity from rat brain. *J Biol Chem* **262**, 14498–14506.
6 Chandler CJ, Wang TTY & Halsted CH (1986) Pteroylpolyglutamate hydrolase from human jejunal brush-borders – purification and characterization. *J Biol Chem* **261**, 928–933.
7 Navratil M, Ptacek J, Sacha P, Starkova J, Lubkowski J, Barinka C & Konvalinka J (2014) Structural and biochemical characterization of the folyl-poly-gamma-L-glutamate hydrolyzing activity of human glutamate carboxypeptidase II. *FEBS J* **281**, 3228–3242.
8 Huber F, Montani M, Sulser T, Jaggi R, Wild P, Moch H, Gevensleben H, Schmid M, Wyder S & Kristiansen G (2015) Comprehensive validation of published immunohistochemical prognostic biomarkers of prostate cancer—what has gone wrong? A blueprint for the way forward in biomarker studies. *Br J Cancer* **112**, 140–148.
9 Queisser A, Hagedorn SA, Braun M, Vogel W, Duensing S & Perner S (2015) Comparison of different prostatic markers in lymph node and distant metastases of prostate cancer. *Mod Pathol* **28**, 138–145.
10 Foss CA, Mease RC, Cho SY, Kim HJ & Pomper MG (2012) GCPII imaging and cancer. *Curr Med Chem* **19**, 1346–1359.
11 Tykvart J, Schimer J, Barinkova J, Pachl P, Postova-Slavetinska L, Majer P, Konvalinka J & Sacha P (2014) Rational design of urea-based glutamate carboxypeptidase II (GCPII) inhibitors as versatile tools for specific drug targeting and delivery. *Bioorg Med Chem* **22**, 4099–4108.
12 Tykvart J, Navratil V, Sedlak F, Corey E, Colombatti M, Fracasso G, Koukolik F, Barinka C, Sacha P & Konvalinka J (2014) Comparative analysis of monoclonal antibodies against prostate-specific membrane antigen (PSMA). *Prostate* **74**, 1674–1690.
13 Collard F, Vertommen D, Constantinescu S, Buts L & Van Schaftingen E (2011) Molecular identification of beta-citrylglutamate hydrolase as glutamate carboxypeptidase 3. *J Biol Chem* **286**, 38220–38230.
14 Miyake M, Kakimoto Y & Sorimachi M (1978) Isolation and identification of beta-citryl-L-glutamic acid from newborn rat-brain. *Biochim Biophys Acta* **544**, 656–666.
15 Miyake M, Kume S & Kakimoto Y (1982) Correlation of the level of beta-citryl-L-glutamic acid with spermatogenesis in rat testes. *Biochim Biophys Acta* **719**, 495–500.
16 Miyake M, Innami T & Kakimoto Y (1983) A beta-citryl-L-glutamate-hydrolysing enzyme in rat testes. *Biochim Biophys Acta* **760**, 206–214.
17 Hamada-Kanazawa M, Kouda M, Odani A, Matsuyama K, Kanazawa K, Hasegawa T, Narahara M & Miyake M (2010) Beta-citryl-L-glutamate is an endogenous iron chelator that occurs naturally in the developing brain. *Biol Pharm Bull* **33**, 729–737.
18 Rovenská M, Hlouchová K, Sácha P, Mlcochová P, Horák V, Zámecník J, Barinka C & Konvalinka J (2008) Tissue expression and enzymologic characterization of human prostate specific membrane antigen and its rat and pig orthologs. *Prostate* **68**, 171–182.
19 Tykvart J, Sacha P, Barinka C, Knedlik T, Starkova J, Lubkowski J & Konvalinka J (2012) Efficient and versatile one-step affinity purification of in vivo biotinylated proteins: expression, characterization and structure analysis of recombinant human glutamate carboxypeptidase II. *Protein Expr Purif* **82**, 106–115.
20 Zhang AX, Murelli RP, Barinka C, Michel J, Cocleaza A, Jorgensen WL, Lubkowski J & Spiegel DA (2010) A remote arene-binding site on prostate specific membrane antigen revealed by antibody-recruiting small molecules. *J Am Chem Soc* **132**, 12711–12716.

21 Hlouchova K, Barinka C, Konvalinka J & Lubkowski J (2009) Structural insight into the evolutionary and pharmacologic homology of glutamate carboxypeptidases II and III. *FEBS J* **276**, 4448–4462.
22 Klusak V, Barinka C, Plechanovova A, Mlcochova P, Konvalinka J, Rulisek L & Lubkowski J (2009) Reaction mechanism of glutamate carboxypeptidase II revealed by mutagenesis, X-ray crystallography, and computational methods. *Biochemistry* **48**, 4126–4138.
23 Mesters JR, Barinka C, Li WX, Tsukamoto T, Majer P, Slusher BS, Konvalinka J & Hilgenfeld R (2006) Structure of glutamate carboxypeptidase II, a drug target in neuronal damage and prostate cancer. *EMBO J* **25**, 1375–1384.
24 DeLano WL (2004) Use of PYMOL as a communications tool for molecular science. *Abstr Pap Am Chem Soc* **228**, U313–U314.
25 Diederichs K & Karplus PA (1997) Improved R-factors for diffraction data analysis in macromolecular crystallography. *Nat Struct Biol* **4**, 269–275.
26 Vaguine AA, Richelle J & Wodak SJ (1999) SFCHECK: a unified set of procedures for evaluating the quality of macromolecular structure-factor data and their agreement with the atomic model. *Acta Crystallogr D* **55**, 191–205.
27 Dodson EJ, Winn M & Ralph A (1997) Collaborative computational project, number 4: providing programs for protein crystallography. *Methods Enzymol* **277**, 620–633.
28 Davis IW, Leaver-Fay A, Chen VB, Block JN, Kapral GJ, Wang X, Murray LW, Arendall WB, Snoeyink J, Richardson JS *et al.* (2007) MolProbity: all-atom contacts and structure validation for proteins and nucleic acids. *Nucleic Acids Res* **35**, W375–W383.
29 Chen VB, Arendall WB III, Headd JJ, Keedy DA, Immormino RM, Kapral GJ, Murray LW, Richardson JS & Richardson DC (2010) MolProbity: all-atom structure validation for macromolecular crystallography. *Acta Crystallogr D* **66**, 12–21.
30 Ryden SE, Kirkish LS & McCann DS (1976) Evaluation of serum ionic calcium measurement in a general hospital population. *Am J Clin Pathol* **66**, 634–638.
31 Magneson GR, Puvathingal JM & Ray WJ (1987) The concentrations of free Mg2 + and free Zn2 + in equine blood plasma. *J Biol Chem* **262**, 11140–11148.
32 Frederickson CJ, Suh SW, Silva D, Frederickson CJ & Thompson RB (2000) Importance of zinc in the central nervous system: the zinc-containing neuron. *J Nutr* **130**, 1471s–1483s.
33 Kelleher SL, McCormick NH, Velasquez V & Lopez V (2011) Zinc in specialized secretory tissues: roles in the pancreas, prostate, and mammary gland. *Adv Nutr* **2**, 101–111.
34 Tykvart J, Schimer J, Jančařík A, Bařinková J, Navrátil V, Starková J, Šrámková K, Konvalinka J, Majer P & Šácha P (2015) Design of highly potent urea-based, exosite-binding inhibitors selective for glutamate carboxypeptidase II. *J Med Chem* **58**, 4357–4363.
35 Cunha AC, Weigle B, Kiessling A, Bachmann M & Rieber EP (2006) Tissue-specificity of prostate specific antigens: comparative analysis of transcript levels in prostate and non-prostatic tissues. *Cancer Lett* **236**, 229–238.
36 Barinka C, Starkova J, Konvalinka J & Lubkowski J (2007) A high-resolution structure of ligand-free human glutamate carboxypeptidase II. *Acta Crystallogr F* **63**, 150–153.
37 Mueller U, Darowski N, Fuchs MR, Förster R, Hellmig M, Paithankar KS, Pühringer S, Steffien M, Zocher G & Weiss MS (2012) Facilities for macromolecular crystallography at the Helmholtz-Zentrum Berlin. *J Synchrotron Radiat* **19**, 442–449.
38 Kabsch W (2010) Xds. *Acta Crystallogr D* **66**, 125–132.
39 Krug M, Weiss MS, Heinemann U & Mueller U (2012) XDSAPP: a graphical user interface for the convenient processing of diffraction data using XDS. *J Appl Crystallogr* **45**, 568–572.
40 Vagin A & Teplyakov A (2000) An approach to multi-copy search in molecular replacement. *Acta Crystallogr D* **56**, 1622–1624.
41 Bailey S (1994) The Ccp4 suite – programs for protein crystallography. *Acta Crystallogr D* **50**, 760–763.
42 Murshudov GN, Vagin AA & Dodson EJ (1997) Refinement of macromolecular structures by the maximum-likelihood method. *Acta Crystallogr D* **53**, 240–255.
43 Murshudov GN, Skubak P, Lebedev AA, Pannu NS, Steiner RA, Nicholls RA, Winn MD, Long F & Vagin AA (2011) REFMAC5 for the refinement of macromolecular crystal structures. *Acta Crystallogr D* **67**, 355–367.
44 Emsley P, Lohkamp B, Scott WG & Cowtan K (2010) Features and development of Coot. *Acta Crystallogr D* **66**, 486–501.
45 Winn MD, Ballard CC, Cowtan KD, Dodson EJ, Emsley P, Evans PR, Keegan RM, Krissinel EB, Leslie AGW, McCoy A *et al.* (2011) Overview of the CCP4 suite and current developments. *Acta Crystallogr D* **67**, 235–242.
46 Ryde U & Olsson MHM (2001) Structure, strain, and reorganization energy of blue copper models in the protein. *Int J Quantum Chem* **81**, 335–347.
47 Ahlrichs R, Bär M, Häser M, Horn H & Kölmel C (1989) Electronic structure calculations on workstation computers: the program system turbomole. *Chem Phys Lett* **162**, 165–169.
48 Maier JA, Martinez C, Kasavajhala K, Wickstrom L, Hauser KE & Simmerling C (2015) ff14SB: improving the accuracy of protein side chain and backbone parameters from ff99SB. *J Chem Theory Comput* **11**, 3696–3713.

49 Perdew JP, Burke K & Ernzerhof M (1996) Generalized gradient approximation made simple. *Phys Rev Lett* **77**, 3865–3868.
50 Tao J, Perdew JP, Staroverov VN & Scuseria GE (2003) Climbing the density functional ladder: nonempirical meta-generalized gradient approximation designed for molecules and solids. *Phys Rev Lett* **91**, 146401.
51 Guo HY, Naser SA, Ghobrial G & Phanstiel O (2002) Synthesis and biological evaluation of new citrate-based siderophores as potential probes for the mechanism of iron uptake in mycobacteria. *J Med Chem* **45**, 2056–2063.
52 Barinka C, Rinnova M, Sacha P, Rojas C, Majer P, Slusher BS & Konvalinka J (2002) Substrate specificity, inhibition and enzymological analysis of recombinant human glutamate carboxypeptidase II. *J Neurochem* **80**, 477–487.
53 Roth M (1971) Fluorescence Reaction for Amino Acids. *Anal Chem* **43**, 880–882.

Supporting information

Additional Supporting Information may be found online in the supporting information tab for this article:
Data S1. Supplementary information.

7.2. Publication II

Knedlik T., Vorlova B., Navratil V., Tykvart J., Sedlak F., Vaculin S., Franek M., Sacha P., and Konvalinka J.:

Mouse glutamate carboxypeptidase II (GCPII) has a similar enzyme activity and inhibition profile but a different tissue distribution to human GCPII.

FEBS Open Bio 2017, 7(9):1362-1378.

FEBS openbio

FEBS PRESS science publishing by scientists

Mouse glutamate carboxypeptidase II (GCPII) has a similar enzyme activity and inhibition profile but a different tissue distribution to human GCPII

Tomáš Knedlík[1,2], Barbora Vorlová[1,3], Václav Navrátil[1,2], Jan Tykvart[1,2,†], František Sedlák[1,3,4], Šimon Vaculín[5], Miloslav Franěk[5], Pavel Šácha[1] and Jan Konvalinka[1,2]

1 Institute of Organic Chemistry and Biochemistry of the Czech Academy of Sciences, Prague, Czech Republic
2 Department of Biochemistry, Faculty of Science, Charles University, Prague, Czech Republic
3 First Faculty of Medicine, Charles University, Prague, Czech Republic
4 Department of Genetics and Microbiology, Faculty of Science, Charles University, Prague, Czech Republic
5 Department of Normal, Pathological and Clinical Physiology, Third Faculty of Medicine, Charles University, Prague, Czech Republic

Keywords
glutamate carboxypeptidase II; mouse animal model; neuronal disorders; prostate cancer; prostate-specific membrane antigen

Correspondence
J. Konvalinka, Institute of Organic Chemistry and Biochemistry of the CAS, v.v.i., Flemingovo n. 2, Prague 6, 16610, Czech Republic
Fax: +420 220 183 578
Tel: +420 220 183 218
E-mail: konval@uochb.cas.cz

†Present address
Donnelly Centre for Cellular and Biomolecular Research, University of Toronto, Toronto, ON, Canada

(Received 18 April 2017, revised 23 June 2017, accepted 19 July 2017)

doi:10.1002/2211-5463.12276

Glutamate carboxypeptidase II (GCPII), also known as prostate-specific membrane antigen (PSMA) or folate hydrolase, is a metallopeptidase expressed predominantly in the human brain and prostate. GCPII expression is considerably increased in prostate carcinoma, and the enzyme also participates in glutamate excitotoxicity in the brain. Therefore, GCPII represents an important diagnostic marker of prostate cancer progression and a putative target for the treatment of both prostate cancer and neuronal disorders associated with glutamate excitotoxicity. For the development of novel therapeutics, mouse models are widely used. However, although mouse GCPII activity has been characterized, a detailed comparison of the enzymatic activity and tissue distribution of the mouse and human GCPII orthologs remains lacking. In this study, we prepared extracellular mouse GCPII and compared it with human GCPII. We found that mouse GCPII possesses lower catalytic efficiency but similar substrate specificity compared with the human protein. Using a panel of GCPII inhibitors, we discovered that inhibition constants are generally similar for mouse and human GCPII. Furthermore, we observed highest expression of GCPII protein in the mouse kidney, brain, and salivary glands. Importantly, we did not detect GCPII in the mouse prostate. Our data suggest that the differences in enzymatic activity and inhibition profile are rather small; therefore, mouse GCPII can approximate human GCPII in drug development and testing. On the other hand, significant differences in GCPII tissue expression must be taken into account when developing novel GCPII-based anticancer and therapeutic methods, including targeted anticancer drug delivery systems, and when using mice as a model organism.

Glutamate carboxypeptidase II (GCPII; EC 3.4.17.21) is a membrane metalloprotease that has been studied intensively over the past 20 years in three different scientific fields: neuroscience, prostate oncology, and dietology. In humans, GCPII is expressed predominantly in the brain [1,2], prostate [3,4], small intestine

Abbreviations
Avi-hGCPII, recombinant extracellular human GCPII; Avi-mGCPII, recombinant extracellular mouse GCPII; GCPII, glutamate carboxypeptidase II; GCPIII, glutamate carboxypeptidase III; NAAG, *N*-acetyl-L-aspartyl-L-glutamate; PSMA, prostate-specific membrane antigen.

[5], and kidney [4,6]. Because GCPII plays different physiological roles in these tissues, three alternative names for the enzyme have historically been used: *N*-acetylated alpha-linked acidic dipeptidase (NAALADase) [7], prostate-specific membrane antigen (PSMA) [8], and folate hydrolase [5]. The close GCPII homolog GCPIII [9,10], recently identified as β-citryl-glutamate hydrolase [11], is also expressed in human tissues.

In the human central nervous system, GCPII hydrolyzes the most abundant peptide neurotransmitter, *N*-acetyl-L-aspartyl-L-glutamate (NAAG), into *N*-acetyl-L-aspartate and glutamate [7]. Inhibition of this proteolytic activity with selective GCPII inhibitors has been shown to be neuroprotective in experiments with mouse models [12]; NAAG activation of metabotropic glutamate type 3 receptors exerts neuroprotective effects toward glutamate-mediated excitotoxicity caused by elevated levels of glutamate released during stroke, traumatic brain injury, and other pathological conditions [13–15]. In addition to the brain, GCPII is expressed on the human jejunal brush border [5,16], where it cleaves the terminal glutamates from poly-γ-glutamylated folates, enabling their transport across the intestinal mucosa (folate absorption) [17]. On the other hand, the function of GCPII in the human prostate is unknown. GCPII is overexpressed in prostate cancer [3,18]; therefore, it has been suggested as a promising target for prostate cancer diagnosis and treatment using targeted strategies [19–21].

An appropriate animal model is necessary for the development and testing of novel therapeutics. Mice, rats, and pigs are among the most promising candidates to become such a model for GCPII research. Several years ago, our laboratory conducted a study comparing human GCPII with its porcine and rat orthologs [22]. The orthologs showed similarity in their enzymatic properties, but considerable differences in terms of their tissue distribution [22]. However, mouse GCPII was not included in the study, even though mice now are the most widely used preclinical models for GCPII-targeted research (stroke [12], traumatic brain injury [23,24], amyotrophic lateral sclerosis [25], inflammatory, and neuropathic pain [26,27], reviewed in Refs [13,28]). Therefore, a comparative analysis of mouse GCPII characterization is needed.

Mouse GCPII shares 91% amino acid similarity with human GCPII and preserves the internalization signal MXXXL, despite low similarity in the intracellular domain [29]. Mouse GCPII also possesses both NAAG-hydrolyzing and folate hydrolase activities [29]. In contrast to the expression pattern of human GCPII, mouse GCPII is expressed in largest amounts in the kidney and, surprisingly, is absent in the mouse prostate [29]. Results from studies with GCPII-knockout mice have been contradictory: some reports have described normal development to adulthood [9,30] and others have noted early embryonic death [31,32].

In the current study, we prepared and characterized recombinant mouse GCPII and compared it with its human counterpart. We put a strong focus on distribution of GCPII in mouse tissues, as this information is highly relevant for the development of novel GCPII-based anticancer and neuroprotective therapies using mouse models.

Results

Efficient one-step purification method yields purified recombinant mouse GCPII (Avi-mGCPII)

As recombinant extracellular human GCPII was shown to correctly represent the endogenous full-length GCPII [33,34], we prepared the recombinant extracellular part of mouse GCPII (Avi-mGCPII) using a *Drosophila* S2 expression system, according to the protocol previously established in our laboratory [34]. Avi-mGCPII has a TEV cleavable Avi-tag sequence attached to the N terminus of the mouse GCPII extracellular domain (amino acids 45–752), enabling fast one-step purification (Fig. 1A).

Avi-mGCPII was purified from the conditioned medium of cells stably transfected with Avi-mGCPII by affinity chromatography based on the biotin–streptavidin interaction [34], yielding 3 mg of pure protein from 1 L conditioned medium (Fig. 1B).

Mouse GCPII has lower catalytic efficiency than human GCPII

To characterize the enzyme activity of Avi-mGCPII, we determined kinetic parameters (K_M and k_{cat}) for cleavage of both substrates: *N*-acetyl-L-aspartyl-L-glutamate (NAAG) and pteroyl-di-L-glutamate (Table 1). The data revealed that the catalytic efficiency of Avi-mGCPII is lower than that of its human counterpart. The enzymes had similar turnover numbers but differed in their K_M values. The differences were more pronounced for pteroyl-di-L-glutamate than for NAAG. Surprisingly, both enzymes had higher catalytic efficiencies for cleavage of pteroyl-di-L-glutamate than for NAAG (Table 1).

Furthermore, to analyze the inhibition profile of Avi-mGCPII, we determined K_i values for several commonly used GCPII inhibitors (using pteroyl-di-L-glutamate as a substrate). The set of GCPII inhibitors included 2-(phosphonomethyl)pentanedioic acid

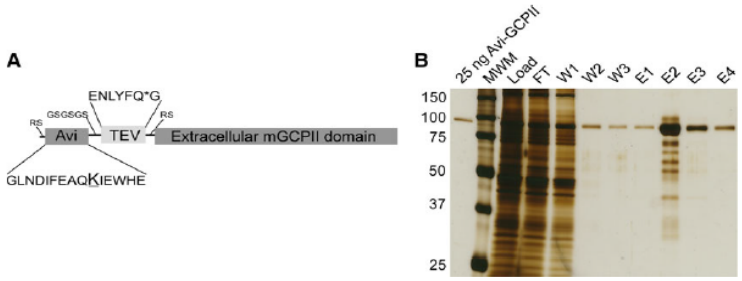

Fig. 1. Schematic structure of Avi-mGCPII and affinity purification. (A) Schematic structure of Avi-mGCPII containing an Avi sequence (the biotinylated lysine residue is enlarged and underlined) and TEV protease cleavage sequence (the cleavage site is marked with an asterisk). (B) Silver-stained SDS/PAGE gel showing affinity purification of Avi-mGCPII expressed in *Drosophila* S2 cells. MWM, molecular weight marker; load, concentrated S2 cell medium; FT, flow-through; W1–W3, wash fractions; E1–E4, elution fractions. Ten microliter samples was loaded onto the gel, except for the E2 fraction (1 μL was loaded).

Table 1. Kinetic parameters of recombinant mouse and human GCPII (Avi-mGCPII and Avi-hGCPII, respectively) for their substrates. Kinetic parameters (K_M and k_{cat}) of *N*-acetyl-L-aspartyl-L-glutamate (NAAG) and pteroyl-di-L-glutamate cleavage were determined using radioenzymatic [34] and HPLC assays [39], respectively. The values shown are mean ± standard deviation of duplicate measurements.

	NAAG			Pteroyl-di-L-glutamate		
Enzymes	K_M [nM]	k_{cat} [s^{-1}]	k_{cat}/K_M [× 10^7 s^{-1} M]	K_M [nM]	k_{cat} [s^{-1}]	k_{cat}/K_M [× 10^7 s^{-1} M]
Avi-mGCPII	1900 ± 100	1.44 ± 0.02	0.077 ± 0.001	290 ± 20	3.63 ± 0.09	1.26 ± 0.08
Avi-hGCPII	550 ± 60	1.45 ± 0.04	0.265 ± 0.007	39 ± 2	5.09 ± 0.09	13.2 ± 0.8

(2-PMPA) [35], (S)-2-(3-((S)-1-carboxy-3-methylbutyl) ureido)pentanedioic acid (ZJ-43) [36], (*S*)-2-(3-((*S*)-1-carboxy-(4-iodobenzamido)pentyl)ureido)pentanedioic acid (DCIBzL) [37], quisqualate, DKFZ-PSMA-11 [38], and beta-citryl-L-glutamate (Table 2). We also tested three compounds recently prepared in our laboratory: JB-352 and JB-277 (originally reported as compounds **3** and **22a** [39]) and JS-686 (originally compound **7** [40]).

Mouse and human GCPII exhibit similar substrate specificities

To obtain information about the substrate specificity of Avi-mGCPII, we screened 19 different dipeptide libraries of the general formula *N*-Ac-A-X [where A represents a given single N-terminal amino acid and X represents a mixture of 19 proteinogenic amino acids (all except for cysteine)]. The *N*-acetylated dipeptide libraries were incubated with the enzymes, and the cleaved amino acids were analyzed by HPLC [41]. As a negative control, the potent and selective GCPII inhibitor 2-PMPA was used to block the specific enzyme activity.

Overall, we found no significant differences in hydrolysis of dipeptide substrates between mouse and human GCPII, as illustrated by heat maps showing mouse and human GCPII processing of individual *N*-acetylated dipeptides (Fig. 2). The enzymes exhibited a clear preference for glutamate in the C-terminal position (i.e., glutamate carboxypeptidase activity); mouse GCPII possesses higher selectivity toward the C-terminal glutamate.

GCPII is highly expressed in mouse kidney, brain, and major salivary glands

To analyze GCPII distribution in mouse tissues, we collected tissues samples from six mice (three females and three males) and analyzed them by western blot using the anti-GCPII antibody GCP-04 [2,42].

Mouse GCPII was expressed predominantly in the mouse kidney and brain (Fig. 3), which is in agreement with previous data [9]. Interestingly, we observed high and variable expression in the mouse major salivary glands. The different apparent molecular weights are likely caused by different glycosylation of GCPII in the tissues.

We also determined the NAAG-hydrolyzing activity in the tissue lysate samples using tritium-labeled NAAG as a substrate and compared these results with

Table 2. Inhibition of recombinant mouse and human GCPII (Avi-mGCPII and Avi-hGCPII, respectively) by a panel of GCPII inhibitors. Inhibition constants (K_i values) were determined using an HPLC-based assay using pteroyl-di-L-glutamate as a substrate. The values shown are mean ± standard deviation of duplicate measurements.

Compound	K_i (Avi-mGCPII) (nM)	K_i (Avi-hGCPII) (nM)
Quisqualate	580 ± 60	520 ± 80
2-PMPA	0.56 ± 0.05	0.26 ± 0.03
ZJ-43	5.9 ± 0.9	0.58 ± 0.07
JB-352	0.66 ± 0.06	0.17 ± 0.04
β-citryl-L-glutamate	24 000 ± 3000	16 000 ± 5000
DCIBzL	0.028 ± 0.003	0.017 ± 0.002
JB-277	0.68 ± 0.07	0.05 ± 0.02
DKFZ-PSMA-11	0.10 ± 0.01	0.018 ± 0.002
JS-686	0.049 ± 0.005	0.021 ± 0.004

the data obtained by western blot analysis. Recombinant mouse GCPII was used as a standard, and the observed levels of NAAG-hydrolyzing activity were converted to amounts of GCPII, which were then normalized to the total protein concentrations in the homogenates (Fig. 4).

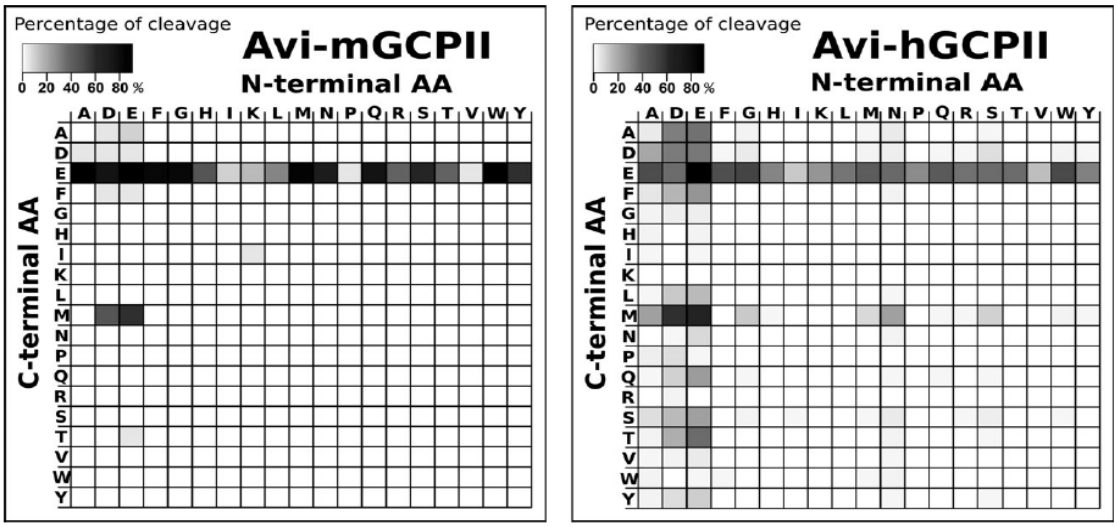

Fig. 2. Heat maps representing the substrate specificities of mouse and human GCPII. Recombinant mouse and human GCPII (Avi-mGCPII and Avi-hGCPII, respectively) were incubated with 19 dipeptide libraries of the general formula *N*-Ac-A-X-OH [where A represents a given single N-terminal amino acid and X represents a mixture of 19 proteinogenic amino acids (all except for cysteine)]. The samples were incubated for 1.5 h at 37 °C, and the cleaved C-terminal amino acids were quantified using HPLC. As negative controls, experiments either with the GCPII-specific inhibitor 2-PMPA or without Avi-mGCPII/Avi-hGCPII were performed. The grayscale key represents the percentage of conversion of the particular amino acid in the reaction mixture.

The results confirmed high expression of GCPII in the kidney, brain, and major salivary glands. We did not detect GCPII in the mouse prostate (Fig. 4).

To further examine the location of GCPII in the highly expressing tissues, we performed immunohistochemistry using the anti-GCPII antibody GCP-04 [2,42]. We found relatively high expression in the white matter in the brain, on luminal side of proximal tubules in the kidney and in the abluminal cells in the major salivary glands (mainly in the sublingual gland) (Fig. 5).

mRNA expression profile differentiates GCPII and GCPIII expression levels in mouse tissues

The GCP-04 antibody cross-reacts with GCPIII, which also cleaves NAAG [11,43]. Therefore, we decided to further analyze the tissue distribution of both homologs by quantitative RNA determination (qPCR). For these analyses, we used either commercially available panels of mouse tissue cDNA libraries (Fig. 6A) or cDNA libraries prepared from mouse tissues (female 1 and male 1; Fig. 6B,C).

The results from commercial cDNA libraries represent the average tissue distribution of both transcripts in the mouse population. Each library was pooled from several hundred mice and normalized by the vendor to several different housekeeping genes (beta-actin, G3PDH, phospholipase A2, and ribosomal protein S29). The highest expression of mouse GCPII mRNA was in the kidney, brain, and testis, while mouse GCPIII mRNA was predominantly expressed in the testis, heart, lung, and skeletal muscle (Fig. 6A).

To gain insight into expression of both transcripts in individual mice, we also quantified mRNA transcripts in cDNA libraries prepared from mouse tissues dissected from one female and one male mouse. The results were normalized to the starting amount of total RNA and are in good agreement with findings from the pooled libraries (Fig. 6B,C).

Discussion

GCPII is a potential pharmaceutical target for a number of pathological conditions caused by glutamate excitotoxicity in the central nervous system, including stroke and traumatic brain injury. Moreover, GCPII has been intensively studied as a target for diagnosis and treatment of prostate cancer, as it is overexpressed in the malignant prostate. In last two decades, a large

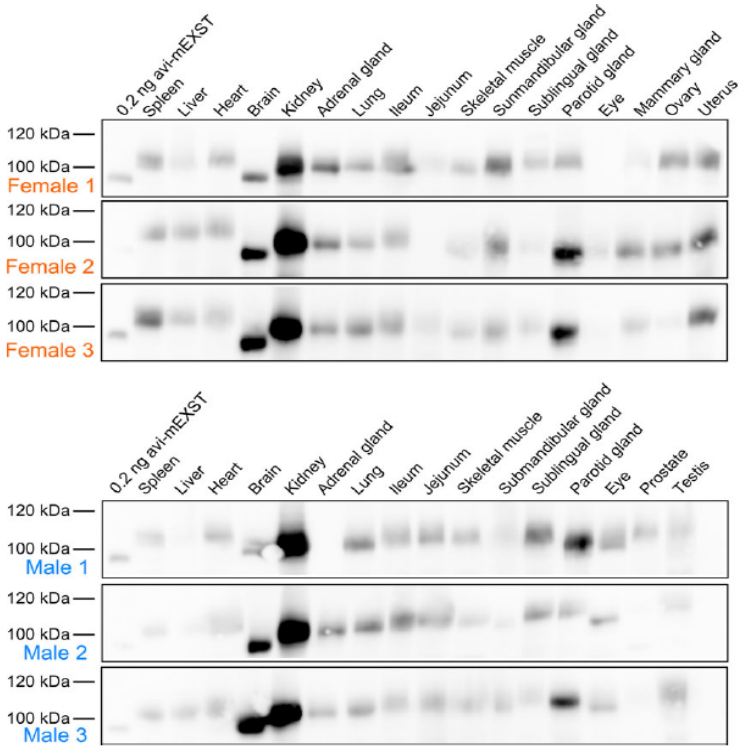

Fig. 3. Western blot analysis of GCPII expression in a panel of mouse tissues. Mouse tissue samples (from three males and three females) were homogenized, and lysates were resolved by SDS/PAGE (50 µg of total protein per lane). Mouse GCPII was visualized using the anti-GCPII primary antibody GCP-04 [2] and HRP-conjugated goat anti-mouse secondary antibody.

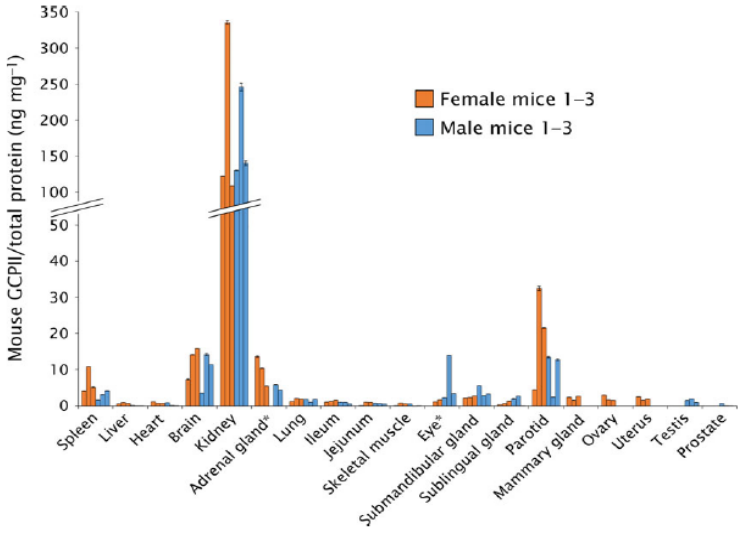

Fig. 4. GCPII expression in mouse tissues determined by radioenzymatic assay. The amount of GCPII in mouse tissues was determined by radioenzymatic assay using [^{3}H]NAAG as a substrate and recombinant mouse GCPII (Avi-mGCPII) as a standard. Each tissue sample was measured in duplicate using 1–50 µg total protein in the reaction; the amount of mouse GCPII was normalized to total protein concentration (ng GCPII per mg total protein). The assay was performed with the same tissue samples used in the western blot analysis. *Not determined (adrenal gland: sample M1; eye: sample F1).

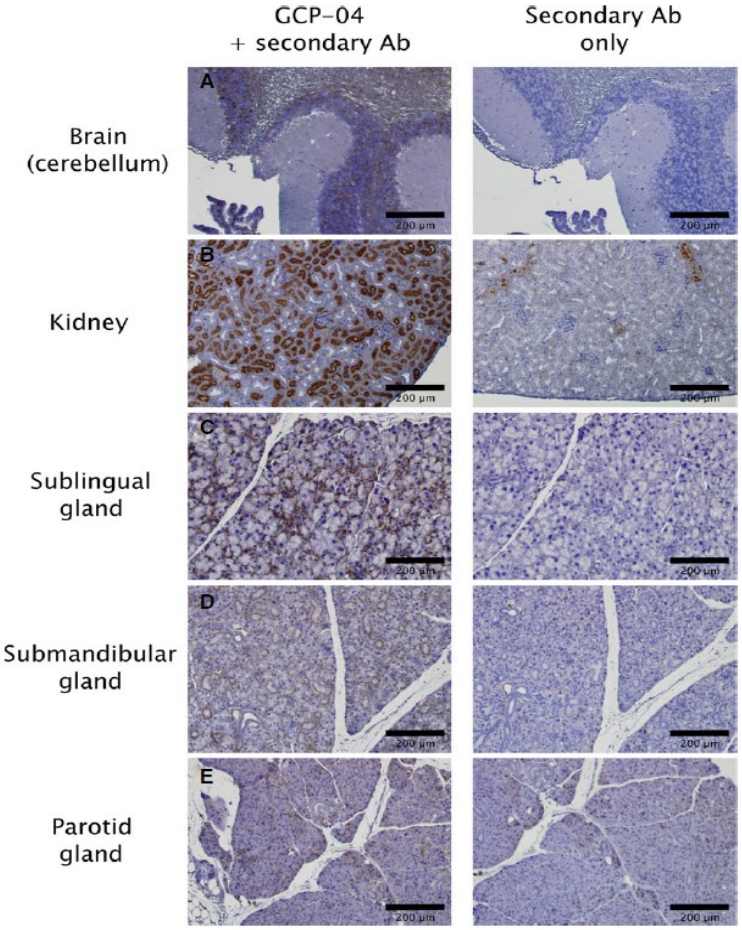

Fig. 5. Immunohistochemical staining of chosen mouse tissue sections. Formalin-fixed, paraffin-embedded mouse tissue sections were incubated with anti-GCPII antibody GCP-04 (at 10 $\mu g \cdot mL^{-1}$ concentration) to visualize and localize mouse GCPII expression [42]. (A) Brain (cerebellum): positive choroid plexus, stratum granulare, white matter. (B) Kidney: positive luminal side of proximal tubules, Bowman capsule; little crossreactivity of secondary anti-mouse antibody with capillaries and blood vessels could be seen in the negative control. (C) Sublingual gland: positive staining of abluminal cells (probably myoepitelial cells). (D) Submandibular gland: faint staining of intercallated ducts and some non-glandular abluminal cells. (E) Parotid gland: faint staining of some non-glandular abluminal cells.

number of papers have been published describing novel GCPII inhibitors acting as neuroprotective drugs [28,44] and GCPII inhibitor-based tools for imaging and/or treating prostate cancer [19,20,45–47]. Most of these compounds and methods were evaluated using mouse models. However, there has been no direct comparison of mouse and human GCPII, which would provide important information to assess the usefulness of such mouse models. Therefore, we set out to perform a systematic and detailed study to compare the enzymatic properties of mouse and human GCPII, as well as tissue distributions on both the mRNA and protein levels.

We expressed the recombinant extracellular part of mouse GCPII with an N-terminal Avi-tag (Avi-mGCPII), which enables fast and efficient one-step purification [34]. Even though GCPII is a transmembrane enzyme, its extracellular domain is the catalytically active portion and correctly represents endogenous full-length GCPII [33]. To compare the enzymatic properties of mouse and human GCPII, we analyzed the cleavage of their substrates: *N*-acetyl-L-aspartyl-L-glutamate (NAAG), which is cleaved by GCPII in the brain, and pteroyl-di-L-glutamate, which is a model substrate for poly-gamma-glutamylated folates hydrolyzed by GCPII in the small intestine. Because mouse and human GCPII have high sequence similarity (86% identity and 97% similarity in the extracellular part; Fig. 7), we did not expect to find any significant differences in their enzymatic

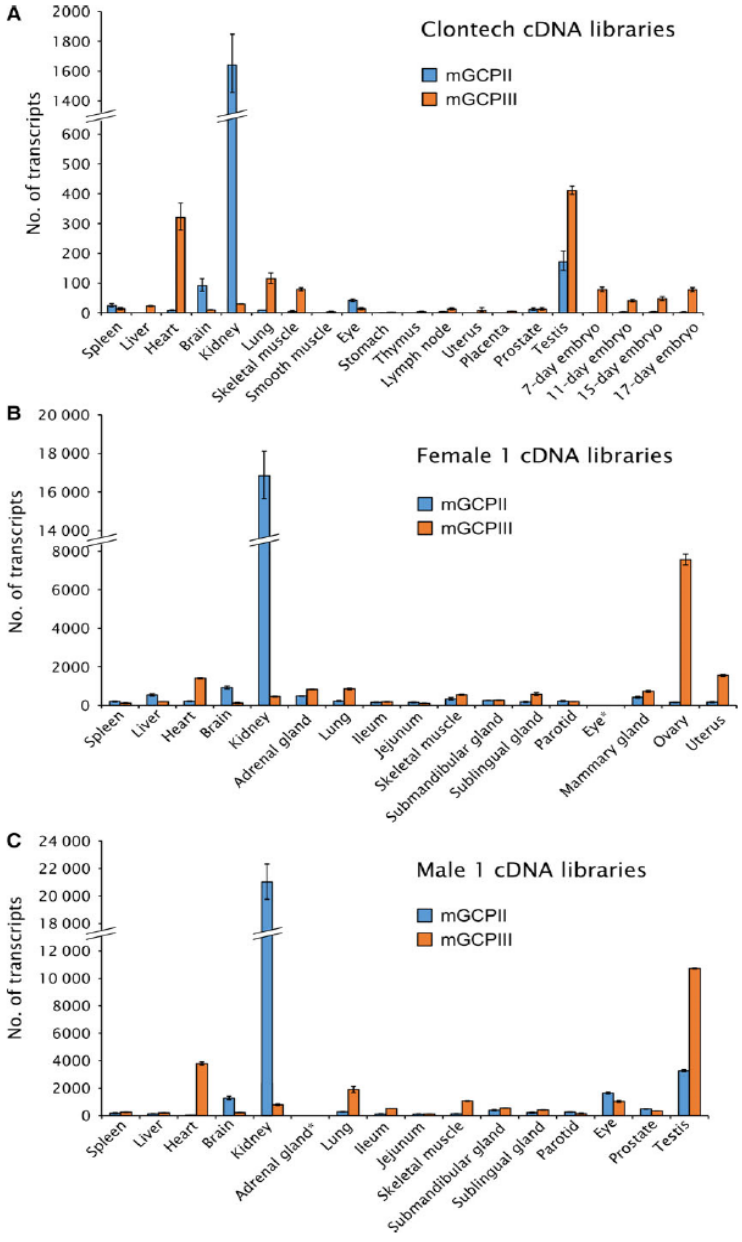

Fig. 6. Quantification of mouse GCPII and GCPIII (mGCPII and mGCPIII, respectively) transcripts using qPCR. (A) Quantification of mGCPII and mGCPIII transcripts using qPCR in commercial mouse tissue cDNA libraries from Clontech. The 'number of transcripts' corresponds to the amount of transcripts in 1.0 μL of 10-fold diluted cDNA libraries (for experimental details, see Experimental procedures). Error bars show standard deviations from triplicate measurements. (B, C) Quantification of mGCPII and mGCPIII transcripts using qPCR in cDNA libraries prepared from mouse tissues dissected from one female (B) and one male mouse (C). The 'number of transcripts' corresponds to the amount of transcripts per 10 ng of total RNA as a starting material for cDNA synthesis (for experimental details, see Experimental procedures). Error bars show standard deviations from triplicate measurements. *Not determined.

properties. In fact, we found that while the enzymes are quite similar in NAAG-hydrolyzing activity, there is an order-of-magnitude difference in their catalytic efficiencies for cleavage of pteroyl-di-L-glutamate. This difference lies in the K_M values of mouse and human GCPII (290 vs. 39 nM for pteroyl-di-L-glutamate and

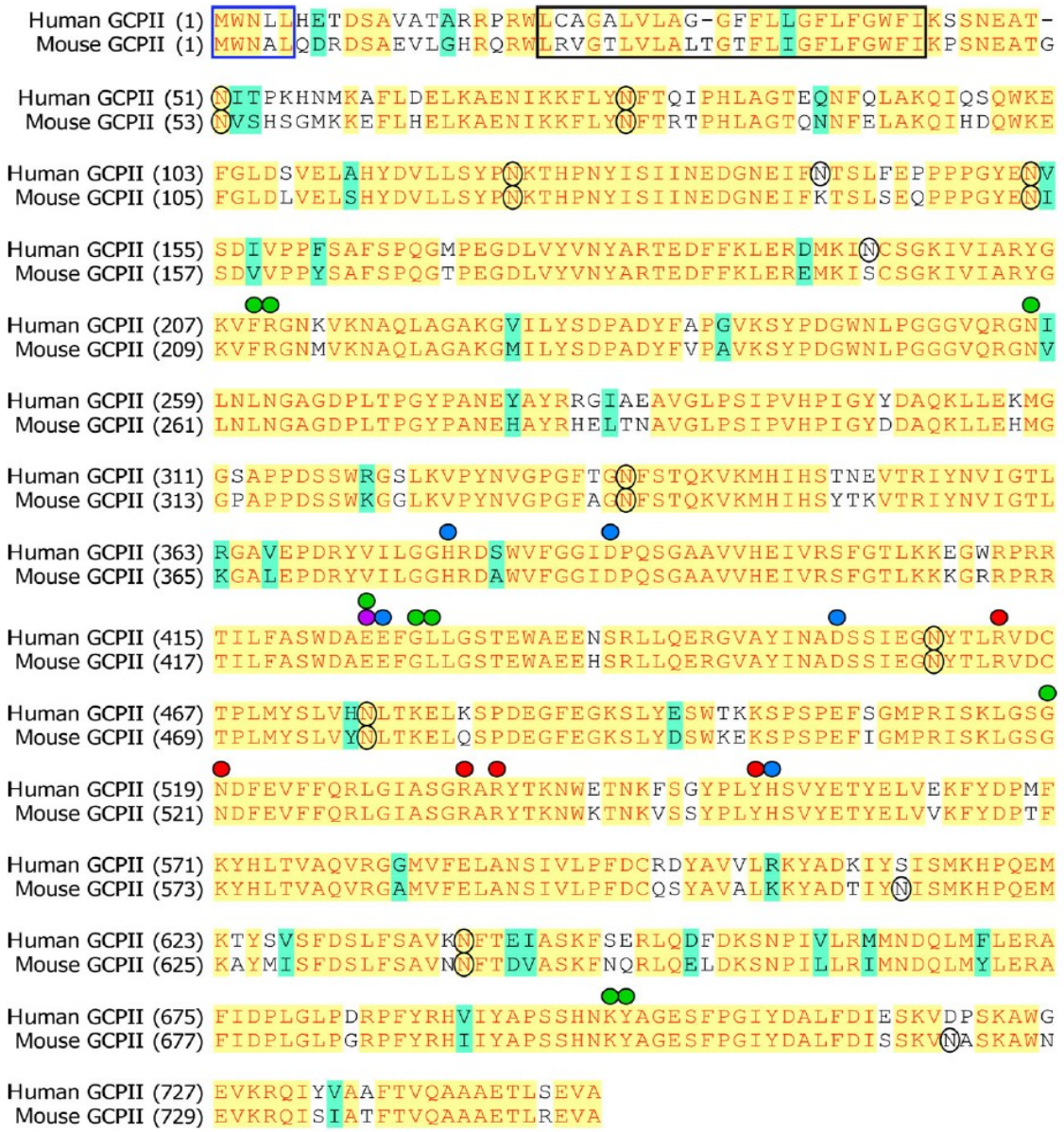

Fig. 7. Sequence alignment of the mouse and human GCPII proteins. Identical amino acid residues are highlighted in yellow, similar residues in green, and different residues in white. A blue frame marks the internalization signal MXXXL [54], and a black frame corresponds to predicted GCPII transmembrane domain (predicted by TMHMM Server v. 2.0). Black circles denote potential N-glycosylation sites ('N-X-S/T'). Green spheres: residues defining the S1′ pocket [49]; red spheres: residues forming the S1 pocket [48]; purple sphere: proton shuttle catalytic base [55]; blue spheres: zinc ligands [56,57].

1900 vs. 550 nM for NAAG). Their turnover numbers are quite similar (3.6 vs. 5.1 s^{-1} and 1.4 vs. 1.5 s^{-1}, respectively) (see Table 1). Slightly surprisingly, our data revealed that the catalytic efficiency of NAAG cleavage by mouse and human GCPII is significantly lower than that of pteroyl-di-L-glutamate cleavage (20-fold and 50-fold, respectively) (see Table 1).

Additionally, we analyzed the inhibition profile of Avi-mGCPII using several GCPII inhibitors commonly used in research, including 2-PMPA, ZJ-43, DCIBzL, DKFZ-PSMA-11, and quisqualate. We also tested several other inhibitors that were prepared in our laboratory. Generally, we did not observe considerable differences in the K_i values obtained for mouse and human GCPII. However, inhibitors ZJ-43 and JB-277 were exceptions; the K_i values for Avi-mGCPII were 10-fold higher (Table 2). Both compounds belong to the urea-based group of GCPII inhibitors, together with DCIBzL. Surprisingly, the K_i value of DCIBzL was identical for both enzymes. As seen in Fig. 7, mouse and human GCPII are highly similar and key amino acid residues participating in substrate binding and hydrolysis are identical [48–50]. Thus, in the absence of an experimentally determined structure of mouse GCPII, it is difficult to explain the observed differences in inhibitor binding and catalytic efficiency.

Next, we assessed the substrate specificity of Avi-mGCPII. We screened dipeptide libraries covering almost all *N*-acetylated dipeptide substrates, not including cysteine-containing dipeptides. Unsurprisingly, mouse GCPII exhibited a strong preference for glutamate in the P1′ position, cleaving almost any dipeptide with a C-terminal glutamate (i.e., glutamate carboxypeptidase activity). It also cleaves dipeptides with methionine in the P1′ position and an acidic amino acid (aspartate or glutamate) in the P1 position. Dipeptides containing any other C-terminal amino acid were not hydrolyzed by mouse GCPII. The substrate specificity of mouse GCPII thus seems to be even more pronounced than that of the human enzyme (Fig. 2).

In addition to the enzymatic properties of mouse GCPII, its tissue distribution is a relevant aspect both to understand the physiological function of the enzyme and to assess the use of mouse models for targeted drug delivery and GCPII inhibition experiments. Therefore, we set out to elucidate GCPII expression in mouse tissues. To see individual differences, we collected tissue samples from six mice (three females and three males).

To assess GCPII expression on the protein level, we prepared mouse tissue lysates and detected mouse GCPII by western blot using the anti-GCPII antibody GCP-04, which was raised against human GCPII [2,42]. Because GCP-04 recognizes a linear epitope in the GCPII primary structure (amino acids 100–104: WKEFG [22]), which is conserved in the mouse GCPII sequence, the antibody can be used for selective and sensitive detection of mouse GCPII as well. We confirmed very high expression of GCPII in the mouse kidney and high expression in the mouse brain, which is in agreement with high GCPII expression in the corresponding human tissues [22]. Furthermore, we observed high expression of GCPII in the mouse major salivary glands. Relatively high variability among individual samples of major salivary glands is probably caused by close association of salivary glands that are macroscopically quite similar. This makes the proper dissection of topographically complicated ventral cervical region particularly cumbersome and might lead to cross-contamination. Therefore, we localized GCPII expression by immunohistochemistry using anti-GCPII antibody GCP-04. We observed GCPII expression in all three salivary glands (sublingual, submandibular, and parotid); however, GCPII is expressed predominantly in the sublingual gland, while the expression in the submandibular and parotid glands is lower (Fig. 5).

Mouse prostate contains negligible levels of GCPII, which is consistent with previous findings [9] and in contrast with human prostate, which expresses large amounts of GCPII [6,22,51]. Additionally, as human and mouse prostates differ considerably in their morphology, we dissected a mouse prostate into its individual parts (anterior, dorsal, and lateral prostate) and searched for potential GCPII expression in each part separately. Nevertheless, we did not detect GCPII expression in any of the tested parts of mouse prostate. Our data suggest that GCPII might also be absent in the mouse jejunum, a tissue where human GCPII cleaves off glutamates from glutamylated folates [17]. Rat jejunum and ileum were shown not to contain GCPII, in contrast to the corresponding human tissues, which express large amounts of GCPII [22]. Folates in rat intestine are hydrolyzed by γ-glutamyl hydrolase, not GCPII [52], and the situation in mice may be thus similar.

Furthermore, we verified GCPII tissue distribution obtained by western blot analysis by quantification of NAAG-hydrolyzing activity in mouse tissues. The activity-based GCPII expression profile correlated well with the western blot results, confirming strong GCPII expression in the mouse kidney, brain, and salivary glands and no expression in mouse prostate and jejunum.

GCPIII is a close GCPII homolog found both in humans and in mouse. The GCP-04 antibody also

recognizes GCPIII but is roughly 10-fold less sensitive toward GCPIII than toward GCPII [42]. Moreover, GCPIII also hydrolyzes NAAG, although with a lower catalytic efficiency [10,11,43]. Therefore, GCPII distribution in mouse tissues obtained by western blot analysis with GCP-04 and activity assay based on NAAG hydrolysis could be distorted by a high amount of GCPIII and low amount of GCPII in a particular tissue. Because there is no specific antibody against GCPIII, we explored GCPII/GCPIII expression in mouse tissues on the mRNA level to differentiate between the two homologs. We quantified GCPII and GCPIII transcripts in both commercially available mouse tissue cDNA libraries and cDNA libraries we prepared from isolated mouse tissues (Fig. 6). Taking these qPCR data into account, GCPIII appears to be the source of the NAAG-hydrolyzing activity in the mouse ovary, uterus, and heart. GCPIII was most strongly expressed in the testis but was accompanied by rather high quantities of GCPII.

To conclude, we prepared and characterized recombinant mouse GCPII and compared it with human GCPII. We found that the differences in enzymatic activity, inhibition profile, and substrate specificity between mouse and human GCPII are rather small; therefore, mouse GCPII can serve as a suitable substitute for human GCPII in enzymological studies.

Due to the observed lack of GCPII expression in the mouse prostate, mouse might not seem to be an ideal model for the development of prostate cancer diagnostic/therapeutic agents. However, most such studies employ human tumor xenografts in mouse models. For this purpose, mice are generally suitable, because the distribution of GCPII in other tissues is quite similar to that in humans. Therefore, mouse GCPII appears to be a good model for the development of GCPII-targeted drugs for treatment of prostate cancer and neuronal disorders.

Experimental procedures

Cloning of mouse GCPII (Avi-mGCPII)

The pIRES/mGCPII plasmid encoding full-length mouse GCPII (amino acids 1-752) was a kind gift from Warren Heston (Cleveland Clinic, USA).

Because the sequence contained two conflicts compared to the annotated mouse GCPII sequence, we performed site-directed mutagenesis to remove them (G240A and E287N). The primers 5′-gctgactactttgttcctGCGgtgaagtc ctatcc-3′ and 5′-ggataggacttcacCGCaggaacaaagtagtcagc-3′ were used to remove the sequence conflict at position 240, and the primers 5′-catgagttgacaAACgctgttggccttc-3′ and 5′-gaaggccaacagcGTTtgtcaactcatg-3′ to remove the sequence conflict at position 287 (changed deoxyribonucleotides are underlined, changed codons capitalized). The mutagenesis was carried out according to the manufacturer's protocol (QuikChange™ Site-Directed Mutagenesis; Stratagene, San Diego, CA, USA).

Then, the sequence corresponding to the extracellular part of mouse GCPII (amino acids 45-752) was amplified by PCR using primers 5′-aaaagatctaaaccttccaatgaagctactgg-3′ and 5′-aaactcgagttaagctacttccctcagagtc-3′ (restriction sites introduced into the sequence are underlined; the primers introduced a *Bgl*II site at the 5′ end and an *Xho*I site at the 3′ end). The resulting DNA fragment was cleaved with *Bgl*II and *Xho*I and ligated into pMT/BiP/AviTEV/rhGCPII plasmid [34] cleaved with the same endonucleases. The correct sequence of the resulting plasmid pMT/BiP/Avi-mGCPII was verified by DNA sequencing.

Transfection of *Drosophila* S2 cells and expression of Avi-mGCPII

Drosophila S2 cells expressing BirA biotin-protein ligase localized in the endoplasmic reticulum (described in Ref. [34]) were used to prepare stable Avi-mGCPII transfectants. The cells were transfected using Calcium Phosphate Transfection Kit (Invitrogen, Waltham, MA, USA) with 9 μg of pMT/BiP/Avi-mGCPII together with 0.5 μg of pCoBlast (Invitrogen), as previously described [10]. The transfected cells were cultivated in the presence of both blasticidin (5 $\mu g \cdot mL^{-1}$, Invitrogen) and hygromycin B (300 $\mu g \cdot mL^{-1}$; Invitrogen).

To express Avi-mGCPII, approximately 2×10^6 stably transfected cells was transferred into a 35-mm Petri dish supplemented with 2 mL SF900II medium (Invitrogen). The following day, protein expression was induced by adding $CuSO_4$ (Sigma-Aldrich, St. Louis, MO, USA) to a final concentration of 1 mM. After three days, cells were harvested by centrifugation, and the medium was analyzed by western blot.

The large-scale expression of Avi-mGCPII was performed as previously described [33]. The final volume of cell suspension was 1000 mL.

Purification of Avi-mGCPII

Purification of Avi-mGCPII was performed as previously described [34]. Briefly, cell medium (1000 mL) containing secreted biotinylated Avi-mGCPII was centrifuged at 3400 ***g*** for 45 min. Then, it was concentrated 10-fold using a LabScale TFF System (Merck Millipore, Billerica, MA, USA) with a Pellicon® XL 50 Cassette, Biomax 100. The concentrated medium was centrifuged again at 3400 ***g*** for 20 min and equilibrated with 300 mM Tris/HCl, 450 mM NaCl, pH 7.2 in a 2 : 1 ratio. The equilibrated

concentrated Avi-mGCPII medium was then mixed with 1 mL Streptavidin Mutein Matrix (Roche, Basel, Switzerland) and incubated with gentle shaking at 6 °C for 15 h. Afterward, the resin was washed with 50 column volumes of 100 mM Tris/HCl, 150 mM NaCl, pH 7.2. Bound biotinylated proteins were eluted with 5 mL of 100 mM Tris/HCl, 150 mM NaCl, 2 mM D-biotin, pH 7.2, in five consecutive elution fractions (after the first elution fraction, the resin was incubated with elution buffer for 1 h). After regeneration of the resin, the flow-through fraction was again mixed with the resin, and the purification procedure was repeated.

Determination of kinetic parameters by radioenzymatic assay

Kinetic parameters (K_M and k_{cat}) of *N*-acetyl-L-aspartyl-L-glutamate (NAAG) cleavage by Avi-mGCPII were determined as previously described [34], with a minor modification: The reactions were performed in a 96-well plate, and appropriate amounts of Avi-mGCPII were mixed with 25 mM Bis-Tris propane, 150 mM NaCl, 0.001% octaethylene glycol monododecyl ether (Affymetrix, Santa Clara, CA, USA), pH 7.4.

Determination of kinetic and inhibition constants by HPLC

Kinetic parameters (K_M and k_{cat}) of pteroyl-di-L-glutamate cleavage by Avi-mGCPII, as well as K_i values for all inhibitors, were determined as previously described [39]. Briefly, in a 96-well plate, Avi-mGCPII was mixed with 25 mM Bis-Tris propane, 150 mM NaCl, 0.001% octaethylene glycol monododecyl ether (Affymetrix), pH 7.4 (and tested inhibitor, if used), into a final volume of 90 µL. Reactions were started by adding 10 µL of 4 µM pteroyl-di-L-glutamate and incubated at 37 °C for 20 min. The reactions were stopped with 20 µL of 25 µM 2-PMPA and subsequently analyzed on an Agilent 1200 Series system using an Acquity UPLC HSS T3 1.8 µm column (2.1 × 100 mm; Waters, Milford, MA, USA).

Animals and tissue isolation

Six C57BL/GJ mice (three males (M) and three females (F)) were sacrificed by cervical dislocation with agreement of the local ethical commission. The ages of the mice were as follows: M1: 5 months; M2: 8 months; M3: 12 months; F1: 8 months; F2 and F3: 12 months. Samples of tissues (for preparation of tissue lysates) were immediately transferred into microtubes and frozen at −80 °C. Samples of tissues (for qPCR quantification) were immediately transferred into RNAlater, impregnated with it for 2 days at 4 °C, and then stored at −80 °C.

Tissue lysate sample preparation

A small piece of tissue (approx. 30 mg) was transferred into 250 µL of 50 mM Tris/HCl, 100 mM NaCl, pH 7.4, in a 2-mL microtube. Tissue samples were homogenized using TissueLyser II (30 Hz, 3 min). The homogenates were then diluted with 250 µL of the lysis buffer. Octaethylene glycol monododecyl ether (Affymetrix) was added to reach 1% final concentration, and the homogenate was sonicated in a water bath for 5 min at 0 °C. Finally, the samples were centrifuged at 600 ***g*** for 15 min, and the resulting supernatant was stored at −80 °C until further use. The lysate protein concentration was determined using Bradford 1 × Dye Reagent (Bio-Rad, Hercules, CA, USA).

Radioenzymatic determination of NAAG-hydrolyzing activity in mouse tissues

The determination of NAAG-hydrolyzing activity in mouse tissues was performed as previously described [53]. A sample of tissue lysate was mixed with 20 mM Tris/HCl, 150 mM NaCl, 0.1% Tween 20, pH 7.4, to a final volume of 90 µL. Reactions were started by adding 10 µL of 1 µM NAAG (containing 50 nM tritium-labeled NAAG), and incubated at 37 °C for 15 h. The reactions were stopped with 100 µL of ice-cold 200 mM KH_2PO_4, 2 mM 2-mercaptoethanol, pH 7.4. The released glutamate was separated from the unreacted substrate using ion-exchange AG1-X resin (Bio-Rad). The radioactivity of the sample was quantified by liquid scintillation using the Rotiszint ECO Plus scintillation cocktail (Roth) in a Tri-Carb Liquid Scintillation Counter (Perkin-Elmer, Waltham, MA, USA). The samples were measured in duplicate.

SDS/PAGE and western blotting

Protein samples were resolved by reducing SDS/PAGE. Proteins were electroblotted onto a nitrocellulose membrane (wet blotting: 100 V/1 h). After blotting, the membrane was blocked with 0.55% (w/v) casein solution in PBS (Casein Buffer 20X-4X Concentrate, SDT, Baesweiler, Germany) at room temperature for 1 h. To visualize GCPII, the blots were probed with the antibody GCP-04 (described in [2]) for 12 h at 4 °C (200 $ng \cdot mL^{-1}$; diluted in 0.55% casein solution), washed three times with PBS containing 0.05% Tween 20 (PBST buffer), and incubated with goat anti-mouse antibody conjugated with horseradish peroxidase (Thermo Scientific, Waltham, MA, USA; diluted in 0.55% casein solution, 1 : 25 000). The blots were then washed three times with PBST to remove unbound antibodies and developed with SuperSignal West Femto Chemiluminescent Substrate (Thermo Scientific).

Chemiluminescence was captured with a ChemiDoc-It™ 600 Imaging System (UVP, Upland, CA, USA).

Immunohistochemistry

Immunohistochemistry was performed according to the protocol described previously using anti-GCPII antibody GCP-04 [2] with minor modifications [42]. Briefly, after standard histological processing (fixation, dehydration, embedding into paraffin, cutting, paraffin removal, rehydration), heat antigen retrieval was performed using 10 mM sodium citrate, 0.1% Tween 20, pH 6.0 buffer and heating to 110 °C for 15 min in an autoclave. Afterward, samples were incubated in 1.5% hydrogen peroxide solution for 20 min to reduce endogenous peroxidase activity and in 10% fetal bovine serum in PBS to block unspecific interactions. The slides were then stained by primary anti-GCPII antibody GCP-04 (10 $\mu g \cdot mL^{-1}$ in 4 °C, overnight), followed by extensive washing (five times with PBS containing 0.1% Tween 20) and incubation with secondary antibody Histofine® Simple Stain™ MAX PO (MULTI) (Nichirei Bioscience Inc., Tokyo, Japan) diluted 1 : 2 with 10% fetal bovine serum in PBS at room temperature for 1 h. After further extensive washing (five times with PBS containing 0.1% Tween 20), GCPII was visualized using DAB/Plus kit (Diagnostic BioSystems, Pleasanton, CA, USA, 60 s). The slides were counterstained with Harris' hematoxylin and mounted in polyvinyl alcohol-based media.

Carboxypeptidase activity assay

Carboxypeptidase activity (i.e., substrate specificity) of mouse GCPII was determined using *N*-Ac-A-X peptide libraries according to a previously published method [41]. Briefly, 1.2 μg Avi-mGCPII was diluted into 25 mM Bis-Tris propane, 150 mM NaCl, 0.001% octaethylene glycol monododecyl ether (Affymetrix), pH 7.4, and incubated in the presence of 25 μM dipeptide for 1.5 h at 37 °C. As negative controls, reactions without the enzyme and in the presence of 1 mM 2-PMPA, a highly selective GCPII inhibitor, were performed. The reaction mixture was then analyzed using HPLC, as previously described [41].

Total RNA isolation and reverse transcription

First, tissue samples were transferred from RNA later solution (Invitrogen, #AM7021) to RLT buffer (part of the RNEasy Mini Kit, Qiagen, Hilden, Germany, #74106) supplied with β-mercaptoethanol and homogenized with 5-mm steel beads (Qiagen; #69989) using TissueLyser II (#85300; Qiagen). Total RNA was isolated using RNeasy Mini Kit according to the manufacturer's instructions. The concentration and purity of isolated RNA were determined spectrophotometrically using a Nanodrop ND-1000 spectrophotometer. The integrity of each RNA sample was analyzed using the Agilent RNA 6000 Nano kit run on an Agilent 2100 Bioanalyzer. Only samples without significant degradation were used for subsequent steps.

RNA was then reverse-transcribed using M-MLV (#28025013; Invitrogen) according to the manufacturer's instructions. Each 20 μL reaction contained up to 2 μg total RNA, 2.5 μM oligo$(dT)_{20}$ primers (#18418020; Invitrogen), 50 ng random hexamers (100 ng if more than 1 μg RNA was transcribed), 40 units of RNAseOUT, 200 units of M-MLV reverse transcriptase, and other components as specified by the manufacturer.

Quantitative PCR (qPCR) analysis

All qPCRs were carried out in triplicate in FrameStar 480/96 multiwell plates (#4ti-0951; 4titude, Wotton, UK) sealed with adhesive optical foil (#4729692001; Roche) using a LightCycler 480 II instrument (Roche) in a total volume of 10 μL. Each reaction consisted of LightCycler 480 Probe Master (Roche) diluted according to the manufacturer's instructions, forward and reverse primers (1 μM final concentration each), fluorescent probe (see description of individual assays for final concentration), and 1 μL of sample or template DNA (positive and nontemplate controls as well as interplate calibrators were included on each plate). Initial denaturation for 3 min at 95 °C was followed by 45 cycles of 10 s at 95 °C, 30 s at 66 °C, and 30 s at 72 °C. The threshold cycle numbers (C_q) were then determined from fluorescence intensities acquired during the qPCR runs by the second-derivative maximum method using LightCycler 480 software (Roche). The presence and size of PCR products were analyzed by agarose gel electrophoresis.

The amount of mouse GCPII (encoded by the gene Folh1) was quantified by an assay set of forward and reverse primers (sequences 5′-gattgccagatatgggaaagtg-3′ and 5′-cctgccagttgagcattttt-3′) and fluorescent hydrolysis probe #6 from the Roche Universal Probe Library (LNA octamer sequence 5′-cagaggaa-3′; final concentration 100 nM). This set was designed to amplify nucleotides 714–773 in mouse GCPII transcript NM_016770 to yield an amplified product of 60 bps, which spans the region of exons 5 and 6 and corresponds to amino acids 202–223 in the longest open reading frame (ORF). This assay should not amplify genomic sequence because it spans a 1029-bp intron.

The amount of mouse GCPIII transcript (encoded by the gene Naalad2) was quantified by an assay set of forward and reverse primers (sequences 5′-aatgatgcagagagactattacgc-3′ and 5′-ccagcttttgtctggtggag-3′) and fluorescent hydrolysis probe #52 from the Roche Universal Probe Library (LNA octamer sequence 5′-gggaggag-3′; final concentration 50 nM). This set was designed to amplify nucleotides 922–981 in mouse GCPIII transcript NM_028279 to yield an amplified product of 60 bps, which spans the region of exons 7 and 8 and corresponds to

amino acids 289–309 in the longest ORF. This assay should not amplify genomic sequence because it spans a 880-bp intron.

As a standard for absolute quantification, serial 10-fold dilutions covering concentrations from 10^8 to 10^2 copies per reaction of either pcDNA4 plasmid with subcloned coding sequence of full-length mouse GCPII (longest ORF from NM_016770 coding amino acids 1–752) or pMT/BiP plasmid with subcloned coding sequence of extracellular part of mouse GCPIII (part of longest ORF from NM_028279 coding amino acids 36–740) were amplified with the corresponding assay set. The initial concentration of plasmid DNA (purified by QIAprep Spin Miniprep Kit, #27106; Qiagen) prior to dilution was determined spectrophotometrically at 260 nm (Nanodrop ND-1000; Thermo Scientific).

To enable precise absolute comparison between the determined amounts of both transcripts, obtained calibration curves were further normalized against each other by quantification of a common region of both plasmids. The region containing the ampicillin resistance gene was quantified by a set of primers with sequences 5′-gcagaagtggtcctgcaact-3′ and 5′-agcttcccggcaacaatta-3′ and fluorescent hydrolysis probe #58 from the Roche Universal Probe Library (final concentration 50 nM). In this way, two calibration curves were obtained for each plasmid, one for the amplification of target transcript and one for the common sequence. Finally, the slope and intercept values of both curves were transformed for each plasmid so that the transformed slope and intercept values of the curves for the common sequence were equal between the two plasmids and corresponded to the average value between the two plasmids.

The amount of both transcripts was determined in the prepared tissue cDNA libraries. In each qPCR, an amount of cDNA corresponding to the starting amount of total RNA of 5–10 ng was used, and the amount of GCPII and GCPIII transcripts were normalized to the total amount of RNA. Both transcripts were also quantified in 1.0 μL of 10-fold diluted commercial tissue cDNA libraries (Mouse MTC Panels I and III supplied by Clontech, Mountain View, CA, USA, #636745 and 636757), which had been normalized to several control genes by the vendor (beta-actin, G3PDH, phospholipase A2, and ribosomal protein S29).

Statistical analysis

All values are presented as the mean ± standard deviation.

Acknowledgements

We would like to thank Warren Heston (Lerner Research Institute, Cleveland Clinic) for providing us with a plasmid encoding mouse GCPII, Jana Starková and Karolína Šrámková for their excellent technical support, Radko Souček for HPLC analyses, and Hillary Hoffman for language editing. This work was supported by Grant No. GA16-02938S from the Grant Agency of the Czech Republic and InterBioMed Project LO 1302 from the Ministry of Education of the Czech Republic.

Author contributions

The manuscript was written through contributions of all authors. All authors have given approval to the final version of the manuscript. JK and PS conceived the project and analyzed data, TK, BV, JT, VN, PS and JK wrote the manuscript, TK, BV, VN, JT, FS, SV and MF designed, performed and interpreted the experiments.

References

1 Berger UV, Carter RE, Mckee M and Coyle JT (1995) N-acetylated alpha-linked acidic dipeptidase is expressed by non-myelinating Schwann-cells in the peripheral nervous-system. *J Neurocytol* **24**, 99–109.

2 Sacha P, Zamecnik J, Barinka C, Hlouchova K, Vicha A, Mlcochova P, Hilgert I, Eckschlager T and Konvalinka J (2007) Expression of glutamate carboxypeptidase II in human brain. *Neuroscience* **144**, 1361–1372.

3 Bostwick DG, Pacelli A, Blute M, Roche P and Murphy GP (1998) Prostate specific membrane antigen expression in prostatic intraepithelial neoplasia and adenocarcinoma: a study of 184 cases. *Cancer* **82**, 2256–2261.

4 Silver DA, Pellicer I, Fair WR, Heston WD and Cordon-Cardo C (1997) Prostate-specific membrane antigen expression in normal and malignant human tissues. *Clin Cancer Res* **3**, 81–85.

5 Pinto JT, Suffoletto BP, Berzin TM, Qiao CH, Lin SL, Tong WP, May F, Mukherjee B and Heston WDW (1996) Prostate-specific membrane antigen: a novel folate hydrolase in human prostatic carcinoma cells. *Clin Cancer Res* **2**, 1445–1451.

6 Kinoshita Y, Kuratsukuri K, Landas S, Imaida K, Rovito PM Jr, Wang CY and Haas GP (2006) Expression of prostate-specific membrane antigen in normal and malignant human tissues. *World J Surg* **30**, 628–636.

7 Robinson MB, Blakely RD, Couto R and Coyle JT (1987) Hydrolysis of the brain dipeptide N-acetyl-L-aspartyl-L-glutamate. Identification and characterization of a novel N-acetylated alpha-linked acidic dipeptidase activity from rat brain. *J Biol Chem* **262**, 14498–14506.

8 Horoszewicz JS, Kawinski E and Murphy GP (1987) Monoclonal-antibodies to a new antigenic marker in epithelial prostatic cells and serum of prostatic-cancer patients. *Anticancer Res* **7**, 927–936.
9 Bacich DJ, Ramadan E, O'Keefe DS, Bukhari N, Wegorzewska I, Ojeifo O, Olszewski R, Wrenn CC, Bzdega T, Wroblewska B *et al.* (2002) Deletion of the glutamate carboxypeptidase II gene in mice reveals a second enzyme activity that hydrolyzes N-acetylaspartylglutamate. *J Neurochem* **83**, 20–29.
10 Hlouchova K, Barinka C, Klusak V, Sacha P, Mlcochova P, Majer P, Rulisek L and Konvalinka J (2007) Biochemical characterization of human glutamate carboxypeptidase III. *J Neurochem* **101**, 682–696.
11 Collard F, Vertommen D, Constantinescu S, Buts L and Van Schaftingen E (2011) Molecular identification of beta-citrylglutamate hydrolase as glutamate carboxypeptidase 3. *J Biol Chem* **286**, 38220–38230.
12 Slusher BS, Vornov JJ, Thomas AG, Hurn PD, Harukuni I, Bhardwaj A, Traystman RJ, Robinson MB, Britton P, Lu XCM *et al.* (1999) Selective inhibition of NAALADase, which converts NAAG to glutamate, reduces ischemic brain injury. *Nat Med* **5**, 1396–1402.
13 Neale JH, Olszewski RT, Gehl LM, Wroblewska B and Bzdega T (2005) The neurotransmitter N-acetylaspartylglutamate in models of pain, ALS, diabetic neuropathy, CNS injury and schizophrenia. *Trends Pharmacol Sci* **26**, 477–484.
14 Wroblewska B, Wroblewski JT, Pshenichkin S, Surin A, Sullivan SE and Neale JH (1997) N-acetylaspartylglutamate selectively activates mGluR3 receptors in transfected cells. *J Neurochem* **69**, 174–181.
15 Bruno V, Wroblewska B, Wroblewski JT, Fiore L and Nicoletti F (1998) Neuroprotective activity of N-acetylaspartylglutamate in cultured cortical cells. *Neuroscience* **85**, 751–757.
16 Halsted CH, Ling EH, Luthi-Carter R, Villanueva JA, Gardner JM and Coyle JT (1998) Folylpoly-gamma-glutamate carboxypeptidase from pig jejunum – molecular characterization and relation to glutamate carboxypeptidase II. *J Biol Chem* **273**, 20417–20424.
17 Chandler CJ, Wang TT and Halsted CH (1986) Pteroylpolyglutamate hydrolase from human jejunal brush borders. Purification and characterization. *J Biol Chem* **261**, 928–933.
18 Mhawech-Fauceglia P, Zhang S, Terracciano L, Sauter G, Chadhuri A, Herrmann FR and Penetrante R (2007) Prostate-specific membrane antigen (PSMA) protein expression in normal and neoplastic tissues and its sensitivity and specificity in prostate adenocarcinoma: an immunohistochemical study using multiple tumour tissue microarray technique. *Histopathology* **50**, 472–483.
19 Chen Z, Penet MF, Nimmagadda S, Li C, Banerjee SR, Winnard PT Jr, Artemov D, Glunde K, Pomper MG and Bhujwalla ZM (2012) PSMA-targeted theranostic nanoplex for prostate cancer therapy. *ACS Nano* **6**, 7752–7762.
20 Heck MM, Retz M, D'Alessandria C, Rauscher I, Scheidhauer K, Maurer T, Storz E, Janssen F, Schottelius M, Wester HJ *et al.* (2016) Systemic radioligand therapy with (177)Lu labeled prostate specific membrane antigen ligand for imaging and therapy in patients with metastatic castration resistant prostate cancer. *J Urol* **196**, 382–391.
21 Hrkach J, Von Hoff D, Ali MM, Andrianova E, Auer J, Campbell T, De Witt D, Figa M, Figueiredo M, Horhota A *et al.* (2012) Preclinical development and clinical translation of a PSMA-targeted docetaxel nanoparticle with a differentiated pharmacological profile. *Sci Transl Med* **4**, 128ra39.
22 Rovenska M, Hlouchova K, Sacha P, Mlochova P, Horak V, Zamecnik J, Barinka C and Konvalinka J (2008) Tissue expression and enzymologic characterization of human prostate specific membrane antigen and its rat and pig orthologs. *Prostate* **68**, 171–182.
23 Zhong C, Zhao X, Van KC, Bzdega T, Smyth A, Zhou J, Kozikowski AP, Jiang J, O'Connor WT, Berman RF *et al.* (2006) NAAG peptidase inhibitor increases dialysate NAAG and reduces glutamate, aspartate and GABA levels in the dorsal hippocampus following fluid percussion injury in the rat. *J Neurochem* **97**, 1015–1025.
24 Zhong CL, Zhao XR, Sarva J, Kozikowski A, Neale JH and Lyeth BG (2005) NAAG peptidase inhibitor reduces acute neuronal degeneration and astrocyte damage following lateral fluid percussion TBI in rats. *J Neurotraum* **22**, 266–276.
25 Ghadge GD, Slusher BS, Bodner A, Canto MD, Wozniak K, Thomas AG, Rojas C, Tsukamoto T, Majer P, Miller RJ *et al.* (2003) Glutamate carboxypeptidase II inhibition protects motor neurons from death in familial amyotrophic lateral sclerosis models. *Proc Natl Acad Sci USA* **100**, 9554–9559.
26 Chen SR, Wozniak KM, Slusher BS and Pan HL (2002) Effect of 2-(phosphono-methyl)-pentanedioic acid on allodynia and afferent ectopic discharges in a rat model of neuropathic pain. *J Pharmacol Exp Ther* **300**, 662–667.
27 Nagel J, Belozertseva I, Greco S, Kashkin V, Malyshkin A, Jirgensons A, Shekunova E, Eilbacher B, Bespalov A and Danysz W (2006) Effects of NAAG peptidase inhibitor 2-PMPA in model chronic pain – relation to brain concentration. *Neuropharmacology* **51**, 1163–1171.
28 Zhou J, Neale JH, Pomper MG and Kozikowski AP (2005) NAAG peptidase inhibitors and their potential

for diagnosis and therapy. *Nat Rev Drug Discov* **4**, 1015–1026.
29 Bacich DJ, Pinto JT, Tong WP and Heston WD (2001) Cloning, expression, genomic localization, and enzymatic activities of the mouse homolog of prostate-specific membrane antigen/NAALADase/folate hydrolase. *Mamm Genome* **12**, 117–123.
30 Gao Y, Xu SY, Cui ZW, Zhang MK, Lin YY, Cai L, Wang ZG, Luo XG, Zheng Y, Wang Y *et al.* (2015) Mice lacking glutamate carboxypeptidase II develop normally, but are less susceptible to traumatic brain injury. *J Neurochem* **134**, 340–353.
31 Tsai G, Dunham KS, Drager U, Grier A, Anderson C, Collura J and Coyle JT (2003) Early embryonic death of glutamate carboxypeptidase II (NAALADase) homozygous mutants. *Synapse* **50**, 285–292.
32 Han LQ, Picker JD, Schaevitz LR, Tsai GC, Feng JM, Jiang ZC, Chu HC, Basu AC, Berger-Sweeney J and Coyle JT (2009) Phenotypic characterization of mice heterozygous for a null mutation of glutamate carboxypeptidase II. *Synapse* **63**, 625–635.
33 Barinka C, Rinnova M, Sacha P, Rojas C, Majer P, Slusher BS and Konvalinka J (2002) Substrate specificity, inhibition and enzymological analysis of recombinant human glutamate carboxypeptidase II. *J Neurochem* **80**, 477–487.
34 Tykvart J, Sacha P, Barinka C, Knedlik T, Starkova J, Lubkowski J and Konvalinka J (2012) Efficient and versatile one-step affinity purification of in vivo biotinylated proteins: expression, characterization and structure analysis of recombinant human glutamate carboxypeptidase II. *Protein Expr Purif* **82**, 106–115.
35 Jackson PF, Cole DC, Slusher BS, Stetz SL, Ross LE, Donzanti BA and Trainor DA (1996) Design, synthesis, and biological activity of a potent inhibitor of the neuropeptidase N-acetylated alpha-linked acidic dipeptidase. *J Med Chem* **39**, 619–622.
36 Kozikowski AP, Zhang J, Nan FJ, Petukhov PA, Grajkowska E, Wroblewski JT, Yamamoto T, Bzdega T, Wroblewska B and Neale JH (2004) Synthesis of urea-based inhibitors as active site probes of glutamate carboxypeptidase II: efficacy as analgesic agents. *J Med Chem* **47**, 1729–1738.
37 Chen Y, Foss CA, Byun Y, Nimmagadda S, Pullambahatla M, Fox JJ, Castanares M, Lupold SE, Babich JW, Mease RC *et al.* (2008) Radiohalogenated prostate-specific membrane antigen (PSMA)-based ureas as imaging agents for prostate cancer. *J Med Chem* **51**, 7933–7943.
38 Eder M, Schafer M, Bauder-Wust U, Hull WE, Wangler C, Mier W, Haberkorn U and Eisenhut M (2012) Ga-68-complex lipophilicity and the targeting property of a urea-based PSMA inhibitor for PET imaging. *Bioconjug Chem* **23**, 688–697.
39 Tykvart J, Schimer J, Barinkova J, Pachl P, Postova-Slavetinska L, Majer P, Konvalinka J and Sacha P (2014) Rational design of urea-based glutamate carboxypeptidase II (GCPII) inhibitors as versatile tools for specific drug targeting and delivery. *Bioorg Med Chem* **22**, 4099–4108.
40 Tykvart J, Schimer J, Jancarik A, Barinkova J, Navratil V, Starkova J, Sramkova K, Konvalinka J, Majer P and Sacha P (2015) Design of highly potent urea-based, exosite-binding inhibitors selective for glutamate carboxypeptidase II. *J Med Chem* **58**, 4357–4363.
41 Tykvart J, Barinka C, Svoboda M, Navratil V, Soucek R, Hubalek M, Hradilek M, Sacha P, Lubkowski J and Konvalinka J (2015) Structural and biochemical characterization of a novel aminopeptidase from human intestine. *J Biol Chem* **290**, 11321–11336.
42 Tykvart J, Navratil V, Sedlak F, Corey E, Colombatti M, Fracasso G, Koukolik F, Barinka C, Sacha P and Konvalinka J (2014) Comparative analysis of monoclonal antibodies against prostate-specific membrane antigen (PSMA). *Prostate* **74**, 1674–1690.
43 Navratil M, Tykvart J, Schimer J, Pachl P, Navratil V, Rokob TA, Hlouchova K, Rulisek L and Konvalinka J (2016) Comparison of human glutamate carboxypeptidases II and III reveals their divergent substrate specificities. *FEBS J* **283**, 2528–2545.
44 Majer P, Jancarik A, Krecmerova M, Tichy T, Tenora L, Wozniak K, Wu Y, Pommier E, Ferraris D, Rais R *et al.* (2016) Discovery of orally available prodrugs of the glutamate carboxypeptidase II (GCPII) inhibitor 2-phosphonomethylpentanedioic acid (2-PMPA). *J Med Chem* **59**, 2810–2819.
45 Chen Y, Dhara S, Banerjee SR, Byun Y, Pullambhatla M, Mease RC and Pomper MG (2009) A low molecular weight PSMA-based fluorescent imaging agent for cancer. *Biochem Biophys Res Commun* **390**, 624–629.
46 Gorin MA, Pomper MG and Rowe SP (2016) PSMA-targeted imaging of prostate cancer: the best is yet to come. *BJU Int* **117**, 715–716.
47 Yang X, Mease RC, Pullambhatla M, Lisok A, Chen Y, Foss CA, Wang Y, Shallal H, Edelman H, Hoye AT *et al.* (2016) [(18)F]Fluorobenzoyllysinepentanedioic acid carbamates: new scaffolds for positron emission tomography (PET) imaging of prostate-specific membrane antigen (PSMA). *J Med Chem* **59**, 206–218.
48 Barinka C, Hlouchova K, Rovenska M, Majer P, Dauter M, Hin N, Ko YS, Tsukamoto T, Slusher BS, Konvalinka J *et al.* (2008) Structural basis of interactions between human glutamate carboxypeptidase II and its substrate analogs. *J Mol Biol* **376**, 1438–1450.
49 Barinka C, Rovenska M, Mlcochova P, Hlouchova K, Plechanovova A, Majer P, Tsukamoto T, Slusher BS, Konvalinka J and Lubkowski J (2007) Structural

insight into the pharmacophore pocket of human glutamate carboxypeptidase II. *J Med Chem* **50**, 3267–3273.

50 Mlcochova P, Plechanovova A, Barinka C, Mahadevan D, Saldanha JW, Rulisek L and Konvalinka J (2007) Mapping of the active site of glutamate carboxypeptidase II by site-directed mutagenesis. *FEBS J* **274**, 4731–4741.

51 O'Keefe DS, Bacich DJ and Heston WD (2004) Comparative analysis of prostate-specific membrane antigen (PSMA) versus a prostate-specific membrane antigen-like gene. *Prostate* **58**, 200–210.

52 Shafizadeh TB and Halsted CH (2007) Gamma-glutamyl hydrolase, not glutamate carboxypeptidase II, hydrolyzes dietary folate in rat small intestine. *J Nutr* **137**, 1149–1153.

53 Knedlik T, Navratil V, Vik V, Pacik D, Sacha P and Konvalinka J (2014) Detection and quantitation of glutamate carboxypeptidase II in human blood. *Prostate* **74**, 768–780.

54 Rajasekaran SA, Anilkumar G, Oshima E, Bowie JU, Liu H, Heston W, Bander NH and Rajasekaran AK (2003) A novel cytoplasmic tail MXXXL motif mediates the internalization of prostate-specific membrane antigen. *Mol Biol Cell* **14**, 4835–4845.

55 Klusak V, Barinka C, Plechanovova A, Mlcochova P, Konvalinka J, Rulisek L and Lubkowski J (2009) Reaction mechanism of glutamate carboxypeptidase II revealed by mutagenesis, X-ray crystallography, and computational methods. *Biochemistry* **48**, 4126–4138.

56 Mesters JR, Barinka C, Li WX, Tsukamoto T, Majer P, Slusher BS, Konvalinka J and Hilgenfeld R (2006) Structure of glutamate carboxypeptidase II, a drug target in neuronal damage and prostate cancer. *EMBO J* **25**, 1375–1384.

57 Speno HS, Luthi-Carter R, Macias WL, Valentine SL, Joshi ART and Coyle JT (1999) Site-directed mutagenesis of predicted active site residues in glutamate carboxypeptidase II. *Mol Pharmacol* **55**, 179–185.

7.3. Publication III

Knedlik T., Navratil V., Vik V., Pacik D., Sacha P., and Konvalinka J.:

Detection and quantitation of glutamate carboxypeptidase II in human blood.

Prostate 2014, 74(7):768-780.

Detection and Quantitation of Glutamate Carboxypeptidase II in Human Blood

Tomáš Knedlík,[1,2] Václav Navrátil,[1,2] Viktor Vik,[3] Dalibor Pacík,[4] Pavel Šácha,[1,2] and Jan Konvalinka[1,2]*

[1]Gilead Sciences and IOCB Research Centre, Institute of Organic Chemistry and Biochemistry, Academy of Sciences of the Czech Republic, Prague, Czech Republic
[2]Department of Biochemistry, Faculty of Science, Charles University in Prague, Prague, Czech Republic
[3]Department of Urology, Thomayer Hospital in Prague, Prague, Czech Republic
[4]Department of Urology, Medical School Masaryk University, University Hospital Brno, Brno, Czech Republic

BACKGROUND. Glutamate carboxypeptidase II (GCPII) is a transmembrane enzyme that cleaves *N*-acetyl-L-aspartyl-L-glutamate (NAAG) in the brain. GCPII is highly expressed in the prostate and prostate cancer and might be associated with prostate cancer progression. Another exopeptidase, plasma glutamate carboxypeptidase (PGCP), was reported to be similar to GCPII and to share its NAAG-hydrolyzing activity.
METHODS. We performed a radioenzymatic assay with [^{3}H]NAAG as a substrate to detect and quantify the enzymatic activity of GCPII in plasma. Using a specific antibody raised against native GCPII (2G7), we immunoprecipitated GCPII from human plasma. We also cloned two PGCP constructs, expressed them in insect cells, and tested them for their NAAG-hydrolyzing activity.
RESULTS. We detected GCPII protein in human plasma and found that its concentration ranges between 1.3 and 17.2 ng/ml in volunteers not diagnosed with prostate cancer. Recombinant PGCP was enzymatically active but exhibited no NAAG-hydrolyzing activity.
CONCLUSION. GCPII is present in human blood, and its concentration within a healthy population varies. Recombinant PGCP does not hydrolyze NAAG, suggesting that GCPII alone is responsible for the NAAG-hydrolyzing activity observed in human blood. The potential correlation between GCPII serum levels and the disease status of prostate cancer patients will be further investigated. *Prostate* © 2014 Wiley Periodicals, Inc.

KEY WORDS: **glutamate carboxypeptidase II; prostate-specific membrane antigen; serum marker; prostate cancer; plasma glutamate carboxypeptidase**

INTRODUCTION

Prostate cancer is the most prevalent type of cancer and one of the leading causes of death among men in the United States and Western Europe. An estimated 233,000 men will be diagnosed with prostate cancer in the United States in 2014, and 29,000 men will die of the disease [1].

Glutamate carboxypeptidase II (GCPII), also known as prostate-specific membrane antigen (PSMA), *N*-acetylated-alpha-linked acidic dipeptidase (NAALADase) or folate hydrolase, is a transmembrane metallopeptidase with a short cytoplasmic tail and a large extracellular domain [2–4]. In humans, GCPII is expressed predominantly in the prostate and in lower amounts in several other tissues, such as brain, kidney, and small intestine [5–8]. GCPII possesses two known

Grant sponsor: Grant Agency of the Czech Republic; Grant number: P304-12-0847; Grant sponsor: OPPK project; Grant number: CZ.2.16/3.1.00/24016.

*Correspondence to: Jan Konvalinka, Institute of Organic Chemistry and Biochemistry, ASCR, v.v.i. Flemingovo n. 2, Prague 6, 166 10, Czech Republic. E-mail: jan.konvalinka@uochb.cas.cz
Received 19 December 2013; Accepted 10 February 2014
DOI 10.1002/pros.22796
Published online in Wiley Online Library (wileyonlinelibrary.com).

enzymatic activities: (1) in the central nervous system, it hydrolyzes the abundant peptidic neurotransmitter *N*-acetyl-L-aspartyl-L-glutamate (NAAG) into *N*-acetyl-L-aspartate and free L-glutamate, thus participating in glutamate excitotoxicity [4]; (2) in the small intestine, GCPII cleaves glutamates from poly-gamma-glutamylated folates, enabling folate to be transported across the intestinal mucosa [9]. Although GCPII is highly expressed on prostate epithelial cells, the physiological role of the protein in this tissue has not yet been elucidated. Several hypotheses have been suggested; however, so far none of them has been widely accepted by the scientific community [10–14].

Interestingly, GCPII expression in prostate cancer seems to be 10-fold higher than in benign prostate tissue [15]. Although the function of GCPII in the prostate is still unclear, the protein's potential as a diagnostic and/or therapeutic target was identified many years ago [16]. As a transmembrane protein that undergoes internalization, GCPII seems to be an ideal target for monoclonal antibody or inhibitor-based imaging or therapy [17–19]. An ^{111}In-labeled antibody raised against GCPII (trade name ProstaScint®) currently is used in the first diagnostic scan detecting GCPII expression in prostate cancer. This conjugate is used clinically for imaging prostate cancer and its metastatic invasion into other tissues [20]. However, ProstaScint® can bind only damaged or dead cells, since the antibody recognizes an internal epitope of GCPII [21]. In the past 10 years, scientists have been working on second generation antibodies that recognize the extracellular portion of GCPII, enabling visualization of viable cells [22,23]. These antibodies, coupled with either a radionuclide or a toxic agent, would specifically bind to prostate cancer cells expressing large quantities of GCPII and, following internalization, would cause damage to the cancer cells [24,25] (reviewed in Ref. [26]).

GCPII's potential as a diagnostic and/or prognostic marker motivated efforts to identify the enzyme in human plasma, either as a secreted or shedded species. Although GCPII has been well-studied as a membrane target, its role as a potential serum marker is less clear. GCPII was first found in human serum in a series of works using Western blot analysis, a semi-quantitative method providing results as relative band intensities [27–29]. Wright's group was first unable to detect GCPII in serum using Western blot [30], but they subsequently showed GCPII to be present in serum [31]. Later, Xiao et al. developed a SELDI quantitative immunoassay using ProteinChip mass spectrometry. In contrast to the Western blot results, this approach led to quantitation of serum GCPII in concentrations in the range of hundreds of nanograms per milliliter [32].

The current prostate cancer screening test is based on quantitation of prostate specific antigen (PSA) in a man's blood [33]. PSA levels are elevated in men with prostate cancer. However, benign prostate hyperplasia and some other factors, such as age, race, or prostate infection, also may lead to elevated PSA levels [34]. Consequently, the Centers for Disease Control and Prevention (CDC) and the U.S. Preventive Services Task Force (USPSTF) have recommended against PSA-based screening for men who do not have symptoms of prostate cancer [35]. Measuring the level of GCPII in blood might be an alternative to the PSA-based screening test. Different levels of GCPII in blood also may correlate with prostate cancer stage, as GCPII expression increases in high-grade cancers and metastatic disease. On the other hand, high concentrations of GCPII in blood, if confirmed, might pose a serious problem for drug delivery targeting GCPII on the prostate epithelium.

It is important to note that another metallopeptidase homologous to GCPII, called plasma glutamate carboxypeptidase (PGCP), also has been reported to be present in human blood [36]. PGCP is secreted into blood plasma and has been reported to possess both NAAG-hydrolyzing and SerMet-hydrolyzing activity [36,37]. Due to its potential NAAG-hydrolyzing activity, PGCP might interfere with the detection of GCPII in enzyme-based assays. The function of PGCP is unknown, but it has been suggested to play a role in hydrolysis of circulating peptides and proteins [36].

In this work, we set out to resolve the conflicting reports concerning GCPII's presence in the blood and its potential to serve as a marker for prostate cancer prognosis. We also analyze the potential GCPII-like activity of PGCP, which might interfere with GCPII-based assay.

MATERIALS AND METHODS

Radioenzymatic Determination of NAAG-Hydrolyzing Activity in Human Plasma

The radioenzymatic assay was performed as previously described [4,38,39], with minor modifications. Plasma samples were diluted 10- to 100-fold with 20 mM Tris–HCl, 150 mM NaCl, 0.1% Tween 20, pH 7.4, (and inhibitor solution, if used) to a final volume of 90 μl. Reactions were first incubated for 5 min at 37°C and then started by adding 10 μl of 1 μM NAAG (containing 50 nM tritium-labeled NAAG, labeled at the terminal glutamate moiety; Perkin-Elmer), and incubated at 37°C for 18 hr. The reactions were stopped with 100 μl of ice-cold 200 mM KH_2PO_4, 2 mM 2-mercaptoethanol, pH 7.4. The released glutamate was then separated from the unreacted substrate using ion exchange AG1-X8 resin (Bio-Rad). The radioactivity of

the sample was quantified by liquid scintillation using the Rotiszint ECO Plus scintillation cocktail (Roth) on a Tri-Carb Liquid Scintillation Counter (Perkin-Elmer). The samples were measured in duplicates or triplicates.

Preparation, Purification, and Biotinylation of the GCPII-Specific Antibody 2G7

The novel mouse monoclonal antibody 2G7, which binds an extracellular epitope in native (i.e., enzymatically active) GCPII, was prepared in the laboratory of Vaclav Horejsi (Institute of Molecular Genetics, Academy of Sciences of the Czech Republic, Prague, Czech Republic). Mice (F1 hybrids of BALB/c and B10.A strains) were immunized with recombinant extracellular GCPII (amino acids 44–750) as previously described [40].

The antibody 2G7 was purified from 800 ml of hybridoma-conditioned medium that was concentrated to 10 ml using a LabScale TFF System (with Pellicon® XL 50 Cassette, Biomax 100, MWCO 100 kDa; Millipore). The concentrated medium was mixed in a 3:1 ratio with 4 M NaCl, 2 M glycine, pH 8.5, and the equilibrated concentrated medium was loaded onto a HiTrap™ FF Protein A Sepharose column (1 ml column volume; GE Healthcare Life Sciences) connected to an AKTA PRIME machine. The column was then washed with 50 ml of 1 M NaCl, 0.5 M glycine, pH 8.5. Bound antibodies were eluted with 100 mM sodium citrate, pH 5.0, and elution fractions were immediately neutralized with 1 M HEPES, pH 8.0 (mixed in a 5:1 ratio). The elution fractions were mixed and dialyzed against PBS using Slide-A-Lyzer® MINI Dialysis Units (10 kDa MWCO; Thermo Scientific).

The purified antibody was biotinylated using EZ-Link Sulfo-NHS-LC-Biotin (Thermo Fisher Scientific, Inc.) according to the manufacturer's instructions. Briefly, 1.2 ml of purified 2G7 antibody in PBS (concentration 0.4 mg/ml) was mixed with 24 µl of 10 mM Sulfo-NHS-LC-Biotin, resulting in a 75-fold molar excess of the biotinylation reagent. The reaction was incubated on ice for 12 hr, then stopped by dialysis against 20 mM Tris–HCl, 150 mM NaCl, pH 7.4, using Slide-A-Lyzer® MINI Dialysis Units (10 kDa MWCO; Thermo Scientific).

Immunoprecipitation of GCPII from Human Plasma

GCPII was immunoprecipitated with biotinylated 2G7. First, 10 µg of biotinylated 2G7 was diluted into 1 ml of 20 mM Tris–HCl, 150 mM NaCl, 0.1% Tween-20, pH 7.4 (TBST buffer). The antibody solution was mixed with 50 µl of Streptavidin Sepharose (GE Healthcare Life Sciences) and incubated for 2 hr at 6°C. Afterwards, the resin with bound 2G7 was washed twice with 1 ml TBST. A citrate plasma sample (600 µl) was diluted 20-fold with TBST, mixed with the resin with bound 2G7 and incubated for 18 hr at 6°C. The resin was then washed three times with 1 ml TBST. Proteins were eluted from the Streptavidin Sepharose by adding 50 µl reducing SDS sample buffer and heating to 100°C for 10 min.

Blood Plasma Sample Preparation

Blood plasma samples were provided by healthy volunteers at Thomayer Hospital in Prague, with agreement of the local ethical commission. Blood was withdrawn into Vacuette® tubes (Greiner Bio-One) containing either sodium citrate (# 456323) or lithium heparin (# 456083) and placed in the refrigerator. Within 8 hr, tubes were centrifuged at 2,000*g* for 10 min with minimal decceleration, and blood plasma was transferred into a microtube. Samples were stored at −20°C until analysis.

Measurements of blood PSA levels were carried out according to standard procedure at Thomayer Hospital in Prague using the ARCHITECT Total PSA Reagent Kit (Abbott Diagnostics).

SDS-PAGE and Western Blotting

Protein samples were resolved by reducing sodium dodecyl sulfate polyacrylamide gel electrophoresis (SDS-PAGE). Gels were either silver-stained, stained with colloidal Coomassie G-250 (blue silver) for mass-spectrometry analysis, or electroblotted onto a PVDF membrane.

After blotting, the membrane was blocked with Blocker™ Casein solution (Thermo Scientific) at room temperature for 1 hr. To visualize GCPII, the blots were incubated with the primary antibody GCP-04 (described in Ref. [41]) for 12 hr at 4°C (diluted in Blocker™ Casein, 360 ng/ml), washed three times with PBS containing 0.05% Tween 20 (PBST buffer), and incubated with goat anti-mouse antibody conjugated with horseradish peroxidase (Thermo Scientific; diluted in Blocker™ Casein, 32 ng/ml).

The blots were then washed three times with PBST to remove unbound antibodies and developed with SuperSignal West Femto Chemiluminescent Substrate (Thermo Scientific). Chemiluminiscence was captured with a ChemiDoc-It™ 600 Imaging System (UVP).

Cloning of PGCP Constructs

The pFastBacPGCP plasmid, containing DNA encoding the full-length PGCP sequence (amino acids 1–472), was a kind gift from Dr. Dolenc (Department of Biochemistry and Molecular and Structural Biology, J. Stefan Institute, Ljubljana, Slovenia). To remove the

*Bgl*II restriction site inside the PGCP sequence, we used site-directed mutagenesis with the following two primers: 5′-gcactctcacttattaaggatcttgggctgcg-3′ and 5′-cgcagcccaagatccttaataagtgagagtgc-3′. The mutagenesis was carried out according to the manufacturer's protocol (QuikChange™ Site-Directed Mutagenesis, Stratagene). Then, the mutated pFastBacPGCP plasmid was used for preparation of two PGCP constructs.

The first construct, aviPGCP, contains a peptide sequence corresponding to the biotin ligase substrate (Avi-tag; [42]) and tobacco-etch virus protease (TEV; [43]) cleavage sequence at the N-terminus of mature PGCP (amino acids 45–472). The sequence corresponding to the mature PGCP chain was amplified by standard PCR with the following primers: 5′-aaaagatctgatgttgctaaagcaatcatc-3′ and 5′-aaactcgagcctaggacctaggcag-3′ (restriction sites introduced into the sequence are underlined). The primers introduced a *Bgl*II site at the 5′ end and an *Xho*I site at the 3′ end of the sequence. The resulting DNA fragment was cleaved with *Bgl*II and *Xho*I and ligated into pMT/BiP/AviTEV/rhGCPII plasmid [39] cleaved with the same endonucleases.

The second construct, ProPGCPavi, contains the propeptide part and the mature chain of PGCP (amino acids 21–44 and 45–472, respectively), followed by a DNA sequence corresponding to the AviTag™ sequence (GeneCopoeia, Inc.) at the C-terminus. The DNA sequence encoding PGCP with propeptide was amplified using primers 5′-aaaagatctaaagctatatgcaagaatg-3′ and 5′- aaatgatcatcctccgcttcctccggacctaggcagcattt-3′. Two restriction sites (underlined) were introduced into the sequence: *Bgl*II at the 5′ end and *Bcl*I at the 3′ end of the sequence. The amplicon was cleaved with *Bgl*II and BclI and inserted into plasmid pTRE-Tight/NaalL2_1-124spacAvi cleaved with *Bgl*II (Šácha et al., manuscript in preparation). This ligation led to introduction of a stop codon between the PGCP and Avi-tag sequence; therefore, mutagenesis was performed to remove the stop-codon sequence using primers 5′-ggaggaagcggaggaagatctggcctgaacg-3′ and 5′-cgttcaggccagatcttcctccgcttcctcc-3′. The mutagenesis was carried out according to the manufacturer's protocol (QuikChange™ Site-Directed Mutagenesis, Stratagene). Finally, the C-terminally Avi-tagged ProPGCP sequence in pTRE-Tight vector was cleaved with *Bgl*II and *Xho*I and inserted into pMT/BiP/V5-HisA (Invitrogen).

The correct sequences of both resulting plasmids were verified by DNA sequencing.

Preparation of Stable *Drosophila* S2 Cell Lines Expressing aviPGCP and ProPGCPavi

Previously prepared *Drosophila* S2 cells expressing BirA biotin-protein ligase localized in ER were used for preparation of stable aviPGCP and ProPGCPavi transfectants [39]. BirA ensures specific in vivo biotinylation of the expressed protein at its Avi-tag sequence. The cells were transfected using Calcium Phosphate Transfection Kit (Invitrogen) with 9 μg of either pMT/BiP/aviPGCP or pMT/BiP/ProPGCPavi together with 0.5 μg of pCoBlast (Invitrogen), analogously as previously described [38]. The transfected cells were cultivated in the presence of both blasticidin (5 μg/ml, Invitrogen) and hygromycin B (300 μg/ml, Invitrogen).

Approximately 2×10^6 stably transfected cells were transferred into a 35 mm Petri dish supplemented with 2 ml SF900II medium (Invitrogen). The following day, protein expression was induced by adding $CuSO_4$ (Sigma) to a final concentration of 1 mM. After 3 days, cells were harvested by centrifugation, and the medium was frozen until use.

Large-Scale Expression of ProPGCPavi and aviPGCP in *Drosophila* S2 Cells

The protocol for large-scale expression of PGCP constructs was identical to that described previously [40]. The final volume of cell suspension was 100 ml for aviPGCP and 500 ml for ProPGCPavi.

Purification of PGCP Constructs

Purification of PGCP constructs was performed as previously described [39]. Briefly, cell medium containing secreted biotinylated ProPGCPavi (500 ml) or aviPGCP (100 ml) was centrifuged at 3,400*g* for 45 min. Then, it was concentrated 10-fold using a LabScale TFF System (Millipore) with a Pellicon® XL 50 Cassette, Biomax 100 (ProPGCPavi purification) or 20-fold using a Vivaspin-6 centrifugal concentrator with a 10 kDa MWCO membrane (aviPGCP purification). The concentrated medium was centrifuged again at 3,400*g* for 20 min and equilibrated with 300 mM Tris–HCl, 450 mM NaCl, pH 7.2 (in a 2:1 ratio). The equilibrated concentrated ProPGCPavi medium was then mixed with 1 ml (or 200 μl for aviPGCP purification) of Streptavidin Mutein Matrix (Roche) and incubated with gentle shaking at 6°C for 15 hr. Afterwards, the resin was washed with 50 column volumes of 100 mM Tris–HCl, 150 mM NaCl, pH 7.2. Bound biotinylated proteins were eluted with 5 ml of 100 mM Tris–HCl, 150 mM NaCl, 2 mM D-biotin, pH 7.2, in five consecutive elution fractions (after the first elution fraction, the resin was incubated with elution buffer for 1 hr). After regeneration of the resin, the flow-through fraction was again mixed with the resin, and the purification procedure was repeated.

HPLC Determination of SerMet-Hydrolyzing Activity

Purified enzyme (30 ng), inhibitor solution (if used), and buffer solution (either 100 mM sodium acetate, 15 mM zinc acetate, pH 5.5, or 100 mM Tris–HCl, 1 mM zinc acetate, pH 7.5) were mixed in a final volume of 45 μl. Then, 5 μl of 10 mM L-seryl-L-methionine (Bachem) was added, and reactions were incubated at 37°C for 1 hr. Reactions were stopped by adding 125 μl of 200 mM sodium borate, pH 10. Reaction products were detected and quantified according to a previously described method using *o*-phthalaldehyde (OPA) derivatization [44] and analyzed on an Agilent 1200 Series system using an AccQ-Tag Ultra column (2.1 × 100 mm; Waters).

Protein Identification in Blood Plasma by Liquid Chromatography/Mass Spectrometry Analysis (LC–MS/MS)

Blood plasma samples were resolved by SDS gel electrophoresis and the gel was stained with colloidal Coomassie G-250. The gel was cut to pieces and the proteins in gel were destained, reduced by dithiothreitol, alkylated by iodacetamide and digested by trypsin. The peptides were extracted and dissolved in 0.1% formic acid. Samples were analyzed on UltiMate 3000 RSLCnano system (Dionex) coupled to a TripleTOF 5600 mass spectrometer with a NanoSpray III source (AB Sciex). The peptides were separated on Acclaim PepMap100 analytical column (3 μm, 15 cm × 75 μm ID, Thermo Scientific) using gradient from 5% to 30% over 55 min. MS mass range was set to 350–1,250 m/z, up to 25 ion candidates per cycle was allowed to be fragmented. In MS/MS mode the instrument acquired fragmentation spectra within m/z range from 100 to 1,600. Protein Pilot 4.0 (AB Sciex) was used for protein identification against *Homo Sapiens* Database (UniProt—SwissProt and TrEMBL, November 18, 2013).

RESULTS

NAAG-Hydrolyzing Activity in Human Plasma Can Be Blocked by GCPII Inhibitors

Three citrate plasma samples obtained from three different individuals (denominated PL, PL2, and PL3) were tested for their NAAG-hydrolyzing activity using radioenzymatic assay with tritium-labeled NAAG. Prior to the assay, plasma samples were dialyzed against 50 mM Tris–HCl, 25 mM NaCl, pH 7.4.

We observed NAAG-hydrolyzing activity in all three plasma samples (Fig. 1A). This activity was sensitive to the GCPII-specific inhibitor 2-(phosphonomethyl)pentanedioic acid (2-PMPA, final concentration 500 nM) and was also inhibited by a collection of other specific GCPII inhibitors, including 2-(3-mercaptopropyl)pentanedioic acid (2-MPPA, 100 μM), 2-[(pentafluorophenylmethyl)hydroxyphosphinyl]methyl-pentanedioic acid (GPI-5232, 500 μM; GPI-5495, 200 μM; GPI-5496, 1 mM), (2*S*,3′*S*)-{[(3′-amino-3′-carboxy-propyl)-hydroxyphosphinoyl]methyl}-pentanedioic acid (EPE, 1 mM), and methotrexate (1 mM). Inhibitors GPI-5232, GPI-5495, and GPI-5496 are stereoisomers. The plasma samples PL2 and PL3 were tested only with 2-PMPA (Fig. 1A).

The diluted plasma samples exhibited a linear dependence of substrate conversion on added plasma volume. More concentrated samples (non-diluted or less than 10-fold dilution) reached a conversion plateau (Fig. 1B), presumably due to matrix effects. Therefore, 10- to 100-fold dilution of plasma samples (the linear area of the curve) was used for GCPII quantification in plasma. Standards of recombinant extracellular GCPII (rhGCPII; prepared as described in Ref. [40]) exhibited linear dependence of substrate conversion on rhGCPII amount in the region between 0 and 50 pg rhGCPII (Fig. 1C).

GCPII Can Be Immunoprecipitated from Plasma and Detected by Mass Spectrometry

To verify that GCPII is in fact present in human blood, we immunoprecipitated GCPII from human citrate plasma with biotinylated antibody 2G7 coupled to Streptavidin Sepharose resin. The presence of GCPII in plasma was confirmed by Western blot analysis of the elution fractions with GCPII-specific antibody GCP-04 (Fig. 2) and eventually by mass spectrometry, which detected peptides covering 34% of the GCPII sequence (data not shown).

As a positive control, the diluted plasma sample was spiked with recombinant extracellular GCPII (rhGCPII; prepared as described in Ref. [40]) to a final concentration of 850 pg/ml (Fig. 2, lanes 3 and 8). As a negative control, no 2G7 antibody was bound to the Streptavidin Sepharose resin mixed with the diluted plasma sample (Fig. 2, lanes 4 and 9). The diffuse appearance of the GCPII bands suggests GCPII is heterogenously glycosylated, in contrast to uniform high-mannose glycosylation of rhGCPII standard expressed in insect cells (Fig. 2).

Interestingly, we were unable to immunoprecipitate GCPII with non-biotinylated antibodies raised against native GCPII (including J591) that were bound to Protein G Sepharose rather than Streptavidin Sepharose (data not shown).

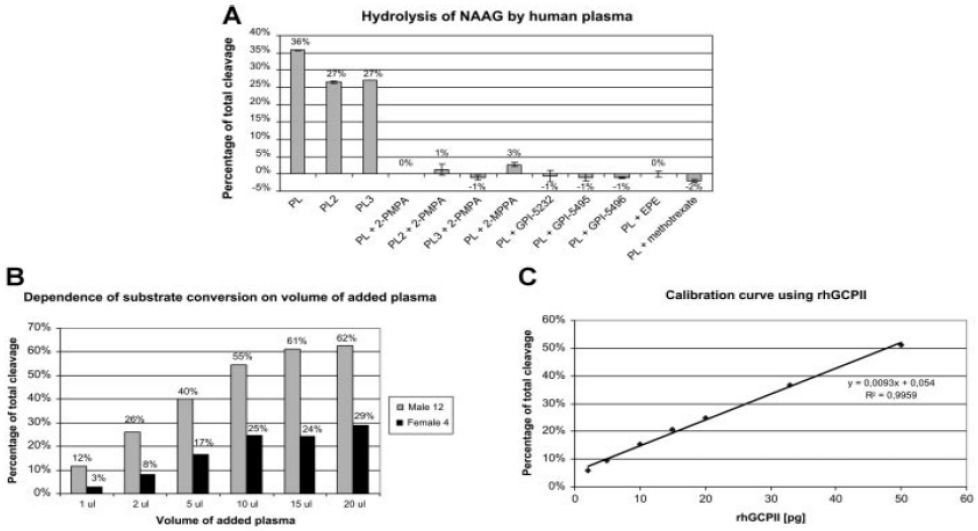

Fig. 1. NAAG-hydrolyzing activity in human plasma and its inhibition by a set of specific GCPII inhibitors. **Panel A**: NAAG-hydrolyzing activity of three different human plasma samples (PL, PL2, PL3) was analyzed using radioenzymatic assay with [^{3}H]NAAG. To probe GCPII inhibition, a panel of GCPII inhibitors was used: 2-PMPA (500 nM), 2-MPPA (100 μM), GPI-5232 (500 μM), GPI-5495 (200 μM), GPI-5496 (1 mM), EPE (1 mM), and methotrexate (1 mM). The activities were measured in duplicate; values are presented as the mean ± standard deviation. Ten microliters of plasma was loaded in each reaction. **Panel B**: Two plasma samples (male #12 and female #4, see Table I) of different GCPII concentration were chosen to illustrate the dependence of substrate conversion on the volume of added plasma. When more than 10 μl of undiluted plasma was added, substrate conversion reached its plateau. **Panel C**: Calibration curve of cleaved [^{3}H]NAAG by recombinant extracellular GCPII (rhGCPII). The analyzed plasma samples were diluted to fit into the linear region of the calibration curve (0–50 pg rhGCPII).

Low Concentrations of GCPII are Present in the Plasma of Healthy Individuals

We set out to analyze the distribution of GCPII concentration in the blood of healthy individuals. Blood samples were collected from volunteers not diagnosed with prostate cancer, including four females. All individuals' PSA levels fell below 2.5 ng/ml (Table I), and therefore they can be considered healthy and without considerable risk of prostate cancer [45]. The GCPII concentration was determined in these samples using radioenzymatic assay with [^{3}H]NAAG as a substrate. Purified recombinant extracellular GCPII (0.01–1 ng/ml; prepared as described in Ref. [40]) was used as a standard. Plasma samples were diluted 10- to 100-fold, which was necessary to fit into the range of the standards. To verify that GCPII is the proteolytic agent, patients' plasma samples were inhibited with 500 nM 2-PMPA. The addition of the GCPII-specific inhibitor led to complete loss of the activity in all tested samples. The GCPII concentration in plasma ranged between 1.3 and 17.2 ng/ml. Since the values for the GCPII amount in the blood are always positive, they should follow log-normal distribution. Therefore, geometrical mean and non-symmetrical standard deviations are used and reach the following values (see Table I): 3.2 ng/ml (+3.3; −1.6 ng/ml); for men only: 3.7 ng/ml (+3.8; −1.9 ng/ml); all female samples fell under 5 ng/ml: 2.0 ng/ml (+1.4; −0.8 ng/ml).

The GCPII concentration in plasma did not correlate with the age of the volunteers (Pearson's correlation coefficient: 0.28; *P*-value: 0.31). The Pearson's correlation analysis revealed no correlation between GCPII and PSA plasma concentrations (Pearson's correlation coefficient: 0.08; *P*-value: 0.81).

Purified Recombinant PGCP Constructs are Enzymatically Active but do not Possess NAAG-Hydrolyzing Activity

We prepared two PGCP constructs to elucidate whether and to what extent PGCP contributes to NAAG-hydrolyzing activity in human plasma.

Endogenous PGCP contains a signal peptide, propeptide, and mature chain. We replaced the endogenous signal peptide with the BiP signal sequence and

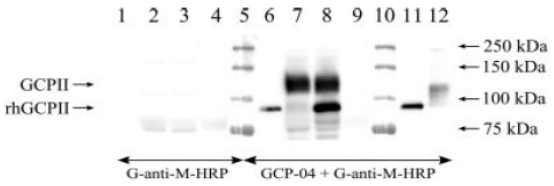

Fig. 2. Immunoprecipitation of GCPII from human plasma. GCPII was immunoprecipitated from 600 μl citrate plasma with biotinylated antibody 2G7 bound to Streptavidin Sepharose. As a negative control, an experiment without antibody 2G7 was performed. As a positive control, diluted plasma sample was spiked with recombinant extracellular GCPII (rhGCPII), lacking its endogenous intracellular and transmembrane parts. The Western blot was performed with the antibody GCP-04 (described in Ref. [41]), recognizing denatured GCPII, followed by HRP-conjugated goat anti-mouse IgG secondary antibody (G-anti-M-HRP; Thermo Scientific). A half of the membrane was probed with G-anti-M-HRP only to visualise the non-specific signal caused by the secondary antibody. The arrows indicate the position of immunoprecipitated GCPII (lanes 7 and 8), rhGCPII in the spiked sample (lane 8), or rhGCPII used as a standard (lanes 6 and 11). (1,6) rhGCPII standard, 1 ng; (2,7) Elution from IP; (3,8) Elution from IP-positive control; (4,9) Elution from IP-negative control; (5,10) All blue standards (Bio-Rad); (11) rhGCPII standard, 2 ng; (12) LNCaP lysate, 1.5 μg total protein. Twenty-five microliters of the elution fraction sample was loaded to each lane.

placed an Avi-tag at the N-terminus or C-terminus. The propeptide part was preserved only in the C-terminally tagged construct, allowing it to remain free for further molecular processing and activation of PGCP (Fig. 3A,C).

Conditioned media from cultures of *Drosophila* S2 cells stably transfected with ProPGCPavi or aviPGCP were concentrated, and Avi-tagged PGCP constructs were purified by affinity chromatography using Streptavidin Mutein Matrix. The purification yield was 3.3 mg of ProPGCPavi (purified from 500 ml of cell-conditioned medium) and 0.22 mg of aviPGCP (purified from 100 ml of cell-conditioned medium). The purity of the proteins was determined by SDS-PAGE (Fig. 3B,D).

The availability of sufficient amounts of recombinant purified PGCP (ProPGCPavi and aviPGCP) enabled determination of PGCP's enzymatic activities. To verify that we obtained properly folded and active PGCP constructs, we determined their proteolytic activity using a cognate substrate of PGCP, the dipeptide L-seryl-L-methionine (SerMet) [37,46]. The determinations were performed in two different buffers: in 100 mM Tris–HCl, 1 mM $ZnCl_2$, pH 7.5 (according to Gingras et al. [36]), and in 100 mM sodium acetate, pH 5.5, including 15 mM zinc acetate (according to Zajc et al. [37]).

TABLE I. GCPII Concentrations in Plasma of Healthy Individuals

	Age (years)	GCPII in plasma (ng/ml)	PSA in plasma (ng/ml)
Female 1	22	1.4 ± 0.3	0.004
Female 2	31	1.3 ± 0.3	N/D
Female 3	43	1.9 ± 0.3	N/D
Female 4	46	4.3 ± 0.3	N/D
Male 1	20	3.7 ± 0.6	0.79
Male 2	22	4.0 ± 0.6	0.41
Male 3	24	2.3 ± 0.4	0.83
Male 4	25	5.7 ± 0.8	2.11
Male 5	26	1.8 ± 0.3	N/D
Male 6	26	1.4 ± 0.3	N/D
Male 7	27	1.3 ± 0.3	0.56
Male 8	27	3.4 ± 0.7	0.95
Male 9	28	4.6 ± 0.7	0.47
Male 10	28	1.5 ± 0.3	0.57
Male 11	33	3.2 ± 0.5	0.90
Male 12	34	17.2 ± 5.0	0.49
Male 13	45	2.4 ± 0.6	0.85
Male 14	50	3.0 ± 0.4	0.62
Male 15	52	9.9 ± 1.0	1.63

Radioenzymatic assay with [^{3}H]NAAG was used to determined GCPII concentrations in heparin-treated plasma samples withdrawn from 19 healthy volunteers. The samples were measured in duplicate using different volumes (2.5 and 5 μl, or 5 and 10 μl) of added plasma in three separate experiments; values are presented as the mean ± standard deviation. PSA concentrations were determined at Thomayer Hospital in Prague. Recombinant extracellular GCPII (0.01–1 ng/ml) was used to construct a calibration curve of NAAG-hydrolyzing activity.

Both ProPGCPavi and aviPGCP possessed SerMet-hydrolyzing activity (Fig. 4A). The enzymes hydrolyzed SerMet in both buffers; however, they exhibited higher activity in the acetate buffer. The activity was sensitive to 25 mM EDTA but completely insensitive to 500 nM 2-PMPA, a GCPII-specific inhibitor (Fig. 4A).

Using a very sensitive radioenzymatic assay for quantification of NAAG-hydrolyzing activity, we did not observe any cleavage of NAAG, even when using 5 μg of ProPGCPavi or 3.3 μg of aviPGCP in a single reaction. For comparison, 5 pg of recombinant GCPII showed significant activity (Fig. 4B).

DISCUSSION

GCPII was identified as a potential target for imaging and therapy of prostate cancer 15 years ago [47,48]. However, the precise physiological role of the enzyme in the prostate and prostate cancer remains unknown. Although GCPII is considered a prostate cancer marker, there currently are no methods available that monitor GCPII levels to predict prostate

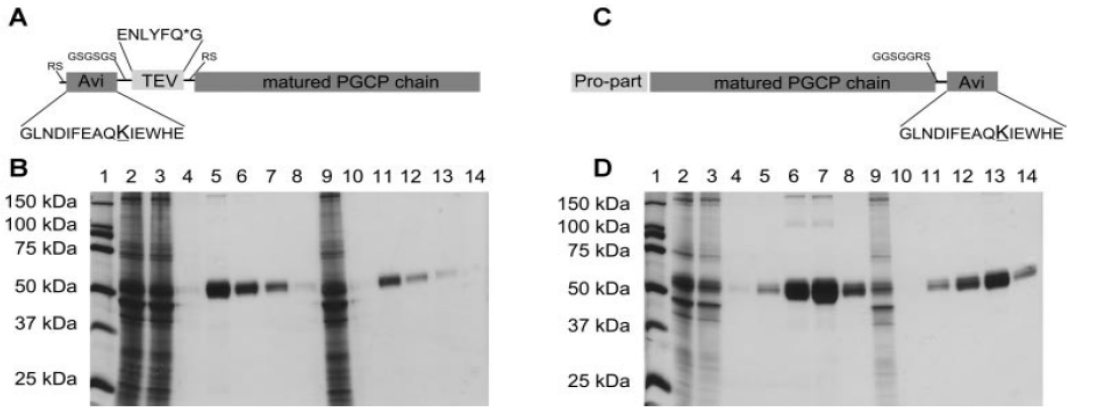

Fig. 3. Recombinant PGCP constructs and their purification. **Panels A,C**: Schematic representation of aviPGCP and ProPGCPavi, respectively. Avi—sequence of 15 amino acids recognized by biotin-protein ligase and biotinylated on the ε-amino group of the lysine residue (underlined); TEV—sequence of 7 amino acids specifically recognized by TEV protease (cleavage site is marked with an asterisk); Pro-part—endogenous propeptide sequence of PGCP. Spacer sequence and amino acids introduced during cloning are depicted in a smaller font size. Created according to Ref. [39]. **Panels B,D**: Analysis of purification of aviPGCP and ProPGCPavi, respectively. Proteins were expressed in *Drosophila* S2 cells, and equilibrated concentrated medium was mixed with Streptavidin Mutein Matrix and incubated overnight at 4°C. The resin with bound biotinylated proteins was separated on a gravity-flow column. The column was washed with Tris buffer, and proteins were eluted with an excess of biotin. Fractions from purification were separated by SDS-PAGE and analyzed by silver-staining. (1) All blue standards (Bio-Rad), recombinant extracellular GCPII (90 kDa); (2) Load; (3) Flow-through; (4) Wash; (5–8) Elutions 1–4; (9) Flow-through; (10) Wash; (11–14) Elutions 1–4. Purification of each protein was performed in two rounds; the first round is represented by lanes 3–8, the second by lanes 9–14. A half microliter of load, flow-through, and E2 and 5 μl of wash, E1, E3, and E4 were loaded onto the gel.

cancer progress. Quantitation of GCPII potentially present in human plasma might be a useful tool for predicting prostate cancer development and prognosis.

Moreover, cancer imaging using antibodies, inhibitors, and other structures, as well as specific drug delivery targeting GCPII, has made remarkable progress in recent years [18,25,49]. Attenuation of GCPII activity might also play an important role in the treatment of neurological disorders associated with excess glutamate [50]. The potential presence of GCPII in blood may compromise these approaches due to non-specific interaction of the ligands with the soluble enzyme circulating in the blood. However, in 2012 Denmeade et al. [51] described a PSMA prodrug that was not hydrolyzed upon prolonged incubation in human plasma. This observation suggests that GCPII concentration in plasma is low and does not suffice to significant hydrolysis of tested prodrugs.

After detecting NAAG-hydrolyzing activity in human blood plasma, we tested the possibility of inhibiting this activity with GCPII-specific inhibitors. We found out that the activity could be inhibited with all inhibitors tested, suggesting the presence of GCPII or its close homolog GCPIII (Fig. 1A). The activity was dependent upon the volume of added plasma but reached a plateau in larger volumes of added sample (Fig. 1B). This is probably caused by matrix effects, a phenomenon often observed when complex matrices such as blood samples are used.

Furthermore, we performed experiments to confirm the presence of GCPII in plasma. In our hands, Western blots yielded irreproducible results due to the very high background caused by the high protein concentrations in plasma samples. Therefore, we used immunoprecipitation for partial purification of the target antigen from a plasma sample. Using a biotinylated mouse monoclonal antibody raised against native GCPII (2G7), we were able to immunoprecipitate GCPII from human plasma samples (Fig. 2). The specificity of the GCPII detection was assured by two additional steps: after the immunoprecipitation, the elution fraction was analyzed with a second previously described anti-GCPII antibody GCP-04 and by mass spectrometry (a direct method of identification). Although the Western blot analysis of immunoprecipitated GCPII was not used for GCPII quantification in the blood, the quantity of immunoprecipitated GCPII roughly corresponded to that predicted by radioenzymatic assay. Mass spectrometry detected 18 different peptides covering 34% of the full-length GCPII sequence. One peptide corresponds to the first 16 amino

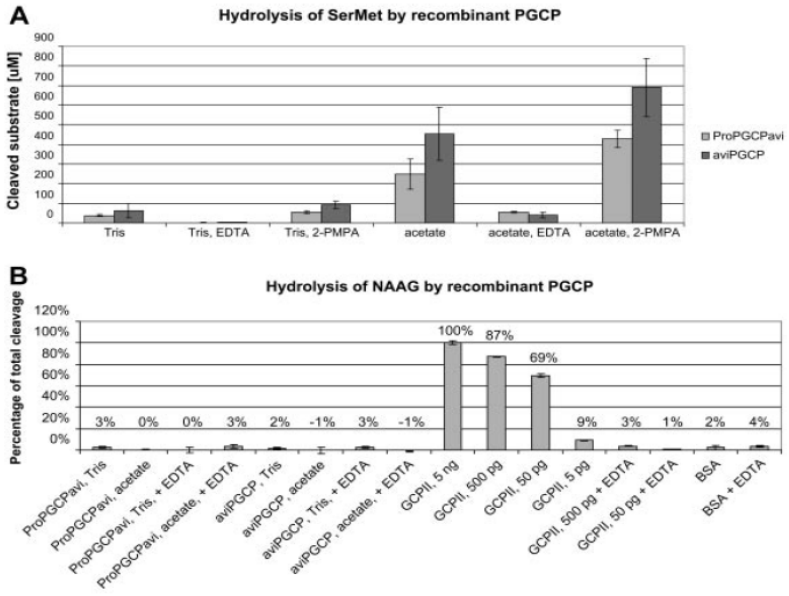

Fig. 4. Analysis of enzymatic activities of PGCP constructs. **Panel A**: SerMet-hydrolyzing activity of PGCP constructs was measured using an HPLC-based method with o-phthalaldehyde (OPA) derivatization. Measurements were performed in two different buffers: 100 mM Tris–HCl, 1 mM $ZnCl_2$, pH 7.5 (according to Gingras et al. [36]) and 100 mM sodium acetate, pH 5.5, including 15 mM zinc acetate (according to Zajc et al. [37]). The amount of ProPGCPavi and aviPGCP in the reaction was 30 ng. The activity of PGCP constructs was inhibited by 25 mM EDTA but not by 500 nM 2-PMPA. **Panel B**: The NAAG-hydrolyzing activity of PGCP constructs was determined using radioenzymatic assay with [^{3}H]NAAG. The assay was performed in two different buffers: 100 mM Tris–HCl, pH 7.5, 1 mM $ZnCl_2$ (according to Gingras et al. [36]) and 100 mM sodium acetate, pH 5.5, including 15 mM zinc acetate (according to Zajc et al. [37]). The amounts of ProPGCPavi and aviPGCP used in the reactions were 5 μg and 3.3 μg, respectively. As the SerMet-hydrolyzing activity of PGCP constructs was inhibited with 25 mM EDTA, the same EDTA concentration was tested in this experimental setup as well. Recombinant GCPII (5 ng to 5 pg) was used as a positive control; GCPII activity was measured in 50 mM Tris–HCl, 150 mM NaCl, pH 7.4, 0.1% Tween-20 (TBST). BSA (5 μg) in TBST served as a negative control.

acids of the intracellular part of GCPII (MWNLLHETDSAVATAR), whereas all other peptides correspond to the extracellular domain of GCPII.

The source of the GCPII that we observed in plasma remains unclear. GCPII, as a transmembrane protein, may be partly shed from the cell surface by the action of an unknown protease, or it could be secreted into plasma in the form of a soluble protein lacking the intracellular and transmembrane regions. Several GCPII splice variants have been described; however, none of them is a secreted protein [52–54]. Lastly, GCPII could stem from an extraprostatic source, which could explain the activity in female plasma samples. We analyzed the immunoprecipitated GCPII by Western blot with the antibody GCP-04, which recognizes denatured GCPII. As shown in Figure 2, GCPII migrated at a molecular weight of about 120 kDa, corresponding to full-length, heavily glycosylated GCPII, rather than to a truncated form of the enzyme. Importantly, we were not able to immunoprecipitate GCPII from plasma with unmodified antibodies including J591 (i.e., not biotinylated or not covalently bound to resin). This might have been caused by high concentrations of endogenous antibodies that blocked binding sites on Protein G Sepharose.

To identify how GCPII concentration in plasma varies within a healthy men and women of various ages, we took blood samples from 19 volunteers and determined GCPII concentrations in the samples using radioenzymatic assay. The GCPII concentration was in the range of 1.3–17.2 ng/ml; geometrical mean and non-symmetrical deviations were 3.2 ng/ml (+3.3; −1.6 ng/ml); for males: 3.7 ng/ml (+3.8; −1.9 ng/ml); for females: 2.0 ng/ml (+1.4; −0.8 ng/ml). We did not observe a correlation between GCPII concentration and the age of volunteers. The Pearson's correlation analysis showed no correlation between GCPII and PSA concentrations in plasma. It would be interesting

to analyze GCPII concentrations in the blood of prostate cancer patients to determine whether there is a correlation between the level of GCPII and prostate cancer stage.

Our quantitation of GCPII in plasma was based on a radioenzymatic assay making use of ability of GCPII to hydrolyze NAAG. This marks the first time that GCPII concentration in plasma has been determined by its enzymatic activity. Previously, GCPII was detected using antibody-based approaches, such as Western blot and SELDI immunoassay [27–32]. Using Western blot, GCPII was detected in the serum of normal men, men with benign prostate hyperplasia (BPH), and prostate cancer patients. The correlation between GCPII concentration and prostate cancer progress remains unclear. Some groups have revealed prognostic correlations in advanced prostate cancer [28], whereas others do not consider GCPII a good serum marker [31]. In the SELDI ProteinChip immunoassay study, significant differences were observed in the mean GCPII concentration between groups of men aged <50, aged >50, with BPH and with prostate cancer; nonetheless, GCPII concentration range was wide and overlapping in all groups [32]. They determined the concentration of GCPII in blood of normal males between 106.4 and 611.5 ng/ml, significantly higher than shown by our work [32]. Both studies showed GCPII concentration in blood of healthy males to be higher than the concentration of PSA.

The NAAG-hydrolyzing activity was inhibited with EDTA, a metallopeptidase inhibitor, as well as with other inhibitors specific to GCPII (Fig. 1A). On the other hand, the activity was not affected by "cOmplete Protease Inhibitor Cocktail, EDTA-free" (Roche; data not shown) suggesting that a metallocarboxypeptidase is responsible for the hydrolysis. To date, there are 27 reviewed metallocarboxypeptidases (EC 3.4.17.) found in humans according to the UniProt [55]. At the same time, only carboxypeptidase B2 (cleaving off C-terminal arginine or lysine residues from biologically active peptides) and PGCP were detected in the blood plasma. NAAG-hydrolyzing activity has been described only for GCPII, its homolog GCPIII, and PGCP. Therefore, only three known enzymes, GCPII, GCPIII, and PGCP can be, in principle, responsible for the observed NAAG-hydrolyzing activity in the plasma samples.

Using the specific substrate of GCPIII, ß-citryl-L-glutamate (BCG) [56], we found out that GCPIII does not contribute to NAAG-hydrolyzing activity. Since the observed BCG-hydrolyzing activity was minimal, we cannot quite exclude the presence of GCPIII in plasma; however, if present, its concentration would be at least 50-fold lower that GCPII (data not shown).

In 1999, Gingras et al. [36] described PGCP, a plasmatic zinc metallopeptidase reportedly possessing the same enzymatic activity as GCPII. PGCP belongs to the MEROPS peptidase family M28 and is a distant homolog of GCPII, sharing 25% amino acid sequence similarity. We prepared two PGCP constructs and expressed them in *Drosophila* S2 cells. Both constructs have an Avi-tag sequence, enabling fast, efficient, and simple purification that makes use of the interaction between the biotinylated Avi-tag and Streptavidin Mutein Matrix [39]. Avi-tag was placed either at the N-terminus of the mature PGCP chain (aviPGCP) or at the C-terminus of the mature PGCP chain, preserving the enzyme's endogenous propeptide part at the N-terminus (ProPGCPavi). PGCP forms enzymatically active dimers, whereas monomers do not possess any enzymatic activity [37]. Removal of the propeptide part is a necessary step for dimer creation, and it is believed to be performed by a protease present in cell medium [37,57]. ProPGCPavi and aviPGCP were purified by affinity chromatography; on SDS-PAGE, we observed a double band for both constructs. The origin of the double band can be explained by cleavage within the sequence of the purified proteins. In the case of aviPGCP, a cleavage similar to that reported within the N-terminal part of purified aviGCPII [39] may have taken place, whereas in the case of ProPGCPavi, removal of the propeptide was observed [37].

To confirm that we purified active and properly folded PGCP constructs, we probed them with a cognate substrate of PGCP, the dipeptide SerMet. Because the activity of PGCP had previously been determined in two different buffers, we performed our assay in both of buffers: 100 mM Tris–HCl, 1 mM $ZnCl_2$, pH 7.5 (according to Gingras et al. [36]), and 100 mM sodium acetate, pH 5.5, including 15 mM zinc acetate (according to Zajc et al. [37]). Both PGCP preparations hydrolyzed SerMet; aviPGCP exhibited higher activity than ProPGCPavi, which was in agreement with our assumption than only a fraction of ProPGCPavi might have been activated by removal of the propeptide. The activity of both constructs was higher in the acetate buffer; however, prolonging the incubation time or using larger amounts of enzyme led to total conversion in both buffers. The activity was sensitive to EDTA, a metalloprotease inhibitor, but not sensitive to 2-PMPA, a GCPII-specific inhibitor (Fig. 4A).

Because we used NAAG-hydrolyzing activity for GCPII quantification and because PGCP has been reported to possess this activity as well, we probed the PGCP preparations with a cognate substrate of GCPII, the dipeptide NAAG. The determination was performed in the Tris and acetate buffers described above. We did not detect any NAAG-hydrolyzing activity

with either PGCP construct, even when high PGCP concentrations were used (Fig. 4B). When compared with recombinant PGCP, a 500,000-fold lower amount of GCPII exhibited significant NAAG-hydrolyzing activity. This result is in direct contradiction to the results previously published by Gingras et al. [36] who purified PGCP from human plasma and placenta and showed that it cleaved NAAG. This discrepancy might be caused by co-purification of GCPII together with PGCP in Gingras' experiment.

In fact, PGCP is the only glutamate carboxypeptidase found in plasma that has ever been shown to exhibit NAAG-hydrolyzing activity, and the inhibitors we used have been previously shown to be very specific for GCPII/GCPIII. The combination of specific immunochemical detection, specific substrate cleavage, specific inhibitory profile, and detection by LC–MS provides, in our opinion, very strong evidence for our conclusion that GCPII is the proteolytic agent responsible for the NAAG hydrolysis in the blood.

The analysis of the clinical relevation of GCPII in plasma and prostate cancer progression will be the focus of further studies.

CONCLUSIONS

We have conclusively shown that GCPII is present in the blood plasma of people not diagnosed with prostate cancer in concentrations between 1.3 and 17.2 ng/ml. The origin, form, and possible function of GCPII in plasma remain unknown and are under further investigation. The concentration of GCPII in plasma likely cannot profoundly influence targeting of imaging probes or drugs using specific anti-GCPII ligands to prostate cancer cells. PGCP, which belongs to the same peptidase family as GCPII, in our hands possesses SerMet-hydrolyzing activity but not NAAG-hydrolyzing activity, and therefore does not contribute to the NAAG-hydrolyzing activity observed in human plasma.

ACKNOWLEDGMENTS

The authors would like to acknowledge Jana Starkova and Karolina Sramkova for their excellent technical support, Radko Soucek for HPLC measurements, Zuzana Demianova, Jana Horakova and Martin Hubalek for mass spectrometry analyses, Hillary Hoffman for language editing, and Vaclav Horejsi and Dobromila Matejkova for preparation of the monoclonal antibody 2G7. The plasmid encoding PGCP was a kind gift from Iztok Dolenc (Department of Biochemistry and Molecular Biology, J. Stefan Institute, Ljubljana, Slovenia) and the inhibitor 2-PMPA was a kind gift from Barbara Slusher (School of Medicine, John Hopkins University, MD, USA). This work was supported by grant P304-12-0847 from the Grant Agency of the Czech Republic and OPPK project CZ.2.16/3.1.00/24016.

REFERENCES

1. Siegel R, Ma J, Zou Z, Jemal A. Cancer statistics, 2014. CA Cancer J Clin 2014;64:9–29.
2. Israeli RS, Powell CT, Fair WR, Heston WD. Molecular cloning of a complementary DNA encoding a prostate-specific membrane antigen. Cancer Res 1993;53:227–230.
3. Horoszewicz JS, Kawinski E, Murphy GP. Monoclonal antibodies to a new antigenic marker in epithelial prostatic cells and serum of prostatic cancer patients. Anticancer Res 1987;7:927–935.
4. Robinson MB, Blakely RD, Couto R, Coyle JT. Hydrolysis of the brain dipeptide N-acetyl-L-aspartyl-L-glutamate. Identification and characterization of a novel N-acetylated alpha-linked acidic dipeptidase activity from rat brain. J Biol Chem 1987;262:14498–14506.
5. Sokoloff RL, Norton KC, Gasior CL, Marker KM, Grauer LS. A dual-monoclonal sandwich assay for prostate-specific membrane antigen: Levels in tissues, seminal fluid and urine. Prostate 2000;43:150–157.
6. Rovenska M, Hlouchova K, Sacha P, Mlcochova P, Horak V, Zamecnik J, Barinka C, Konvalinka J. Tissue expression and enzymologic characterization of human prostate specific membrane antigen and its rat and pig orthologs. Prostate 2008;68:171–182.
7. Kinoshita Y, Kuratsukuri K, Landas S, Imaida K, Rovito PM Jr, Wang CY, Haas GP. Expression of prostate-specific membrane antigen in normal and malignant human tissues. World J Surg 2006;30:628–636.
8. Cunha AC, Weigle B, Kiessling A, Bachmann M, Rieber EP. Tissue-specificity of prostate specific antigens: Comparative analysis of transcript levels in prostate and non-prostatic tissues. Cancer Lett 2006;236:229–238.
9. Chandler CJ, Wang TT, Halsted CH. Pteroylpolyglutamate hydrolase from human jejunal brush borders. Purification and characterization. J Biol Chem 1986;261:928–933.
10. Liu H, Rajasekaran AK, Moy P, Xia Y, Kim S, Navarro V, Rahmati R, Bander NH. Constitutive and antibody-induced internalization of prostate-specific membrane antigen. Cancer Res 1998;58:4055–4060.
11. Conway RE, Joiner K, Patterson A, Bourgeois D, Rampp R, Hannah BC, McReynolds S, Elder JM, Gilfilen H, Shapiro LH. Prostate specific membrane antigen produces pro-angiogenic laminin peptides downstream of matrix metalloprotease-2. Angiogenesis 2013;16:847–860.
12. Conway RE, Petrovic N, Li Z, Heston W, Wu D, Shapiro LH. Prostate-specific membrane antigen regulates angiogenesis by modulating integrin signal transduction. Mol Cell Biol 2006;26:5310–5324.
13. Divyya S, Naushad SM, Murthy PV, Reddy Ch R, Kutala VK. GCPII modulates oxidative stress and prostate cancer susceptibility through changes in methylation of RASSF1, BNIP3, GSTP1 and Ec-SOD. Mol Biol Rep 2013;40:5541–5550.
14. Zhang Y, Guo Z, Du T, Chen J, Wang W, Xu K, Lin T, Huang H. Prostate specific membrane antigen (PSMA): A novel modulator

of p38 for proliferation, migration, and survival in prostate cancer cells. Prostate 2013;73:835–841.

15. Lapidus RG, Tiffany CW, Isaacs JT, Slusher BS. Prostate-specific membrane antigen (PSMA) enzyme activity is elevated in prostate cancer cells. Prostate 2000;45:350–354.
16. Kahn D, Williams RD, Seldin DW, Libertino JA, Hirschhorn M, Dreicer R, Weiner GJ, Bushnell D, Gulfo J. Radioimmunoscintigraphy with 111indium labeled CYT-356 for the detection of occult prostate cancer recurrence. J Urol 1994;152:1490–1495.
17. Bander NH, Milowsky MI, Nanus DM, Kostakoglu L, Vallabhajosula S, Goldsmith SJ. Phase I trial of 177lutetium-labeled J591, a monoclonal antibody to prostate-specific membrane antigen, in patients with androgen-independent prostate cancer. J Clin Oncol 2005;23:4591–4601.
18. Liu T, Nedrow-Byers JR, Hopkins MR, Wu LY, Lee J, Reilly PT, Berkman CE. Targeting prostate cancer cells with a multivalent PSMA inhibitor-guided streptavidin conjugate. Bioorg Med Chem Lett 2012;22:3931–3934.
19. Chen Z, Penet MF, Nimmagadda S, Li C, Banerjee SR, Winnard PT Jr, Artemov D, Glunde K, Pomper MG, Bhujwalla ZM. PSMA-targeted theranostic nanoplex for prostate cancer therapy. ACS Nano 2012;6:7752–7762.
20. Taneja SS. ProstaScint(R) scan: Contemporary use in clinical practice. Rev Urol 2004;6 (Suppl 10): S19–S28.
21. Troyer JK, Feng Q, Beckett ML, Wright GL Jr. Biochemical characterization and mapping of the 7 E11-C5. 3 epitope of the prostate-specific membrane antigen. Urol Oncol 1995;1:29–37.
22. Bander NH, Trabulsi EJ, Kostakoglu L, Yao D, Vallabhajosula S, Smith-Jones P, Joyce MA, Milowsky M, Nanus DM, Goldsmith SJ. Targeting metastatic prostate cancer with radiolabeled monoclonal antibody J591 to the extracellular domain of prostate specific membrane antigen. J Urol 2003;170:1717–1721.
23. Frigerio B, Fracasso G, Luison E, Cingarlini S, Mortarino M, Coliva A, Seregni E, Bombardieri E, Zuccolotto G, Rosato A, Colombatti M, Canevari S, Figini M. A single-chain fragment against prostate specific membrane antigen as a tool to build theranostic reagents for prostate cancer. Eur J Cancer 2013;49:2223–2232.
24. Fracasso G, Bellisola G, Cingarlini S, Castelletti D, Prayer-Galetti T, Pagano F, Tridente G, Colombatti M. Anti-tumor effects of toxins targeted to the prostate specific membrane antigen. Prostate 2002;53:9–23.
25. Tagawa ST, Akhtar NH, Nikolopoulou A, Kaur G, Robinson B, Kahn R, Vallabhajosula S, Goldsmith SJ, Nanus DM, Bander NH. Bone marrow recovery and subsequent chemotherapy following radiolabeled anti-prostate-specific membrane antigen monoclonal antibody j591 in men with metastatic castration-resistant prostate cancer. Front Oncol 2013;3:214.
26. Akhtar NH, Pail O, Saran A, Tyrell L, Tagawa ST. Prostate-specific membrane antigen-based therapeutics. Adv Urol 2012;2012:973820.
27. Rochon YP, Horoszewicz JS, Boynton AL, Holmes EH, Barren RJ III, Erickson SJ, Kenny GM, Murphy GP. Western blot assay for prostate-specific membrane antigen in serum of prostate cancer patients. Prostate 1994;25:219–223.
28. Murphy GP, Kenny GM, Ragde H, Wolfert RL, Boynton AL, Holmes EH, Misrock SL, Bartsch G, Klocker H, Pointner J, Reissigl A, McLeod DG, Douglas T, Morgan T, Gilbaugh J. Measurement of serum prostate-specific membrane antigen, a new prognostic marker for prostate cancer. Urology 1998;51:89–97.
29. Murphy GP, Maguire RT, Rogers B, Partin AW, Nelp WB, Troychak MJ, Ragde H, Kenny GM, Barren RJ III, Bowes VA, Gregorakis AK, Holmes EH, Boynton AL. Comparison of serum PSMA, PSA levels with results of Cytogen-356 ProstaScint scanning in prostatic cancer patients. Prostate 1997;33:281–285.
30. Troyer JK, Beckett ML, Wright GL. Detection and characterization of the prostate-specific membrane antigen (Pmsa) in tissue-extracts and body-fluids. Int J Cancer 1995;62:552–558.
31. Beckett ML, Cazares LH, Vlahou A, Schellhammer PF, Wright GL. Prostate-specific membrane antigen levels in sera from healthy men and patients with benign prostate hyperplasia or prostate cancer. Clin Cancer Res 1999;5:4034–4040.
32. Xiao Z, Adam BL, Cazares LH, Clements MA, Davis JW, Schellhammer PF, Dalmasso EA, Wright GL Jr. Quantitation of serum prostate-specific membrane antigen by a novel protein biochip immunoassay discriminates benign from malignant prostate disease. Cancer Res 2001;61:6029–6033.
33. Catalona WJ, Richie JP, Ahmann FR, Hudson MA, Scardino PT, Flanigan RC, deKernion JB, Ratliff TL, Kavoussi LR, Dalkin BL, Waters WB, Macfarlane MT, Southwick PC. Comparison of digital rectal examination and serum prostate specific antigen in the early detection of prostate cancer: Results of a multicenter clinical trial of 6,630 men. J Urol 1994;151:1283–1290.
34. Nadler RB, Humphrey PA, Smith DS, Catalona WJ, Ratliff TL. Effect of inflammation and benign prostatic hyperplasia on elevated serum prostate specific antigen levels. J Urol 1995;154:407–413.
35. Moyer VA. Screening for prostate cancer: U.S. Preventive Services Task Force recommendation statement. Ann Intern Med 2012;157:120–134.
36. Gingras R, Richard C, El-Alfy M, Morales CR, Potier M, Pshezhetsky AV. Purification, cDNA cloning, and expression of a new human blood plasma glutamate carboxypeptidase homologous to N-acetyl-aspartyl-alpha-glutamate carboxypeptidase/prostate-specific membrane antigen. J Biol Chem 1999;274:11742–11750.
37. Zajc T, Suban D, Rajkovic J, Dolenc I. Baculoviral expression and characterization of human recombinant PGCP in the form of an active mature dimer and an inactive precursor protein. Protein Expr Purif 2011;75:119–126.
38. Hlouchova K, Barinka C, Klusak V, Sacha P, Mlcochova P, Majer P, Rulisek L, Konvalinka J. Biochemical characterization of human glutamate carboxypeptidase III. J Neurochem 2007;101:682–696.
39. Tykvart J, Sacha P, Barinka C, Knedlik T, Starkova J, Lubkowski J, Konvalinka J. Efficient and versatile one-step affinity purification of in vivo biotinylated proteins: Expression, characterization and structure analysis of recombinant human glutamate carboxypeptidase II. Protein Expr Purif 2012;82:106–115.
40. Barinka C, Rinnova M, Sacha P, Rojas C, Majer P, Slusher BS, Konvalinka J. Substrate specificity, inhibition and enzymological analysis of recombinant human glutamate carboxypeptidase II. J Neurochem 2002;80:477–487.
41. Sacha P, Zamecnik J, Barinka C, Hlouchova K, Vicha A, Mlcochova P, Hilgert I, Eckschlager T, Konvalinka J. Expression of glutamate carboxypeptidase II in human brain. Neuroscience 2007;144:1361–1372.
42. Beckett D, Kovaleva E, Schatz PJ. A minimal peptide substrate in biotin holoenzyme synthetase-catalyzed biotinylation. Protein Sci 1999;8:921–929.

43. Kapust RB, Waugh DS. Controlled intracellular processing of fusion proteins by TEV protease. Protein Expr Purif 2000;19: 312–318.

44. Woodward C, Henderson JW Jr. High-speed amino acid analysis (AAA) on 1.8 μm reversed-phase (RP) columns. Wilmington, DE, USA: Agilent Technologies; 2007.

45. Heidenreich PJB, Bellmunt J, Bolla M, Joniau S, Mason MD, Matveev V, Mottet N, van der Kwast TH, Wiegel T, Zattoni F. editors. Guidelines on Prostate Cancer: European Association of Urology, Arnhem 2012.

46. Dolenc I, Mihelic M. Purification and primary structure determination of human lysosomal dipeptidase. Biol Chem 2003;384: 317–320.

47. Foss CA, Mease RC, Cho SY, Kim HJ, Pomper MG. GCPII imaging and cancer. Curr Med Chem 2012;19:1346–1359.

48. Chang SS. Overview of prostate-specific membrane antigen. Rev Urol 2004;6 (Suppl 10): S13–S18.

49. Wu X, Ding B, Gao J, Wang H, Fan W, Wang X, Zhang W, Ye L, Zhang M, Ding X, Liu J, Zhu Q, Gao S. Second-generation aptamer-conjugated PSMA-targeted delivery system for prostate cancer therapy. Int J Nanomed 2011;6:1747–1756.

50. Rahn KA, Watkins CC, Alt J, Rais R, Stathis M, Grishkan I, Crainiceau CM, Pomper MG, Rojas C, Pletnikov MV, Calabresi PA, Brandt J, Barker PB, Slusher BS, Kaplin AI. Inhibition of glutamate carboxypeptidase II (GCPII) activity as a treatment for cognitive impairment in multiple sclerosis. Proc Natl Acad Sci USA 2012;109:20101–20106.

51. Denmeade SR, Mhaka AM, Rosen DM, Brennen WN, Dalrymple S, Dach I, Olesen C, Gurel B, Demarzo AM, Wilding G, Carducci MA, Dionne CA, Moller JV, Nissen P, Christensen SB, Isaacs JT. Engineering a prostate-specific membrane antigen-activated tumor endothelial cell prodrug for cancer therapy. Sci Transl Med 2012;4:140ra186.

52. Schmittgen TD, Teske S, Vessella RL, True LD, Zakrajsek BA. Expression of prostate specific membrane antigen and three alternatively spliced variants of PSMA in prostate cancer patients. Int J Cancer 2003;107:323–329.

53. Cao KY, Mao XP, Wang DH, Xu L, Yuan GQ, Dai SQ, Zheng BJ, Qiu SP. High expression of PSM-E correlated with tumor grade in prostate cancer: A new alternatively spliced variant of prostate-specific membrane antigen. Prostate 2007;67:1791–1800.

54. Su SL, Huang IP, Fair WR, Powell CT, Heston WD. Alternatively spliced variants of prostate-specific membrane antigen RNA: Ratio of expression as a potential measurement of progression. Cancer Res 1995;55:1441–1443.

55. http://www.uniprot.org/uniprot/?query=ec%3A3.4.17.-+reviewed%3Ayes+AND+organism%3A%22Human+[9606]%22&sort=score; searched January 31, 2014.

56. Collard F, Vertommen D, Constantinescu S, Buts L, Van Schaftingen E. Molecular identification of beta-citrylglutamate hydrolase as glutamate carboxypeptidase 3. J Biol Chem 2011; 286:38220–38230.

57. Bromme D, Nallaseth FS, Turk B. Production and activation of recombinant papain-like cysteine proteases. Methods 2004;32: 199–206.

7.4. Publication IV

Navratil V., Schimer J., Tykvart J., Knedlik T., Vik V., Majer P., Konvalinka J., and Sacha P.:

DNA-linked Inhibitor Antibody Assay (DIANA) for sensitive and selective enzyme detection and inhibitor screening.

Nucleic Acids Res 2017, 45(2):e10.

Supplementary information is available online. It is also reprinted here; however, tables showing raw data are omitted here.

Nucleic Acids Research Advance Access published September 26, 2016

Nucleic Acids Research, 2016 1
doi: 10.1093/nar/gkw853

DNA-linked Inhibitor Antibody Assay (DIANA) for sensitive and selective enzyme detection and inhibitor screening

Václav Navrátil[1,2,*], Jiří Schimer[1,2], Jan Tykvart[1,2], Tomáš Knedlík[1,2], Viktor Vik[3], Pavel Majer[1], Jan Konvalinka[1,2,*] and Pavel Šácha[1,2,*]

[1]Gilead Sciences and IOCB Research Centre, Institute of Organic Chemistry and Biochemistry, Academy of Sciences of the Czech Republic, Prague, 166 10, Czech Republic, [2]Department of Biochemistry, Faculty of Science, Charles University in Prague, Prague, 128 43, Czech Republic and [3]Department of Urology, Thomayer Hospital in Prague, Prague, 140 59, Czech Republic

Received June 26, 2016; Revised September 6, 2016; Accepted September 15, 2016

ABSTRACT

Human diseases are often diagnosed by determining levels of relevant enzymes and treated by enzyme inhibitors. We describe an assay suitable for both ultrasensitive enzyme quantification and quantitative inhibitor screening with unpurified enzymes. In the DNA-linked Inhibitor ANtibody Assay (DIANA), the target enzyme is captured by an immobilized antibody, probed with a small-molecule inhibitor attached to a reporter DNA and detected by quantitative PCR. We validate the approach using the putative cancer markers prostate-specific membrane antigen and carbonic anhydrase IX. We show that DIANA has a linear range of up to six logs and it selectively detects zeptomoles of targets in complex biological samples. DIANA's wide dynamic range permits determination of target enzyme inhibition constants using a single inhibitor concentration. DIANA also enables quantitative screening of small-molecule enzyme inhibitors using microliters of human blood serum containing picograms of target enzyme. DIANA's performance characteristics make it a superior tool for disease detection and drug discovery.

INTRODUCTION

Many human diseases are diagnosed and monitored based on selective protein quantification in biological samples, for which the gold standard is sandwich ELISA (1,2), in which an analyte is captured by an immobilized antibody, probed with a second enzyme-linked antibody and quantified via a reaction catalyzed by the linked enzyme. To increase sensitivity, sandwich immunoassays have been developed using DNA-linked antibodies allowing detection by quantitative polymerase chain reaction (qPCR) (3–6).

Many clinically relevant proteins are enzymes that are directly involved in disease pathogenesis and thus represent promising drug targets (7) and many currently marketed drugs are indeed small-molecule enzyme inhibitors. Identifying inhibitors of relevant enzymes typically involves screening small-molecule libraries (8) to find compounds capable of displacing an active site probe or directly influencing the enzyme reaction kinetics (9). A major drawback of currently used protocols is that they usually require purified enzymes which can be difficult and costly to prepare.

Here we describe a multiwell plate-based assay suitable for enzyme detection in complex biological matrices that offers significantly greater sensitivity than sandwich ELISA and that allows screening of small-molecule inhibitors of target enzymes without the need to purify the target. In our DNA-linked Inhibitor ANtibody Assay (DIANA), the enzyme is captured by an immobilized antibody, probed with a detection probe consisting of a DNA oligonucleotide covalently linked to a small molecule that binds to the active site of the target enzyme and is subsequently quantified by qPCR (Figure 1). Dual recognition of the target enzyme by antibody and detection probe provides selectivity, while qPCR provides sensitivity and broad linear range. Since the probe binds to the target enzyme's active site, DIANA selectively detects only the active form of the enzyme, which is likely to be the more clinically relevant form. This novel assay for enzyme detection can also be used to screen for

*To whom correspondence should be addressed. Tel: +420 220 183 218; Fax: +420 220 183 578; Email: konval@uochb.cas.cz
Correspondence may also be addressed to Pavel Šácha. Tel: +420 220 183 452; Fax: +420 220 183 578; Email: pavelsacha@gmail.com
Correspondence may also be addressed to Václav Navrátil. Tel: +420 220 183 241; Fax: +420 220 183 578; Email: vanavratil@gmail.com
Present addresses:
Jiří Schimer, School of Chemistry & Biochemistry, Georgia Institute of Technology, Atlanta, GA 30332-0400, USA.
Jan Tykvart, The Donnelly Centre for Cellular and Biomolecular Research, University of Toronto, Toronto, Ontario M5S 3E1, Canada.

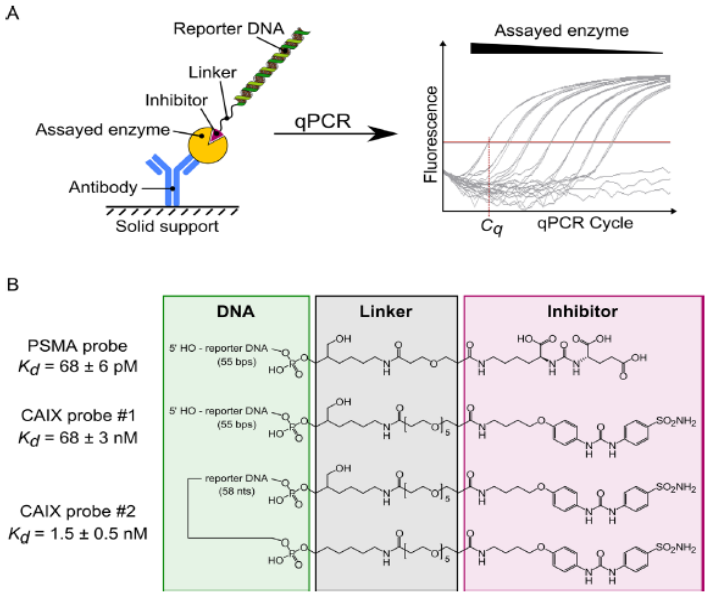

Figure 1. Schematic representation of enzyme detection using DIANA. (**A**) A covalent conjugate comprising an oligonucleotide (reporter DNA) and small-molecule competitive inhibitor of the target enzyme is used as a detection probe. The probe binds to the active site of the enzyme, which has been captured on the solid support by binding to the immobilized antibody. The amount of detection probe bound to the target enzyme is measured by quantitative PCR in terms of the threshold cycle (C_q), which is indirectly proportional to the logarithm of probe concentration. (**B**) Structures of the detection probes used for quantification of PSMA and CAIX. Each probe consists of reporter DNA (green box) covalently attached via a linker region (black box) to a competitive inhibitor of PSMA or CAIX (magenta box). The PSMA probe and CAIX probe #1 contain one copy of inhibitor linked to the 3′ end of the double-stranded reporter DNA, whereas CAIX probe #2 contains two copies of the inhibitor linked to both ends of the single-stranded reporter DNA. Probe affinities (K_d values) were determined by titrating each probe into wells containing the corresponding captured enzyme.

small-molecule inhibitors of those enzymes by assessing the ability of potential inhibitors to compete with the probe for binding to the active site. The sensitivity and selectivity of DIANA means that picogram amounts of unpurified target enzyme can be used, while the broad linear range means that inhibition constants (K_i) can be determined from single-well measurements, without the need for serial dilutions of inhibitor.

We demonstrate the sensitivity and selectivity of DIANA by targeting two clinically relevant enzymes: prostate-specific membrane antigen (PSMA), also known as glutamate carboxypeptidase II (GCPII) and carbonic anhydrase IX (CAIX). Both enzymes are homodimeric integral membrane proteins (10,11) and tumor-associated antigens (12–14) suitable for use in targeted drug delivery (15,16) and diagnostics (17–19). Their direct involvement in pathogenesis of several diseases makes them attractive targets for drug discovery (20–25), and indeed high-affinity competitive inhibitors of both enzymes have been identified by rational design (24,26,27). However, PSMA inhibitors bear multiple negative charges and show poor bioavailability (28,29), while CAIX inhibitors bear a sulfonamide head and act non-selectively (24,30). Therefore, identifying new inhibitor scaffolds is essential for further development of drugs targeting diseases related to these enzymes. We provide evidence that DIANA may be an efficient system not only for identifying leads against these and other target enzymes, but also for selective and sensitive detection of these target enzymes for possible diagnostic purposes.

MATERIALS AND METHODS

Materials

Buffers. Tris buffered saline (TBS): 20 mM Tris (Promega; H5135), 150 mM NaCl (Penta; 16610–31000), pH = 7.4; TBST: TBS with 0.05% Tween 20 (Affymetrix; 20605); TBST': TBS with 0.1% Tween 20; TBST'C: TBST' with 500-fold diluted casein blocker (0.01% final, SDT; CBC1); TBST'CS: TBST' with 500-fold diluted casein blocker (0.01% final) and 0.005% sodium dodecyl sulphate (SDS). HEPES: 100 mM HEPES (Sigma; H4034), 400 mM NaCl (Penta; 16610–31000), pH = 7.5; HEPESTC: HEPES with 0.01% Tween 20 and 500-fold diluted casein blocker (0.01% final); HEPEST'C: HEPES with 0.1% Tween 20 and 500-fold diluted casein blocker (0.01% final).

Detection probes. DNA oligonucleotide of the sequence CCT GCC AGT TGA GCA TTT TTA TCT GCC ACC TTC TCC ACC AGA CAA AAG CTG GAA A with 3′-terminally modified phosphate moiety by 6-amino-2-

(hydroxymethyl)hexyl group (Generi-Biotech, OPC purification) was reacted with NHS-esters of the small-molecule ligands of PSMA and CAIX to prepare the monovalent detection probes. The resulting conjugates were then annealed with equimolar amount of DNA oligonucleotide of complementary sequence CCA GCT TTT GTC TGG TGG AGA AGG TGG CAG ATA AAA ATG CTC AAC TGG CAG G (Generi Biotech, standard purification) prior to use. DNA oligonucleotide of the sequence AAA CCT GCC AGT TGA GCA TTT TTA TCT GCC ACC TTC TCC ACC AGA CAA AAG CTG GAA A containing the 3′-terminal 6-amino-2-(hydroxymethyl) hexyl phosphate modification and the 5′-terminal 6-aminohexyl phosphate modification (custom synthesis Generi-Biotech, OPC purification) was reacted with NHS-esters of the small-molecule ligand of CAIX to prepare the bivalent CAIX detection probe. See Supplementary Data for more details.

Proteins. The recombinant extracellular portion of human PSMA (rhPSMA) was expressed and purified as previously described (31) (designated as rhGCPII) and its molar concentration was determined by amino acid analysis using a Biochrom30 device (Biochrom) according to the manufacturer's instructions. The mass concentration was derived from the molar concentration, whereby the molecular weight of 88.7 kDa for rhPSMA was determined by MALDI-TOF. For long-term storage, purified rhPSMA diluted in TBST' was aliquoted, flash frozen in liquid nitrogen and kept at −80°C.

Human colon cancer cell line HT-29 endogenously expressing CAIX was used as a source of CAIX in DIANA experiments. Cells grown in Petri dishes at 37°C and 5% CO_2 in Dulbecco's modified Eagle's medium (Sigma; D5671) supplemented with 10% Fetal bovine serum (FBS, Sigma; F7524) and 4 mM glutamine to 100% confluency were harvested by resuspending in the medium, and then transferred to a microtube and pelleted at 300 *g* for 2 min and washed twice with TBS. Afterward, the supernatant was removed and cells were lyzed by resuspending in 50 mM Tris, 100 mM NaCl, pH 7.4, with 1% octaethylene glycol monododecyl ether ($C_{12}E_8$, Affymetrix; O330) and 2 h incubation on ice. The crude lysate was centrifuged at 600 *g* for 15 min at 4°C, and the supernatant was transferred to a new tube and centrifuged at 15 000 *g* for 15 min at 4°C. The resulting supernatant, hereafter referred to as the lysate, was transferred to a new tube. The total protein concentration in the lysate was determined using Bio-Rad Protein assay, and the amount of CAIX was determined using Quantikine ELISA for human CAIX (R&D Systems; DCA900) according to the manufacturer's instructions. The lysate was diluted in TBST' and kept in aliquots at −80°C for long-term storage.

Capture antibodies. Mouse monoclonal antibody 2G7, which selectively binds human PSMA (K_d ∼2.9 nM (32)), was prepared and purified as previously described (33). Purified mouse monoclonal antibody M75 selectively recognizing the PG domain of CAIX (34) (K_d ∼1.5 nM (35)), was a kind gift from Pavlína Řezáčová. For long-term storage, the antibodies were aliquoted in TBS or PBS, flash frozen in liquid nitrogen and kept at −80°C.

Blood samples. Samples were drawn from healthy volunteers, patients with histologically proven prostate carcinoma (PCa) or clear cell renal carcinoma (ccRCC) at Thomayer Hospital in Prague, with the agreement of the local ethical commission and with informed consent obtained from all subjects. See Supplementary Table S5 for a more detailed description of the individuals, including gender, age and diagnosis. In case of patients with diagnosed PCa or ccRCC, the blood samples were drawn in the morning before surgical removal of the tumor, i.e. radical prostatectomy, radical nephrectomy or partial nephrectomy. Blood was withdrawn into Vacuette® tubes (Greiner Bio-One) containing clot activator (# 456071; serum) or sodium citrate (# 456323; citrate plasma) and placed in the refrigerator. Within 8 h, tubes were centrifuged at 2000 *g* for 10 min with minimal deceleration and blood serum was transferred into a microtube and stored at −80°C until analysis. At the time of analysis, the serum samples were thawed on ice, mixed thoroughly and centrifuged at 5000 *g* for 15 min at 4°C to remove precipitate if formed.

Methods

General assay protocol. DIANA experiments were done according to this assay protocol. Any experimental conditions not described in this protocol, such as used buffers or used probe concentrations, as well as any divergences from this protocol, such as different incubation times, are described separately in sections describing particular experiments. To emphasize the possibilities of optimization of the duration of the protocol, we report both the incubation times employed in reported experiments and ranges of incubation times that were tested and did not influence the assay performance.

Capture antibody recognizing the protein of interest was immobilized onto the surface of wells of a FrameStar 480/96 multiwell plate (4titude; 4ti-0951) by applying 10 μl of the antibody in TBS at a concentration of 10 ng.μl^{-1} to the bottom of the wells and incubating for 60 min (range 30 to 120 min) at room temperature (RT). To avoid evaporation of the liquid in the wells, plates were covered during all incubations with general adhesive plate seals (4titude; 4ti-0510). The liquid was then tapped out, and the wells were washed three times with 200 μl TBS. Then, for PSMA detection, 100 μl casein blocking agent diluted 5-fold in TBS ('casein blocker biotin free 5.5% w/v'; SDT; CBC1) was applied to the bottom of the wells, while for CAIX detection 10 mg/ml BSA (Sigma; A7906) in TBS was applied. Plates were then incubated overnight (range 2 to 24 h) at RT. The liquid was tapped out again, and the wells were washed three times with 200 μl TBST. Thereafter, 10 μl of the sample containing analyte was applied to the bottom of the wells and incubated; during this step the target enzyme is being captured by the immobilized antibody. The samples were typically diluted in appropriate buffer containing 0.1% Tween 20, and the time of incubation was 2 h (range 1 to 21 h) at RT. The liquid was then tapped out, and the wells were washed three times with 200 μl TBST. Subsequently, 10 μl of detection probe diluted in appropriate buffer (typically containing 0.01 or 0.1% Tween 20 and 0.01% casein blocker to minimize non-selective binding of

the probe) was added to the bottom of wells, and samples were incubated for 45 min (range 15 to 120 min) at RT. The liquid was then tapped out again, and the wells were washed at least six times with 200 μl TBST. Finally, 10 μl of a qPCR reaction mixture composed of LC 480 Probes Master (Roche, cat. no. 04707494001; diluted to the final concentration recommended by the manufacturer), forward and reverse primer (CCA GCT TTT GTC TGG TGG AG and CCT GCC AGT TGA GCA TTT TT; final concentration 1 $\mu mol.l^{-1}$ each) and fluorescent hydrolysis probe #87 from the Roche Universal Probe Library (LNA octamer sequence CTG CCA CC, cat. no. 04689127001; final concentration 100 $nmol.l^{-1}$) was added and the plate was sealed with adhesive optical film (Roche, cat. no. 4729692001). The amount of detection probe was then quantified by qPCR: 3 min at 95°C; then 45 cycles of 10 s at 95°C, 30 s at 66°C and 30 s at 72°C; and finally 2 min at 37°C in a LightCycler 480 II qPCR instrument (Roche) with the excitation and emission filters adjusted to 465 nm and 510 nm respectively. . Threshold cycles (C_q) were obtained from the measured fluorescence curves using the method of maxima of the second derivative in the Light Cycler 480 II Software (Roche). Based on measurements with a dilution series of the PSMA detection probe in water as a template, the linear range of quantification of the probe extended from at least 6 copies to 6×10^8 copies of the probe per well with over 90% amplification efficiency.

Determination of the K_d values of the probes. K_d values were determined according to the general assay protocol by titrating captured enzymes with the appropriate detection probes. For the PSMA detection probe, 1 pg of rhPSMA diluted in 10 μl TBST' was captured onto immobilized antibody 2G7 in each well. Thereafter, different concentrations of the detection probe in TBST' were incubated with the captured rhPSMA. Resulting amounts of bound probe were then fitted using the GraFit v.5.0.11 (Erithacus Software Ltd.) with the function $[EP] = E_{tot} \times P_{tot}/(K_d + P_{tot})$, where [EP] is the amount of bound probe, P_{tot} is the analytical concentration of the probe during the incubation and E_{tot} is the amount of captured enzyme, while E_{tot} and K_d were parameters of the fit to be solved. The same procedure was repeated with the detection probe diluted in TBST' buffer with added casein blocker (TBST'C), or with added casein blocker and SDS (TBST'CS). Finally, the dissociation constant of the probe was determined in the same manner with PSMA captured from 1 μl serum diluted 10-fold in TBST' prior to capture (determined K_d values are listed in Supplementary Table S1).

For the monovalent CAIX detection probe, 0.78 ng of CAIX in HT-29 cell lysate (10 μg total protein) diluted in TBST' was captured onto immobilized M75 antibody in each well. Afterward, different concentrations of the probe in HEPEST'C were incubated with the captured CAIX and resulting amounts of bound probe were used to determine the K_d value in the same way as for PSMA. For the bivalent CAIX detection probe, only 0.078 ng of CAIX in HT-29 cell lysate (1 μg total protein) diluted in TBST' was captured onto immobilized M75 antibody, and subsequently, different concentrations of the probe in HEPEST'C were incubated with captured CAIX. The K_d value of the probe was also determined on captured endogenous CAIX from 1 μl serum diluted 10-fold in TBST' in the same manner (determined K_d values are listed in Supplementary Table S2).

Quantification of PSMA and CAIX in test matrices. Quantification followed the general assay protocol. In case of PSMA detection, serial dilutions of rhPSMA in TBST' were captured via immobilized antibody 2G7 and subsequently detected by PSMA detection probe diluted in TBST'CS to 50 pM concentration. In case of CAIX, serial dilutions of HT-29 cell lysate in TBST' were captured via immobilized antibody M75 and subsequently detected by bivalent CAIX detection probe diluted in HEPEST'C to 500 pM concentration.

Quantification of PSMA in serum samples. Quantification followed the general assay protocol with minor modifications. Known amounts of rhPSMA in TBST' were used as standards. Prior to analysis of the serum samples, 10% stock solution of Tween 20 was added to the samples to a final concentration of 0.1%. The samples were then diluted 10-fold in TBST' and added to the wells coated with the antibody 2G7. After overnight incubation (~21 h) and washing, the wells with standards were incubated with the PSMA detection probe in TBST'CS at a concentration of 100 pM, whereas the wells with serum samples were incubated with the PSMA probe at a concentration of 500 pM (to compensate for the different affinities of the probe toward the recombinant and endogenous proteins). The incubation of serum samples was much longer than incubations used with purified recombinant standards described in general assay protocol in order to minimize matrix effects seen in some samples when analyzing PSMA (non-linear assay response upon serum dilution in both DIANA and ELISA quantifications; see Supplementary Data). However, experiments with limited number of samples indicated that shorter incubation times within the ranges described in general assay protocol were possible without compromising the assay performance even when assaying complex biological matrices, such as blood serum, cell lysate or urine (data not shown).

The amount of PSMA in serum samples was computed by comparing the measured C_q to the standard curve, which was constructed as a linear regression fit of the plot of C_q values versus the logarithm of rhPSMA concentrations in standards (the standards covered the five-log range from 1 fg to 100 pg PSMA per well). To validate the obtained results, replicate wells with serum samples were incubated with the detection probe in the presence of 10 μM compound **16** ($K_i = 0.34 \pm 0.06$ nM as determined by enzyme kinetics), which was designed to completely disrupt the selective binding of the probe to PSMA but not the non-selective binding to the surface.

Quantification of CAIX in serum samples. Quantification followed the general assay protocol with minor modifications. Serial dilutions of HT-29 cell lysate in TBST' of known CAIX concentration (determined by Quantikine ELISA for human CAIX supplied by RnD Systems) were used as a standard. Undiluted serum samples to which 10% stock solution of Tween 20 was added to a final concentration of 0.1% were loaded into the wells coated with the an-

tibody M75. After overnight incubation (~21 h) and washing, wells were incubated with the bivalent CAIX detection probe in HEPEST'C at a concentration of 200 pM.

The amount of CAIX in serum samples was computed by comparing the measured C_q to the standard curve, which was constructed as a linear regression fit of the plot of C_q values versus logarithms of the CAIX concentrations in standards (the standards covered a five-log range from 7.8 fg to 780 pg CAIX per well). To validate the results, replicate wells with serum samples were incubated with the detection probe in the presence of 10 μM acetazolamide (K_i ~25 nM (36)), which was designed to completely disrupt the selective binding of the probe to CAIX but not the non-selective binding to the surface.

Evaluation of enzyme inhibitors. Evaluation of inhibitors followed the general assay protocol. For testing of PSMA inhibitors, 250 pg rhPSMA diluted in 10 μl TBST' was first incubated with immobilized capture antibody 2G7. Thereafter, a few wells were incubated with the PSMA detection probe diluted to 125 pM in TBST'C and the remaining wells were incubated with 125 pM probe in TBST'C in the presence of various tested compounds (listed in Supplementary Table S12) at 100 μM concentration. After extensive washing, the amount of bound probe in each well was quantified by qPCR and the ΔC_q values for each compound were computed as the difference between the C_q value in well(s) incubated with the particular compound and mean C_q value of wells incubated without any compound. The K_i values of the compounds were computed from their tested concentration and the corresponding ΔC_q values according to the equation $K_i = (2^{-\Delta Cq}/(1 - 2^{-\Delta Cq})) \times I_{tot}/(1 + (P_{tot}/K_d))$, where I_{tot} is the total concentration of the tested compound (100 μM), P_{tot} is the total concentration of probe (125 pM) and K_d is the dissociation constant of the probe (~125 pM). The K_i values of the same compounds toward PSMA naturally present in human serum were determined in the same manner, but PSMA from 1 μl of sera diluted 10-fold in TBST' (containing ~6 pg PSMA) was captured via immobilized antibody 2G7 in each well. Then, few wells were incubated with the PSMA detection probe diluted to 70 pM in TBST' (K_d ~200 pM) while the remaining wells were incubated with 70 pM probe in TBST' in the presence of tested compounds at either 100 nM or 100 μM concentration.

For testing of CAIX inhibitors, CAIX from HT-29 cell lysate diluted in TBST' (5 μg total protein containing 390 pg CAIX) was captured via immobilized antibody M75 in each well and a few wells were incubated with the bivalent detection probe diluted to 500 pM in HEPESTC with 10% DMSO, while the remaining wells were incubated with a mixture of 500 pM probe in the same buffer in the presence of various tested compounds (listed in Supplementary Table S17) at either 1 μM or 100 μM concentration. The K_i values of the compounds were computed from their tested concentrations and corresponding ΔC_q values according to the equation: $K_i = ((1 - 2 \times R_{aff})/(1 - R_{aff} - (R_{aff}^2 + (1 - 2 \times R_{aff}) \times 2^{-\Delta Cq})^{0.5}) - 1) \times I_{tot}/(1 + (P_{tot}/K_{d2}))$, where R_{aff} is the ratio of K_{d2} of the double-binding probe to K_{d1} of the single-binding probe ($R_{aff} = K_{d2}/K_{d1}$; K_{d1}~ 70 nM, K_{d2} ~ 1.5 nM; Supplementary Table S2). The K_i values of the same compounds toward CAIX naturally present in human serum were determined in the same manner, but CAIX from 10 μl of human serum (containing ~6 pg CAIX) with Tween 20 added to a concentration of 0.1% was captured via immobilized antibody M75 in each well. Then, few wells were incubated with the bivalent detection probe diluted to 180 pM in HEPESTC with 10% DMSO, while the remaining wells were incubated with the 180 pM probe in the same buffer in the presence of tested compounds at either 1 or 100 μM concentration.

PSMA enzymatic assay. The rate of hydrolysis of pteroyl-di-L-glutamate ($PteGlu_2$) in the presence of serial dilutions of various tested compounds was monitored by HPLC and was used to determine K_i values of the compounds toward PSMA. The procedure was carried out as previously described (37).

CAIX enzymatic assay. The rate of hydration of carbon dioxide in the presence of serial dilutions of compound **10** was monitored by detecting color changes of pH indicator and was used to determine the K_i value of the compound **10** toward CAIX. The procedure was carried out as previously described (38). The K_i values of carborane compounds were taken from ref. (38), and the K_i value of acetazolamide from ref. (36).

Quantification of PSMA by ELISA. ELISA was carried out as described previously (39) with some modifications. Briefly, 2G7 antibody was diluted to 5 ng/μl in 100 mM borate solution, pH 9.5 and 100 μl were loaded to each well of 96-well Maxisorp plate (Nunc, 437 111) and incubated for 1 h at RT. After washing with TBS (3 × 200 μl), the wells were blocked with 250 μl casein blocker (SDT; cat. no. CBC1) diluted 5-fold in TBS for 22 h at RT, followed by TBST wash (3 × 200 μl). Then, 100 μl of 10-fold diluted citrate plasma samples ($n = 34$) or serum samples when no citrate samples were available ($n = 2$) either in TBST' or in TBST' with 4.5 mM ethylenediaminetetraacetic acid (EDTA) were loaded to the wells, and the samples were incubated for 16 h at RT. As standard, rhPSMA (31) serially diluted in TBST' to concentrations ranging from 1 pg to 1 ng per well was used. After subsequent TBST wash (3 × 200 μl), 100 μl biotinylated mouse monoclonal antibody J591 (40) recognizing GCPII diluted in TBST' to 0.25 ng/μl was added and incubated for 1 h at RT. After washing out the unbound biotinylated J591 (3 × 200 μl TBST), 100 μl NeutrAvidin conjugated with horseradish peroxidase (Thermo Scientific) diluted in TBST' to 0.5 ng/μl was added and incubated for 30 min at RT, followed by a TBST wash (5 × 200 μl). Finally, chemiluminescence in 170 μl of luminol substrate (prepared by mixing 0.1 ml 1 M Tris–HCl, pH 8.8; 10 μl 250 mM luminol in DMSO; 22.2 μl 90 mM 4-iodophenol in DMSO and filled to 1 ml with distilled water; 0.6 μl of 30% H_2O_2 was added shortly before use) was measured on a Tecan Infinite M1000 instrument.

To control for false-positive signal due to the presence of heterophilic interfering antibodies, the samples were diluted in replicate wells in TBST' with 4.5 mM EDTA. The EDTA denatures PSMA, which leads to the loss of binding of the antibodies to PSMA. The remaining signal, if any, corresponds to the signal from interfering antibodies. The

PSMA concentration was therefore determined as the difference between wells with and without EDTA.

Statistical analysis. Two-tailed Mann Whitney U-test was used to compare mean PSMA and CAIX serum levels between the groups of individuals. The calculations were run in the past software (41). Because the expression of genes (and consequently also the serum levels) are considered to be log-normally distributed (42), median values and 16th and 84th percentiles for serum levels determined in the sample set were indicated (rather than mean values and standard deviations) to describe the scatter of the values. The non-parametric rank statistical test was chosen because we do not expect the values to be normally distributed. While the amount of available serum samples was limited, the sample size of 12 individuals in each group was chosen to provide reasonable power of the statistical test.

RESULTS

Preparation and characterization of detection probes

To prepare detection probe that binds to the target enzyme active site and allows quantification by qPCR (Figure 1A), we derivatized known competitive inhibitors of PSMA (43) and CAIX (24) to carry a linker bearing a terminal NHS-ester. These derivatives were then reacted with the primary amine group of custom-synthesized DNA oligonucleotides (see Figure 1B for structures and K_d values). Interestingly, attaching the oligonucleotide to the inhibitors improved their binding affinity several-fold (see Supplementary Data for more details on probe synthesis and testing). Because the affinity of the CAIX probe was three orders of magnitude lower than that of the PSMA probe, we conjugated two CAIX inhibitors to a single oligonucleotide, increasing overall affinity nearly 50-fold. This substantial increase may be because each inhibitor of a single probe can bind to one active site in the CAIX homodimer, as described previously for a bivalent small-molecule CAIX inhibitor (16). We used only this bivalent probe #2 in all CAIX experiments.

Quantification of PSMA and CAIX in test matrices

Quantification of PSMA and CAIX consisted of several steps. First, the capture antibody was immobilized onto the bottom of wells in a 96-well polypropylene PCR plate, and wells were then blocked with appropriate reagent. Next, sample was added to the wells, and target enzyme from the sample was selectively bound by the capture antibody. Then the appropriate detection probe was added and allowed to bind to the active site of the target enzyme. Finally, after extensive washing, the amount of bound probe was quantified by qPCR.

To assess the dynamic range and sensitivity of DIANA, we analyzed serial dilutions of enzyme standards diluted in buffered solution; the same standards were later used to quantify both targets in human sera. As a standard for PSMA quantification, we used purified recombinant human PSMA (rhPSMA). The linear range of detection extended over six orders of magnitude, from 3.6 zeptomoles to 3.6 femtomoles (320 ag to 320 pg) in a 10-μl sample. The lowest detected amount, defined as the amount of analyte that gave a signal higher than the blank signal plus two s.d., was 1.1 zeptomole (100 ag). The total range of detection thus extended over seven orders of magnitude from 1.1 zeptomole to 11 femtomoles (100 ag to 1 ng; Figure 2A and Supplementary Table S3). As a standard for CAIX quantification, we used lysate from cultured HT-29 cells; the CAIX concentration in the stock lysate was determined by Quantikine ELISA for human CAIX (RnD Systems). The linear range of detection extended over five orders of magnitude from 140 zeptomoles to 14 femtomoles (7.8 fg to 780 pg) in a 10-μl sample. The lowest detected amount was 46 zeptomoles (2.5 fg), corresponding to a total range of detection over five orders of magnitude from 46 zeptomoles to 14 femtomoles (2.5 fg to 780 pg; Figure 2B and Supplementary Table S4).

Quantification of PSMA and CAIX in human serum

After establishing DIANA performance against target enzymes using purified enzyme or cell lysate, we examined its performance against clinical samples of human serum from 12 healthy men, 12 men with Prostate carcinoma (PCa) and 10 men and 2 women with clear cell renal cell carcinoma (ccRCC). Undiluted samples were assayed for CAIX, while samples were diluted 10-fold before assaying PSMA (for details on testing of the assay linearity and on the recovery of spiked protein standards see Supplementary Data). Thus, the serum volumes used per well were 1 μl for PSMA and 10 μl for CAIX.

Measured PSMA concentrations in serum ranged from 0.10 to 6.0 ng/ml, with a median value of 0.45 ng/ml (16th and 84th percentiles were 0.23 and 1.1 ng/ml, respectively; Supplementary Table S9). Mean concentration did not differ significantly among the three groups, suggesting that serum PSMA is not elevated in either ccRCC or PCa (Supplementary Figure S1a). This contrasts with a previous report of elevated PSMA protein levels in serum from PCa patients as determined by semiquantitative SELDI assay (17). Measured CAIX concentrations ranged from 0.034 to 0.61 ng/ml, with a median value of 0.12 ng/ml (16th and 84th percentiles were 0.059 and 0.25 ng/ml, respectively; Supplementary Table S10). Mean CAIX concentration was significantly lower in healthy individuals than in patients with ccRCC (two tailed Mann-Whitney test, $P = 0.033$) or PCa ($P = 0.021$; Supplementary Figure S1b). This is the first report showing the elevated level of CAIX in patients with prostate cancer. The elevated level of CAIX in serum of ccRCC patients is in line with previous reports (18,19).

To further validate the serum levels obtained by DIANA, we reanalyzed the samples by sandwich ELISA. We are not aware of any commercially available ELISA validated for quantification of PSMA in blood serum or plasma, so we used our previously reported ELISA protocol (39) with some modifications. We used this ELISA to determine PSMA concentrations in control citrate plasma samples drawn from the same individuals on the same occasion as samples used in DIANA determinations. PSMA concentrations determined by ELISA showed excellent agreement with values obtained by DIANA ($R^2 = 0.898$; Figure 2C). Similarly, we validated CAIX concentrations by reanalyzing the serum samples with a commercially available Quan-

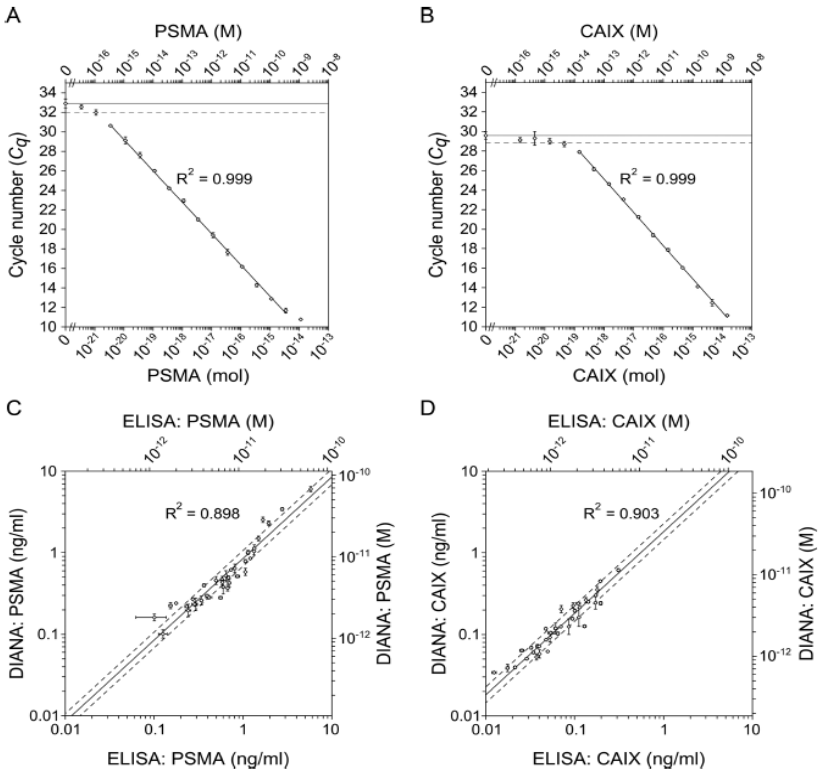

Figure 2. Ultrasensitive detection of PSMA and CAIX by DIANA. (**A** and **B**) Plots of average C_q values versus amount of human recombinant purified PSMA standard diluted in buffered solution (A), or average C_q values versus amount of human CAIX present in HT-29 cell lysate diluted in buffered solution (**B**). Upper x-axes indicate molar concentration, while lower x-axes indicate the corresponding molar amount per well. Horizontal lines show the average background signal; dashed horizontal lines show the average background signal plus 2 s.d. Error bars show s.d. of quadruplicate measurements (A and B). (**C** and **D**) Plots of concentrations of PSMA (C) and CAIX (D) determined using DIANA in 36 human serum samples versus concentrations determined using ELISA in the same serum samples (CAIX) or in control citrate plasma samples (PSMA) drawn from the same individuals on the same occasion.Lines show the linear regression fit of log-transformed concentrations; dashed lines indicate values 1.25-fold higher or lower than the linear regression. Error bars show s.d. of triplicate (C) or duplicate (D) measurements.

tikine ELISA for human CAIX and CAIX concentrations determined by both methods showed excellent agreement ($R^2 = 0.903$; Figure 2D). Reference ELISA thus confirmed the accuracy of serum levels of both enzymes determined by DIANA, and it corroborated our observations of PSMA and CAIX levels in clinical samples.

Next, we used the serum samples to examine the sensitivity and selectivity of DIANA by attempting to outcompete the binding of the detection probe using known competitive inhibitors of the target enzymes. We hypothesized that these inhibitors would quantitatively outcompete the selective binding of the probe to the target enzyme, without affecting possible non-selective binding of the probe to other proteins. Therefore, we reasoned that PSMA or CAIX concentrations determined in wells containing a suitable concentration of competitive inhibitor should provide an estimate of the limit of detection, reflecting non-selective binding of the probe. In this manner, we estimated the average limit of detection of PSMA in a 1-μl serum sample to be 0.8 pg/ml (range 0.4 to 2.4 pg/ml; Supplementary Table S9) and of CAIX in a 10-μl serum sample to be 1.1 pg/ml (range 0.7 to 2.8 pg/ml; Supplementary Table S10). These detection limits were much lower than the actual enzyme concentrations in the set of clinical samples analyzed; the limits for PSMA were on average 870-fold lower than the actual PSMA concentration (range 140- to 2800-fold), while the limits for CAIX were on average 210-fold lower than the actual CAIX concentrations (range 12- to 930-fold).

Using DIANA to evaluate inhibitors of target enzymes

Determination of inhibitor binding affinities (expressed as K_i values) followed the same general protocol as enzyme quantification, with slight modifications (Figure 3A). An identical amount of target enzyme was captured onto the

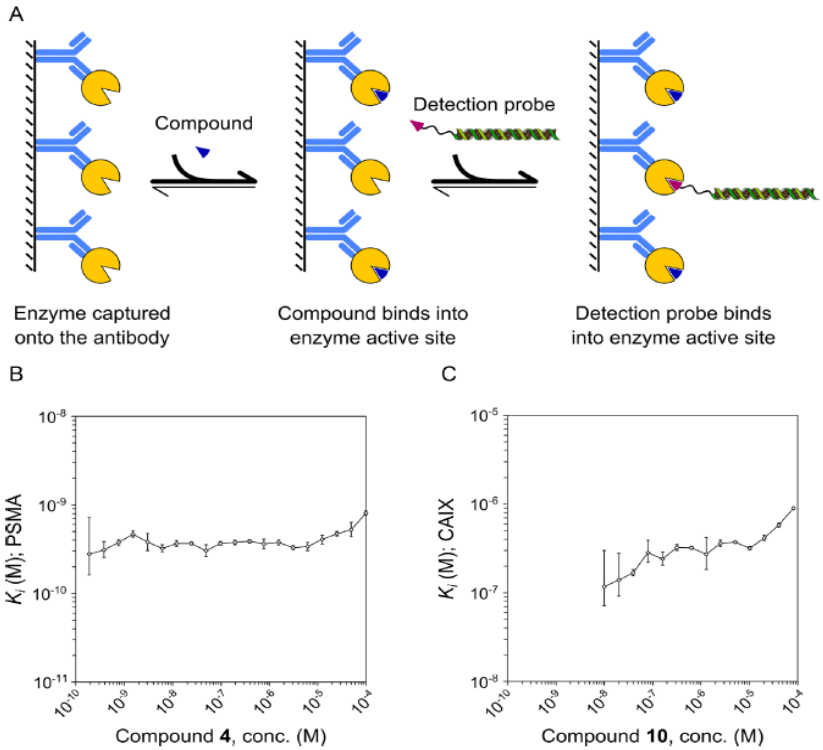

Figure 3. Determination of inhibition constants from single inhibitor concentrations by DIANA and its validation by inhibitor titration. (**A**) Detection probe was incubated with target enzyme in the presence of putative inhibitor. The binding of the test compound resulted in lower amount of the bound probe. The amount of bound probe together with concentration of compound was then used to determine the inhibition constant at each dilution of the compound. (**B**) Purified PSMA standard was titrated with PSMA inhibitor (compound **4**) and detected using the monovalent detection probe against PSMA. Measured inhibition constants were constant over more than five orders of magnitude of inhibitor concentration. (**C**) CAIX from cell lysate was titrated with CAIX inhibitor (compound **10**) and detected using the bivalent detection probe against CAIX. Measured inhibition constants were constant over more than two orders of magnitude. The lowest inhibitor concentrations were lower than their respective K_i values, which leads to insufficient inhibition and therefore larger errors of determinations. K_i values determined at the highest inhibitor concentrations are higher than the average because of background signal. Error bars show s.d. of triplicate (**B**) or duplicate (**C**) measurements.

immobilized antibody in each well; this amount was within the linear range of detection. Some wells were incubated with detection probe alone, and the rest were incubated with a mixture of the probe and a known concentration of putative inhibitor, present in molar excess with respect to the enzyme. Inhibitor affinity (K_i value) was calculated from the inhibitor concentration and from the difference in the number of PCR cycles needed to amplify the reporter DNA (ΔC_q) in wells incubated in the presence or absence of inhibitor. Given the broad linear range of the assay, we were able to calculate the K_i value for each inhibitor from each well after assuming that the monovalent PSMA probe bound non-cooperatively to its target, while the bivalent CAIX probe bound cooperatively (see Supplementary Data for more details). These calculations are presented in detail in the next two sections.

Evaluation of PSMA inhibitors

To examine the accuracy of our model to determine K_i values of PSMA inhibitors using single inhibitor concentrations (Supplementary Figure S2a), we incubated captured rhPSMA with serial dilutions of competitive inhibitor (compound **4**; $K_i = 1.1 \pm 0.1$ nM based on enzyme kinetics) ranging from 100 pM to 100 μM. Then we determined the K_i from each measured data point (Supplementary Table S13). Measured K_i values were constant over the entire dilution series except at the extremes (Figure 3B); mean K_i calculated over the range from 200 pM to 50 μM was 0.37 ± 0.06 nM. This indicates that DIANA can accurately determine K_i values from single concentrations of small-molecule inhibitors over the broad linear range of the assay, covering six orders of magnitude in the case of PSMA.

To further verify this, we determined K_i values of 41 known competitive inhibitors of PSMA (listed in Sup-

plementary Table S12) using single-well measurements at a constant inhibitor concentration (100 μM). We then compared DIANA-determined values with those using an HPLC-based substrate cleavage assay (37) which requires testing serial dilutions of inhibitors (see Figure 4A). The two methods showed excellent agreement ($R^2 = 0.991$) over the entire range of K_i determinations covering seven orders of magnitude from mid-picomolar to mid-micromolar values (Supplementary Table S15). This confirms that DIANA can accurately measure K_i values from a single inhibitor concentration.

The high selectivity and sensitivity of DIANA allowed us to determine K_i values for the 41 known PSMA inhibitors using only 1 μl of human serum (containing ∼6 pg of PSMA) rather than purified rhPSMA. Because of the low amount of PSMA present, we tested inhibitor concentrations of 100 μM and 100 nM in order to cover the range of K_i values. The values measured in this way agreed well with those determined using rhPSMA (Figure 4B), over the entire range of K_i values ($R^2 = 0.989$; Supplementary Table S16).

To evaluate the robustness of DIANA, we examined the standard deviations of the assay and evaluated its response to different buffer compositions and solvents. Standard errors in the presence or absence of inhibitors were typically lower than 0.15, corresponding to a CV of 11%. Together with signal-to-background ratios of up to 22 qPCR cycles, these standard errors translated into a Z' factor of over 0.9. Such Z' values were obtained not only when assaying purified PSMA standard but also when assaying PSMA in human serum. The expected precision of the determined K_i values is shown in Supplementary Figure S2a. We found no significant variation in the signal-to-background ratio when we screened different concentrations of detergent, casein blocker or, most notably, organic solvents such as methanol, acetonitrile and DMSO at concentrations of up to 10%. These findings suggest that DIANA can serve as a highly versatile screening platform for testing small-molecule libraries dissolved in 100% DMSO (Supplementary Table S14).

To explore the possibility of omitting the capture antibody, which would expand the assay to include target enzymes for which specific antibodies are unavailable, we tested a panel of PSMA inhibitors against recombinant biotinylated PSMA captured on neutravidin. This led to nearly identical results as using untagged PSMA captured by an immobilized antibody (Supplementary Figure S3). Since the detection probe also binds the PSMA homolog GCPIII (44) (with K_d of ∼5 nM), we tested a subset of these PSMA inhibitors against recombinant biotinylated GCPIII captured on neutravidin and obtained K_i values corresponding to those obtained by conventional enzyme kinetics assays (Supplementary Figure S4; experimental details on assaying both proteins are described in Supplementary Data). The binding of the probe to both enzymes together with capturing of their tagged variants onto neutravidin thus enabled us to rapidly develop screening assay for both targets, but such promiscuity also may have compromised the selectivity of the PSMA detection in biological matrices. To examine the selectivity of the DIANA protocol which employs an immobilized anti-PSMA antibody 2G7 and which we used previously to quantify untagged PSMA, we assayed different amounts of GCPIII using this protocol. We found that the presence of GCPIII did not interfere with PSMA quantification even at very high concentrations (Supplementary Table S22). The selectivity ratio toward PSMA was more than six orders of magnitude, which suggests that using a highly selective capture antibody ensures detection of only the desired target, even when the probe can bind other proteins in the sample.

Evaluation of CAIX inhibitors

Determination of K_i values was more complex for CAIX inhibitors than for PSMA inhibitors because we used the bivalent probe against CAIX, which presumably binds cooperatively to the target. Therefore we altered the model for calculating K_i values (Supplementary Figure S2b). To test the accuracy of the model, we incubated CAIX captured from a lysate of HT-29 cells with serial dilutions of a competitive CAIX inhibitor (compound **10**; $K_i = 408 \pm 64$ nM based on enzyme kinetics) ranging from 0.6 nM to 80 μM, and we determined the K_i from each measured data point (Supplementary Table S18). We obtained a mean K_i of 323 ± 54 nM over a range of inhibitor concentrations spanning more than two orders of magnitude, from 80 nM to 20 μM. This validated our assumption that the detection probe binds CAIX cooperatively (Figure 3C).

This inhibitor concentration range over two orders of magnitude useful for determining K_i from single measurements is narrower than the concentration range giving a linear response for CAIX quantification. This result reflects (1) relatively low endogenous expression of CAIX by HT-29 cells, (2) higher non-selective binding of probe after CAIX capture from lysate versus capture from buffer or serum and (3) bivalence of the CAIX probe, which leads to a larger change in C_q with increasing inhibitor concentration than would be observed with a monovalent probe. These factors narrow the range of determined K_i values, but the last factor at the same increase precision and therefore sensitivity, which may make DIANA useful for identifying weak inhibitors (Supplementary Figure S2b).

Using our validated model for calculating K_i, we determined the K_i values of 10 CAIX inhibitors (listed in Supplementary Table S17) by incubating the inhibitors at 1 μM and 100 μM with CAIX captured from cell lysate in the presence of 10% DMSO, which was necessary because of the low solubility of some inhibitors. We compared these values with those determined from enzyme kinetics (38) (Supplementary Table S19) and found good agreement ($R^2 = 0.816$, Figure 4C) over the entire range of K_i values covering three orders of magnitude from mid-nanomolar to mid-micromolar values. We assumed that the solvent did not influence our results, since we found that DMSO at final concentrations up to 10% did not affect selective or non-selective binding of the detection probe.

Finally, we determined K_i values using 10 μl human serum (containing approximately 6 pg of CAIX) and inhibitor concentrations of 1 μM and 100 μM in the presence of 10% DMSO. The resulting K_i values agreed well with those obtained previously using CAIX from cell lysate ($R^2 = 0.888$, Figure 4D). Despite the very small amount of

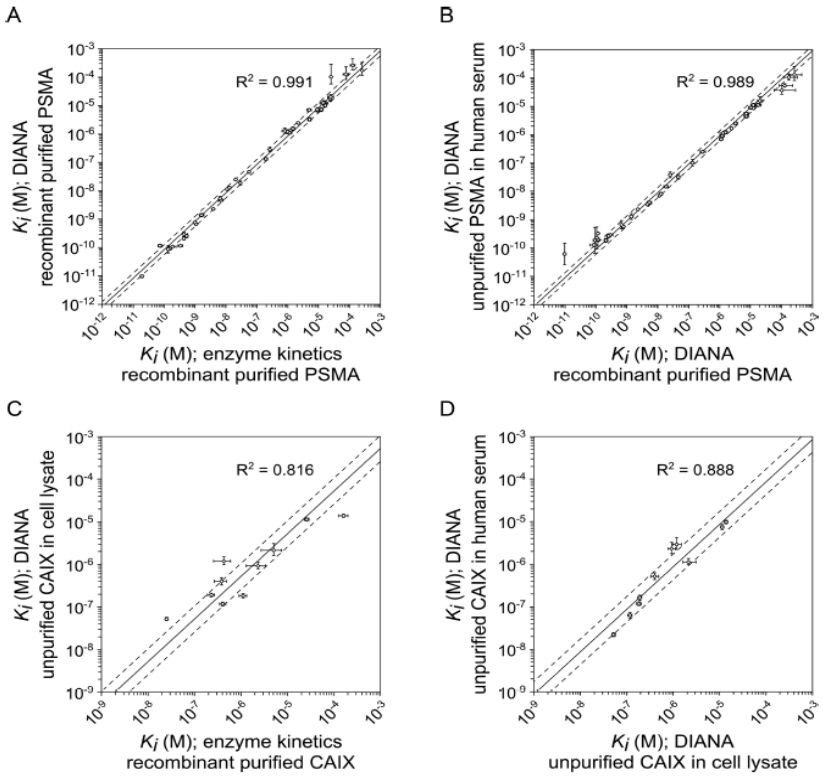

Figure 4. Validation of single-well determination of inhibition constants of PSMA and CAIX inhibitors using DIANA. (**A**) Plot of K_i values of 41 PSMA inhibitors determined by titrating recombinant purified PSMA with inhibitor and measuring kinetics (x-axis) versus K_i values determined by DIANA from a single well containing 100 μM inhibitor and recombinant purified PSMA (y-axis). (**B**) Plot of K_i values of 41 PSMA inhibitors determined by DIANA from a single well containing 100 μM inhibitor with recombinant purified PSMA (x-axis) versus K_i values determined by DIANA from two measurements with unpurified endogenous PSMA in 1 μl of human serum in the presence of either 100 μM or 100 nM inhibitor (y-axis). (**C**) Plot of K_i values of 10 CAIX inhibitors determined by titrating recombinant purified CAIX with inhibitor and measuring kinetics (x-axis) versus K_i values determined by DIANA from two measurements with unpurified CAIX in cell lysate in the presence of either 100 μM or 1 μM inhibitor (y-axis). (**D**) Plot of K_i values of 10 CAIX inhibitors determined by DIANA from two measurements with unpurified CAIX in cell lysate in the presence of either 100 μM or 1 μM inhibitor (x-axis) and by DIANA from two measurements with unpurified endogenous CAIX in 10 μl of human serum in the presence of either 100 μM or 1 μM inhibitor (y-axis). (A–D) Lines show linear regression of log-transformed values; dashed lines indicate values that are 1.5-fold (PSMA) or 2-fold (CAIX) higher or lower than the linear fit. Error bars show s.d. of duplicate measurements in the case of DIANA, or s.e. of the titration in the case of enzyme kinetics.

CAIX in cell lysate and human serum, Z' values were reproducibly higher than 0.8. These results confirm the applicability of the assay to screen enzyme inhibitors with low-abundance enzymes in different biological matrices.

DISCUSSION

Here, we report the development of DIANA assay suitable for enzyme detection and screening of enzyme inhibitors. This assay is analogous to the immuno-PCR assay described in (3), in which the target protein is captured by an immobilized antibody and then detected by another DNA-linked antibody. However, in DIANA assay, the DNA-linked antibody has been replaced by detection probe consisting of a DNA oligonucleotide covalently linked to a small molecule that binds to the active site of a target enzyme. The use of conjugates of DNA and small molecules as affinity reagents has been proposed more than 20 years ago (45) and they have been since then employed in a number of contexts. Nevertheless, we show that DIANA represents a novel and powerful way of using such conjugates with some important implications which are discussed in following paragraphs.

We show that DIANA is a straightforward and extremely sensitive method for quantifying enzymes suitable for complex biological matrices. We estimated the limits of detection for two integral membrane proteins, PSMA and CAIX, in human sera to be, respectively, 10×10^{-21} mol and 200×10^{-21} mol. Such sensitivity is comparable to that of the most sensitive sandwich immunoassays available for complex bi-

ological matrices, including sandwich ELISA (10×10^{-18} mol; e.g. Abbott Architect total PSA kit, IVD Ref. 7K70), immuno-PCR (3) (100×10^{-21} mol), immuno-PCR on gold nanoparticles (Bio-Barcode assay (4); 300×10^{-21} mol), proximity ligation assay (5) (1×10^{-21} mol), and proximity extension assay (6) (100×10^{-21} mol). Additionally, DIANA is advantageous when assaying clinical samples: the synthetic nature of the detection probe means that the DIANA sandwich cannot be cross-linked by interfering antibodies present in human blood, which occasionally cause false-positive results in sandwich immunoassays (46,47).

The amount of target enzyme is quantified via quantitative PCR (qPCR), which has broad linear range and is extremely sensitive. This is achieved by geometrical amplification of the template DNA during PCR cycles. However, this is connected with slightly lower precision than by other linear readouts, such as colorimetric or chemiluminiscent detection. Depending on the amount of template, a typical qPCR machine has standard deviation of 0.10–0.25 cycle, which translates into coefficient of variation of 7–19% compared to few percent achieved in ELISA readout. Although such precision should be sufficient for most diagnostic tests, we suggest that in cases when small changes in enzyme levels need to be detected, either replicates could be run or other more precise DNA detection techniques could be employed, such as isothermal rolling circle amplification (48) or commercially available digital PCR.

The binding of the detection probe to the enzyme active site, the extremely high sensitivity and wide linear range of DIANA also make it well-suited for screening of competitive inhibitors of target enzymes. The sensitivity enables testing of inhibitors using tiny amounts of unpurified targets, and the wide range enables determination of K_i from a single well, minimizing the amount of reagents required. DIANA can identify both tight and weak inhibitors. The highest inhibitor affinity that can be accurately determined is limited by the assay sensitivity and therefore lies approximately in the K_i range of five to six orders of magnitude below the K_d of the probe. DIANA also correctly identifies inhibitors that bind even more tightly and ranks them as the most tightly binding in the screen, though it underestimates their affinities. The ability of DIANA to identify weak inhibitors is limited only by their solubility; thus, every inhibitor at a concentration at or above its K_i should be detectable in principle. Target binding by the detection probe does not compete with target binding by weak inhibitors, since the probe is used at concentrations below its K_d regardless of the magnitude of the K_d, which is made possible by ultrasensitive qPCR detection. Indeed, in the present study, we detected PSMA inhibitors with an affinity 10^6-fold lower than that of the detection probe, even when the inhibitor was present at a concentration similar to or lower than its K_i. The solid-phase assay format also allows testing of fluorescent or colored compounds, since they are washed out before analysis and therefore cannot interfere with the qPCR readout.

As with other ultrasensitive solid-phase assays, the sensitivity of DIANA is limited by non-selective adsorption of the detection probe, since every single probe molecule bound to the surface, including those that are non-selectively adsorbed, is detected by qPCR. In our hands, this non-selective background binding was low but detectable even at subnanomolar probe concentrations and in the presence of casein blocker and it increased with increasing probe concentration. This implies that a high-affinity ligand is essential for ultrasensitivity as lower probe affinity cannot be compensated for by increasing probe concentration.

We showed that a probe with subnanomolar affinity enabled detection of zeptomole amounts of PSMA. However, such potent ligands have been identified for a limited number of targets. As we showed here for CAIX, tight-binding probes can be prepared from weaker ligands by including several copies of the ligand moiety in order to induce multiple binding of the probe, though this strategy is likely to work only for multimeric enzymes and/or enzymes bearing at least two distinct active sites. Otherwise, the sensitivity will decrease in proportion to the decreasing affinity of the ligand, which may limit the use of weaker ligands for DIANA-based diagnostics. However, these ligands may still be useful for DIANA-based inhibitor screening, since in this case the assay's linear range is more important than its sensitivity. While loss of sensitivity also means loss of dynamic range, the range may be partially restored by capturing larger amounts of target enzyme. We therefore predict that even ligands that bind with micromolar affinity may be useful for DIANA-based inhibitor screening, offering linear response over several orders of magnitude.

The ability to use subnanomolar concentrations of probe without losing sensitivity or dynamic range, regardless of probe affinity, means that extremely small amounts of probe are needed. As nanomole amounts of probe are easily synthesized from milligram amounts of ligand, preparing sufficient probe for billions of measurements is straightforward. Since the probe is stable to multiple freeze-thaw cycles, we expect that a single probe synthesis will yield enough material for any size of project, facilitating replication studies, reagent sharing and long-term archiving. We obtained similar assay performance in evaluating enzyme inhibitors when we captured PSMA via an immobilized antibody as when we omitted the antibody and instead captured recombinant biotinylated PSMA onto neutravidin. This shows that DIANA can be adapted to screen inhibitors of target enzymes for which specific antibodies are unavailable; in these cases, immobilization can be achieved by derivatizing the surface to bind an affinity tag recombinantly fused to the target enzyme, i.e. biotin or his-tag. This eliminates the need for antibody while still allowing unpurified target to be used. This approach will enable rapid development of platforms for testing compounds against panels of enzymes and quantitative evaluation of their selectivity, which will be facilitated by the use of detection probes prepared from class-specific inhibitors, such as pepstatin (49), staurosporin (50) or acetazolamide (30), together with production and capture of tagged enzymes.

Detection probes prepared from promiscuous inhibitors are still useful for detection of enzymes in complex biological matrices, in such cases a selective antibody is used for capturing of the enzyme which complements the assay selectivity. By testing recombinant purified enzyme standards, we showed that in combination with suitable antibody we selectively detected PSMA over its closest homolog

GCPIII even when using detection probe binding to both targets. Selectivity ratio of at least six orders of magnitude was achieved, even though the selectivity ratio of the probe itself was only about 60-fold. Moreover, despite both proteins share approximately 70% amino acid sequence identity without any dissimilar regions, there is a number of selective anti-PSMA antibodies available (32). This shows that it is possible to develop selective DIANA assay even for highly similar enzymes for which a selective inhibitor is not available. Similarly, we used probe prepared from non-selective inhibitor of several human carbonic anhydrases (24) for CAIX detection. There are 15 human carbonic anhydrases and 12 of them are enzymatically active and many potent yet non-selective inhibitors are known, while the development of selective inhibitors still remain challenge of current medicinal chemistry (30). Nevertheless, the low sequence homology between the carbonic anhydrases allowed us to use anti-CAIX antibody M75 which recognizes the proteoglycan-like domain of CAIX (34) absent from any other human carbonic anhydrase. The selectivity of resulting DIANA sandwich was validated by the excellent agreement of CAIX serum levels detected using DIANA and values determined using the commercial CAIX ELISA (Quantikine, R&D Systems), which has been tested by the vendor for selectivity against all other human carbonic anhydrases.

In principle, DIANA is not limited to enzymes and could be applied to any functional protein, including receptors or transporters, for which a sufficiently potent small-molecule ligand is available. Additionally, because DIANA does not require purified target, it may be especially advantageous for transmembrane proteins and other proteins that are difficult to prepare and purify. Moreover, the unique ability of DIANA to determine the compound's K_i from a single tested concentration might be especially useful for high-throughput inhibitor screening or for profiling inhibitor selectivity against a panel of enzymes. Finally, DIANA's simple and straightforward protocol, similar to that of sandwich ELISA or immuno-PCR, and its compatibility with multiwell plates, make it suitable for automation and high throughput.

SUPPLEMENTARY DATA

Supplementary Data are available at NAR Online.

ACKNOWLEDGEMENTS

We acknowledge Pavlína Řezáčová for generously providing the CAIX inhibitors, the HT-29 cell line and M75 antibody; Klára Pospíšilová for determining the reference K_i value of compound **10**; Neil Bander for generously providing the J591 antibody; Josef Lazar and Barbora Vorlová for critical reading of the manuscript; and Radko Souček and Jana Starková for excellent technical support.

Author contributions. V.N., P.Š. and J.K. conceived the project; V.N., P.Š., J.S. and J.K. designed the experiments; V.N., J.S., J.T., T.K., P.M. and V.V. performed the experiments; V.N., P.Š. and J.K. analyzed the data; V.N. and J.K. wrote the manuscript; and all authors contributed to the editing of the manuscript.

FUNDING

Ministry of Education of the Czech Republic [NPU I project LO 1302]. Funding for open access charge: Ministry of Education of the Czech Republic [NPU I project LO 1302].

Conflict of interest statement. V.N., J.S., P.M., J.K. and P.Š have filed an international patent application (PCT/CZ2015/000084), which is owned by the Institute of Organic Chemistry and Biochemistry of the Academy of Sciences of the Czech Republic.

REFERENCES

1. Engvall,E. and Perlmann,P. (1971) Enzyme-linked immunosorbent assay (Elisa) quantitative assay of immunoglobulin-G. *Immunochemistry*, **8**, 871–874.
2. Lequin,R.M. (2005) Enzyme immunoassay (EIA)/Enzyme-linked immunosorbent assay (ELISA). *Clin. Chem.*, **51**, 2415–2418.
3. Hendrickson,E.R., Truby,T.M., Joerger,R.D., Majarian,W.R. and Ebersole,R.C. (1995) High sensitivity multianalyte immunoassay using covalent DNA-labeled antibodies and polymerase chain reaction. *Nucleic Acids Res.*, **23**, 522–529.
4. Thaxton,C.S., Elghanian,R., Thomas,A.D., Stoeva,S.I., Lee,J.S., Smith,N.D., Schaeffer,A.J., Klocker,H., Horninger,W., Bartsch,G. *et al.* (2009) Nanoparticle-based bio-barcode assay redefines 'undetectable' PSA and biochemical recurrence after radical prostatectomy. *Proc. Natl. Acad. Sci. U.S.A.*, **106**, 18437–18442.
5. Fredriksson,S., Dixon,W., Ji,H., Koong,A.C., Mindrinos,M. and Davis,R.W. (2007) Multiplexed protein detection by proximity ligation for cancer biomarker validation. *Nat. Methods*, **4**, 327–329.
6. Lundberg,M., Eriksson,A., Tran,B., Assarsson,E. and Fredriksson,S. (2011) Homogeneous antibody-based proximity extension assays provide sensitive and specific detection of low-abundant proteins in human blood. *Nucleic Acids Res.*, **39**, e102.
7. Robertson,J.G. (2005) Mechanistic basis of enzyme-targeted drugs. *Biochemistry*, **44**, 5561–5571.
8. Hughes,J.P., Rees,S., Kalindjian,S.B. and Philpott,K.L. (2011) Principles of early drug discovery. *Brit. J. Pharmacol.*, **162**, 1239–1249.
9. Inglese,J., Johnson,R.L., Simeonov,A., Xia,M.H., Zheng,W., Austin,C.P. and Auld,D.S. (2007) High-throughput screening assays for the identification of chemical probes. *Nat. Chem. Biol.*, **3**, 466–479.
10. Mesters,J.R., Barinka,C., Li,W.X., Tsukamoto,T., Majer,P., Slusher,B.S., Konvalinka,J. and Hilgenfeld,R. (2006) Structure of glutamate carboxypeptidase II, a drug target in neuronal damage and prostate cancer. *EMBO J.*, **25**, 1375–1384.
11. Alterio,V., Hilvo,M., Di Fiore,A., Supuran,C.T., Pan,P.W., Parkkila,S., Scaloni,A., Pastorek,J., Pastorekova,S., Pedone,C. *et al.* (2009) Crystal structure of the catalytic domain of the tumor-associated human carbonic anhydrase IX. *Proc. Natl. Acad. Sci. U.S.A.*, **106**, 16233–16238.
12. Kinoshita,Y., Kuratsukuri,K., Landas,S., Imaida,K., Rovito,P.M., Wang,C.Y. and Haas,G.P. (2006) Expression of prostate-specific membrane antigen in normal and malignant human tissues. *World J. Surg.*, **30**, 628–636.
13. Wykoff,C.C., Beasley,N.J.P., Watson,P.H., Turner,K.J., Pastorek,J., Sibtain,A., Wilson,G.D., Turley,H., Talks,K.L., Maxwell,P.H. *et al.* (2000) Hypoxia-inducible expression of tumor-associated carbonic anhydrases. *Cancer Res.*, **60**, 7075–7083.
14. Zhou,G.X., Ireland,J., Rayman,P., Finke,J. and Zhou,M. (2010) Quantification of carbonic anhydrase IX expression in serum and tissue of renal cell carcinoma patients using enzyme-linked immunosorbent assay: prognostic and diagnostic potentials. *Urology*, **75**, 257–261.
15. Heck,M.M., Retz,M., D'Alessandria,C., Rauscher,I., Scheidhauer,K., Maurer,T., Storz,E., Janssen,F., Schottelius,M., Wester,H.J. *et al.* (2016) Systemic Radioligand Therapy with (177)Lu Labeled Prostate Specific Membrane Antigen Ligand for Imaging and Therapy in Patients with Metastatic Castration Resistant Prostate Cancer. *J. Urol.*, **196**, 382–391.

16. Krall,N., Pretto,F. and Neri,D. (2014) A bivalent small molecule-drug conjugate directed against carbonic anhydrase IX can elicit complete tumour regression in mice. *Chem. Sci.*, **5**, 3640–3644.
17. Xiao,Z., Adam,B.L., Cazares,L.H., Clements,M.A., Davis,J.W., Schellhammer,P.F., Dalmasso,E.A. and Wright,G.L. (2001) Quantitation of serum prostate-specific membrane antigen by a novel protein biochip immunoassay discriminates benign from malignant prostate disease. *Cancer Res.*, **61**, 6029–6033.
18. Zavada,J., Zavadova,Z., Zat'ovicova,M., Hyrsl,L. and Kawaciuk,I. (2003) Soluble form of carbonic anhydrase IX (CA IX) in the serum and urine of renal carcinoma patients. *Brit. J. Cancer*, **89**, 1067–1071.
19. Sim,S.H., Messenger,M.P., Gregory,W.M., Wind,T.C., Vasudev,N.S., Cartledge,J., Thompson,D., Selby,P.J. and Banks,R.E. (2012) Prognostic utility of pre-operative circulating osteopontin, carbonic anhydrase IX and CRP in renal cell carcinoma. *Brit. J. Cancer*, **107**, 1131–1137.
20. Slusher,B.S., Vornov,J.J., Thomas,A.G., Hurn,P.D., Harukuni,I., Bhardwaj,A., Traystman,R.J., Robinson,M.B., Britton,P., Lu,X.C.M. *et al.* (1999) Selective inhibition of NAALADase, which converts NAAG to glutamate, reduces ischemic brain injury. *Nat. Med.*, **5**, 1396–1402.
21. Bacich,D.J., Wozniak,K.M., Lu,X.C.M., O'Keefe,D.S., Callizot,N., Heston,W.D.W. and Slusher,B.S. (2005) Mice lacking glutamate carboxypeptidase II are protected from peripheral neuropathy and ischemic brain injury. *J. Neurochem.*, **95**, 314–323.
22. Olszewski,R.T., Bzdega,T. and Neale,J.H. (2012) mGluR3 and not mGluR2 receptors mediate the efficacy of NAAG peptidase inhibitor in validated model of schizophrenia. *Schizophr. Res.*, **136**, 160–161.
23. Chiche,J., Ilc,K., Laferriere,J., Trottier,E., Dayan,F., Mazure,N.M., Brahimi-Horn,M.C. and Pouyssegur,J. (2009) Hypoxia-inducible carbonic anhydrase IX and XII promote tumor cell growth by counteracting acidosis through the regulation of the intracellular pH. *Cancer Res.*, **69**, 358–368.
24. Pacchiano,F., Carta,F., McDonald,P.C., Lou,Y.M., Vullo,D., Scozzafava,A., Dedhar,S. and Supuran,C.T. (2011) Ureido-substituted benzenesulfonamides potently inhibit carbonic anhydrase IX and show antimetastatic activity in a model of breast cancer metastasis. *J. Med. Chem.*, **54**, 1896–1902.
25. Lou,Y.M., McDonald,P.C., Oloumi,A., Chia,S., Ostlund,C., Ahmadi,A., Kyle,A., Keller,U.A.D., Leung,S., Huntsman,D. *et al.* (2011) Targeting tumor hypoxia: suppression of breast tumor growth and metastasis by novel carbonic anhydrase IX inhibitors. *Cancer Res.*, **71**, 3364–3376.
26. Jackson,P.F., Cole,D.C., Slusher,B.S., Stetz,S.L., Ross,L.E., Donzanti,B.A. and Trainor,D.A. (1996) Design, synthesis, and biological activity of a potent inhibitor of the neuropeptidase N-acetylated alpha-linked acidic dipeptidase. *J. Med. Chem.*, **39**, 619–622.
27. Kozikowski,A.P., Nan,F., Conti,P., Zhang,J.H., Ramadan,E., Bzdega,T., Wroblewska,B., Neale,J.H., Pshenichkin,S. and Wroblewski,J.T. (2001) Design of remarkably simple, yet potent urea-based inhibitors of glutamate carboxypeptidase II (NAALADase). *J. Med. Chem.*, **44**, 298–301.
28. van der Post,J.P., de Visser,S.J., de Kam,M.L., Woelfler,M., Hilt,D.C., Vornov,J., Burak,E.S., Bortey,E., Slusher,B.S., Limsakun,T. *et al.* (2005) The central nervous system effects, pharmacokinetics and safety of the NAALADase-inhibitor GPI 5693. *Brit. J. Clin. Pharmacol.*, **60**, 128–136.
29. Rais,R., Wozniak,K., Wu,Y., Niwa,M., Stathis,M., Alt,J., Giroux,M., Sawa,A., Rojas,C. and Slusher,B.S. (2015) Selective CNS uptake of the GCP-II inhibitor 2-PMPA following intranasal administration. *PLoS One*, **10**, e0131861.
30. Supuran,C.T. (2008) Carbonic anhydrases: novel therapeutic applications for inhibitors and activators. *Nat. Rev. Drug Discov.*, **7**, 168–181.
31. Barinka,C., Rinnova,M., Sacha,P., Rojas,C., Majer,P., Slusher,B.S. and Konvalinka,J. (2002) Substrate specificity, inhibition and enzymological analysis of recombinant human glutamate carboxypeptidase II. *J. Neurochem.*, **80**, 477–487.
32. Tykvart,J., Navratil,V., Sedlak,F., Corey,E., Colombatti,M., Fracasso,G., Koukolik,F., Barinka,C., Sacha,P. and Konvalinka,J. (2014) Comparative analysis of monoclonal antibodies against prostate-specific membrane antigen (PSMA). *Prostate*, **74**, 1674–1690.
33. Knedlik,T., Navratil,V., Vik,V., Pacik,D., Sacha,P. and Konvalinka,J. (2014) Detection and quantitation of glutamate carboxypeptidase II in human blood. *Prostate*, **74**, 768–780.
34. Zavada,J., Zavadova,Z., Pastorek,J., Biesova,Z., Jezek,J. and Velek,J. (2000) Human tumour-associated cell adhesion protein MN/CA IX: identification of M75 epitope and of the region mediating cell adhesion. *Brit. J. Cancer*, **82**, 1808–1813.
35. Chrastina,A., Zavada,J., Parkkila,S., Kaluz,T., Kaluzova,M., Rajcani,J., Pastorek,J. and Pastorekova,S. (2003) Biodistribution and pharmacokinetics of I-125-labeled monoclonal antibody M75 specific for carbonic anhydrase IX, an intrinsic marker of hypoxia, in nude mice xenografted with human colorectal carcinoma. *Int. J. Cancer*, **105**, 873–881.
36. Vullo,D., Scozzafava,A., Pastorekova,S., Pastorek,J. and Supuran,C.T. (2004) Carbonic anhydrase inhibitors: inhibition of the tumor-associated isozyme IX with fluorine-containing sulfonamides. The first subnanomolar CA IX inhibitor discovered. *Bioorg. Med. Chem. Lett.*, **14**, 2351–2356.
37. Tykvart,J., Schimer,J., Barinkova,J., Pachl,P., Postova-Slavetinska,L., Majer,P., Konvalinka,J. and Sacha,P. (2014) Rational design of urea-based glutamate carboxypeptidase II (GCPII) inhibitors as versatile tools for specific drug targeting and delivery. *Bioorg. Med. Chem.*, **22**, 4099–4108.
38. Brynda,J., Mader,P., Sicha,V., Fabry,M., Poncova,K., Bakardiev,M., Gruner,B., Cigler,P. and Rezacova,P. (2013) Carborane-based carbonic anhydrase inhibitors. *Angew. Chem. Int. Edit.*, **52**, 13760–13763.
39. Sacha,P., Knedlik,T., Schimer,J., Tykvart,J., Parolek,J., Navratil,V., Dvorakova,P., Sedlak,F., Ulbrich,K., Strohalm,J. *et al.* (2016) iBodies: modular synthetic antibody mimetics based on hydrophilic polymers decorated with functional moieties. *Angew. Chem. Int. Ed. Engl.*, **55**, 2356–2360.
40. Liu,H., Moy,P., Kim,S., Xia,Y., Rajasekaran,A., Navarro,V., Knudsen,B. and Bander,N.H. (1997) Monoclonal antibodies to the extracellular domain of prostate-specific membrane antigen also react with tumor vascular endothelium. *Cancer Res.*, **57**, 3629–3634.
41. Hammer,O. and Harper,D.A.T. (2006) *Paleontological Data Analysis*. Blackwell Publishing, Malden.
42. Bengtsson,M., Stahlberg,A., Rorsman,P. and Kubista,M. (2005) Gene expression profiling in single cells from the pancreatic islets of Langerhans reveals lognormal distribution of mRNA levels. *Genome Res.*, **15**, 1388–1392.
43. Maresca,K.P., Hillier,S.M., Femia,F.J., Keith,D., Barone,C., Joyal,J.L., Zimmerman,C.N., Kozikowski,A.P., Barrett,J.A., Eckelman,W.C. *et al.* (2009) A series of halogenated heterodimeric inhibitors of prostate specific membrane antigen (PSMA) as radiolabeled probes for targeting prostate cancer. *J. Med. Chem.*, **52**, 347–357.
44. Hlouchova,K., Barinka,C., Konvalinka,J. and Lubkowski,J. (2009) Structural insight into the evolutionary and pharmacologic homology of glutamate carboxypeptidases II and III. *FEBS J.*, **276**, 4448–4462.
45. Brenner,S. and Lerner,R.A. (1992) Encoded combinatorial chemistry. *Proc. Natl. Acad. Sci. U.S.A.*, **89**, 5381–5383.
46. Henry,N., Sebe,P. and Cussenot,O. (2009) Inappropriate treatment of prostate cancer caused by heterophilic antibody interference. *Nat. Clin. Pract. Urol.*, **6**, 164–167.
47. Poyet,C., Hof,D., Sulser,T. and Muntener,M. (2012) Artificial prostate-specific antigen persistence after radical prostatectomy. *J. Clin. Oncol.*, **30**, E62–E63.
48. Ali,M.M., Li,F., Zhang,Z.Q., Zhang,K.X., Kang,D.K., Ankrum,J.A., Le,X.C. and Zhao,W.A. (2014) Rolling circle amplification: a versatile tool for chemical biology, materials science and medicine. *Chem. Soc. Rev.*, **43**, 3324–3341.
49. Rich,D.H., Bernatowicz,M.S., Agarwal,N.S., Kawai,M., Salituro,F.G. and Schmidt,P.G. (1985) Inhibition of aspartic proteases by pepstatin and 3-Methylstatine derivatives of pepstatin - evidence for collected-substrate enzyme-inhibition. *Biochemistry*, **24**, 3165–3173.
50. Karaman,M.W., Herrgard,S., Treiber,D.K., Gallant,P., Atteridge,C.E., Campbell,B.T., Chan,K.W., Ciceri,P., Davis,M.I., Edeen,P.T. *et al.* (2008) A quantitative analysis of kinase inhibitor selectivity. *Nat. Biotechnol.*, **26**, 127–132.

DNA-linked Inhibitor Antibody Assay (DIANA) for sensitive and selective enzyme detection and inhibitor screening

Supplementary information:

Further validation of PSMA and CAIX quantification in serum samples.

To test the linearity of the detection with dilution of the samples, differentially diluted samples were analyzed. The protocol was equal to that described in **materials and methods**, with the exception of the dilution of the analyzed sample.

For PSMA detection, not only 10 µl of 10 fold diluted samples was analyzed, but a dilution series of 10 µl of six serum samples ranging from undiluted (with added Tween 20 to final conc. 0.1%) to 100 fold diluted samples was analyzed instead. The results listed in **Supplementary Table S7** show that the PSMA concentrations were almost invariable throughout all dilutions in five samples. In the remaining one sample, the PSMA concentration was significantly underestimated in dilutions lower than tenfold while constant in dilutions tenfold and higher. Afterwards, all 36 serum samples were analyzed undiluted and 10 times diluted (**Supplementary Table S6**). The determined PSMA concentrations were in most cases slightly lower in diluted *vs*. undiluted samples, but in few cases significantly higher in diluted *vs*. undiluted samples. The reason for this phenomenon is not known to us, but we have observed exactly the same behavior with our PSMA ELISA and we therefore conclude that it is caused probably due to some target specific matrix effects rather than by assay specific interference. We also investigated whether this phenomenon might be caused by the presence of heterophilic interfering antibodies which would crosslink the ELISA sandwich even in the absence of the antigen. In this respect, we analyzed the samples by ELISA also after dilution in buffer with EDTA, which causes denaturation of PSMA but does not hinder the binding of the interfering antibodies and we found that EDTA almost completely suppressed the signal (**Supplementary Table S9**). Moreover, the DIANA sandwich cannot be cross-linked by these antibodies, as the detection probe does not consist of immunoglobulin and therefore we conclude that observed signals arise from selective binding of assay reagents to PSMA rather than from cross-linking of the sandwich by interfering antibodies. Nevertheless, because of this behavior exclusively tenfold diluted serum samples were used for PSMA quantifications.

The same experiments were done for CAIX detection (**Supplementary Tables S6** and **S8**), which showed only slightly decreasing CAIX concentrations with increasing dilution of the samples. No nonlinear response as in the case of PSMA was observed for CAIX quantifications. CAIX concentration determined in undiluted samples was approx. two to three times higher than in tenfold diluted samples, which might also explain approx. two times higher concentrations determined by DIANA (exclusively undiluted samples were analyzed) *vs*. by commercial ELISA (50 µl of assay diluent added to the 100 µl sample prior analysis).

To further asses the accuracy of the determined amounts of PSMA and CAIX, two different concentration of rhPSMA and HT-29 cell lysate were spiked into two serum samples and concentration of both proteins was

determined afterwards. The recovery of PSMA and CAIX ranged between 100 to 120% and 70 to 110%, respectively (**Supplementary Table S11**).

Derivation of equations for the determination of K_i of tested competitive inhibitors.

The equation for the dissociation constant K_d of the detection probe is:

$$K_d = [E] * [P] / [EP] \quad (1),$$

where [E] is the concentration of free enzyme, [P] is the concentration of free detection probe and [EP] is the concentration of the enzyme in complex with the detection probe. The concentration of free enzyme corresponds to the difference of the total (analytical) enzyme concentration (E_{tot}) and of the concentration of enzyme in complex with the probe ([EP]), and by substituting this relation into the previous equation and solving for [EP] we get (analogously to the determination of Michaelis constant of substrate and enzyme):

$$[EP] = E_{tot} * [P] / (K_d + [P]) \quad (2).$$

The concentration of the free detection probe [P] is not known, but either if the total concentration of enzyme is lower than the K_d of the detection probe, or if the total concentration of enzyme is lower than the total (analytical) concentration of the detection probe P_{tot}, [P] can be approximated by P_{tot} and the last relation can then be written as:

$$[EP] = E_{tot} * P_{tot} / (K_d + P_{tot}) \quad (3).$$

The concentration of bound probe in a complex EP is quantity measured by qPCR. The actual dissociation constant is determined by plotting the measured values of EP quantities against the used analytic concentration of detection probe and their fitting to a function described by equation (3) connected for example with numerical determination of dissociation constant of the probe (and of analytical concentration of the analyte that may not be known in advance).

The dissociation constant corresponds to the inhibition constant K_i in case of competitive inhibition, the equation for K_i of the tested compound is then:

$$K_i = [E] * [I] / [EI] \quad (4),$$

where [I] is the concentration of free tested compound and [EI] the concentration of the enzyme in complex with the bound tested compound, whereas designations of other variables remain same as in previous equation. It applies to the total amount of enzyme:

$$E_{tot} = [E] + [EP] + [EI] \quad (5),$$

and the proportion of enzyme occupied by the tested compound x is defined as:

$$[EI] / E_{tot} = x \quad (6),$$

After solving the equation (6) for E_{tot} and substituting into equation (5), solving and substituting [EP] from equation (1), substituting [EI] from equation (4) and solving, an equation for K_i is obtained:

$$K_i = (1 / x - 1) * [I] / (1 + ([P] / K_d)) \quad (7),$$

after expressing the concentration of the unbound tested compound [I] using the total (analytical) concentration of the tested compound I_{tot}, which is the sum of the concentrations of bound and unbound compound (I_{tot} = [I] + [EI]), substituting for [EI] from equation (6) and solving for [I] we get:

$$[I] = I_{tot} - x * E_{tot} \quad (8).$$

The resulting equation for calculating K_i is then:

$$K_i = (1 / x - 1) * (I_{tot} - x * E_{tot}) / (1 + ([P] / K_d)) \quad (9).$$

Practically, however, the fraction x of inhibited enzyme by the tested compound is not measured directly, but the amount of bound probe in well incubated with the tested compound is compared to the amount of bound probe in well incubated without the tested compound. Within the linear range of enzyme quantification and by assumption of non-cooperative binding of the probe into the active site of the enzyme, the amount of bound probe is directly proportional to the amount of free enzyme, i.e., the binding of competitive inhibitor to portion x of the enzyme leads to the decrease in amount of bound probe by the same proportion. Therefore, the ratio of amount of bound probe after incubation with the tested compound to the amount of bound probe after incubation without the tested compound is equal to the ratio of remaining amount of free enzyme unoccupied by the tested compound in its presence ([E] = E_{tot} - [EI]) to the total amount of enzyme (E_{tot}), i.e., to (E_{tot} - [EI]) / E_{tot}.

For each of the two quantities the C_q value is measured, which is inversely proportional to the logarithm of bound probe, i.e., with decreasing amount the measured C_q increases, and if ΔC_q is defined as C_q measured for an incubation without the tested compound subtracted from C_q measured for incubation with the tested compound, then applies:

$$(E_{tot} - [EI]) / E_{tot} = (1 + eff.)^{-\Delta Cq} \quad (10),$$

where *eff.* is the efficiency of the PCR reaction, which under optimal conditions is equal to one. Equation (9) is then reformulated using the previously mentioned relations:

$$K_i = ((1 + eff.)^{-\Delta Cq} / (1 - (1 + eff.)^{-\Delta Cq})) * (I_{tot} - x * E_{tot}) / (1 + ([P] / K_d)) \quad (11).$$

within the quantitative range of the method, this equation is further simplified by replacing concentration of free detection probe [P] with analytic concentration of the probe P_{tot}, which is known (explained in commentary in next paragraph). Virtually always, I_{tot} is significantly higher than E_{tot}, the entire member (x * E_{tot}) can therefore be neglected compared I_{tot}. The simplified equation is then:

$$K_i = ((1 + eff.)^{-\Delta Cq} / (1 - (1 + eff.)^{-\Delta Cq})) * I_{tot} / (1 + (P_{tot} / K_d)) \quad (12).$$

Thank to the sensitivity of qPCR readout, P_{tot} is kept lower than its K_d, i.e., the value of term 1 + (P_{tot} / K_d) describing the degree of competition between the probe and the tested compound for binding into the active site is approximately equal one, which in turn means that I_{tot} responsible for 50% inhibition is approx. equal to K_i which makes this assay sensitive in hit discovery. Graphical representation of equation (12) for *eff.* equal one is shown in **Supplementary Figure S2a**.

Commentary: the linear range of enzyme quantification is determined empirically by serial dilution of the enzyme and its quantification, but important relations are also easily derived theoretically. It follows from equation (1) that [EP] / [E] is directly proportional when [P] / K_d is constant. Because [P] = P_{tot} – [EP], the ratio of [P] / K_d is constant when [P] ~ P_{tot} which is valid when [EP] is significantly lower than P_{tot}. This is fulfilled when E_{tot} is smaller than P_{tot} or when [E] is smaller than K_d, because [EP] / [P] = [E] / K_d and when [E] < K_d then [EP] < [P] which is always lower than P_{tot}.

The above described model also assumes that there is no cooperativity of binding neither of the probe nor of the tested compound. This is true either when there is only one active site on the enzyme or when the binding to one site does not influence the affinity of binding to other sites, which is the case of homodimeric protein PSMA and monovalent detection probe.

More complicated model applies to the bivalent probe capable of cooperative binding to both active sites of CAIX homodimer: as we have shown, the bivalent probe has almost fifty fold higher potency than the monovalent probe, which causes non-linear proportionality of amount of bound probe on the fraction x of enzyme unoccupied by the tested competitive inhibitor. More specifically, by assuming non-cooperative binding of the tested competitive inhibitor, the binding of the inhibitor into both active sites of the CAIX homodimer is random, i.e., when portion x of the total amount of active sites is occupied by the tested compound, then the amount of CAIX homodimers with both sites occupied is x^2, whereas one site is occupied in $2x * (1 - x)$ and no site is occupied in $(1 - x)^2$. The probe binds with high affinity to CAIX homodimers having both active sites unoccupied by the tested compound, and although it binds also to CAIX homodimers having just one of the active sites occupied by the tested compound, the affinity is much lower. Also, the probe does not bind to CAIX homodimers having both sites occupied by the tested compound. The ratio R_{aff} of affinities of bivalently *vs.* monovalently bound probe is roughly determined as the ratio of K_d of probe containing two copies of CAIX ligand K_{d2} and of probe containing only one CAIX ligand K_{d1}, i.e., $R_{aff} = K_{d2} / K_{d1}$ which is equal to 0.022 ± 0.007 for our CAIX bivalent detection probe (**Figure 1b**). The ratio of amount of bound probe after incubation with tested compound [EP_i] *vs.* amount of bound probe after incubation without compound [EP_0] is then:

$$[EP_i] / [EP_0] = (1 + eff.)^{-\Delta Cq} = (1 - x)^2 + 2x * (1 - x) * R_{aff} \quad (13).$$

Solving for x leads to the equation (note that [E] / E_{tot} = 1 – x):

$$x = (1 - R_{aff} - (R_{aff}^2 + (1 - 2 * R_{aff}) * (1 + eff.)^{-\Delta Cq})^{0.5}) / (1 - 2 * R_{aff}) \quad (14).$$

After substituting for x into equation (9) and simplifying, K_i is calculated from I_{tot} and measured ΔC_q as follows:

$$K_i = ((1 - 2 * R_{aff}) / (1 - R_{aff} - (R_{aff}^2 + (1 - 2 * R_{aff}) * (1 + eff.)^{-\Delta Cq})^{0.5}) - 1) * I_{tot} / (1 + (P_{tot} / K_d)) \quad (15),$$

graphical representation of this equation for R_{aff} = 0.022 and *eff.* = 1 is plotted in **Supplementary Figure S2b**, which shows that the slope of dependency of K_i on ΔC_q is less steep than for monovalent probe (**Supplementary Figure S2a**). In other words equal change in K_i makes bigger difference in ΔC_q, which means that the K_i is determined with higher precision than with monovalent probe (standard error of the ΔC_q remains the same but its change is bigger)

but on the other hand the dynamic range of K_i determination gets narrower. More precisely, the ratio [E] / E_{tot} can be approximated by $(1 + eff.)^{-\Delta Cq/2}$ for ΔC_q smaller than ten cycles for R_{aff} = 0.022. With increasing cooperativity of the probe binding (i.e., with decreasing R_{aff}), this approximation is valid to increasingly higher values of ΔC_q.

Testing of inhibitors on biotinylated PSMA and GCPIII.

Purified recombinant human PSMA consisting of extracellular portion of PSMA with N-terminally attached biotinylated Avi-tag used for purification (designated Avi-rhPSMA) was prepared and purified as described (1) (wherein designated as Avi-GCPII). The only difference when compared to rhPSMA protein standard used elsewhere is the presence of the purification tag and both proteins are therefore nearly identical in terms of catalytic efficiency. Purified recombinant human GCPIII consisting of extracellular portion of GCPIII with N-terminally attached biotinylated Avi-tag used for purification (designated Avi-GCPIII) was prepared and purified as described (2). For long term storage, the purified proteins (diluted in TBST') were aliquoted and flash frozen in liquid nitrogen and then kept at -80 °C.

The K_i values of tested compounds toward both proteins were determined by DIANA in analogous way as described for rhPSMA in **materials and methods** with several modifications: in case of Avi-rhPSMA, 2 ng of purified protein diluted in TBST' was captured onto immobilized neutravidin (Pierce) in each well and thereafter incubated with the PSMA detection probe in TBST' at 63 pM concentration (K_d of the probe determined by titration ~ 70 pM) alone or in the presence of tested compounds at 100 µM concentration. The K_i values of the compounds were computed from their tested concentration and ΔC_q values between wells incubated with and without the compound as described for rhPSMA using equation $K_i = (2^{-\Delta Cq} / (1 - 2^{-\Delta Cq})) * I_{tot} / (1 + (P_{tot} / K_d))$. In case of Avi-GCPIII, 1 ng of purified protein diluted in TBST' with 1 mM $ZnCl_2$ was captured onto immobilized neutravidin in each well and thereafter incubated with the PSMA detection probe in TBST' at 100 pM concentration (K_d of the probe determined by titration ~ 4.4 nM) alone or in the presence of tested compounds at either 1 µM or 100 µM concentration. The K_i values of the compounds were computed in the same way as for Avi-rhPSMA.

Plot of K_i values determined by DIANA with Avi-rhPSMA captured on neutravidin vs. K_i values determined by reference enzyme kinetics (described in (3)) shows an excellent agreement between the two methods for all tested compounds, with the K_i values determined from single concentration ranging from subnanomolar to mid micromolar (R^2 = 0.982, **Supplementary Figure S3** and **Supplementary Table S20**). Plot of K_i values determined by DIANA with the homologous protein Avi-rhGCPIII captured on neutravidin vs. K_i values determined by reference enzyme kinetics (described in (4)) show also an excellent agreement between the two methods for all tested compounds, with determined K_i values ranging from 10 nM to 100 µM (**Supplementary Figure S4** and **Supplementary Table S21**).

Detection probes

PSMA detection probe was prepared by linking of a known potent urea based PSMA inhibitor *S,S*-2-(3-(5-amino-1-carboxypentyl)-ureido)-pentanedioic acid (5) to the DNA. For this purpose, derivative of this inhibitor with attached linker bearing NHS ester at its end was synthetised (compound **3**) which was then reacted with DNA oligonucleotide bearing amine group. This compound was also reacted with ethanolamine and the resulting compound (compound **4**) was used as a reference in PSMA enzymatic assay to asses the impact of linking of the DNA oligonucleotide on the inhibition potency (see **Supplementary Figure S5**).

As determined by enzyme kinetics, the K_i value of the inhibitor with linker alone (compound **4**) was 1.1 ± 0.1 nM while the K_i value of the resultant detection probe the inhibition was only 0.34 ± 0.03 nM. The inhibition potency of the probe translated into its K_d value of 0.068 ± 0.006 nM as determined by titration of the probe on PSMA captured via immobilized antibody 2G7 (**Supplementary Table S1**). For comparison, the K_d value of compound **4** determined in the same way was 0.37 ± 0.06 nM (**Supplementary Table S13**). Despite lower values determined by the latter method, both methods are in agreement, that the attachment of oligonucleotide improved the binding potency at about three to five fold.

To prepare CAIX probe, derivative of CAIX inhibitor 4-(3-phenylureido)benzenesulfonamide (6) with attached linker bearing NHS ester was synthetised (compound **9**; **Supplementary Figure S6**) and conjugated to the oligonucleotide. K_i value of the inhibitor with linker alone (compound **10** bearing amine instead of NHS ester in compound **9**) determined by enzyme kinetics was 408 ± 64 nM; K_i value of the prepared CAIX detection probe was not determined in the same way, since the consumption of the probe would be too high. To accurately asses the influence of oligonucleotide attachment, K_d values of the probe (68 ± 3 nM; **Supplementary Table S2**) and of the compound **10** (323 ± 54 nM; **Supplementary Table S18**) were determined by titration on CAIX captured via immobilized antibody M75. Consequently, the attachment of the oligonucleotide improved the binding affinity at about five fold, but this was still three orders of magnitude lower than that of the PSMA probe.

To prepare more tightly binding probe, compound **9** was reacted with DNA oligonucleotide with amine group attached at either 3' end and 5' end which led to the formation of bivalent detection probe with K_d value of 1.5 ± 0.5 nM as determined by titration on CAIX captured via immobilized antibody M75. The almost fifty fold improvement of the binding affinity compared to the monovalent probe is probably due to the ability of the bivalent probe to bind to both active sites of the CAIX homodimer simultaneously, similar phenomenon was previously observed for bivalent small molecule inhibitor of CAIX (7). This bivalent probe was used for CAIX detection as well as testing of CAIX inhibitors.

The positions on inhibitors amenable to derivatization with linker moiety as well as the length of the linkers were chosen based on evidence from literature and known crystal structures of both proteins. The way of derivatization of the PSMA inhibitors is well known (5) and it has been shown that attachment of nucleotides via short linker may improve their affinity (8). The position of the linker attachment on CAIX inhibitor was derived from structures of

such inhibitors in active site of carbonic anhydrase II showing their mode of binding (6). The length was then guessed from crystal structure of CAIX (9) showing that linker containing five ethylenglycol units is of sufficient length to connect the active site to the protein surface.

We conjugated those inhibitors to single stranded DNA oligonucleotide (designated as ssDNA) and subsequently tested the influence of both single stranded and double stranded DNA-reporter on assay performance. To prepare double stranded DNA-reporter, we annealed both mono-substituted PSMA and CAIX detection probes with two different complementary strands: with first oligonucleotide being complementary to all bases of the probe (designated as dsDNA) and with second oligonucleotide being complementary to all bases of the probe except the last 3 bases at the 3' termini where the inhibitors were attached (designated as dsDNA_3A). We then compared their performance in DIANA assay; while we have not seen any significant difference in either K_d or the assay signal between ssDNA a dsDNA_3A, we have seen a decline in affinity for dsDNA of approximately two- to three-fold. At the same time, the non-selective adsorption of both double stranded variants was lower resulting in background lowered by about two PCR cycles. However, we cannot exclude that different experimental settings could result in variation of non-selective binding and we therefore suggest to compare single and double stranded DNA reporters in cases where the maximum sensitivity is crucial. The dsDNA_3A detection probes thus achieved highest signal-to-noise ratio and were used in subsequent DIANA experiments with the only exception of the bivalent CAIX probe where we used single stranded DNA reporter as this should allow maximum flexibility for optimal simultaneous binding into both active sites of the homodimer.

Interestingly, the prepared conjugates were better binders than the original inhibitors with linker; we think that this effect might be caused by the binding of DNA bases to some exosites at the protein surface near the active site. This hypothesis is also supported by the fact, that we have seen a decline in the affinity after pairing the 3' termini proximal bases with complementary oligonucleotide as described in previous paragraph.

Detailed description of synthesis of the detection probes

Chemicals were purchased from Sigma-Aldrich, unless stated otherwise. The purity of compounds was tested on analytical Jasco PU-1580 HPLC (flow rate 1 ml/min, invariable gradient 2-100% (vol./vol.) ACN in 30 minutes, RT shown for each compound) with column Watrex C18 Analytical Column, 5 µm, 250 x 5 mm. Final products used for conjugation with the oligonucleotides were purified using preparative scale HPLC Waters Delta 600 (flow rate 7 ml/min, gradient and RT shown for each compound) with column Waters SunFire C18 OBD Prep Column, 5 µm, 19 x 150 mm. All final products were of at least 99% purity. Structure of these products was further confirmed by HRMS at LTQ Orbitrap XL (Thermo Fisher Scientific) and by NMR (Bruker Avance I™ 500 MHz equipped with Cryoprobe or Bruker Avance I™ 400 MHz). Initial oligonucleotides and prepared detection probes were analyzed by LC/ESI-MS method on the Agilent 6230 TOF LC/MS device (Agilent Technologies) equipped with dual AJS ESI source in the settings for detecting negative ions (4GHz, HiRes). Separation was carried out at room temperature on

Agilent Zorbax Extend-C18 1.8 µm (2.1x50 mm) column by gradient elution in changing ratio of mobile phase and acetonitrile, at a flow rate of 0.3 ml.min^{-1} (2-45% (vol./vol.) ACN in 6 minutes).

PSMA:

Preparation of 3,3'-oxydipropanoic acid (compound **1**): 2.38 ml (20 mmol) of 3,3'-oxydipropanenitrile was dissolved in 7 ml of concentrated HCl and was heated to 50 °C for 24 hours. The reaction mixture was then left to cool down overnight and the hydrochloric acid was removed by flow of nitrogen. The resulting slurry was dissolved in water and lyophilized; 2.25 g of white product was obtained (yield 70%). The spectral analysis of this product was identical to that described (10).

Preparation of bis(2,5-dioxopyrrolidin-1-yl) 3,3'-oxydipropanoate (compound **2**): To a solution of compound **1** (260 mg, 1.6 mmol, 1.0 eq) and N-hydroxy succinimide (660 mg, 3.2 mmol, 2.0 eq) in 10 ml of THF, solid DCC (368 mg, 3.2 mmol, 2.0 eq) was added in one portion. The reaction was left overnight, after which the formed DCU was filtered of and the volatiles were rotary evaporated. The crude product was further purified by chromatography (He:EtOAc 1:2); 338 mg of pure product obtained (isolated yield 60%). Analytical HPLC RT = 16.2 min.

^{1}H NMR (400 MHz, $CDCl_3$): δ 3.85 (t, *J* = 6.4 Hz, 4H), 2.90 (t, *J* = 6.4 Hz, 4H), 2.83 (bs, 8H).

^{13}C NMR (101 MHz, $CDCl_3$): δ 169.07, 166.77, 65.78, 32.20, 25.73.

HRMS (ESI+): calculated mass of $C_{14}H_{16}O_9N_2$ $[MNa]^+$ 379.07480, detected mass 379.07469.

Preparation of 19-((2,5-dioxopyrrolidin-1-yl)oxy)-5,13,19-trioxo-16-oxa-4,6,12-triazanonadecane-1,3,7-tricarboxylic acid (compound **3**): To a stirring solution of compound **2** (69 mg, 193 µmol, 1.2 eq) dissolved in 1 ml of DMF, a solution of di-tert-butyl 2-(3-(6-amino-1-(tert-butoxy)-1-oxohexan-2-yl)ureido)pentanedioate (100 mg, 161 µmol, 1.0 eq, prepared as previously described (11)) and DIEA (34 µl, 193 µmol, 1.2 eq) in 1 ml of DMF was added dropwise during 1 hour. The reaction mixture was left stirring for 2 hours after which an HPLC analysis proved total disappearance of second reactant. The solvents were then removed by rotary vacuo and the compound was fully dried. 1 ml of TFA was then added into the crude mixture to yield crude title compound. After 1 hour incubation at room temperature the trifluoracetic acid was removed by flow of nitrogen. The crude product was purified using preparative HPLC (gradient 5-50% (vol./vol.) ACN in 40 minutes, RT 18 minutes); 20 mg of the product was obtained (isolated yield after two steps 22%). Analytical HPLC RT = 13.7 min.

^{1}H NMR (500 MHz, DMSO-d6): δ 7.80 (t, J = 5.6, 1H, **NH**-Lys-6), 6.32 (d, J = 8.3, 1H, **NH**-Glu-2), 6.29 (d, J = 8.2, 1H, **NH**-Lys-2), 4.09 (m, 1H, **Glu-2**), 4.03 (m, 1H, **Lys-2**), 3.55 (m, 4H, O-**CH_2**-CH_2-COO, Lys-CO-CH_2-**CH_2**-O), 3.00 (m, 2H, **Lys-6**), 2.80 (bs, 4H, CO-**CH_2**-**CH_2**-CO), 2.41 (t, J = 6.3, 2H, O-CH_2-**CH_2**-COO), 2.31-2.20 (m, 4H, Lys-CO-**CH_2**-CH_2, **Glu-4**), 1.91 (m, 1H, **Glu-3b**), 1.71 (m, 1H, **Glu-3a**), 1.63 (m, 1H, **Lys-3b**), 1.51 (m, 1H, **Lys-3a**), 1.37 (m, 2H, **Lys-5**), 1.26 (m, 2H, **Lys-4**).

^{13}C NMR (125.7 MHz, DMSO-d6): δ 174.77 (**Lys-1**), 174.40 (**Glu-1**), 173.95 (**Glu-5**), 172.89 (O-CH_2-CH_2-**COO**), 170.39 (**CO**-NH-**CO**), 170.00 (lys-**CO**-CH_2-CH_2-O), 157.52 (NH-**CO**-NH), 66.87 (lys-CO-CH_2-**CH_2**-O), 66.07 (O-**CH_2**-CH2-COO), 52.46 (**Lys-2**), 51.85 (**Glu-2**), 38.54 (**Lys-6**), 36.25 (Lys-CO-**CH_2**-CH_2-O), 34.84 (O-CH_2-**CH_2**-COO), 31.97 (**Lys-3**), 30.09 (**Glu-4**), 29.00 (**Lys-5**), 27.71 (**Glu-3**), 25.66 (CO-**CH_2**-**CH_2**-CO), 22.82 (**Lys-4**).
HRMS (ESI+): calculated mass of $C_{22}H_{32}O_{13}N_4$ $[MNa]^+$ 583.18581; detected mass 583.18596.

Preparation of 1-hydroxy-4,10,18-trioxo-7-oxa-3,11,17,19-tetraazadocosane-16,20,22-tricarboxylic acid, compound **4**: 10 µl of stock DMSO solution containing 0.28 mg (0.5 µmol, 1.0 eq) of compound **3** was mixed with 50 µl of aqueous solution of ethanolamine at concentration of 100 mmol.l^{-1} (5 µmol, 10 eq) and left overnight at room temperature. The mixture was then diluted in ACN/water and lyophilized three times (to evaporate all the remaining ethanolamine and DMSO). This compound was used without further purification (the only contaminant is free NHS).
HRMS (ESI-): calculated mass of $C_{20}H_{33}O_{11}N_4$ $[M]^-$ 505.21513, detected mass 505.21515.

The detection probe for selective binding to PSMA was prepared by reacting the compound **3** with single-stranded DNA oligonucleotide of the sequence CCT GCC AGT TGA GCA TTT TTA TCT GCC ACC TTC TCC ACC AGA CAA AAG CTG GAA A and with 3'-terminally modified phosphate moiety by 6-amino-2-(hydroxymethyl)hexyl group (custom synthesis by Generi-Biotech, OPC purification; hereinafter *iqPCR_amino*): 6.9 µl of 1 mol.l^{-1} HEPES buffered to pH = 8.0 were added to 10 µl of the oligonucleotide *iqPCR_amino* at a concentration of 1.02 mmol.l^{-1} (10.2 nmol, 1.0 eq) in 100 mmol.l^{-1} phosphate, 150 mmol.l^{-1} NaCl, pH 7.8 (hereinafter modification buffer) and after stirring, 3.1 µl of a solution of compound **3** at a concentration of 100 mmol.l^{-1} in anhydrous DMSO (307 nmol, 30.0 eq) was added. The resulting mixture was incubated at room temperature for 24 hours and then purified from compound **3** and its hydrolyzed form via ultrafiltration on Amicon Ultra 0.5 ml 10K column (Millipore, cat. No. UFC501096). The retained solution contained 9.2 nmol of the detection probe as determined spectrophotometrically (1 OD = 1744 pmol; yield ~ 90%). This detection probe containing single stranded reporter DNA and the original oligonucleotide *iqPCR_amino* were analyzed using LC/MS (mobile phase: aqueous solution of HFIP (1,1,1,3,3,3-hexafluoro-2-propanol) at concentration of 200 mmol.l^{-1} adjusted to pH 7.0 by addition of triethylamine): RT of the original oligonucleotide was 4.84 min and observed mass was 16981.87 (predicted 16979.91); RT of the detection probe was 4.85 min and the observed mass was 17426.84 (predicted 17425.08). The observed mass difference between the detection probe and the original oligonucleotide was 444.97 which corresponded to the predicted difference of 445.17. As retention times of both species were virtually the same, the purity had to be estimated solely based on the mass spectrum; signals corresponding to *m/z* ratio of the original oligonucleotide were not observed in the mass spectrum of the detection probe, we therefore conclude that the purity of the probe exceeded 90%. Prior to use, the detection probe has been annealed with equimolar amount of DNA oligonucleotide of complementary sequence CCA GCT TTT GTC TGG TGG AGA AGG TGG CAG ATA AAA ATG CTC AAC TGG CAG G

(Generi Biotech, desalting purification; 1 OD = 1721 pmol) in TBS by rapid heating to 98°C followed by slow cooling to room temperature in thermal cycler.

CAIX:

Preparation of methyl 4-(4-((tert-butoxycarbonyl)amino)butoxy)benzoate (compound **5**): To a solution of 161 mg (1.06 mmol, 1.0 eq) of methyl 4-hydroxybenzoate, 300 mg (1.59 mmol, 1.5 eq) of tert-butyl (4-hydroxybutyl) carbamate and 400 mg (1.59 mmol, 1.5 eq) of triphenylphosphine in 10 ml of THF was added 312 µl (1.59 mmol, 1.5 eq) of DIAD in one portion and the reaction was left stirring overnight. The reaction mixture was then evaporated and the crude product was purified by column chromatography on silica (He:EtOAc 4:1, R_f = 0.25; note: the methyl 4-hydroxybenzoate has identical RF with the product, therefore 1.5 eq of other reactants was used) 260 mg of white powder was obtained (isolated yield 75%).

^{1}H NMR (400 MHz, $CDCl_3$): δ 7.95 (d, *J* = 8.9 Hz, 2H), 6.87 (d, *J* = 8.9 Hz, 2H), 3.99 (t, *J* = 6.2 Hz, 2H), 3.85 (s, 3H), 3.17 (dd, *J* = 12.8, 6.3 Hz, 2H), 1.86 – 1.75 (m, 2H), 1.69 – 1.61 (m, 2H), 1.42 (s, 9H).

^{13}C NMR (101 MHz, $CDCl_3$): δ 166.92, 162.78, 156.10, 131.64, 122.57, 114.12, 79.20, 67.73, 51.89, 40.29, 28.49, 26.86, 26.49.

MS (ESI+): calculated mass $C_{17}H_{25}O_5N$ $[MNa]^+$ 346.17; detected mass 346.2.

Preparation of 4-(4-((tert-butoxycarbonyl)amino)butoxy)benzoic acid (compound **6**): 270 mg of compound **5** were dissolved in 5 ml of methanol and 5 ml of 5 mol.l^{-1} NaOH were added. The mixture was refluxed until TLC analysis showed complete disappearance of compound **5** (6 hours). The reaction mixture was evaporated and dissolved water/EtOAc (20/20 ml), the water phase was acidified by 10% $KHSO_4$ (wt./vol.) to acidic pH and extracted 2 more times by 20 ml of EtOAc. 240 mg of oily product which turned to crystalline white after removal of solvent traces was obtained (isolated yield 95%).

^{1}H NMR (400 MHz, $CDCl_3$): δ 8.03 (d, *J* = 8.9 Hz, 2H), 6.91 (d, *J* = 9.0 Hz, 2H), 4.04 (t, *J* = 6.2 Hz, 2H), 3.27-3.20 (m, 2H), 1.91 – 1.78 (m, 2H), 1.69 (dd, *J* = 14.8, 7.2 Hz, 2H), 1.44 (s, 9H).

^{13}C NMR (101 MHz, $CDCl_3$): δ 171.51, 163.46, 156.20, 132.42, 121.92, 114.28, 79.42, 67.86, 40.36, 28.56, 26.89, 26.53.

MS (ESI-): calculated mass $C_{16}H_{22}O_5N$ $[M]^-$ 308.16; detected mass 308.2.

Preparation of tert-butyl (4-(4-(3-(4-sulfamoylphenyl)ureido)phenoxy)butyl)carbamate (compound **7**): 720 mg (2.33 mmol, 1.0 eq) of compound **6** were dissolved in 15 ml of dry toluene and 810 µl (4.65 mmol, 2 eq) of DIEA were added. DPPA (552 µl, 2.56 mmol, 1.1 eq) was added to the reaction mixture in one portion and the reaction temperature was raised to 90 °C for 2 hours. The reaction mixture was then evaporated and dissolved in dry ACN; 601 mg (3.49 mmol, 1.5 eq) of sulfanilamide was added in one portion and reaction mixture was heated up to 60 °C

overnight while stirring. All volatiles were evaporated after 12 hours and the crude product was purified by column chromatography on silica (He: EtOAc, 2:5, R_f = 0.25). 340 mg of product were obtained (isolated yield 30%).
^{1}H NMR (400 MHz, DMSO): δ 8.98 (s, 1H), 8.59 (s, 1H), 7.71 (d, *J* = 8.8 Hz, 2H), 7.59 (d, *J* = 8.9 Hz, 2H), 7.34 (d, *J* = 9.0 Hz, 2H), 7.20 (s, 2H), 6.91 – 6.81 (m, 3H), 3.91 (t, *J* = 6.4 Hz, 2H), 2.96 (dd, *J* = 12.9, 6.7 Hz, 2H), 1.71 – 1.61 (m, 2H), 1.51 (dt, *J* = 13.1, 6.5 Hz, 2H), 1.37 (s, 9H).
^{13}C NMR (101 MHz, DMSO): δ 155.37, 154.02, 152.16, 142.99, 136.40, 132.04, 126.61, 120.14, 117.12, 114.50, 77.06, 67.05, 40.35 (overlap with solvent peak) 27.77, 26.85, 25.73.
MS (ESI+): calculated mass of $C_{22}H_{30}O_6N_4S$ $[MNa]^+$ 501.17; detected mass 501.2.

Preparation of 4-(4-(3-(4-sulfamoylphenyl)ureido)phenoxy)butan-1-aminium 2,2,2-trifluoroacetate, (compound **8**): 500 mg of compound **7** were dissolved in 1 ml of TFA and the reaction mixture sonicated and stirred alternately for 5 minutes. TFA was then removed by flow of nitrogen and the product was used in further steps without any further purification.

Preparation of 2,5-dioxopyrrolidin-1-yl 19-oxo-24-(4-(3-(4-sulfamoylphenyl)ureido)phenoxy)-4,7,10,13,16-pentaoxa-20-azatetracosan-1-oate (compound **9**): 33 mg (67 µmol, 1.0 eq) of compound **8** were added slowly (during 1 hour) into a solution of bisNHS-PEG5 (36 mg, 67 µmol, 1.0 eq; Broadpharm) and DIEA (22 µl, 168 µmol, 2.5 eq) in DMF (1 ml). The reaction mixture was left stirring for further 3 hours and then all the volatiles were evaporated. The final product was purified by preparative scale HPLC (gradient: 15-50% (vol./vol.) ACN in 40 minutes, RT 30 minutes). 15 mg of product were isolated with purity well above 99% (yield 28%). Analytical HPLC RT = 18.7 min. **HRMS (ESI+):** calculated mass of $C_{35}H_{50}O_{14}N_5S$ $[MH]^+$ 795.30695, detected mass 796.30678.

Preparation of 18-oxo-23-(4-(3-(4-sulfamoylphenyl)ureido)phenoxy)-3,6,9,12,15-pentaoxa-19-azatricosan-1-aminium 2,2,2-trifluoroacetate (compound **10)**: 46 mg (112 µmol, 1 eq) of Boc-PEG5-COOH was dissolved in 0.5 ml of DMF along with 36 mg (112 µmol, 1.0 eq) of TBTU and 49 µl (279 µmol, 2.5 eq) of DIEA. To this solution 55 mg (112 µmol, 1.0 eq) of compound **8** was added and the mixture was stirred overnight. The solvent was then evaporated and the crude product dissolved in 10 ml of EtOAc. The organic phase was washed two times with saturated bicarbonate, two times by 10% (wt./vol.) $KHSO_4$, and once with brine dried and evaporated; 53 mg of intermediate were isolated. 1 ml of TFA was then added to the crude intermediate and the reaction mixture was alternately sonicated and stirred for 15 minutes. The TFA was then removed by flow of nitrogen and the product was purified by preparative scale HPLC (gradient: 10-50% ACN in 40 minutes, RT = 22 minutes). 17 mg of product were isolated (isolated yield over two steps 31%). Analytical HPLC RT = 16.5 min. **HRMS (ESI+):** calculated mass $C_{30}H_{48}O_{10}N_5S$ $[MH]^+$ 670.31164; detected mass 670.31164.

The detection probe for selective binding to CAIX was prepared by reacting the compound **9** with single-stranded DNA oligonucleotide: 2 µl of 1 mol.l^{-1} HEPES buffered to pH 8.0 were added to 10 µl of the oligonucleotide *iqPCR_amino* at a concentration of 820 µmol.l^{-1} (8.2 nmol, 1.0 eq) in the modification buffer and after stirring, 8.2 µl of a solution of compound **9** at a concentration of 50 mmol.l^{-1} in anhydrous DMSO (410 mmol, 50 eq) was added and stirred again. Finally, 5 µl of anhydrous DMSO was added to the mixture to prevent precipitation and after stirring incubated overnight at room temperature. The resulting mixture was then diluted in 900 µl of an aqueous solution of 0.1 mol.l^{-1} HEPES, pH 8.0, incubated another day at room temperature and then purified from compound **9** and its hydrolyzed form by ultrafiltration on Amicon Ultra 0.5 ml 10K. The resulting retenate contained 8.1 nmol of the detection probe as determined spectrophotometrically (yield ~ 99%) and was analyzed using LC/MS (mobile phase: 0.05% (wt./vol.) aqueous ammonium acetate solution): retention time of the prepared detection probe was 5.14 min with the observed mass of 17663.28 (predicted 17663.86); according to the LC chromatogram at 260 nm the conversion of the conjugation was approx. 80%. The difference between observed masses of the detection probe and the original oligonucleotide was 681.41 which corresponded to the predicted difference of 680.30. Prior use, the detection probe has been annealed with equimolar amount of DNA oligonucleotide of complementary sequence CCA GCT TTT GTC TGG TGG AGA AGG TGG CAG ATA AAA ATG CTC AAC TGG CAG G (Generi Biotech, desalting purification; 1 OD = 1721 pmol) in TBS by rapid heating to 98 °C followed by slow cooling to room temperature in thermal cycler.

The bivalent detection probe for selective binding of CAIX was prepared by reacting of compound **9** and single-stranded DNA oligonucleotide of the sequence AAA CCT GCC AGT TGA GCA TTT TTA TCT GCC ACC TTC TCC ACC AGA CAA AAG CTG GAA A containing the 3'-terminal 6-amino-2-(hydroxymethyl) hexyl phosphate modification and the 5'-terminal 6-aminohexyl phosphate modification (custom synthesis Generi-Biotech, OPC purification; hereinafter *iqPCR_bis_amino*): 3.4 µl of 1 mol.l^{-1} HEPES buffered to pH 8.0 were added to 2.7 µl of the oligonucleotide *iqPCR_bis_amino* at a concentration of 1.9 mmol.l^{-1} (5.0 nmol, 1.0 eq) in the modification buffer and after stirring, 5.0 µl of a solution of compound **9** at a concentration of 50 mmol.l^{-1} in anhydrous DMSO (250 mmol, 50 eq) were added and stirred again. The resulting mixture was purified and analyzed using LC/MS identically as described above for monovalent probe. Two major peaks were observed: first with RT of 5.13 min corresponding to the single substituted oligonucleotide and second with RT of 5.29 min corresponding to the double substituted oligonucleotide. Observed mass of the double substituted oligonucleotide was 19462.36, while the observed mass of the original *iqPCR_bis_amino* oligonucleotide analyzed in the same way was 18100.85 (predicted 18101.88, RT = 4.85 min), corresponding to weight difference of 1361.50 which corresponds to twice the mass of the conjugated compound **9** (680.30). The mixture containing approx. 40% of single and 50% of double substituted detection probes (according to the LC chromatogram at 260 nm) was used without any further purification and is referred as the

"bivalent probe", the total obtained amount of both species was 4.8 nmol as determined spectrophotometrically (yield approx. 96%, yield of the bivalent probe approx. 50%).

Supplementary Figures:

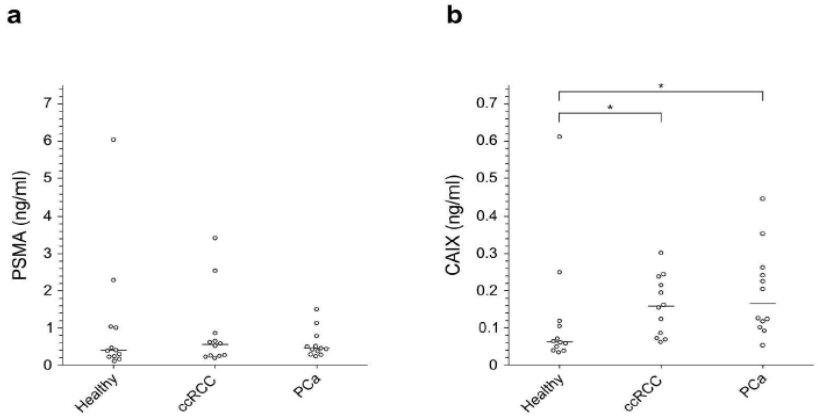

Supplementary Figure S1 Comparison of PSMA and CAIX serum levels between healthy and diseased state. (**a**,**b**) Plots of PSMA (**a**) and CAIX (**b**) serum levels determined by DIANA in samples from 12 healthy males, 12 males with histologically proven PCa and 10 males and 2 females with histologically proven ccRCC. Horizontal lines indicate median concentrations; * indicates statistically significant differences between the groups with $p < 0.05$ as determined by the two tailed Mann-Whitney test.

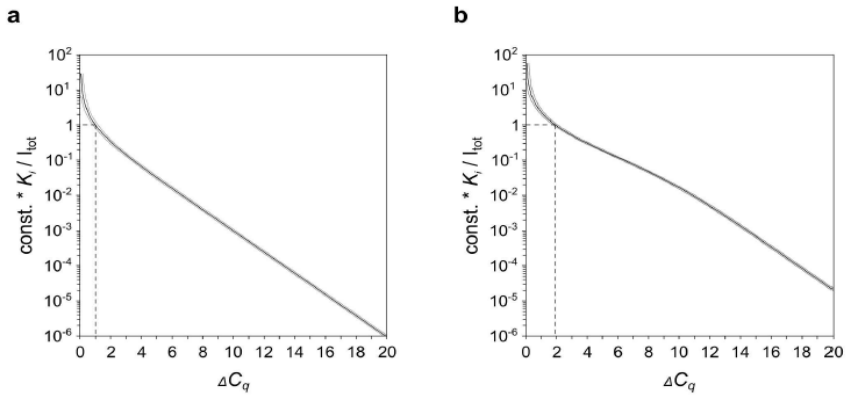

Supplementary Figure S2 Theoretical background of inhibitor testing by DIANA.

(**a**) Dependency of the determined inhibition constant (K_i) of tested inhibitor on measured ΔC_q valid for monovalent probe and plotted based on $K_i = (2^{-\Delta Cq} / (1 - 2^{-\Delta Cq})) * I_{tot} / (1 + (P_{tot} / K_d))$, used to determine the K_i values of PSMA inhibitors. I_{tot} is the total concentration of the tested inhibitor, P_{tot} is the total concentration of probe and K_d is the dissociation constant of the probe. Constant is equal to the term $1 + (P_{tot} / K_d)$, which can be approximated by one if probe concentration P_{tot} is held below its K_d.

(**b**) Dependency of the determined inhibition constant (K_i) of tested inhibitor on measured ΔC_q valid for bivalent probe and plotted based on $K_i = ((1 - 2 * R_{aff}) / (1 - R_{aff} - (R_{aff}^2 + (1 - 2 * R_{aff}) * 2^{-\Delta Cq})^{0.5}) - 1) * I_{tot} / (1 + (P_{tot} / K_{d2}))$, used to determine the Ki values of CAIX inhibitors. R_{aff} is the ratio of K_{d2} of the double-binding probe to K_{d1} of the single-binding probe ($R_{aff} = K_{d2} / K_{d1}$; $K_{d1} \sim 70$ nM, $K_{d2} \sim 1.5$ nM for CAIX probe).

Grey lines show +/- s.d. of the determined K_i under the assumption that C_q is measured with s.d. of 0.15 cycle. Dashed lines indicate the IC_{50} value; which corresponds to the inhibitor concentration at which 50% of the probe has been displaced by the inhibitor.

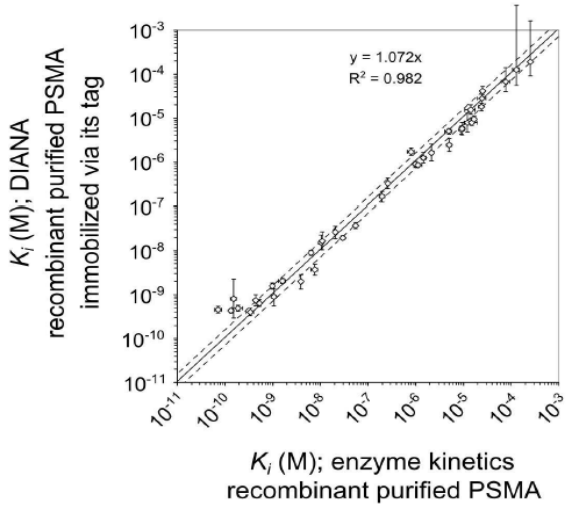

Supplementary Figure S3

Plot of K_i values of 39 compounds determined by enzyme kinetics from titration of recombinant purified Avi-rhPSMA with inhibitor (x-axis) versus K_i values determined by DIANA from single measurement with 100 µM inhibitor (10^{-4} M) and recombinant purified Avi-rhPSMA captured via its tag onto neutravidin (y-axis). Lines show linear regression of log transformed values, dashed lines indicates values 1.5 times higher or lower than the linear regression. Error bars, s.d. over duplicates for DIANA, s.e. of the titration for enzyme kinetics.

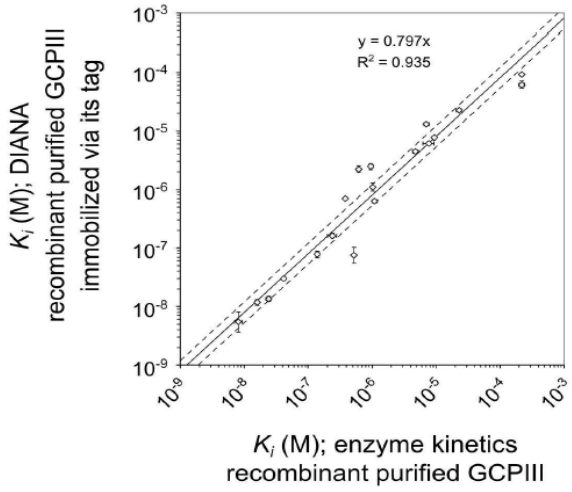

Supplementary Figure S4

Plot of K_i values of 19 compounds determined by enzyme kinetics from titration of recombinant purified Avi-GCPIII with inhibitor (x-axis) versus K_i values determined by DIANA from measurements with 1 µM (10^{-6} M) and 100 µM inhibitor (10^{-4} M) with recombinant purified Avi-GCPIII captured via its tag onto neutravidin (y-axis). Lines show linear regression of log transformed values, dashed lines indicates values 1.5 times higher or lower than the linear regression. Error bars, s.d. over duplicates for DIANA, s.e. of the titration for enzyme kinetics.

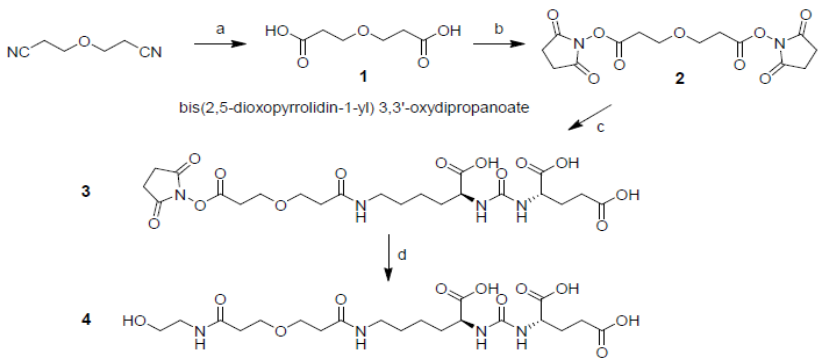

a) conc. HCl, 50 °C, 24h; b) NHS-OH, DCC, THF; c) 1) di-*tert*-butyl 2-(3-(6-amino-1-(*tert*-butoxy)-1-oxohexan-2-yl)ureido)pentanedioate, DIEA, DMF, 2) TFA; d) ethanolamine, DMF, DIEA

Supplementary Figure S5 Synthesis of PSMA inhibitors

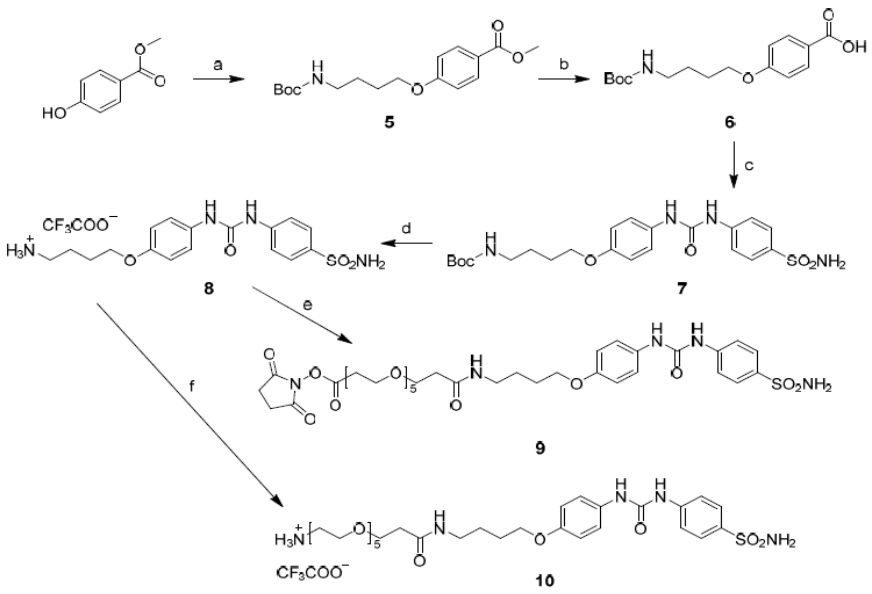

a) *tert*-butyl (4-hydroxybutyl)carbamate, $(Ph)_3P$, DIAD, THF; b) 5M NaOH,MeOH/H_2O, reflux 6h; c) 1) DPPA, DIEA, Tol, RT to 90 °C 2) sulfanilamide, ACN, 60 °C; d) TFA; e) bisNHS-PEG_5, DIEA, DMF; f) 1) Boc-PEG_5-COOH TBTU, DIEA, DMF 2) TFA

Supplementary Figure S6 Synthesis of CAIX inhibitors

Supplementary tables 1-22 on pages S20-S41 are skipped here (available online).

Supplementary materials references:

1. Tykvart, J., Sacha, P., Barinka, C., Knedlik, T., Starkova, J., Lubkowski, J. and Konvalinka, J. (2012) Efficient and versatile one-step affinity purification of in vivo biotinylated proteins: Expression, characterization and structure analysis of recombinant human glutamate carboxypeptidase II. *Protein Expres. Purif.*, **82**, 106-115.
2. Tykvart, J., Navratil, V., Sedlak, F., Corey, E., Colombatti, M., Fracasso, G., Koukolik, F., Barinka, C., Sacha, P. and Konvalinka, J. (2014) Comparative analysis of monoclonal antibodies against prostate-specific membrane antigen (PSMA). *Prostate*, **74**, 1674-1690.
3. Tykvart, J., Schimer, J., Barinkova, J., Pachl, P., Postova-Slavetinska, L., Majer, P., Konvalinka, J. and Sacha, P. (2014) Rational design of urea-based glutamate carboxypeptidase II (GCPII) inhibitors as versatile tools for specific drug targeting and delivery. *Bioorg. Med. Chem.*, **22**, 4099-4108.
4. Tykvart, J., Schimer, J., Jancarik, A., Barinkova, J., Navratil, V., Starkova, J., Sramkova, K., Konvalinka, J., Majer, P. and Sacha, P. (2015) Design of Highly Potent Urea-Based, Exosite-Binding Inhibitors Selective for Glutamate Carboxypeptidase II. *J. Med. Chem.*, **58**, 4357-4363.
5. Maresca, K.P., Hillier, S.M., Femia, F.J., Keith, D., Barone, C., Joyal, J.L., Zimmerman, C.N., Kozikowski, A.P., Barrett, J.A., Eckelman, W.C. *et al.* (2009) A Series of Halogenated Heterodimeric Inhibitors of Prostate Specific Membrane Antigen (PSMA) as Radiolabeled Probes for Targeting Prostate Cancer. *J. Med. Chem.*, **52**, 347-357.
6. Pacchiano, F., Carta, F., McDonald, P.C., Lou, Y.M., Vullo, D., Scozzafava, A., Dedhar, S. and Supuran, C.T. (2011) Ureido-Substituted Benzenesulfonamides Potently Inhibit Carbonic Anhydrase IX and Show Antimetastatic Activity in a Model of Breast Cancer Metastasis. *J. Med. Chem.*, **54**, 1896-1902.
7. Krall, N., Pretto, F. and Neri, D. (2014) A bivalent small molecule-drug conjugate directed against carbonic anhydrase IX can elicit complete tumour regression in mice. *Chem. Sci.*, **5**, 3640-3644.
8. Wang, X.N., Tian, H.B., Lee, Z. and Heston, W.D.W. (2012) Structure-Activity Relationships of 2 ',5 '-Oligoadenylate Analogue Modifications of Prostate-Specific Membrane Antigen (Psma) Antagonists. *Nucleos. Nucleot. Nucl.*, **31**, 432-444.
9. Alterio, V., Hilvo, M., Di Fiore, A., Supuran, C.T., Pan, P.W., Parkkila, S., Scaloni, A., Pastorek, J., Pastorekova, S., Pedone, C. *et al.* (2009) Crystal structure of the catalytic domain of the tumor-associated human carbonic anhydrase IX. *Proc. Natl. Acad. Sci. USA*, **106**, 16233-16238.
10. White, D.E. and Jacobsen, E.N. (2003) New oligomeric catalyst for the hydrolytic kinetic resolution of terminal epoxides under solvent-free conditions. *Tetrahedron-Asymmetry*, **14**, 3633-3638.
11. Murelli, R.P., Zhang, A.X., Michel, J., Jorgensen, W.L. and Spiegel, D.A. (2009) Chemical Control over Immune Recognition: A Class of Antibody-Recruiting Small Molecules That Target Prostate Cancer. *J. Am. Chem. Soc.*, **131**, 17090-17092.

Jméno a příjmení	Číslo OP	Datum vypůjčení	Poznámka